Vol. 294, No. 3, August 30, 1994
Completing Volume 294

ISSN 0003-2670

ANALYTICA CHIMICA ACTA

An international journal devoted to all branches of analytical chemistry

Editors: Harry L. Pardue (West Lafayette, IN, USA)
Alan Townshend (Hull, Great Britain)
J.T. Clerc (Berne, Switzerland)
Willem E. van der Linden (Enschede, Netherlands)
Paul J. Worsfold (Plymouth, Great Britain)

Associate Editor: Sarah C. Rutan (Richmond, VA, USA)

Editorial Advisers:

F.C. Adams, Antwerp
M. Aizawa, Yokohama
W.R.G. Baeyens, Ghent
C.M.G. van den Berg, Liverpool
A.M. Bond, Bundoora, Vic.
M. Bos, Enschede
J. Buffle, Geneva
R.G. Cooks, West Lafayette, IN
P.R. Coulet, Lyon
S.R. Crouch, East Lansing, MI
R. Dams, Ghent
P.K. Dasgupta, Lubbock, TX
Z. Fang, Shenyang
P.J. Gemperline, Greenville, NC
W. Heineman, Cincinnati, OH
G.M. Hieftje, Bloomington, IN
G. Horvai, Budapest
T. Imasaka, Fukuoka
D. Jagner, Gothenburg
G. Johansson, Lund
D.C. Johnson, Ames, IA
A.M.G. Macdonald, Birmingham
D.L. Massart, Brussels
P.C. Meier, Schaffhausen
M. Meloun, Pardubice
M.E. Meyerhoff, Ann Arbor, MI
H.A. Mottola, Stillwater, OK
M. Otto, Freiberg
D. Pérez-Bendito, Córdoba
A. Sanz-Medel, Oviedo
T. Sawada, Tokyo
K. Schügerl, Hannover
M.R. Smyth, Dublin
R.D. Snook, Manchester
J.V. Sweedler, Urbana, IL
M. Thompson, Toronto
G. Tölg, Dortmund
Y. Umezawa, Tokyo
J. Wang, Las Cruces, NM
H.W. Werner, Eindhoven
O.S. Wolfbeis, Graz
Yu.A. Zolotov, Moscow
J. Zupan, Ljubljana

ELSEVIER

ANALYTICA CHIMICA ACTA

Scope. *Analytica Chimica Acta* publishes original papers, rapid publication letters and reviews dealing with every aspect of modern analytical chemistry. Reviews are normally written by invitation of the editors, who welcome suggestions for subjects. Letters can be published within **four months** of submission. For information on the Letters section, see inside back cover.

Submission of Papers

Americas

Prof. Harry L. Pardue
Department of Chemistry
1393 BRWN Bldg, Purdue University
West Lafayette, IN 47907-1393
USA

Tel:(+1-317) 494 5320
Fax:(+1-317) 496 1200

Computer Techniques

Prof. J.T. Clerc
Universität Bern
Pharmazeutisches Institut
Baltzerstrasse 5, CH-3012 Bern
Switzerland

Tel:(+41-31) 6314191
Fax:(+41-31) 6314198

Prof. Sarah C. Rutan
Department of Chemistry
Virginia Commonwealth University
P.O. Box 2006
Richmond, VA 23284-2006
USA
Tel:(+1-804) 367 7517
Fax:(+1-804) 367 8599

Other Papers

Prof. Alan Townshend
Department of Chemistry
The University
Hull HU6 7RX
Great Britain

Tel:(+44-482) 465027
Fax:(+44-482) 466410

Prof. Willem E. van der Linden
Laboratory for Chemical Analysis
Department of Chemical Technology
Twente University of Technology
P.O. Box 217, 7500 AE Enschede
The Netherlands
Tel:(+31-53) 892629
Fax:(+31-53) 356024

Prof. Paul Worsfold
Dept. of Environmental Sciences
University of Plymouth
Plymouth PL4 8AA
Great Britain

Tel:(+44-752) 233006
Fax:(+44-752) 233009

Submission of an article is understood to imply that the article is original and unpublished and is not being considered for publication elsewhere. *Anal. Chim. Acta* accepts papers in English only. There are no page charges. Manuscripts should conform in layout and style to the papers published in this issue. See inside back cover for "Information for Authors".

Publication. *Analytica Chimica Acta* appears in 16 volumes in 1994 (Vols. 281–296). *Vibrational Spectroscopy* appears in 2 volumes in 1994 (Vols. 6 and 7). Subscriptions are accepted on a prepaid basis only, unless different terms have been previously agreed upon. It is possible to order a combined subscription (*Anal. Chim. Acta* **and** *Vib. Spectrosc.*).
Our p.p.h. (postage, packing and handling) charge includes surface delivery of all issues, except to subscribers in the U.S.A., Canada, Australia, New Zealand, China, India, Israel, South Africa, Malaysia, Thailand, Singapore, South Korea, Taiwan, Pakistan, Hong Kong, Brazil, Argentina and Mexico, who receive all issues by air delivery (S.A.L.–Surface Air Lifted) at no extra cost. For Japan, air delivery requires 25% additional charge of the normal postage and handling charge; for all other countries airmail and S.A.L. charges are available upon request.

Subscription orders. Subscription prices are available upon request from the publisher. Subscription orders can be entered only by calendar year and should be sent to: Elsevier Science B.V., Journals Department, P.O. Box 211, 1000 AE Amsterdam, The Netherlands. Tel: (+31-20) 5803 642, Telex: 18582, Telefax: (+31-20) 5803598, to which requests for sample copies can also be sent. Claims for issues not received should be made within six months of publication of the issues. If not they cannot be honoured free of charge. Readers in the U.S.A. and Canada can contact the following address: Elsevier Science Inc., Journal Information Center, 655 Avenue of the Americas, New York, NY 10010, U.S.A. Tel: (+1-212) 6333750, Telefax: (+1-212) 6333990, for further information, or a free sample copy of this or any other Elsevier Science journal.
Advertisements. Advertisement rates are available from the publisher on request.

US mailing notice – Analytica Chimica Acta (ISSN 0003-2670) is published 3 times a month (total 48 issues) by Elsevier Science B.V. (Molenwerf 1, Postbus 211, 1000 AE Amsterdam). Annual subscription price in the USA US$ 3035.75 (valid in North, Central and South America), including air speed delivery. Second class postage paid at Jamaica, NY 11431. *USA Postmasters*: Send address changes to Anal. Chim. Acta, Publications Expediting, Inc., 200 Meacham Av., Elmont, NY 11003. Airfreight and mailing in the USA by Publication Expediting.

ANALYTICA CHIMICA ACTA

An international journal devoted to all branches of analytical chemistry

(Full texts are incorporated in CJELSEVIER, a file in the Chemical Journals Online database available on STN International; Abstracted, indexed in: Aluminum Abstracts; Anal. Abstr.; Biol. Abstr.; BIOSIS; Chem. Abstr.; Curr. Contents Phys. Chem. Earth Sci.; Engineered Materials Abstracts; Excerpta Medica; Index Med.; Life Sci.; Mass Spectrom. Bull.; Material Business Alerts; Metals Abstracts; Sci. Citation Index)

VOL. 294 NO. 3 CONTENTS AUGUST 30, 1994

ELSEVIER

Analytica Chimica Acta 294 (1994) 227–242

ANALYTICA CHIMICA ACTA

Neural networks for library search of ultraviolet spectra

C.R. Mittermayr *[a], A.C.J.H. Drouen [b], M. Otto [c], M. Grasserbauer [a]

[a] *Institute for Analytical Chemistry, Technical University of Vienna, Getreidemarkt 9-151, A-1060 Vienna, Austria*
[b] *Hewlett Packard GmbH, Hewlett-Packard-Strasse, D-76337 Waldbronn, Germany*
[c] *Department of Chemistry, Institute for Analytical Chemistry, TU Bergakademie Freiberg, Leipziger Strasse 29, D-09559 Freiberg, Germany*

Received 13th October 1993; revised manuscript received 21st March 1994

Abstract

An artificial neural network is used to implement a spectral library search system for UV spectra obtained from a diode-array detector after liquid chromatographic separation. The net is trained by a slightly modified backpropagation algorithm. Several parameters were optimized to ensure convergence and to speed up learning. Sets of up to 200 UV spectra can successfully be learned by a neural network. The neural net is not able to classify unknown spectra as unknown. This is due to the feedforward algorithm used. On the other hand in the case of noisy spectra a well trained net can produce results superior to classical methods of library search like the correlation coefficient. The crucial point is the selection of the appropriate training data set. To facilitate a correct identification the training data have to include the full dynamic range of noise. Extrapolation beyond the training data space is not recommended since the results are not reliable. In the case of impurities the net is better than the correlation coefficient, although the training data consisted only of pure spectra. If one is aware of the limitations neural networks are a powerful tool for a robust identification of UV spectra.

Key words: Chromatography; Artificial neural networks; Library search of UV spectra

1. Introduction

The on-line combination of chromatographic and spectroscopic methods generally produces a huge amount of data. The spectra are used to identify a chromatographic peak and to confirm its purity.

For compound identification a spectrum of the chromatographic peak is compared with a set of spectra of known compounds. A similarity index is calculated to compare spectra. This similarity index is influenced by background absorptions, noise, non-linearity of the detector signal and instrumental differences [1,2].

As these factors are normally not quantitatively known, some experience is needed to evaluate and to interpret the similarity index together with the spectral data. An alternative approach to spectra identification is the use of neural networks.

The number of applications of neural networks in spectroscopy was steadily increasing over the last 5 years. The main subjects are spectra interpretation, especially infrared (IR) [3–7] and mass

* Corresponding author.

0003-2670/94/$07.00 © 1994 Elsevier Science B.V. All rights reserved
SSDI 0003-2670(94)294144-B

spectrometry (MS) [8–10], calibration [2,11–23] and pattern recognition/classification [24–29]. While these applications need a high degree of generalization, the use of neural networks for identification/spectral library search [30–34] rely rather on exact learning.

The present article is the first study on using neural networks for spectral library search applied to UV–visible data, which is more difficult than using IR spectra[30,33], because of the rather "unresolved" shape of the UV–visible spectra.

Since neural networks are robust in respect to small variances in data, such as noise, they may avoid some of the problems encountered with the similarity index. Another disadvantage of the classical sequential comparison of an unknown target spectrum with a set of library spectra is that the search and matching procedure is time consuming for large libraries. A neural network could speed up the process due to its parallel structure.

We used data from the on-line combination of liquid chromatography (LC) with UV–visible detection, to explore these promising properties of neural networks. Since UV spectra are highly dependent on the solvent, the solvent was kept constant. The main issue was to study the robustness of a neural network against noise and small quantities of impurities. The tests were conducted with simulated data.

The results of neural networks are compared with the results of a conventional similarity measure, the correlation coefficient. Since the training of neural networks is very time consuming and a classical library search can be performed in a straightforward manner, this comparison can help to choose the appropriate method for a problem.

2. Theory

2.1. Neural networks

There are already a lot of different types of neural networks and the choice of the type of the neural network is one of the most critical problems which has to be solved.

Hopfield neural networks are often suggested as autoassociative memories, but it is known that there is no guarantee for reaching a stable equilibrium if nonorthogonal input vectors are applied.

Kohonen and counterpropagation neural networks are certainly a good choice for data clustering, classification or compression, but since the activation of a neuron is based on the smallest distance between the neuron's weight vector and the input pattern, there is no advantage in comparison to classical distance based methods. Another unfavourable feature of the Kohonen net is that due to the competitive learning, no matter which pattern is presented, always one neuron is activated, so the performance can be even worse than achieved be a classical distance based method.

Multilayer, feedforward neural networks using the backpropagation algorithm seem to be a good choice due to their ability to produce "hidden features" in a nonlinear fashion which might make it easier to distinguish between very similar spectra. The enhancement of small differences is necessary, because some of the spectra seem even visually to be nearly identical. Multilayer, feedforward neural networks consist of a large number of simple processing units (also called neurons), which are highly interconnected. The neurons are arranged in layers. The first layer is called input layer, because the input vector is presented to it. It can be considered as an interface between the external world and the neural net. The last layer produces the output of the neural network and is therefore called the output layer. Layers between the input and the output layer are called hidden layers and have no connections to the external world. Most problems can be solved using only one hidden layer.

First a neuron i calculates the weighted sum net_i of the inputs inp_j.

$$net_i = \sum_j W_{ij} \cdot inp_j \qquad (1)$$

whereby W_{ij} is the weight, which connects the neuron i with neuron j.

The weighted sum of the input is passed through a transfer function which may be a lin-

ear, a threshold or a sigmoid function. The output o_i of the transfer function is also the output of the neuron. The mathematical description is:

$$o_i = \mathrm{f}(net_i) \tag{2}$$

The backpropagation algorithm is used to train these multilayer, feedforward neural networks. This algorithm requires a monotonically increasing transfer function [35], whose values must be confined to the interval [0,1]. These requirements are fulfilled by the sigmoid function:

$$\mathrm{f}(\mathrm{net_i}) = \frac{1}{1 + \mathrm{e}^{-(\alpha \cdot \mathrm{net_i} + \vartheta)}} \tag{3}$$

It was shown that the parameter α can be removed without loss of generality. The parameter θ can be treated as another weight, if each input vector is augmented by one component which has a permanent value of 1. This additional weight is called bias [35].

The backpropagation algorithm represents one kind of supervised learning. Learning is performed by presenting a number of input pattern to the network several times. The training patterns are presented randomly and this is repeated every epoch. The output o_i of the neural network is compared with the desired output t_i. The error is used to adjust the weights according to the generalized delta rule:

$$\Delta W_{ij} = k \cdot \delta_i \cdot \mathrm{inp_j} \tag{4}$$

k is a constant called learning rate, δ_i the correction term and inp_j the input of neuron j to neuron i. There are different correction terms for the output layer:

$$\delta_i = \mathrm{f}'(\mathrm{net_i}) \cdot (t_i - o_i) \tag{5}$$

and for the hidden layer:

$$\delta_i = \mathrm{f}'(\mathrm{net_i}) \cdot \sum_k (\delta_k \cdot w_{ki}) \tag{6}$$

whereby δ_k is the correction term of the output neuron k.

The total error of the network is described by the root mean square error (RMS) of all patterns in the data set.

$$RMS = \sqrt{\frac{\Sigma(t_i - o_i)^2}{n}} \tag{7}$$

It is monitored during the iterative learning procedure. If it becomes smaller than a predefined threshold (the convergence criterium), learning is stopped.

The original backpropagation algorithm [36],described above, was modified to some extent, to speed up the convergence of the network. Eq. 4 can be augmented with the scaled change of the weights of the previous iteration, the momentum (μ is the momentum factor).

$$\Delta W_{ij}(t) = k \cdot \delta_i \cdot inp_j + \mu \cdot \Delta W_{ij}(t-1) \tag{8}$$

If the scaled correction term of the previous layer is added to the input of the neuron, the algorithm is called "fast backpropagation" algorithm [37].

$$\Delta W_{ij}^L = k \cdot \delta_i^L \cdot \left[\mathrm{inp_j} + k_M \cdot \delta_i^{L-1}\right] \tag{9}$$

Another possibility to speed up the convergence is to add a small constant value F' to the derivative of the sigmoid function [37].

$$\delta_i = \left[f'(\mathrm{net_i}) + F'\right] \cdot (t_i - o_i) \tag{10}$$

The addition of uniform noise to the net_i can also speed up the training [2].

2.2. Library search and correlation coefficient

Library search systems [38] compare unknown spectra with known spectra in the spectral library. Generally they are based on the hypothesis that compounds exhibiting similar spectra have similar chemical structures. A spectrum can be considered as an n-dimensional vector. The determination of the similarity between two vectors can be based on either the angle between the vectors or the distance of their tips. Both measures need some kind of normalization.

The measure of the angle is the cosine, the distance can be determined with the Euclidian distance. Since the correlation coefficient for two spectra is identical with the cosine for the vector-normalized mean centered spectra [1], it involves what statisticians call the z-transform of the spectra which, in chemometrics terminology, is also referred to as autoscaling. Mean-centering eliminates all spectral differences due to a fixed baseline offset that might be present in an individual spectrum. Since similar spectra show only

slightly different cosine values and consequently correlation coefficients, the ability to discriminate these spectra is enhanced by squaring these values.

3. Experimental

3.1. Software and hardware

The calculations presented in this paper were done using two software packages. The simulation of the neural networks was performed by the NeuralWorks II Plus software package of NeuralWare. The library search was conducted by the HPLC^{3D} Chemstation from Hewlett-Packard. All calculations were performed on a personal computer with an Intel 486 processor and 14 MByte RAM.

3.2. Data

A number of small spectral libraries containing various UV spectra gathered for different purposes has been combined to a large spectral library, regardless of the solvent used.

All spectra were recorded in 2 nm steps, but they had to be shifted in the wavelength domain to the next even integer wavelength, since the spectra were not measured at the same wavelengths. Then all spectra were truncated to the same wavelength range of 212–400 nm resulting in 95 data points. Spectra with a squared correlation coefficient above 0.995 were eliminated leaving 256 spectra for the data set.

In a preliminary study we used 30 spectra of polyaromatic hydrocarbons in order to optimize several parameters. These spectra show substantial differences and identification is consequently straightforward.

In order to simulate noise, 232 spectra of a pure solvent (methanol) were recorded and their background interferences were eliminated. The identity of the spectra was represented by a unique integer starting at 1 up to n, the number of spectra in the training set. This identification number (ID) was coded either as a binary digit or as a n-dimensional vector. The vector consisted of $(n-1)$ zeroes and a single "one" at the ith element (for i = ID). This kind of coding is called "1-out-of-n" by the authors. These vectors are all orthonormal to each other.

3.3. Preprocessing

All spectra have been normalized before presenting them to the network. The spectra were either normalized to a maximum value of 1 or to a area of 100.

Input and target output data were linearly transformed before presenting them to the net. For this purpose a table was generated which contained the minimum and the maximum of all values presented to a specific neuron. While all inputs to a specific input neuron i were mapped from the interval $[\min_i, \max_i]$ to the interval [0,1], the output values were mapped to two different intervals [0,1] and [0.2,0.8], respectively.

3.4. Network topology

There were 95 neurons in the input layer according to the number of data points. The number of neurons in the output layer depended on the coding of the identity of the spectra. The output layer consisted of 8 neurons if coding binary (allowing 255 different spectra) and of n spectra in the case of "1-out-of-n".

During the optimization of parameters the number of hidden neurons was 30. When the capabilities of the neural networks were evaluated afterwards, the number of neurons in the hidden layer was 1.4 times the number of spectra being learned, due to the results of the optimization.

The transfer function of the hidden and the output layer was the sigmoid function. The weights were randomly initialized in the interval $[-0.1,0.1]$.

3.5. Classification

In order to classify the results of the network two thresholds were used. If none of the outputs was above the lower threshold (0.2) the answer was negative, i.e., the network considered the

spectrum as unknown. If only the ith output is larger than the higher threshold (0.8) (and all other outputs are below), this spectrum was positively identified as spectrum ID = i. In all other cases the result was uncertain.

4. Optimization of parameters

Because training a neural network is a rather time consuming task, it is necessary to ensure convergence within a reasonable time. Furthermore some combinations of parameters do not allow convergence at all. Although such parameter values are sometimes obvious or at least easy to detect some efforts have to be made in this direction.

4.1. Noise / F' Offset

According to the literature the addition of noise to the input data can speed up convergence [2]. Besides that it is possible to add noise to the summation values of each neuron. This kind of noise is analog to the temperature in the simulated annealing method. Adding a small constant to the derivative of the sigmoid function in the correction term is also mentioned to achieve faster convergence [37].

Results show clearly that adding a small constant F' (in the range [0.0,0.2]) in Eq. 10 can reduce the necessary iterations till convergence to half, while the addition of noise slows down learning. Increasing values of the constant F' make the training faster up to a point were suddenly divergence occurs. The learning rate and the momentum were 1.0 and 0.0, respectively.

4.2. Learning rate / momentum

During the optimization of the learning rate and the momentum (Fig. 1), no noise was added and the F'Offset was kept at 0.2. While a two factorial ANOVA showed that the influence of the momentum was of no significance ($\alpha = 5\%$), the learning rate showed a similar behaviour as the F'Offset. Increasing learning rates provided faster convergence until suddenly divergence occurred. Yet the change in behaviour was less sharp than with the F'Offset, because there was a small range of instability between the optimum and the point when the learning rate caused always divergence. The optimum found for the learning rate was 1.5 (Fig. 1).

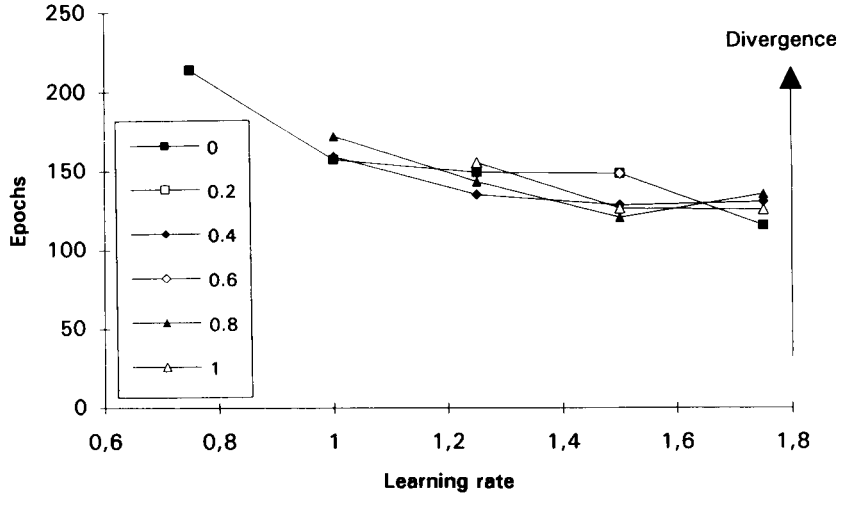

Fig. 1. Dependence of the number of epochs to converge on the learning rate and the momentum. At a learning rate of 1.75 about half of the experiments diverged, so the stable optimum was at a learning rate of 1.5.

4.3. Hidden units

The implementation of a library search system stipulates two contradicting conditions. On the one hand the spectra must be learned very *exactly* to identify very similar spectra and on the other hand the neural network has to be robust enough to identify also noisy data or data with other deviations like an offset or small impurities. In terms of classification exact learning (identification) can be considered as *desired overfitting*, since an own class is assigned to each compound.

From theory [39], for exact learning of n arbitrary input patterns $(n - 1)$ hidden units are sufficient. This can be interpreted such that each unit in the hidden layer represents a hyperplane separating the input space in such a way that in each hyper "polyeder" (one and) only one input pattern is contained [40]. If the input patterns are rather similar, it seems to be obvious that it is more difficult to obtain a good separation. The optimization of the number of hidden units shows in our case that $(n - 1)$ hidden units are not only sufficient but necessary. We used more than the sufficient number of hidden units, since the more such hyperplanes are available for the separation, the faster and the easier the separation is obtained.

If too many hidden units are used, the hyperpolyeder dedicated to a certain compound might be too small to account for the deviations from noise or impurities. This would be a case of overfitting and loss of (our limitedly required) generalization. To compensate for this one has to choose the training set appropriately.

In order to ensure convergence at RMS = 0.025 with a number of hidden units smaller than 30 it was necessary to use a smaller F'Offset than the optimum found for 30 hidden units. The F'Offset of 0.15 was then kept constant for the optimization of the number of hidden units. The learning rate was 1.5 and the momentum 0.7 to suppress eventually occurring oscillations.

35 units in the hidden layer were found to be optimal in respect to the speed of convergence (Fig. 2). The ratio of 35 units in the hidden layer to 30 units in the output layer, which equalled to the number of spectra, was 7:6. In the following experiments with larger networks the ratio of 7:5 was used for practical reasons.

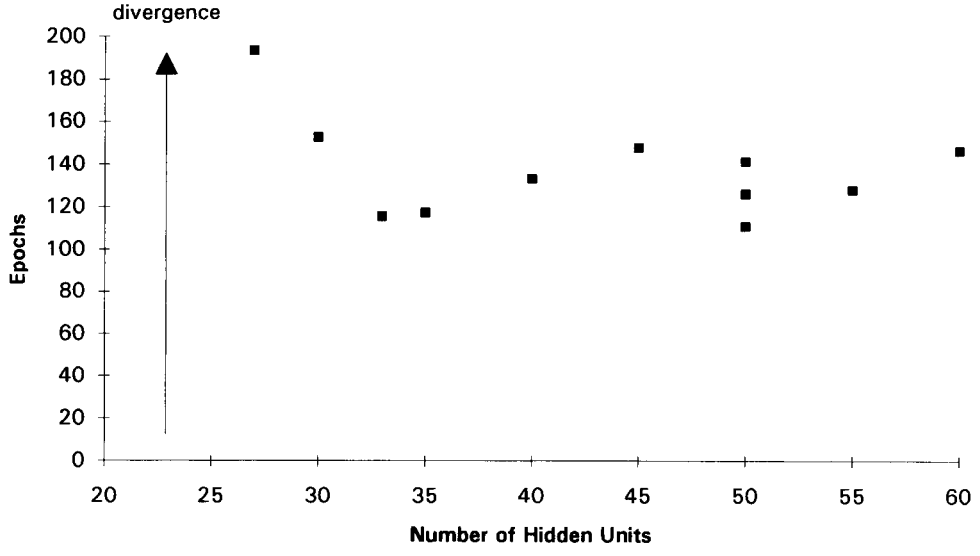

Fig. 2. Dependence of the number of epochs to converge on the number of units in the hidden layer. The network architecture was 95 input, n hidden, 30 output units. Below 27 hidden units no convergence was obtained at all.

4.4. Internal scaling of the output data

As mentioned above the choice of the interval to which the output data were scaled influences the speed and the way the net converges. Two different intervals were compared: [0.2,0.8] and [0.0,1.0]. In Fig. 3, which shows two typical graphs for the two different intervals, one can see different trends. Although the network trained with the larger interval for the scaling of the output starts with a higher RMS error it converges much faster. Especially with larger networks we obtained complete learning only with the interval [0.0,1.0].

4.5. Influence of the coding of the output data

The advantage of the binary coding (see data section) of the output would be a smaller number of weights for the same number of spectra and therefore a smaller number of calculations per iteration.

It was found, however, that this reduction in the number of calculations per iteration is weighted out by a larger number of iterations necessary to reach convergence. And furthermore the parameters (learning rate, momentum, F') have to be optimized again. (It was found that only with a $F'\text{Offset} = 0$ convergence could be obtained.) Another drawback is that the interpretation of the results is more difficult, since it might be necessary to use different decision criteria for each bit and if one bit is set false the output pattern shows no similarity at all, 1-out-of-n coding provides that even spectra having been classified as uncertain can reflect to some degree similarity with a stored spectrum. Because of these problems binary coding was not studied more intensively.

4.6. Net capacity

Up to 200 spectra could be learned correctly. Using the available hardware this took 28 h for neural networks whose output were coded 1-out-of-n. Therefore larger networks were not further investigated due to time limits. Remarkably no changes in the optimized parameters were necessary compared with former smaller nets (for less spectra).

5. Selection of training data set

Since the influence of the data set composition on the performance of the net was emphasized in

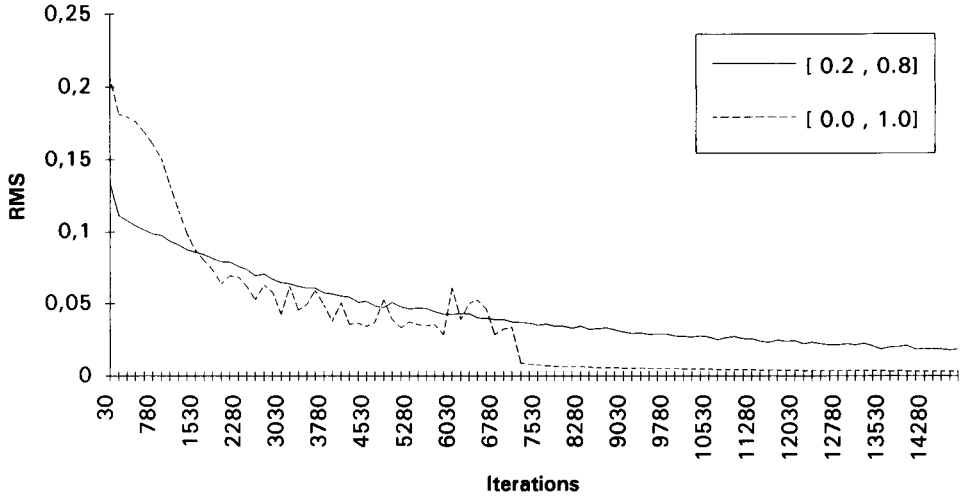

Fig. 3. RMS error monitored during the training for different internal scaling of the target outputs. scaling interval [0.2,0.8] and scaling interval [0.0,1.0].

literature [27,35,41,42], it was a major goal of this work to find an appropriate training data set. This was explored for the case of noisy data.

5.1. Generation of noisy data

To explore the influence of noise (which should not be mixed up with the noise in the optimization section), data which contains a certain degree of noise were generated. The mean value of the noise was not zero, but had an offset. Therefore it was necessary to center the "pure" noisy spectra to a mean value of zero. The addition of noise to the spectra was performed by the following procedure:

First the maximum of the input spectrum was scaled to a certain absorbance value (5 or 2), then the original or mean centered noise spectra were added to the scaled spectra, resulting in a lower and higher noise level (noise level I and II), respectively. From a random selected starting point n subsequent noise spectra were added to the n library spectra. This procedure was repeated 3 or 5 times, resulting in 3 or 5 noisy spectra per compound. Afterwards the spectra were normalized as described in the data preprocessing section. The maximum absorbance to which the spectra were scaled is a measure proportional to the signal-to-noise (S/N) ratio [1]. All experiments were conducted with a different number of spectra: 30, 50 and 75.

5.2. Training neural networks for spectra with noise

Training with pure spectra

At first exclusively noiseless data from the spectral library were used as training data set. The robustness against noise was tested by means

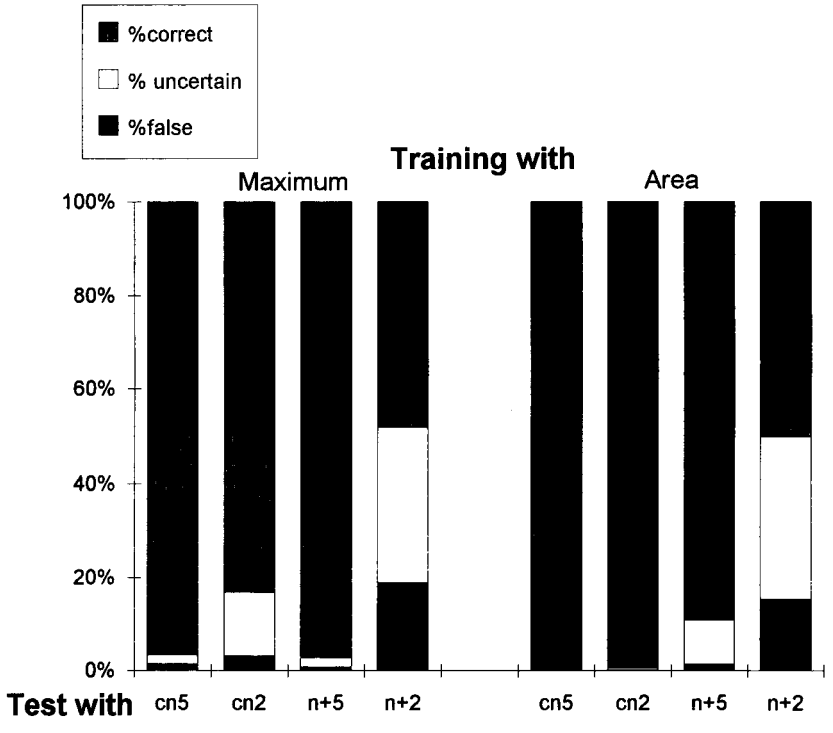

Fig. 4. The neural networks were trained with noisefree spectra from the library either maximum (left bars) or area (right bars) normalized. The performance of the networks is tested with 4 different test sets. The abbreviations for the test sets are: cnI and cnII stand for spectra with mean centered noise at a noise level I and II, respectively; n + I and n + II stands for spectra with noise with offset at a noise level I and II, respectively. Each test set contained 3 noisy spectra of each compound. The results are classified into three categories: correct, uncertain and false, as described in the text.

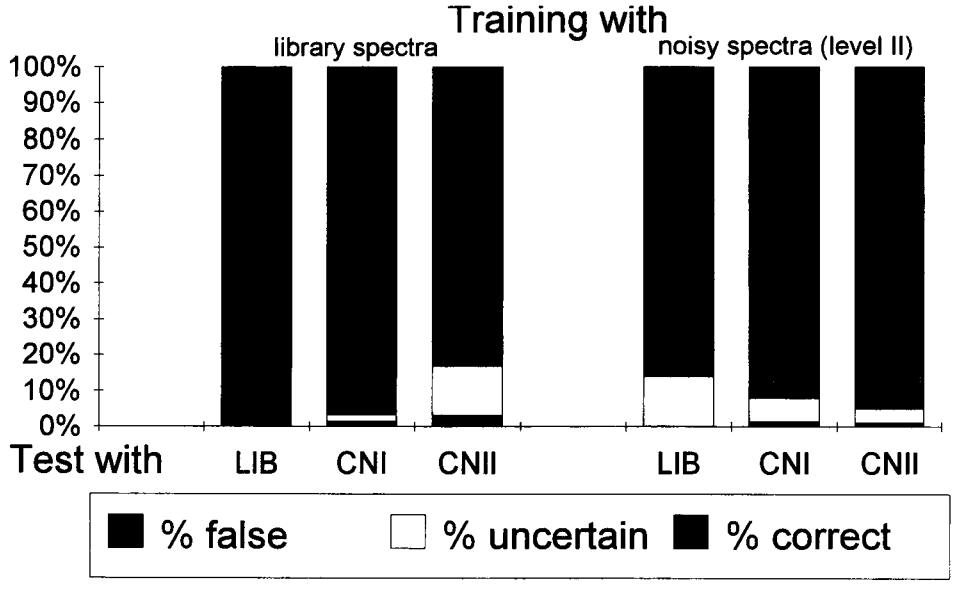

Fig. 5. Comparison of the results of the training with noisefree spectra (see Fig. 6) and a training set with 3 spectra of each compound with mean centered noise at a noise level II. The spectra were maximum normalized. Three different test sets were used: cnI, cnII (as defined above) and pure spectra abbreviated with "lib".

of spectra containing mean centered noise and noise with offset, respectively. Both types of test data were used at different noise levels. Both tests show the same trend (Fig. 4): the higher the noise level the higher the amount of false and uncertain identifications. If the test spectra have mean centered noise, the percentage of correct identifications is higher than for noise with an offset. In the case of mean centered noise area normalization is better than maximum normalization.

It can be concluded from these results that a training data set containing noisefree spectra is only able to identify spectra with a small amount of mean centered noise. Therefore noisy spectra were used as training data set in the next step.

Training with mean centered noisy spectra

The training data set consisted of three noisy spectra per substance at noise level II.

Results of tests with pure spectra from the library were not as satisfying as desired because there appeared a large number of spectra classified as uncertain. Yet it is remarkable that no false identification was made among them. This might be a consequence of the "average" character of the pure spectra in respect to the noisy spectra.

Tests with mean centered noisy data at different noise levels (I and II) revealed that the more similar (with respect to the noise level) the test data are to the training data, the higher is the number of correct identifications.This trend is more pronounced in the data which are maximum normalized. (Fig. 5).

Training with noisy spectra with offset

Three different data sets were used. The first data set contained 3 noisy spectra per substance, the second 5 and the third 3 noisy spectra and the noisefree spectrum itself. All noisy data had a noise level II.

The same trend as described above for mean centered noise spectra can be seen here too. The more similar test and training data, the better the results (Fig. 6). The number of noisy spectra per substance biases the results. The more spectra of noise level II are in the training data set, the less correct are the results of test with data containing a smaller level or no noise at all.

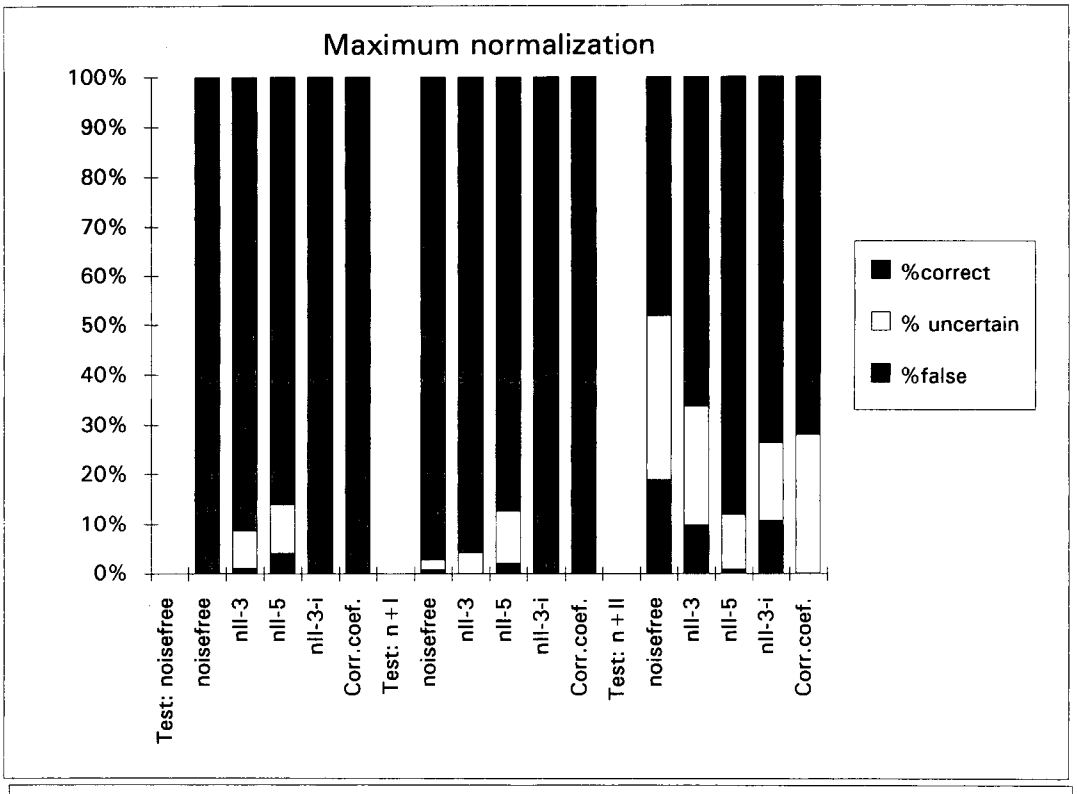
Maximum normalization
100%
90%
80%
70%
60%
50%
40%
30%
20%
10%
0%
%correct
% uncertain
%false
Test: noisefree
noisefree
nll-3
nll-5
nll-3-i
Corr.coef.
Test: n+l
noisefree
nll-3
nll-5
nll-3-i
Corr.coef.
Test: n+ll
noisefree
nll-3
nll-5
nll-3-i
Corr.coef.

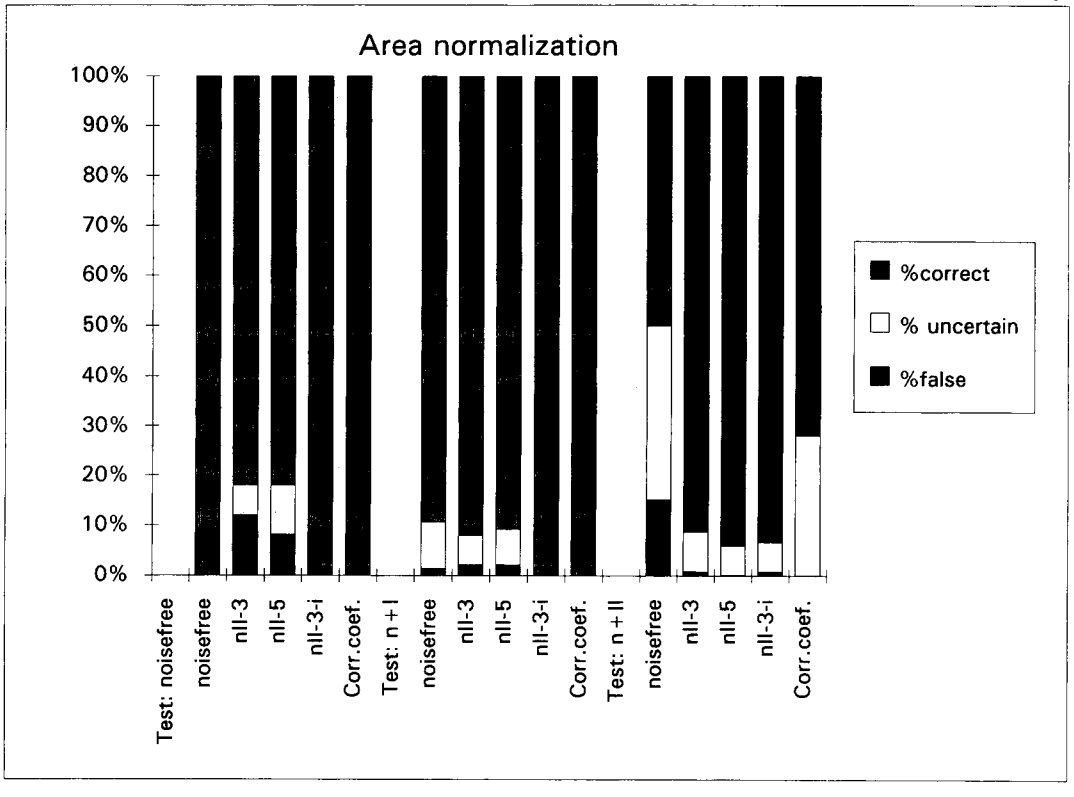
Area normalization
100%
90%
80%
70%
60%
50%
40%
30%
20%
10%
0%
%correct
% uncertain
%false
Test: noisefree
noisefree
nll-3
nll-5
nll-3-i
Corr.coef.
Test: n+l
noisefree
nll-3
nll-5
nll-3-i
Corr.coef.
Test: n+ll
noisefree
nll-3
nll-5
nll-3-i
Corr.coef.

The data set consisting of noisefree spectra as well as noisy spectra of noise level II produced the best results at all. This might be on the one hand due to the fact, that the presence of noisy and noisefree spectra increased the potential of the network to discriminate noise more exactly and on the other hand, because the data span the range from no noise to noise level II. We conclude that the noisy training pattern of one compound span the hyperpolyeder which is centered around the noisefree library spectrum.

The fact that test spectra containing a noise level I, which lie in the spanned range, are identified correctly to 100%, implies the interpolation capabilities of the network and stresses the importance of the right choice of the training data set.

5.3. *"unknown" spectra*

Unknown spectra (spectra which have not been trained) were presented to neural networks trained either only with library spectra or with 3 noisy spectra and library spectra. In both cases the neural network produced about 40% false positive and 50% indifferent identifications. A desired output for "unknown" spectra would have been zero for all output units or in less favourable cases only indifferent, but the network produced sometimes even higher scores for the false positive results than for correct ones. This emphasizes the fact that unknown spectra cannot readily detected by feedforward neural network.

5.4. *Impurities*

Data were generated by adding appropriately scaled spectra so that the desired impurity content (1, 5 or 20%) was obtained. The ratio of the maximum absorbance of two spectra added corresponded to the percentage given. Three spectra each scaled to the 3 different levels of impurity were added to 10 other spectra, resulting in 90 test spectra. Afterwards the spectra were maximum normalized again.

The networks tested were trained only with pure spectra. The answer of the net was considered as correct when the "main" compound was recognized correctly. As expected: the higher the level of impurity, the poorer the results of the test (Fig. 7).

In order to be able to compare the results with those obtained by a classical library search, a different method of classification was performed. If similarity measures are used, hit lists are produced normally as a result, whereby the correct spectrum should be in the first place. A possible additional condition for the identification is that the similarity measure has to exceed a predefined threshold.

The comparison of the results obtained with the original method using an upper and a lower threshold and the method using the maximum output and only a lower threshold (0.25) shows that in some cases the spectrum is recognized correctly but the output value is not large enough to result in a positive identification for the former method. A further raising of the lower threshold in the latter method reduces the number of false positive identifications but the number of correct positive identifications does not improve because the output values are already very high. The number of spectra classified as uncertain increases due to the stricter classification criteria (Fig. 8).

6. Comparison between correlation coefficient and neural networks

To get an equivalent representation of the results each test spectrum was compared with all

Fig. 6. Comparison of results of different training sets and the result of the correlation coefficient. The spectra are either (a) maximum normalized or (b) area normalized. The training sets were noisefree spectra (lib), noisy spectra with offset at a noise level II with either 3 or 5 spectra per compound ("nII − 3", respectively, "nII − 5"). The training set "nII − 3 − i" contained additionally to the training set "nII − 3" the noisefree library spectra. The test sets were noisefree spectra (lib), and noisy spectra with offset at a noise level I and II (n + I, n + II). (see Fig 5.)

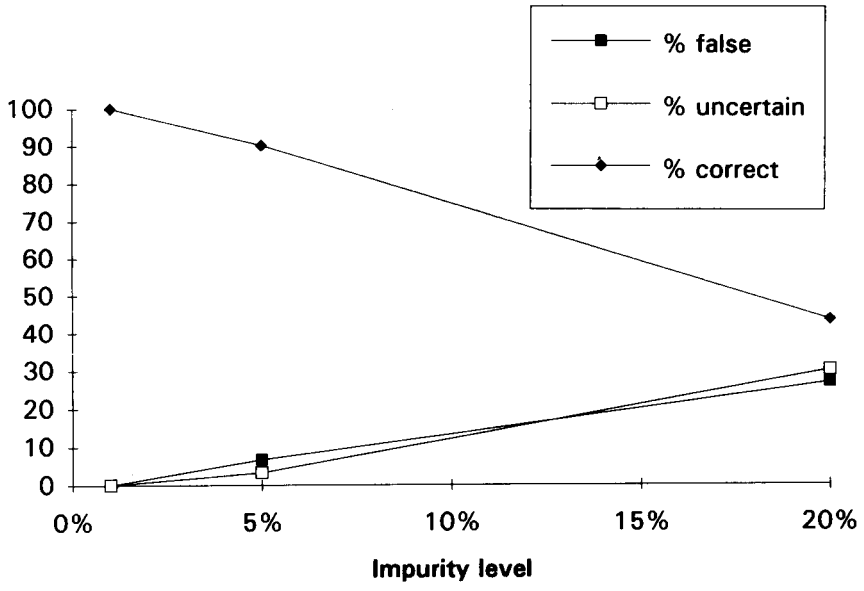

The percentage of correctly, uncertainly and falsely identified spectra depending on the percentage of impurity.

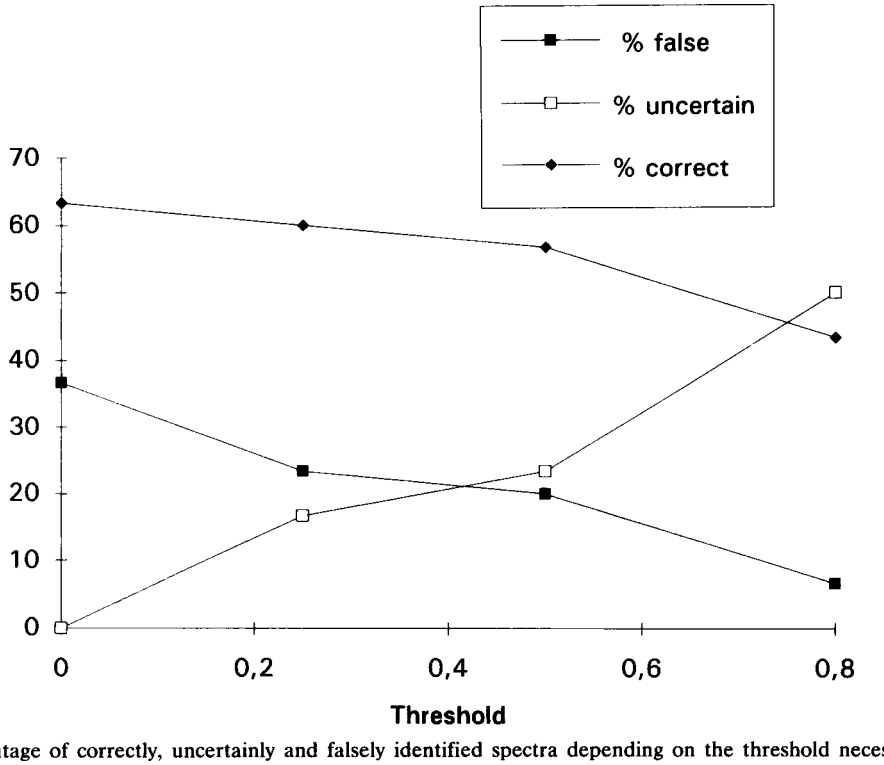

Fig. 8. The percentage of correctly, uncertainly and falsely identified spectra depending on the threshold necessary for positive identification.

library spectra. All correlation coefficients of a test spectrum were arranged as n-dimensional vectors. This vector corresponds to the output vector of a network. The classification of the result was performed the same way as this was done with the output vector of the networks. The main difference was that the thresholds for the classification scheme had to be different, instead of 0.2 and 0.8, 0.95 and 0.995 were used.

The test with *unknown spectra* shows the crucial problem with feedforward neural networks. If unknown spectra are presented to the network, the network produces a high percentage of false positive (40%) and uncertain (50%) identifications. The network has apparently learned to tolerate slight deviations and to produce positive identifications.

On the other hand it is principally impossible to train a network to classify unknown spectra as unknown, since the spectra cannot be determined in advance and therefore they cannot be given to the training data set.

If the test data consisted of *mean centered noisy spectra*, a neural network trained with area normalized noise free spectra yielded superior results. At a low noise level the results were comparable. At a higher noise level the portion of correctly identified spectra by using the correlation coefficient fell drastically (Fig. 9).

The performance of the correlation coefficient in respect to test data containing *noise with offset* is nearly the same, since the correlation coefficient is not influenced by an offset according to the theory. The best network results were obtained by a network trained with a data set containing a noisefree and three noisy (with offset with a noise level II) spectra, which were area normalized. Although the network identified

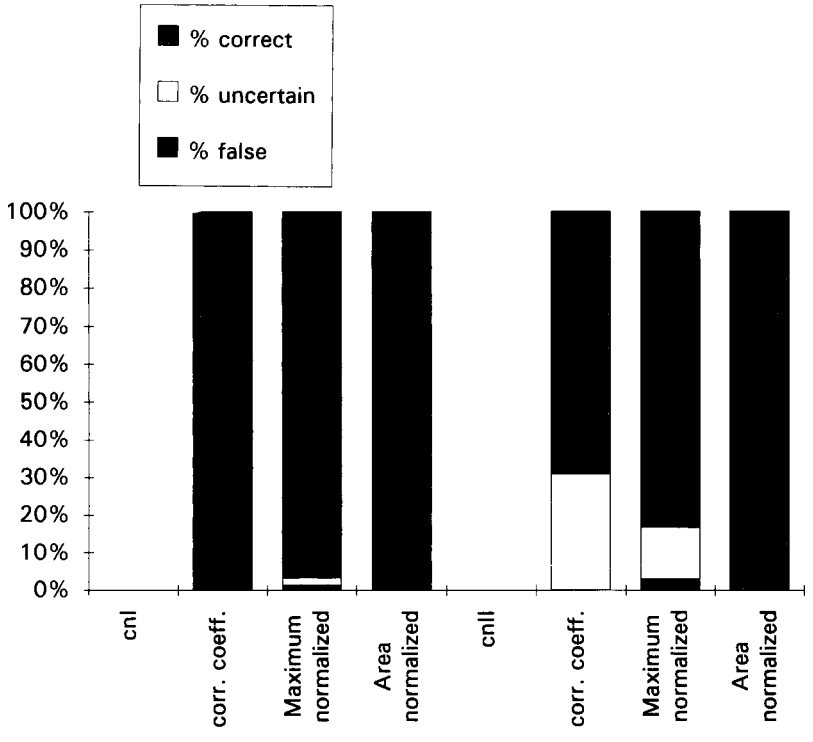

Fig. 9. Comparison of results obtained by a neural network and the correlation coefficient. Test data were mean centered noisy spectra at different noise levels (cnI, cnII, see Fig. 5). Results for the neural network are shown for different normalizations (maximum and area, respectively).

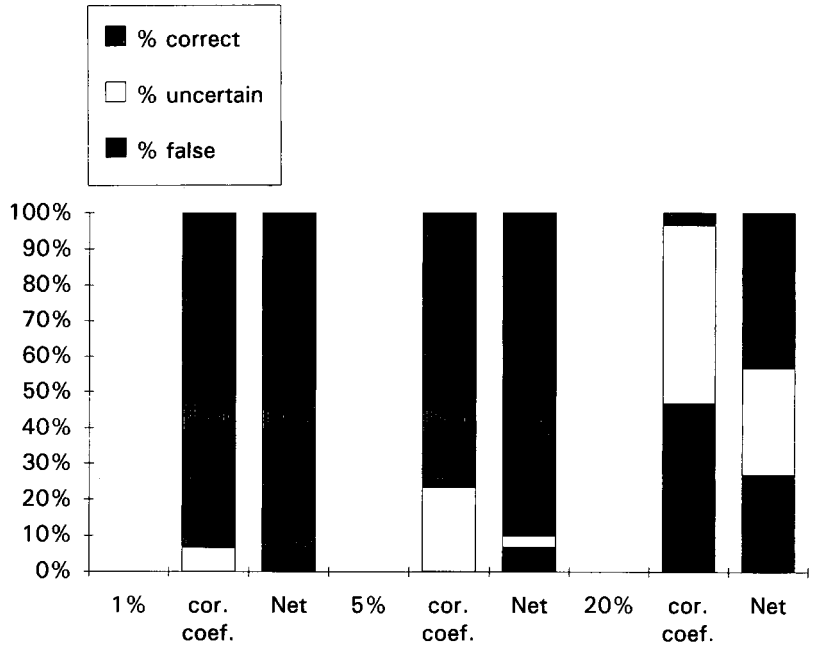

Fig. 10. Comparison of the results obtained by a neural network and the correlation coefficient. Test data were impure data with an impurity content of 1, 5 or 20%. <

93.3% of the spectra correctly, 0.67% were identified false positively, while the correlation coefficient never yielded false identifications (Fig. 6).

6.1. *Impurities at a 1, 5 or 20% level*

If the same scheme of classification was applied as described above (using an upper and a lower threshold) to classify the results, the neural network was always better than the correlation coefficient (Fig. 10). While the correlation coefficient produces only false negative failures the neural network yields also false positive results at the 20% level of impurities.

For mixtures the correlation coefficient degrades rapidly, which is a desired behaviour for a similarity measure. Nevertheless the "main" compound has often the highest similarity score.

Consequently using only the highest score for the identification would improve the performance of the correlation coefficient. But it is also reasonable to demand that the highest similarity score exceeds a certain threshold, since a correlation coefficient smaller than 0.8 is not very meaningful for identifying spectra. That is why the highest similarity score is used for identification only if it exceeds a certain threshold. By varying the threshold a different number of correct, uncertain or false identifications are obtained. The same method was used for the neural network. To be able to compare the results of both methods regardless the different absolute values of the thresholds a Recall-Reliability-Plot was used (Fig. 11) [9].

$$\text{Recall} = I_c/N_c \tag{11}$$

$$\text{Reliability} = I_c/(I_c + I_f) \tag{12}$$

Where N_c is the total number of spectra, and I_c and I_f represent the number of correct and false positive classified spectra, respectively.

If the threshold, which must be exceeded for a positive identification is raised, the result moves from high recall and low reliability to high reliability and low recall. If the value to be exceeded is minimal, the recall is maximal. The graphs (Fig.

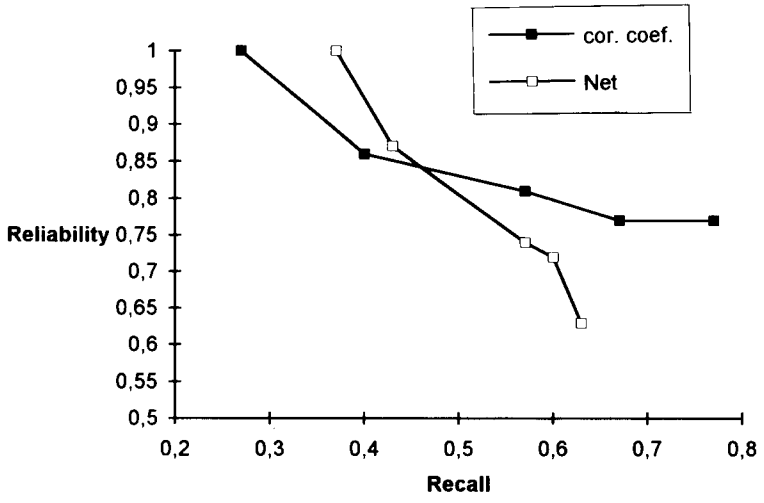

Fig. 11. The reliability (Eq. 12) is plotted against the recall (Eq. 11). The values are calculated from a test with impure data at 20% impurity level by changing the threshold for positive identification. <

11) obtained leave a possibility to optimize to individual problems.

7. Conclusions

All spectra from the training data set can be learned correctly if the appropriate parameter set is chosen. Tanabe et. al. [30] found similar parameter values for the storage of IR spectra, especially the learning rate and the number of hidden units. Although Tanabe et al. do not state that they also had a rather abrupt divergence, after a region of instability, we conclude this from the fact that they did not use the values of the learning rate or momentum, which seems optimal from that table.

The capacity of the neural network depends mainly on the number of hidden units (if the number of output units is changed according to the number of the spectra and the coding scheme used), since it has been proven that a backpropagation neural network with sigmoid transfer function and at least 2 hidden layers (in practice one hidden layer is often sufficient) can accomplish every arbitrary mapping.

The goal of this work was to achieve a compromise between two contradicting requirements. On the one hand the spectra should be learned exactly, and on the other hand the neural network should also be robust enough in respect to noise and impurities. The crucial point to fulfil these requirements is the selection of the training data set. The data set has to represent the whole data space, which could be presented to the neural network in the recall phase. Due to the interpolation capabilities the amount of necessary data is reduced, since not all different levels have to be present in the data set. Extrapolations beyond the training data set are limited, because the performances decreases drastically.

Comparing the neural network approach with a well-established method of distance measures, like the correlation coefficient, the neural network can show its benefits in being more robust against noise and impurities. The higher the amount of noise the greater the advantage of the net. The strongest limitation of feedforward neural networks for spectral identification are unknown spectra, since there seems to be no reasonable method how to train such a network to classify a spectrum as unknown. Unless this problem is solved applications of feedforward neural networks to spectral identification are limited to problems where all spectra to be analyzed come from a known set of possible spectra. Possible

solutions to this problems might be obtained by an ART-2 or RBF neural network, which have some kind of vigilance parameter which accounts for extrapolative situations [43].

Acknowledgments

This work was financially supported by the European Communities as part of the COMETT – Eurochemometrics Project.

References

[1] H.-J. P. Sievert and A. C. J. H. Drouen, in L. Huber and S. A. George (Eds.), Diode Array Detection In HPLC, Marcel Dekker, New York, 1993, pp. 51–126.
[2] P.J. Gemperline, J.R. Long and V.G. Gregoriou, Anal. Chem., 63 (1991) 2313.
[3] M. Meyer and T. Weigelt, Anal. Chim. Acta, 265 (1992) 183.
[4] R.J. Fessender and L. Györgyi, J. Chem. Soc., Perkin. Trans. II, (1991) 1755.
[5] J.R.M. Smits, P. Schoemakers, A. Stehmann, F. Sijstermans and G. Kateman, Chemom. Intell. Lab. Syst., 18 (1993) 27.
[6] E.W. Robb and M.E. Munk, Mikrochim. Acta (Wien), (1990) 131.
[7] E.W. Robb, M.S. Madison and M.E. Munk, Mikrochim. Acta (Wien), (1991) 505.
[8] H. Lohninger and F. Stancl, Fresenius' J. Anal. Chem., 344 (1992) 186.
[9] B. Curry and D.E. Rumelhart, Tetrahedron Comp. Methodol., 3 (1990) 213.
[10] H. Lohninger, in J. Gmehling (Ed.), Software Development in Chemistry 5, Springer, Berlin, 1991.
[11] C.Borggaard and H.H. Thodberg, Anal. Chem., 64 (1992) 545.
[12] A. Bos, M. Bos and W.E. van der Linden, Anal. Chim. Acta, 256 (1992) 133.
[13] C. Schierle and M. Otto, Fresenius' J. Anal. Chem., 344 (1992) 190.
[14] P.J. Gemperline, Chemom. Intell. Lab. Syst., 15 (1992) 115.
[15] C. Schierle, M. Otto and W. Wegscheider, Fresenius' J. Anal. Chem., 343 (1992) 561.
[16] T.J. McAvoy, et al., Biotechnol. Bioeng., 40 (1992) 53.
[17] P.Olmos et al., IEEE Trans. Nucl. Sci., 38 (1991) 971.
[18] M. Bos, A. Bos and W.E. van der Linden, Analyst, 118 (1993) 323.
[19] T.B. Blank and S.D. Brown, Anal. Chim. Acta, 277 (1993) 273.
[20] A. Bos, M. Bos and W.E. van der Linden, Anal. Chim. Acta, 277 (1993) 289.
[21] J.R. Long, V.G. Gregoriou and P.J. Gemperline, Anal. Chem., 62 (1990) 1791.
[22] M.Bos, A. Bos and W.E. van der Linden, Anal. Chim. Acta, 233 (1990) 31.
[23] M. Bos and H.T. Weber, Anal. Chim. Acta, 247 (1991) 97.
[24] M. Glick and G.M. Hieftje, Appl. Spectrosc., 45 (1991) 1706.
[25] J.R.M Smits, L.W. Breedveld, M.W.J. Derksen, G. Kateman, H.W. Balfoort, J. Snoek and J.W. Hofstraat, Anal. Chim. Acta, 258 (1992) 11.
[26] J.W. Ball and P.C. Jurs, Anal. Chem., 65 (1993) 505.
[27] M. Hartnett, D. Diamond and P.G. Barker, Analyst, 118 (1993) 347.
[28] B.J. Withoff, S.P. Levine and S.A. Sterling, Anal. Chem., 62 (1990) 2709.
[29] E. Yee and J. Ho, Appl. Optic., 29 (1990) 2929.
[30] K. Tanabe, T. Tamura and H. Uesaka, Appl. Spectrosc., 46 (1992) 807.
[31] A.L. Allanic, J.Y. Jezequel and J.C. Andre, Anal. Chem., 64 (1992) 2618.
[32] B. Meyer et al., Science, 38 (1991) 542.
[33] A. Bruchmann, H.J. Götze and P. Zinn, Chemom. Intell. Lab. Syst., 18 (1993) 59.
[34] M. Otto and U. Hörchner, in J. Gasteiger (Ed.), Software Development in Chemistry 4, Springer, Berlin, 1990, pp. 377–384.
[35] J. Zupan and J. Gasteiger, Anal. Chim. Acta, 248 (1991) 1.
[36] D. E. Rumelhart, J. L. McClelland and the PDP Research Group, Parallel Distributed Processing, MIT Press, Cambridge, MA, 1986.
[37] Neural Computing, Manual of NeuralWork II Plus, Pittsburgh, PA, 1991.
[38] A. Drouen and L. Huber, HP Technical Note, 12-5954-6268 (1986)
[39] M.A. Sartori and P.J. Antsaklis, IEEE Trans. Neural Networks, 2 (1991) 467.
[40] S.-C.Huang and Y.-F. Huang, IEEE Trans. Neural Networks, 2 (1991) 47
[41] G. Kateman and J.R.M. Smits, Anal. Chim. Acta, 277 (1993) 179.
[42] J. Zupan and J. Gasteiger, Neural Networks for Chemists, VCH, Weinheim, 1993.
[43] H. Lohninger, J. Chem. Inf. Comput. Sci., 33 (1993) 736.

ELSEVIER

Analytica Chimica Acta 294 (1994) 243–249

ANALYTICA CHIMICA ACTA

Evaluation of pH field effect transistor measurement signals by neural networks

Bernd Hitzmann *, Thomas Kullick

Institut für Technische Chemie, Universität Hannover, Callinstr. 3, 30167 Hannover, Germany

Received 14th February 1994; revised manuscript received 21st March 1994

Abstract

A method is described which allows to evaluate analyte concentrations from flow-injection analysis signals of a pH field effect transistor (pH-FET) detector independently of the buffer capacity of the probe. The enzyme penicillin-G amidase was employed as the biocompound to monitor penicillin concentrations. Measurements have been carried out by using samples with various penicillin concentrations (penicillin-G: 1.5, 2.5, 5.0, 7.5 and 10.0 g/l) as well as various buffer ion concentrations (phosphate: 5, 15, 20, 25, 35, 45 and 50 mM). Depending on the penicillin concentration as well as the buffer ion concentration the peak shaped measurement signals did not only change their height but also their contour. Using the standard evaluation methods (peak height, integral or width) no unambiguous relation to the considered concentration could be found. In contrast to this, neural networks have been found to be able to evaluate the different contours. The relative errors were 4.7% for the determination of the penicillin concentration and 4.9% for the buffer ion concentration. The possibility of broadening the scope of this method to other pH-FET systems is discussed.

Key words: Biosensors; Enzyme field effect transistors; Flow injection; Neural networks; Evaluation methods

1. Introduction

Enzyme field effect transistors (EnFET sensors) are a special type of biosensor, which employ a pH-sensitive field effect transistor as transducer. The biological compound is directly fixed at the gate of the FET by using a polymer matrix. One reason to use enzymes as biocompounds is that they catalyze just one specific reaction. pH-EnFETs using enzymes induce a reaction of the analyte to an acid or base product. The pH shift is then detected by the FET. The shift is most frequently proportional to the analyte concentration. However, the buffer capacity has a tremendous influence on the pH shift [1]. For example, using an EnFET with penicillin-G amidase in a flow-injection analysis (FIA) system as a detector for penicillin measurements, the height of the peak-shaped measurement signal as well as their integral is highly influenced by the puffer capacity of the sample solution. To be able to evaluate penicillin concentration one has to take care that

* Corresponding author.

0003-2670/94/$07.00 © 1994 Elsevier Science B.V. All rights reserved
SSDI 0003-2670(94)00145-C

the buffer capacity does not change very much, otherwise the error of penicillin evaluation increases drastically. Shul'ga et al. [2] and Soldatkin et al. [3] reduced the influence of buffer concentration by using additional permselective membranes. These membranes block the transport of protons as well as hydroxy ions inside the membrane, thus eliminating the buffer effect on the measurement signal of the biosensor.

In this contribution an evaluation method is presented which provides the penicillin concentration as well as information about the buffer capacity, e.g., the buffer ion concentration, from ordinary (not pretreated) FIA signals. This evaluation method is based on the application of a neural network [4]. Until now neural networks are applied in FIA for signal modeling [5] as well as a reliable signal evaluation [6] even of FI patterns severely distorted by noise addition, peak height variation and baseline shift [7]. The measurement signals of samples with various penicillin as well as various buffer ion concentrations cannot be adequately evaluated by peak height, integral or peak width. These standard evaluation methods just use one characteristic feature of the whole measurement signal to calculate the considered concentration; i.e., all the information of the measurement signal is condensed to the signal height, integral or width. The contour of the measurement signals presented here, however, are too complex to be reduced to just one of these characteristic feature of the whole signal. Therefore, we used a neural network which enables us to relate many discrete measurement points of the whole signal to the concentrations, i.e., the penicillin as well as the buffer ion concentration.

2. Materials and methods

2.1. The En-FET-sensor-system

The pH-FETs of ABC Co. (Puchheim, Germany) are employed, which have at $U_{DS} = 2$ V and $I_D = 100$ μA a pH response of 53 mV/pH-decade. The gate consists of Si_3N_4. The enzyme penicillin-G amidase (EC 3.5.11, Hoechst, Frankfurt) was utilized as biocompound, which catalyzes the dissociation of the amide linkage (bond) between the side chain and the penicillin fundamental lattice. The immobilization of the enzyme suspension ($(NH_4)_2SO_4$) has been carried out directly on the gate of the FET by formation of cross-bonds with a 25% water–glutaraldehyde solution (G5882, Sigma, Deisenhofen).

The EnFET was employed as a detector in a FI system (EVA, Eppendorf, Hamburg). The buffer ion concentration (phosphate) of the carrier solution was 20 mM at pH 7.0. Sample solutions with different penicillin concentrations (1.5, 2.5, 5.0, 7.5 and 10.0 g/l) as well as different buffer ion concentrations (phosphate: 5, 15, 20, 25, 35, 45 and 50 mM) were prepared for the measurements at pH 7.0. The automation of the FI system as well as the measurement recording was accomplished by CAFCA [8] (*C*omputer *A*ssisted *F*low *C*ontrol and *A*nalysis, Anasyscon, Hannover). The uptake rate for the measurement signal was 2 Hz. One measurement cycle took 150 s.

2.2. The neural network

For the measurement signal evaluation a structured feed-forward network was developed in Turbo Pascal 6.0 using a toolbox [9]. Several neural network structures have been applied all with three layers: an input layer always consisted of 7 input neurons, one hidden layer with various numbers of neurons (3–9), and an output layer with 1 neuron (for penicillin buffer ion concentration using different networks) or 2 neurons (for simultaneous determination of penicillin and buffer ion concentrations). For the calculation of the net input of a neuron the bias was taken into account. As nonlinear transfer function the most widely used sigmoidal function has been applied. To calculate concentrations from the net output a linear function was used, i.e., the penicillin as well as the buffer ion concentrations have been pre-scaled into the 0.2–0.8 interval. The back-propagation algorithm was employed for correcting the weights using the generalized delta rule (momentum constant = 0.9).

3. Results and discussion

3.1. The characteristic contours of the measurement signals

In Fig. 1 fragments of measurement signals of several probes, all with a fixed penicillin concentration (10 g/l) but with various buffer ion concentrations (5, 15, 25, 35 and 50 mM), are shown. It is clearly recognizable that with increasing buffer ion concentration the contours of the measurement signals are decreasing, the rising of the signals starts earlier, but the initially large increase continues to be smaller until the maximum is reached. In Fig. 2 the same fragments of the measurement signals are shown as in Fig. 1. Again the same ion concentrations are used but at lower fixed penicillin concentration (1.5 g/l). The contours are different to those of the higher penicillin concentrations but the characteristic features are the same. The intensities of these signals are all much lower. The lower the buffer ion concentration, the slender is the contour of the signal, i.e., the smaller is the width of half intensity. The higher the buffer ion concentration is the faster the signal begins to rise. The measurements with penicillin concentrations between 10 and 1.5 g/l have a hybrid contour. The heights of the maxima have values between those shown in Figs. 1 and 2. The signals corresponding to the higher buffer ion concentration always have a rising phase which starts earlier. From multiple measurements of the same sample the characteristic contours of the signal were proved to be reproducible. From all measurement signals one can derive that the higher the buffer concentration is, the earlier the signal starts to rise, but that the height of the signal is smaller. To relate these characteristic contours to the corresponding concentrations we used neural networks.

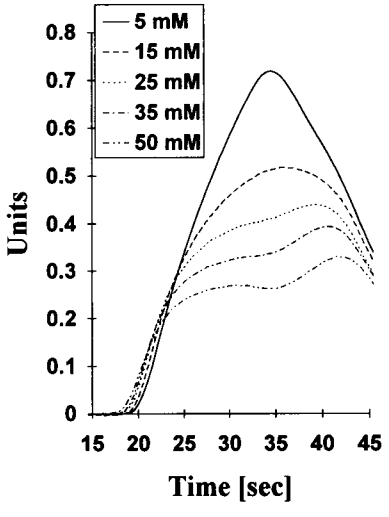

Fig. 1. Fragments of measurement signals of several probes all with a fixed penicillin concentration (10 g/l) but with various buffer ion concentrations (5, 15, 25, 35 and 50 mM).

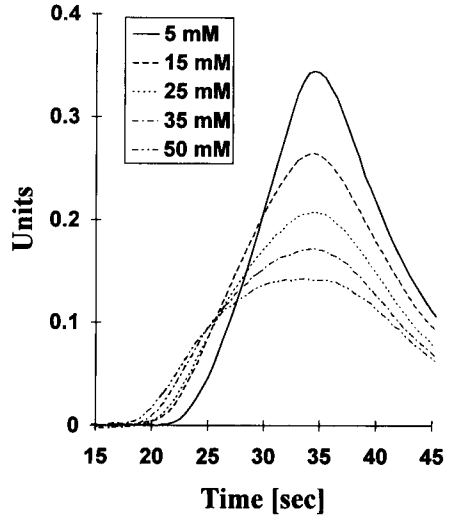

Fig. 2. Fragments of measurement signals of several probes all with a fixed penicillin concentration (1.5 g/l) but with various buffer ion concentrations (5, 15, 25, 35 and 50).

3.2. The training of the network

The task of the neural network was to calculate the penicillin as well as the buffer ion concentration from the characteristic variation of the measurement contour. A typical structure of a three-layer neural net used for simultaneous determination of penicillin and buffer ion concentrations can be seen in Fig. 3. To investigate the influence of the number of neurons of the hidden layer, multiple training runs have been carried out with 3–9 neurons of the hidden layer. Furthermore, the number of neurons of the third

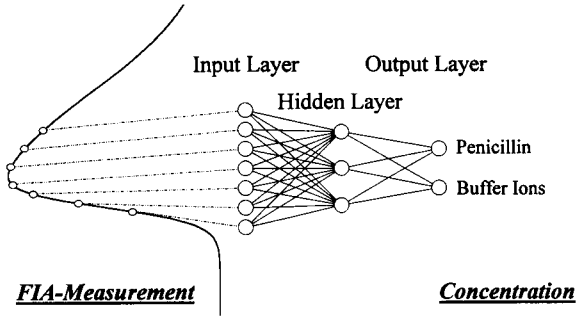

Fig. 3. The typical structure of the neural net used for the determination of penicillin and buffer ion concentration.

layer was changed from 1 to 2. In the case of one neuron in the output layer different nets have been used for the prediction of penicillin and buffer ion concentrations.

From all samples prepared, only a few were taken as a training set: all combinations of 1.5, 5 and 10 g/l penicillin with 5, 20, 35 and 50 mM buffer ion as well as all combinations of 2.5 and 7.5 g/l penicillin with 15, 25 and 45 mM buffer ion concentration. This was done, so that the other combinations can be used exclusively for testing the generalization (interpolation) capacity of the network. To eliminate the influence of a drifting baseline, all data of a particular measurement cycle were shifted so that their baseline was given the value zero. As input values for the neural network, 7 measurements during the time interval of 20–44 s in 4-s steps have been taken from each measurement cycle. The change of these values is significant for their characteristic contour. From each sample one measurement cycle was taken for the training of the neural net, that is $3*4+2*3=18$ training patterns were applied. For the back-propagation learning scheme the epoch learning procedure was used, which means that the weights were changed after all 18 training patterns were applied (one epoch) and not after each pattern input. During all training phases the average of the percentage error between real and predicted concentration improves almost monotonically. After 100000 epochs the training was stopped and started again with new random initialized weights to investigate the influence of this procedure.

3.3. The prediction of the network

For a comparison of the results coming from different network structures an average error of the concentration prediction from measurement signals was calculated.

$$\overline{error} = \frac{100}{N} \sum_{i=1}^{N} \frac{|c_i^t - c_i^p|}{c_i^t}$$

$\overline{error}$ = average error, N = number of measurements, c_i^t = true concentration, c_i^p = predicted concentration.

In Fig. 4 the typical evolution of the average error of the penicillin prediction as well as buffer ion concentration prediction depending on the number of learning epochs are shown. In both cases the error propagation was calculated from two different neural nets, both consisting of three neurons in the hidden layer and one neuron in the third layer. The error was calculated as average value from the determination of measurement signals not used for training. Almost half of these measurement signals belong to concentration combinations which were not trained. As can be seen, the error of the penicillin determination drops very fast. After the minimum of the error is reached, the values increase slowly. This indicates that overtraining has taken place. The error of the buffer ion concentration goes down slowly reaching no minimum. A minimum is obtained only after 10^7 training cycles.

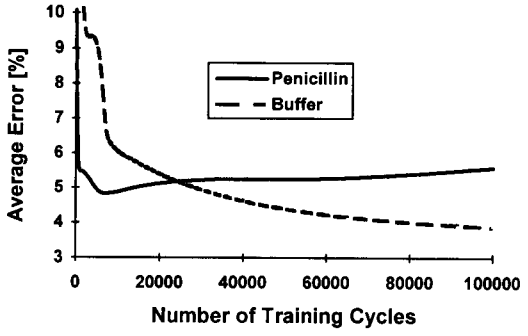

Fig. 4. The evolution of the average error of penicillin and buffer ion concentration determination depending on numbers of training cycles. These results are obtained from two networks with 3 hidden neurons and one output neuron.

Table 1
The average values of the predicted penicillin concentrations (g/l) determined by 4 or 5 (italic and bold values) measurements of each probe. The italic and bold values are concentration combinations which were not used for training. The values are predicted by a net consisting of 3 neurons in the hidden layer and one neuron in the output layer after 6500 training cycles

Phosphate (mM)	Penicillin (g/l)				
	1.5	2.5	5.0	7.5	10
5	1.47	***2.36***	4.98	***8.29***	10.26
15	***1.59***	2.52	***5.53***	7.52	***10.30***
20	1.53	***2.46***	4.85	***7.90***	10.30
25	***1.58***	2.51	***5.26***	7.91	***10.19***
35	1.58	***2.41***	4.85	***7.72***	10.22
45	***1.59***	2.37	***4.85***	7.32	***10.30***
50	1.58	***2.49***	4.95	***7.89***	9.98

In Table 1 and Table 2 the average of predicted concentrations and in Tables 3 and 4 their average errors are shown for penicillin and buffer ion concentrations, respectively. These results were obtained by neural nets which have also been used for the error calculation of Fig. 4. The penicillin results originate from a network whose average error gained the minimum value (at 6700 training cycles). Because the error of buffer ion determination was always decreasing in Fig. 4 the weights at 30000 training cycles were selected for further analysis. The values in Tables 1–4 which are printed italic and bold are obtained from concentration combinations which were not used for training, i.e., the network has to interpolate these values. The italic and bold values in the tables are average values calculated from 5 samples, the other values are obtained from 4 samples.

Table 2
The average values of the predicted buffer ion concentrations (mM) determined by 4 or 5 (italic and bold values) measurements of each probe. The italic and bold values are concentration combinations which had not been used for training. The values are predicted by a net consisting of 3 neurons in the hidden layer and one neuron in the output layer after 30000 training cycles

Phosphate (mM)	Penicillin (g/l)				
	1.5	2.5	5.0	7.5	10
5	5.66	***6.90***	5.22	***5.02***	4.41
15	***13.1***	15.8	***15.4***	15.6	***15.8***
20	18.5	***20.1***	19.6	***20.0***	20.2
25	***24.6***	24.9	***24.6***	25.1	***24.9***
35	38.2	***36.2***	35.2	***35.7***	35.8
45	***46.0***	44.8	***45.4***	44.5	***45.1***
50	49.1	***50.3***	49.7	***50.2***	50.2

Table 3
The average error (%) calculated from the values of Table 1

Phosphate (mM)	Penicillin (g/l)				
	1.5	2.5	5.0	7.5	10
5	2.0	***5.7***	2.7	***10.4***	2.6
15	***6.1***	2.0	***10.6***	3.4	***4.2***
20	3.0	***1.8***	5.6	***6.5***	4.8
25	***5.5***	5.1	***7.6***	8.3	***3.8***
35	5.2	***3.6***	4.2	***3.6***	3.0
45	***7.0***	6.4	***3.4***	8.2	***3.1***
50	5.6	***3.9***	1.4	***5.1***	0.5

As can be seen from the average error of the penicillin prediction the two largest errors are 10.6 and 10.4%. Both are obtained from measurements of which the concentration combination was not used for training. The next two largest errors, however, are obtained from measurements of which the concentration combinations were used for training. The total average of all errors of untrained concentration combinations is 5.4% whereas that of trained concentration combinations is 4.1%. The difference is 1.3%. However, if one analyses the prediction of the buffer ion concentration the largest errors are obtained by small penicillin and small phosphate concentrations. Again, the largest average error originates from an untrained concentration combination (38.9%). If this value is not considered

Table 4
The average error (%) calculated from the values of Table 2.

Phosphate (mM)	Penicillin (g/l)				
	1.5	2.5	5.0	7.5	10
5	14.5	***38.9***	5.1	***8.5***	11.2
15	***13.5***	5.8	***2.9***	3.9	***5.6***
20	7.3	***0.9***	2.3	***1.3***	0.7
25	***3.1***	3.1	***2.3***	2.4	***0.3***
35	9.2	***3.3***	2.2	***2.8***	2.3
45	***4.1***	2.3	***1.7***	1.9	***0.8***
50	2.1	***1.2***	0.8	***0.7***	1.4

Table 5
The minimum error (%) as well as the number of training cycles obtaining that error depending on number of hidden neurons as well as different training runs of the penicillin determination

No. of hidden neurons	No. of training		
	I	II	III
3	5.0	5.1	4.6
	25500	18000	2400
5	4.8	4.5	4.5
	4700	4100	1800
7	4.6	5.3	4.7
	18700	3200	3700
9	5.6	4.4	5.5
	2600	5000	16800

for the calculation of a total average error of all untrained concentration combinations, then a value of 3.3% is obtained. This must be compared to the average error of all trained concentration combinations (4.4%). Employing a *t*-test on the errors of trained and untrained concentration combinations, no significant difference could be found. Therefore, one can conclude, that there is no significant difference between trained and untrained concentration combinations. The network is able to interpolate unknown analyte concentrations. The total average errors of all predictions are 4.7 and 4.9% for penicillin and phosphate, respectively.

For a more practicable use of the evaluation of measurements by neural nets it would be easier to predict the penicillin as well as the buffer ion concentration by just one neural net. Therefore, we used nets with 2 neurons as output layer. Results are shown for various numbers of hidden neurons in Tables 5 and 6 for penicillin and buffer ion concentrations, respectively. In each row of the tables the minimum total average error as well as the number of training cycles obtaining that minimum error can be seen. In the columns these values are presented for various runs, i.e., the results of different training runs with different random initialized weights. The largest total average error of penicillin evaluation of all runs is 5.6%. This is in the order of the typical measurement quality of this kind of sensor. These indicate that in each run the net was able to evaluate the signals. As can be seen for the prediction of the penicillin concentrations the smallest error is 4.4% obtained after 5000 training cycles by a net consisting of 9 hidden neurons. The largest error of penicillin prediction, however, is 5.6% obtained after 2600 training cycles by the same number of hidden neurons. This indicates that the learning algorithm was not always able to find the lowest minimum of error, i.e., finding the best weights for this specific application. If one compares the number of training cycles necessary to obtain the best prediction it is clear to see that the best prediction of buffer ion concentration is obtained after many more cycles than that of the penicillin concentration. The same behaviour was observed when using different nets for the penicillin and buffer ion concentration, i.e., networks with only one output neuron.

4. Conclusions

The results of this investigation show that the measurement signals of the EnFET can be well evaluated by a neural network. The penicillin concentration as well as the buffer ion concentration from unknown (untrained) samples have been determined with an error that is of the same

Table 6
The minimum error (%) as well as the number of training cycles obtaining that error depending on number of hidden neurons as well as different training runs of the buffer ion determination

No. of hidden neurons	No. of training		
	I	II	III
3	5.8	5.8	6.7
	96700	87100	54000
5	5.1	4.5	3.5
	46200	97700	71300
7	4.3	5.5	3.6
	99400	99400	24900
9	3.1	3.8	3.6
	69300	44700	99700

order as for measurements with constant buffer ion concentration evaluated by peak height.

To calculate the time for the whole calibration procedure using neural nets one has to add the time for measurement of the signals and for the training and testing of the net. The measurements for the training and the testing set lasted about 2 h. The training period of the nets, with the results that have been shown in detail, lasted for about 30 min. If one also considers the time for testing the net sum is about 3 h. This is not too long, and therefore this evaluation method can also be applied for practical applications.

This signal evaluation method has been applied for a particular EnFET system. However, it provides the prospect to evaluate other pH-based sensor system measurements, which also have a dependence of buffer ion concentration. No further treatment of the sample or the sensor system, such as additional membranes, is necessary. Furthermore, this evaluation method might also quantify other measurement signals changing their contour with respect of properties of various analytes.

References

[1] M.J. Eddowes, Sensors Actuators, 7 (1985) 97.
[2] A.A. Shul'ga, V.I. Strikha, A.P. Soldatkin, A.V. El'skaya, H. Maupas, C. Martelet and P. Clechet, Anal. Chim. Acta, 278 (1993) 233.
[3] A.P. Soldatkin, A.V. El'skaya, A.A. Shul'ga, L.I. Netchiporouk, A.M. Nyamsi Hendji and N. Jaffrezic-Renault, Anal. Chim. Acta, 283 (1993) 695.
[4] J. Zupan and J. Gasteiger, Anal. Chim. Acta, 248 (1991) 1.
[5] C. Campmajó, M. Poch, J. Robusté, F. Valero and J. Lafuente, Analysis, 20 (1992) 127.
[6] A. Wassmann and B. Hitzmann, Chem. Ing. Tech., 65 (1993) 947.
[7] M. Hartnett, D. Diamond and P.G. Barker, Analyst, 118 (1993) 347
[8] B. Hitzmann, F. Lammers, B. Weigel and A. Van Putten, BioForum, 16 (1993) 450.
[9] H. Kruse, R. Mangold, B. Melcher and O. Penger, Programmierung Neuronaler Netze, Eine Turbo Pascal Toolbox, Addison-Wesley, Bonn, 1991.

ELSEVIER

Analytica Chimica Acta 294 (1994) 251–260

ANALYTICA CHIMICA ACTA

Optimization of the amperometric detection of nitrite by reaction with iodide in a post-column reactor for liquid chromatography of non-volatile nitrosamines.

G.A. Sacchetto *, G. Favaro, P. Pastore, M. Fiorani

Department of Inorganic, Organometallic and Analytical Chemistry, University of Padova, via Marzolo 1, 35131 Padova, Italy

Received 16th November 1993; revised manuscript received 16th March 1994

Abstract

Following previous studies on this subject, the use of iodide reagent in acidic medium for the liquid chromatographic amperometric determination of non-volatile nitrosamines has been investigated in a two-line flow-injection manifold coupled with a voltammetric flow-through detector. The peak current signals obtained for the nitrite–iodide reaction were compared with those obtained for the iodate–iodide reaction used as a reference for the production of the electroactive species I_3^-. The effect of adsorption–desorption phenomena on the reactor walls was investigated and analyzed by the "exponentially modified Gaussian" model applied to flow-injection peaks obtained under different experimental conditions, as to composition of the carrier liquid (water and water–acetonitrile mixtures), concentration of the reagent and temperature of the reactor. From an analytical point of view, the method ensures a satisfactory linear response, a higher sensitivity and a much lower detection limit (about 1×10^{-8} M) than those found with the cerium(IV) reagent, and a comparable band broadening and tailing.

Key words: Flow injection; Amperometry; Nitrite; Liquid chromatography; Nitrosamines

1. Introduction

In two previous papers [1,2] the suitability of Ce(IV) in acidic medium as a post-column reagent for the oxidation and the electrochemical detection of nitrite (nitrous acid) produced by the warm acid decomposition of some classes of nitrosamines was demonstrated.

The electrochemical behaviour of the Ce(IV)–Ce(III) couple in 0.5–2.0 M sulphuric acid solutions was first investigated on different electrode materials, and gold was found the most suitable one for the oxidative detection of Ce(III) produced by the reaction of nitrite with excess Ce(IV) reagent, provided that prepolarization in the anodic "oxygen chemisorption" potential range was performed. Then, the behaviour of an on-line post-column reactor (PCR) system based on the use of the Ce(IV) reagent was investigated in a two-line flow manifold coupled with a flow-through voltammetric detector equipped with twin gold electrodes for both mono- and biamperometric detection modes. The performance of the

* Corresponding author.

0003-2670/94/$07.00 © 1994 Elsevier Science B.V. All rights reserved
SSDI 0003-2670(94)00140-H

flow reactor elements was evaluated by flow injection (FI) of both Ce(III) and nitrite in aqueous and mixed water–acetonitrile carriers, as the usual eluent media for the liquid chromatographic separation of the above mentioned compounds [3].

In this work the previously described flow manifold [2], including the post-column reactor system, was used to investigate the suitability of iodide solutions in 0.5 M sulphuric acid for the post-column reduction and electrochemical detection of nitrite (nitrous acid) produced in the denitrosation reaction of the above mentioned non-volatile nitrosamines. The iodine–iodide couple is a highly reversible electrochemical system on both gold and platinum electrodes in sulphuric acid media [4] and the reductive detection of iodine (I_3^-) as the reaction product of nitrite with excess iodide can be easily performed by both mono- and biamperometric modes [5]. A much lower background current is expected in this case, as the presence of iodine in the iodide reagent solutions can be effectively limited, if solutions are deoxygenated. On the other hand, the possibility of controlling the iodine production by a proper choice of the flow rate in the presence of oxygen [5] seemed to be a rather cumbersome practice leading to further sources of irreproducibility.

Both water and water–acetonitrile (70 + 30, v/v) mixtures were tested as carrier liquids (eluents). Various reagent concentrations were utilized, and the influence of the reactor temperature on the FI response was investigated.

2. Experimental

2.1. Apparatus

The flow-injection experiments were performed by means of the two-channel flow manifold shown in Fig. 1. Details on the design and the features of the flow manifold and of the EG Model 400 (Princeton Applied Research) electrochemical detector employed can be found in a previous paper [2]. To further reduce the PCR dispersion, the cooling coil was replaced by a short PTFE knitted coil (1 m × 0.5 mm i.d., Supelco) immersed in cold circulating water. Flow rates of 0.5 ml min^{-1} were usually adopted in each of the two channels. Samples were generally injected (intercalated) by a metal-free rotary valve by using a 20 μl loop, filled with a gastight glass syringe with a PTFE piston (Hamilton Model 1725 RNR), to prevent any prolonged contact of the analyte samples with metallic surfaces.

The potential values throughout this paper are referred to the saturated calomel electrode (SCE).

2.2. Reagents

KI (RP Normapur, Prolabo), KIO_3 (RP-ACS, Carlo Erba), $NaNO_2$ (RPE-ACS, Carlo Erba), H_2SO_4 (95%, RP Normapur, Prolabo) and acetonitrile (LC grade, Prolabo) were used as purchased. Solutions of KI were freshly prepared by dissolving the salt in 0.5 M H_2SO_4 previously deaerated by bubbling presaturated nitrogen

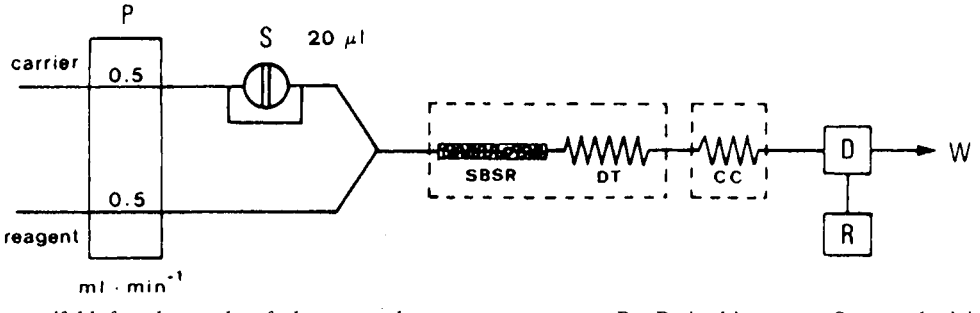

Fig. 1. Flow manifold for the study of the post-column reactor system. P = Peristaltic pump; S = sample injection valve; SBSR = single-bead string reactor; DT = delay tube; CC = cooling coil; D = detector; R = recorder; W = waste.

(S.I.O., 99.999% purity) for at least 20 min. A slight flow of nitrogen was maintained over the solution during the experiments. The carrier liquids, water or water–acetonitrile (70 + 30, v/v), were flushed in the same way. After thorough deaeration special care was devoted to avoid any contact of the sodium nitrite solutions with the atmosphere.

From the values of the background current measured at 0.2 V (reduction of iodine to iodide) the background concentration of iodine (I_3^-) was estimated to amount to about 1.5×10^{-6} M, i.e., less than 0.3% of the iodide content of the reagent, about one order of magnitude lower than the residual Ce(III) in the Ce(IV) reagent [2].

2.3. Procedure

The mechanical polishing and the electrochemical cleaning procedures of the gold electrodes were similar to those described in a previous paper [1], but for the anodic prepolarization finishing step, which was not necessary in the present case.

3. Results and discussion

The main problem in utilizing the reduction of nitrite by iodide, according to the usual reaction:

$$2HNO_2 + 3I^- + 2H^+ \rightarrow 2NO + I_3^- + 2H_2O \quad (1)$$

is the interference of oxygen, which may directly slowly oxidize I^- according to the scheme:

$$3I^- + 1/2O_2 + 2H^+ \rightarrow I_3^- + H_2O \quad (2)$$

or oxidize nitric oxide produced in reaction (1):

$$NO + 1/2O_2 \rightarrow NO_2 \quad (3)$$

$$NO_2 + 3I^- + 2H^+ \rightarrow NO + I_3^- + H_2O \quad (4)$$

The latter two reactions lead to production of iodine and regeneration of nitric oxide at a not negligible rate in the time scale of the residence time in the PCR system; thus both the carrier and the reagent must be accurately deoxygenated.

The amperometric response for FI of nitrite and iodate, the latter being used as a reference analyte for the reaction with I^- to produce I_3^-, was evaluated in the light of the "exponentially modified gaussian" (EMG) model [6,7]. The EMG model describes chromatographic or FI peaks as the result of a convolution of a gaussian and of an

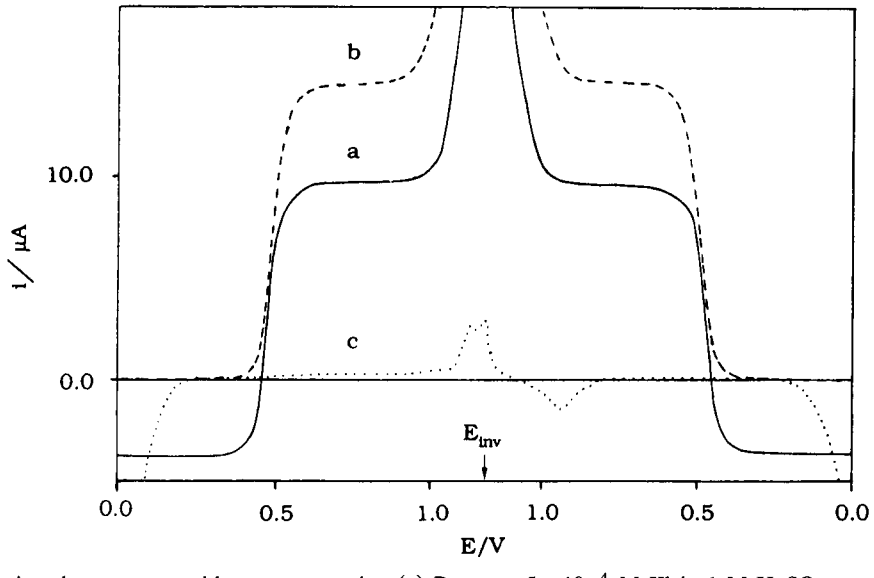

Fig. 2. Hydrodynamic voltammogram with aqueous carrier. (a) Reagent, 5×10^{-4} M KI in 1 M H_2SO_4; carrier, 2.0×10^{-5} M KIO_3. (b) Reagent, as for (a); carrier, water. (c) Reagent, 1 M H_2SO_4; carrier, water. Scan rate, 10 mV s^{-1}; reactor temperature, 25°C; flow rate, 1.0 ml min^{-1}.

exponential decay function, which should account for the asymmetry of the peak (tailing). This model allows to evaluate the variance of the peak, σ^2, as the sum of two components, a purely gaussian one, σ_G^2, and a purely exponential one, τ^2, and its validity is assessed by its ability to reliably calculate peak areas. Different kinds of peaks can be compared on the basis of their experimentally derived EMG model parameters, and also a comparison of peak areas obtained in the above mentioned cases (NO_2^- and IO_3^- as analytes) can be performed. Areas are related to the amounts of I_3^- produced by the two reactions, under the very reasonable assumption of an invariant electrochemical conversion yield of the amperometric detector. On the other hand, on the basis of the EMG parameters, both physical and chemical dispersion effects in the PCR system are put into evidence. Furthermore any other possible effect on the dispersion due to other causes (for instance adsorption of reaction products) can be investigated and quantified. This is a way to control the extra-broadening effects of the PCR on the incoming chromatographic bands.

3.1. Hydrodynamic voltammograms of the triiodide–iodide couple in the flow system

A preliminary voltammetric study was made to investigate the electrochemical behaviour of the I_3^-/I^- couple in a continuous flow system.

Slow-scan hydrodynamic voltammograms (10 mV s^{-1}) were performed by continuously pumping a 2×10^{-5} M KIO_3 aqueous solution into the carrier tube, while a 5×10^{-4} M KI solution in 1.0 M H_2SO_4 flowed in the reagent tube.

Flow rates of 0.5 ml min^{-1} were used in both stream tubes. One of the resulting voltammograms is shown in Fig. 2 (curve a). In the strongly acidic medium iodate rapidly reacts with excess iodide to give triiodide. At low potentials the reduction wave of the triiodide ion to iodide is clearly visible. At potentials higher than about 0.5 V iodide is oxidized to iodine (I_3^-) and then to iodate in the potential range where the oxygen chemisorption wave begins to develop on the gold electrode (see curve c). On reversing the scan direction the couple exhibits the same features of the anodic scan, thus showing that the oxygen chemisorption/desorption effect is very limited in the explored potential range, while it is clearly visible in the background voltammogram obtained in the absence of iodide (curve c). This finding can be ascribed to the possibility that even a faint adsorption of iodine on the electrode surface completely prevents the usual oxygen chemisorption [8]. The current due to iodine traces in the iodide solution (curve b) is practically negligible on this scale; however, it will be considered below in the evaluation of the detection limit for nitrite.

The most suitable working potential for monoamperometric measurements falls around 0.2–0.3 V; for the biamperometric detection modes a potential difference of 0.1–0.2 V is sufficient to get a linear current response, while not less than 0.3 V were required when Ce(IV) was used as the reagent [2].

Further voltammograms were performed by pumping into the carrier line a 2.0×10^{-5} M solution of KIO_3 in water–acetonitrile (70 + 30, v/v), acetonitrile being the most frequently used organic modifier, to simulate the operative conditions for the reversed-phase liquid chromatographic separation of nitrosamines [3]. The voltammograms appear to be essentially the same as those for the aqueous carrier (Fig. 2), but with a decrease of the limiting current of about 10% for both the I_3^- reduction and the iodide oxidation. This finding can be ascribed to a decrease of the diffusion coefficients of both triiodide and iodide ions, mainly due to the increase of the kinematic viscosity of the medium on increasing acetonitrile content [2].

3.2. Amperometric responses for iodine (I_3^-) in the flow system

Two series of flow-injection experiments were performed to investigate the nature of the amperometric responses for both the iodate–iodide reference reaction and the nitrite–iodide reaction of analytical interest. The iodate reaction with excess iodide acidic reagent was used as a reference

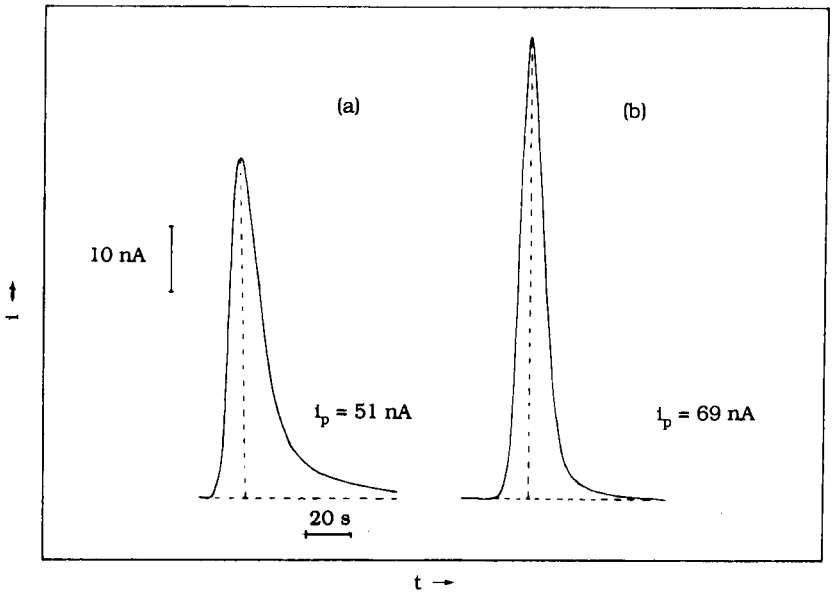

Fig. 3. Amperometric peaks obtained by FI of iodate (a) and nitrite (b) in aqueous carrier. Reagent, KI 5×10^{-4} M in 1 M H_2SO_4; analyte concentration, 2×10^{-5} eq l^{-1}; reactor temperature, 25°C; flow rate, 1.0 ml min^{-1}.

for the flow production of iodine (I_3^-), according to the usual reaction scheme:

$$IO_3^- + 8I^- + 6H^+ \rightarrow 3I_3^- + 3H_2O \quad (5)$$

in which I_3^- is the only product. The nitrite reaction under the same conditions is actually producing iodine and nitrogen monoxide according to reaction (1). Nitrogen monoxide, NO, can

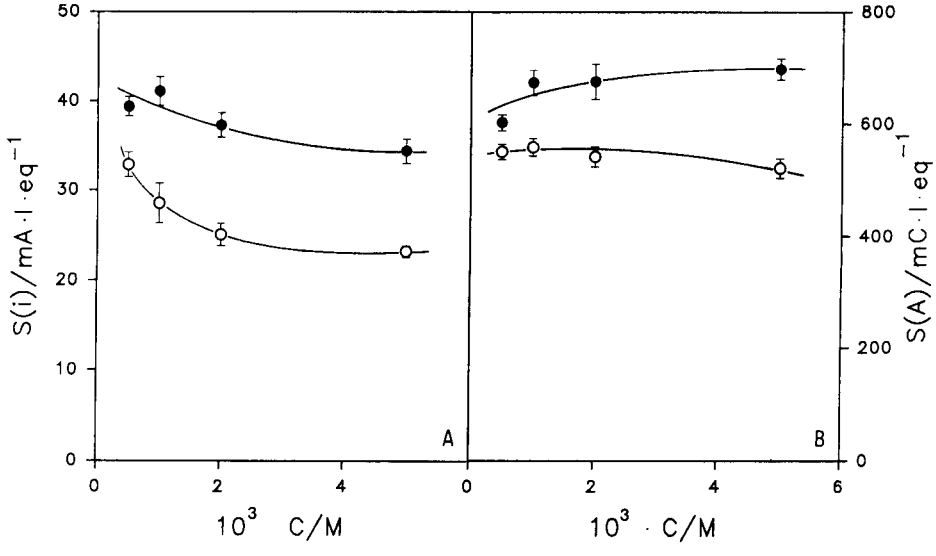

Fig. 4. Dependence of amperometric sensitivity on iodide reagent concentration for FI of nitrite (•) and iodate (○). (A) Peak height sensitivity; (B) peak area sensitivity. Carrier, water; analyte concentration, $(1.0–4.0) \times 10^{-5}$ eq l^{-1}; reactor temperature, 25°C; applied potential, 0.2 V vs. SCE.

Table 1
Amperometric peak height responses of FI experiments for nitrite and iodate ($(1.0–4.0)\times10^{-5}$ eq l^{-1}), at variable reagent concentration. Equation: $i(\text{nA}) = (a \pm s_a) + (b \pm s_b)\cdot 10^5 \cdot C(\text{eq } l^{-1})$

Analyte	$10^3 \cdot C_{KI}$ (M)	a	b	s_a	s_b	r
IO_3^-	0.5	−11.5	32.8	3.8	1.4	0.995
IO_3^-	1.0	−9.4	28.6	5.9	2.2	0.983
IO_3^-	2.0	−6.8	25.1	3.4	1.2	0.993
IO_3^-	5.0	−6.1	23.2	1.8	0.7	0.998
NO_2^-	0.5	−6.9	39.4	2.9	1.1	0.998
NO_2^-	1.0	−2.5	41.1	4.3	1.6	0.996
NO_2^-	2.0	−3.1	37.3	3.8	1.4	0.999
NO_2^-	5.0	−14.3	34.4	3.8	1.4	0.998

in fact produce more iodine by a further, although slower, reaction with I^- [9] :

$$2NO + 3I^- + 2H^+ \rightarrow H_2N_2O_2 + I_3^- \quad (6)$$

In the confined FI manifold volume, reaction (6) can proceed to some extent during the residence time of the sample plug.

A good linearity of the response signal dependence on the analyte concentration has been derived from FI experiments for both IO_3^- and NO_2^-, in the same concentration range for several iodide reagent concentrations ranging between 5.0×10^{-4} and 5.0×10^{-3}M. Some results are reported in Table 1. As a general finding, current sensitivities (parameter b in the table) for nitrite are substantially larger than those found for iodate. For the sake of comparison two peaks are reported in Fig. 3. Peaks obtained with nitrite injections (b) are higher, but less broad and especially less skewed than those obtained for iodate injections (a). While a difference in peak height could be immediately ascribed to, e.g., a contribution of reaction (6), the discrepancy of their shapes needs a more profound investigation.

Table 2
Amperometric peak area responses of FI experiments for nitrite and iodate ($(1.0–4.0)\times10^{-5}$ eq l^{-1}), at variable reagent concentration. Equation: $A(\text{nC}) = (a' \pm s'_a) + (b' \pm s'_b)\cdot 10^5 \cdot C(\text{eq } l^{-1})$

Analyte	$10^3 \cdot C_{KI}$ (M)	a'	b'	s'_a	s'_b	r
IO_3^-	0.5	−155	549	38	14	0.991
IO_3^-	1.0	−103	557	43	16	0.988
IO_3^-	2.0	−45	540	50	18	0.984
IO_3^-	5.0	−14	520	47	17	0.984
NO_2^-	0.5	−90	522	40	14	0.989
NO_2^-	1.0	−105	672	61	22	0.984
NO_2^-	2.0	−52	674	86	32	0.985
NO_2^-	5.0	−304	696	53	19	0.995

In order to generalize this finding, Fig. 4A is given to show the averaged current sensitivities, $S(i)$, derived from current vs. analyte concentration plots (see Table 1, column 4), as a function of the iodide reagent concentration. The above observations on peak heights are then confirmed.

3.3. Time-domain characteristics of FI peaks at variable reagent concentration.

Attention has then been paid to the time-domain characteristics of the FI peaks and a tentative hypothesis has been formulated that excess peak broadening and especially tailing may be ascribed to adsorption of the reaction product I_3^- on the manifold walls, essentially PTFE tubings and SBSR (single bead string reactor) glass spheres. The problem of analyte adsorption has been recently mentioned by Ruzicka and Hansen [10] as an interesting subject for further investigation. Using the above assumptions, it must be taken into consideration that the adsorption effect is controlled by the rate of production of I_3^- according to the two main involved reactions (1) and (5). In other words the faster the reaction the more immediate and the more effective the adsorption is. Adsorption/desorption effects would lower peak height and increase both broadening and tailing, without substantially changing peak area. In Fig. 4A it clearly appears that the amperometric sensitivity decreases on increasing iodide reagent concentration for both analytes. In fact, on increasing reagent concentration both reaction rates increase and I_3^- adsorption effects increase too.

Peak area sensitivities calculated according to the EMG model [6,7] are reported in Table 2 for the same experiments of Table 1. Averaged peak area sensitivities are also plotted against iodide concentration in Fig. 4B: they exhibit a substantial independence from reagent concentration, because both reactions (1) and (5) are to be considered as complete in the residence time of

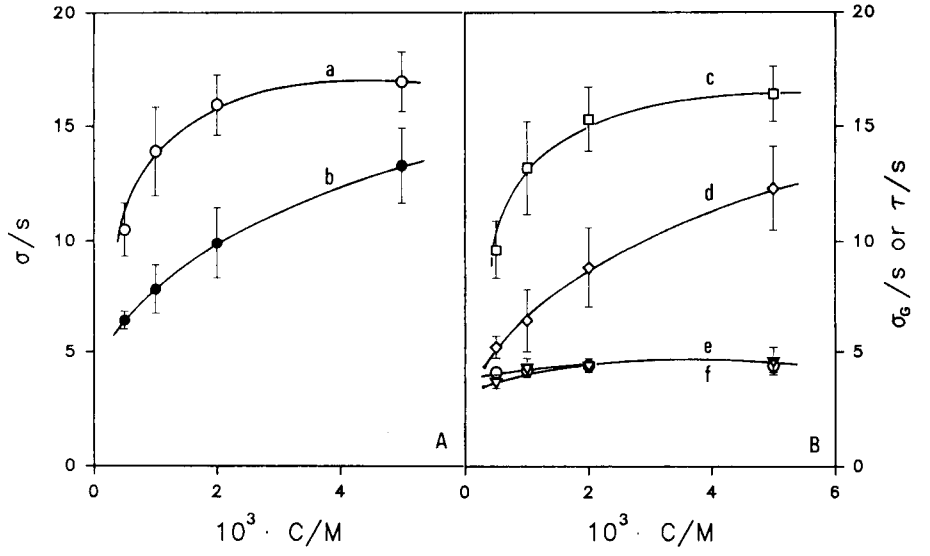

Fig. 5. Dependence of time-domain EMG parameters on KI reagent concentration for FI of nitrite and iodate. (a) σ for iodate; (b) σ for nitrite; (c) τ for iodate; (d) τ for nitrite; (e) σ_G for iodate; (f) σ_G for nitrite. Carrier, water; analyte concentration, $(1.0–4.0) \times 10^{-5}$ eq l^{-1}; applied potential, 0.2 V vs. SCE.

the sample plug (about 90 s). Nitrite–iodate peak area sensitivity ratios are not far from unity, while peak height sensitivity ratios range between 1.3 and 1.5 (Fig. 4A).

On the other hand, the time-domain parameters σ, σ_G and τ, obtained by applying the EMG model [6,7] to both iodate and nitrite analyte peaks, give support to the above considerations on peak height and area trends with reagent concentration. As it is seen in Fig. 5A and B the peak standard deviation σ and its "exponential" component τ increase with reagent concentration

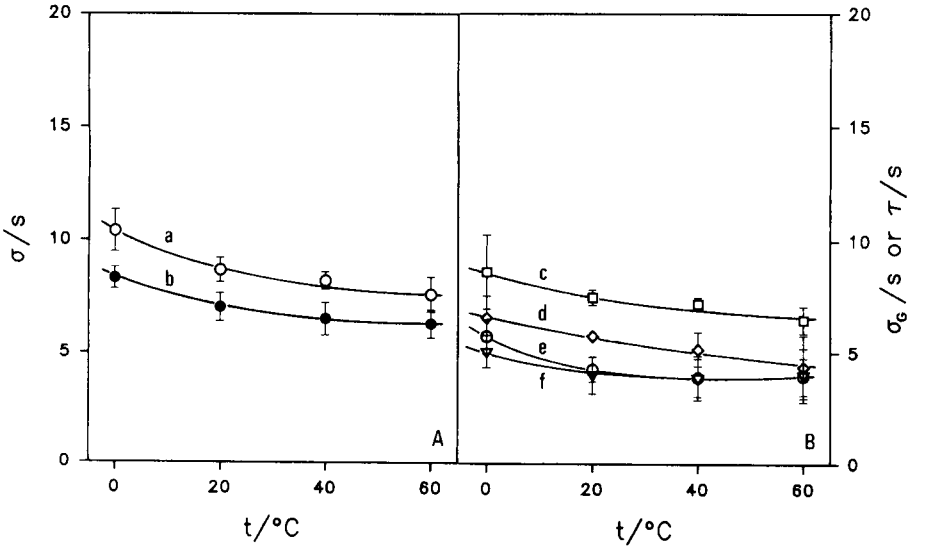

Fig. 6. Dependence of time-domain EMG parameters on reactor temperature (0–60°C) for FI of nitrite and iodate. (a) σ for iodate; (b) σ for nitrite; (c) τ for iodate; (d) τ for nitrite; (e) σ_G for iodate; (f) σ_G for nitrite. Carrier, water; reagent, 5×10^{-4} M KI in 1 M H_2SO_4; analyte concentration, 5.0×10^{-5} eq l^{-1}; applied potential, 0.2 V vs. SCE.

for both iodate and nitrite FI peaks, thus supporting peak broadening and especially peak tailing dependence on reagent concentration, and then on reaction rates. Values of σ and τ for nitrite are, in all cases, smaller than those for iodate. On the contrary, as expected, the "gaussian" component, σ_G, is essentially independent of the reagent concentration and its values are the same for both analytes. All these results support the formulated hypothesis of reaction product adsorption in the flow system.

3.4. Flow injections of nitrite and iodate at varying reactor temperature

As mentioned in the Introduction the yields of the acid denitrosation reactions of nitrosamines are greatly enhanced by temperatures exceeding 50–60°C. On the other hand, it is expected that both reaction rates of iodate and nitrite with the iodide reagent become larger at higher temperatures, while adsorption of the reaction product should be weaker and less effective; on the whole, less skewed FI peaks should be obtained for both analytes at increasing temperature of the PCR. In general, smaller variances (σ^2) are also expected as a consequence of the decrease of the medium kinematic viscosity already pointed out and of the corresponding increase of the diffusion coefficients [2].

The results obtained from measurements performed with aqueous carrier at increasing PCR temperature from 0 to 60°C are presented in Fig. 6A and B. The time-domain EMG parameters exhibit a steadily decreasing trend on increasing temperature. The values for the analyte NO_2^- are generally appreciably lower than those found for IO_3^-, with a slight tendency to equalization at the highest temperatures. As expected, peak heights (see Fig. 7A) increase at increasing temperatures in both cases, but their ratios remain approximately invariant around the value 1.2. In the meantime (see Fig. 7B), peak areas are found to vary just a little with temperature for both iodate and nitrite, while their ratio remains substantially equal to 1.

However, the above formulated hypothesis that reaction (6) can be a bit effective in the "confined" space of the reaction system cannot be fully rejected, taking into account that peak area ratios are generally slightly larger than 1.

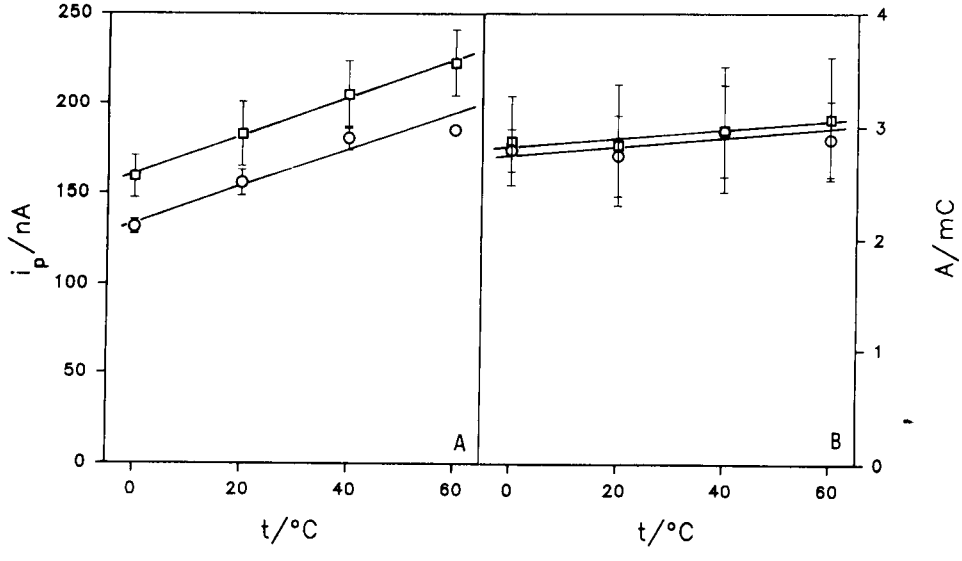

Fig. 7. Dependence of peak characteristics on reactor temperature for FI of nitrite (□) and iodate (○). (A) Peak height, i_p, vs. temperature T; (B) peak area, A, vs. temperature, T; carrier, water; reagent, 5×10^{-4} M KI in 1 M H_2SO_4; analyte concentration, 5.0×10^{-5} eq l^{-1}; applied potential, 0.2 V vs. SCE.

3.5. Optimized experimental conditions for the analytical determination of non-volatile nitrosamines

Despite the problems discussed above, the monoamperometric as well as the biamperometric determination of nitrite is satisfactory both in terms of response linearity, sensitivity and noise. By the usual chromatographic flow rates (about 1 ml min^{-1}) the residence time amounts to about 90 s, a time generally sufficient for a good denitrosation yield of the previously considered non-volatile nitrosamines at temperatures just above 50–60°C [2,3]. By enhancing the temperature of the reactor both peak broadening and tailing are decreased ($\sigma < 5$ s, $\tau/\sigma_G < 1.3$, respectively). The iodide reagent concentration should not be higher than $(1–2) \times 10^{-3}$ M; this choice helps to control broadening and tailing effects within the above limits even at ambient temperature of the reactor. The limited value of the reagent concentration helps to reduce the background current to at least one order of magnitude less than in the case of the Ce(IV) reagent [2]. As a consequence, the noise, which appears mainly as a low-frequency fluctuation of the background current (pumping pulsation), is substantially lower and the theoretical limit of detection amounts to about 1×10^{-8} M. This limit corresponds to a minimum detectable amount of nitrite of about 10 pg in the 20 μl sample loop.

3.6. The use of the iodide reagent as an alternative to Ce(IV)

As mentioned above, in previous work [2] Ce(IV) acidic solutions were employed for the detection of nitrite (nitrous acid) released by the denitrosation of non-volatile nitrosamines. Ce(IV) is a strong oxidant, and on using its solutions as flow reagent one must operate at the very high potential values where the Ce(III) product can be efficiently oxidized. However, under those conditions, very low values of the limit of detection of nitrite cannot be obtained, due to the not negligible background current, mainly arising from unavoidable Ce(III) traces present in the reagent. In contrast, the iodide reagent does not suffer from troubles of this kind, provided an effective deoxygenation is performed. Moreover, the triiodide–iodide couple is highly reversible, and this is a remarkable advantage for biamperometric detection modes.

A direct comparison was made by injecting nitrite into the FI manifold both on flowing Ce(IV) and I^- reagents under the same experimental conditions. Of course, both electrochemical parameters (e.g., applied potential) and intrinsic properties of the hydrodynamic analyte units (e.g., diffusion coefficients, solvation state, etc.) were different, but the general geometric and hydrodynamic parameters of the flow system (flow-rate, kinematic viscosity, etc.) were the same.

The results exhibit a slightly better response sensitivity with Ce(IV), but the detection limit with iodide is at least one order of magnitude lower, due to the smaller noise (see above). The ratio of current sensitivities $S(\mathrm{Ce(III)})/S(I_3^-)$ experimentally obtained by reacting nitrite with the two reagents was found to amount to 1.16. This value can be compared with that calculated by the following approach. The limiting current in a thin-layer rectangular-channel cell is given by the following equation [11] :

$$i_l = 1.47 \cdot nFAD^{2/3}C^{\circ}l^{2/3}U^{1/3} \qquad (7)$$

where n is the number of electrons, A is the electrode area, D is the diffusion coefficient, L is the length of the cell and U is the flow velocity. On changing the reactor product from Ce(III) to I_3^-, the n value changes from 1 to 2, and the diffusion coefficients from 5.2×10^{-6} cm^2 s^{-1} to 1.11×10^{-5} cm^2 s^{-1} [12,13]; based on the stoichiometry of the two reactions, which leads to $C^{\circ}(\mathrm{Ce(III)})/C^{\circ}(I_3^-) = 4$, one finally gets:

$$S(\mathrm{Ce(III)})/S(I_3^-) = i_l(\mathrm{Ce(III)})/i_l(I_3^-) = 1.2$$

a value which is in good agreement with the above reported experimental one.

Peak shapes are similar in the two cases, although the peaks are a bit sharper if Ce(IV) is used. This finding can be ascribed to the above discussed adsorption effect of the analyte I_3^- on the PCR walls, and can be considered as a further confirmation of our hypothesis.

4. Conclusions

The use of iodide solutions in 0.5 M sulphuric acid as the flow reagent for the amperometric detection of the nitrite produced in the warm acid denitrosation of non-volatile nitrosamines has been investigated in a two-lines flow manifold coupled to a flow-through voltammetric detector.

Peak current signals for FI of iodate, taken as a reference analyte for iodine production, and of nitrite were recorded in a variety of experimental conditions: different carrier liquids, water and water–acetonitrile mixtures, different reactor temperatures and different iodide reagent concentrations. The different characteristics of the FI signals obtained for the two analytes are ascribed to the possible adsorption–desorption phenomena of the electroactive I_3^- product on the walls of the reactor system.

An analysis of the results including peak height, peak area and time-domain parameters (peak variances) by using the EMG model strongly supports the above hypothesis and evidences the role of the different rates of the iodate–iodide and nitrite–iodide reactions on the FI signal shape. Moreover, the above analysis suggests that, in general, the use of peak areas, instead of peak heights, which is much more usual in chromatography than in FIA, could give more reliable and reproducible data, due to the smaller dependence of the peak area on such spurious phenomena as analyte adsorption.

From the point of view of the analytical application for nitrosamines determination the use of iodide reagent offers some advantages over Ce(IV), although it requires a rigorous deoxygenation of the solutions. By performing the analytical operations at relatively high reactor temperatures ($T > 50$–60°C), as required to reach a good conversion yield of the denitrosation reactions in the above defined flow conditions, peak broadening and tailing effects for nitrite are limited and comparable with those obtained with Ce(IV). However, the much lower background current found at the "mild" working potential for I_3^- detection helps to reach detection limits for nitrite lower by about one order of magnitude (about 1.0×10^{-8} M).

Further work is in progress along the indicated lines.

Acknowledgments

This work has been financially supported by the Italian Consiglio Nazionale delle Ricerche (CNR) and by the Italian Ministero dell'Università e della Ricerca Scientifica e Tecnologica (MURST).

References

[1] G.A. Sacchetto, P. Pastore, G. Favaro and M. Fiorani, Anal. Chim. Acta, 258 (1992) 99.
[2] G. Favaro, G.A. Sacchetto, P. Pastore and M. Fiorani, Anal. Chim. Acta, 273 (1993) 457.
[3] S.H. Lee and L.R. Field, J. Chromatogr., 386 (1987) 137.
[4] P.G. Desideri, L. Lepri and D. Heimler, in A.J. Bard (Ed.), Encyclopedia of the Electrochemistry of the Elements, Vol. 1, Dekker, New York, 1973, p. 104.
[5] A. Hulanicki, W. Matuszewski and M. Trojanowicz, Anal. Chim. Acta, 194 (1987) 119.
[6] S.H. Brooks, D.V. Leff, M.A. Hernandez Torres and J.G. Dorsey, Anal. Chem., 60 (1988) 2737.
[7] S.H. Brooks and J.G. Dorsey, Anal. Chim. Acta, 229 (1990) 35.
[8] R. Woods, in A.J. Bard (Ed.), Electroanalytical Chemistry, Vol. 9, Dekker, New York, 1976, p. 119.
[9] W.J. Plieth, in A.J. Bard (Ed.), Encyclopedia of the Electrochemistry of the Elements, Vol. VIII-5, Dekker, New York, 1978, p. 369.
[10] J. Ruzicka and E.H. Hansen, Flow Injection Analysis, Wiley, New York, 2nd edn., 1988, p. 135.
[11] K. Stulik and V. Pacakova, Electroanalytical Measurements in Flowing Liquids, Ellis-Horwood, Chichester, 1987, p. 60.
[12] T.H. Randle and A.T. Kuhn, J. Chem. Soc., Faraday Trans. 1, 79 (1983) 1741.
[13] P.G. Desideri, L. Lepri and D. Heimler, in A.J. Bard (Ed.), Encyclopedia of the Electrochemistry of the Elements, Vol. 1, Dekker, New York, 1973, p. 106.

ELSEVIER

Analytica Chimica Acta 294 (1994) 261–270

ANALYTICA CHIMICA ACTA

Voltammetric studies of composite ceramic carbon working electrodes

G. Gun, M. Tsionsky, O. Lev *

Division of Environmental Sciences, Fredy and Nadin Herrmann School of Applied Science, The Hebrew University of Jerusalem, Jerusalem 91904, Israel

Received 16th December 1993; revised manuscript received 24th February 1994

Abstract

Sol-gel derived indicator ceramic carbon electrodes (CCEs) made of graphite powder entrapped in hydrophobically modified silica gel are presented. Voltammetric characteristics of the electrodes are compared with other classes of graphite electrodes. Background current, double layer capacitance and metrological characteristics, including renewal repeatability, interelectrode reproducibility and operational stability for various solvents are presented. The indicator CCEs exhibit better stability than carbon paste electrodes and their renewal is easier and more reproducible than that of glassy carbon electrodes.

Key words: Voltammetry; Ceramic carbon electrodes

1. Introduction

The high conductivity, relative inertness and wide operational voltage window of graphite in aqueous solution gave rise to a phalanx of carbon based electrodes. Different forms of monolithic carbon electrodes, such as glassy carbon and graphite rods, carbon pastes and solid composite carbon electrodes (composed of graphite powder dispersed in organic polymers) are routinely used for electroanalytical applications. Carbon paste electrodes made of graphite powder mixed with paraffin oil, nujol, or some other viscous and hydrophobic oil [1] proved to be suitable for many electroanalytical applications [2] due to their simple preparation procedures and the ease of surface renewal after contamination. However, application of carbon paste electrodes is practically confined to aqueous solutions, and their low operational stability and interelectrode reproducibility limit their usefulness in liquid chromatography (LC), flow-injection analysis (FIA) and other routine electroanalytical applications, especially when a long operational lifetime is required. Solid composite carbon electrodes, including, for example, different types of carbon powders immobilized in poly(chlorotrifluoroethylene) [3], silicone rubber [4], PTFE [5], polyethylene [6], polyacrylonitrile foam [7], epoxy resin [8], crosslinked polystyrene [9], crosslinked polyacrylamide [10] and other organic materials [11] exhibit a voltammetric response of microelectrode

* Corresponding author.

0003-2670/94/$07.00 © 1994 Elsevier Science B.V. All rights reserved
SSDI 0003-2670(94)00146-D

ensembles and their surface can be renewed by polishing. However, even this class of solid composite electrodes suffers from the inherent disadvantages of the organic polymer supports.

The evolution of sol-gel technology, a fusionless method for the synthesis of ceramic [12] and organically modified ceramic materials [13] created new possibilities for the production of photometric [14] and electroanalytical sensors [15–17]. In a recent article [18] we introduced a new class of sol-gel derived composite carbon–silica electrodes. The electrodes are comprised of graphite powder, homogeneously dispersed in modified silica matrices. It was demonstrated that by changing of the silicon precursors the porous electrodes can exhibit hydrophobic or hydrophilic surface properties. Hydrophilic electrodes (made, e.g., of tetramethoxysilane or 2-cyanoethyltriethoxysilane precursors) are water permeable, and therefore useful when large surface area electrodes are desirable (e.g., electrocatalysis, and some reference electrodes). When hydrophobic glass forming precursors (e.g., methyltrimethoxysilane or diphenyldimethoxysilane) are used the electrode surface repels water, leaving only the outermost section of the electrode exposed and active. Electroanalytical applications of modified hydrophobic ceramic carbon electrodes (CCEs) are discussed elsewhere [18,19]. In this paper, the voltammetric characteristics of the indicator CCEs are explored and compared with other classes of graphite electrodes.

2. Experimental

2.1. Materials

All the organosilanes were purchased from ABCR Inc. (Karlsruhe). High-purity carbon powder (ca. 10–20 μm) was purchased from Ultra

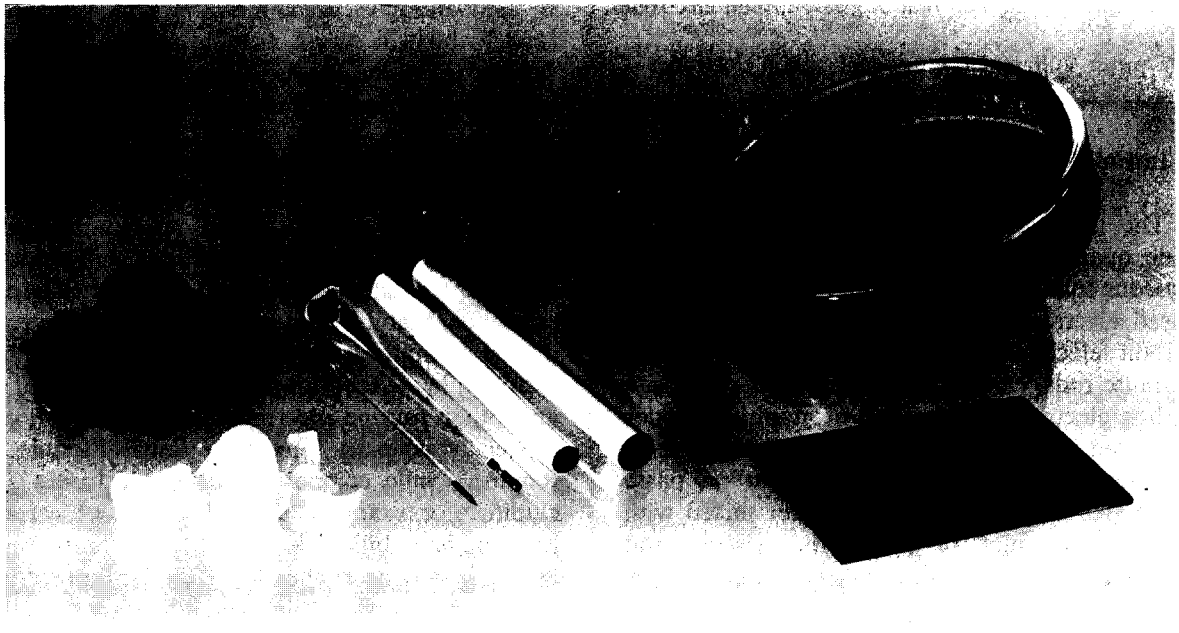

Fig. 1. Sol-gel derived electrodes: from left to right, carbon powder, sol-gel derived silica monoliths, miniature sol-gel electrode, monolithic rod electrodes, unsupported flat CCE plate (before polish), the casting petri dish and polished thin layer of silica–carbon material on a supporting glass

Carbon Co. (Bay City, MI). Glassy carbon, 3 mm diam. was obtained from Atomergic Chemicals (Farmingdale, NY). Platinum foil (99.99% purity) was purchased from Alfa. Unless otherwise specified analytical grade reagents and triply distilled water (resistivity greater than 20 MΩ/cm) were used.

2.2. Apparatus

An EG&G PARC Model 273 potentiostat-galvanostat, in conjunction with a Watanabe WX 4421 x-y recorder was used for voltammetric and steady state studies. A three-electrode cell, equipped with a Pt-flag counter and a saturated calomel electrode (SCE), was used. AC experiments were conducted using an EG&G PARC Model 378 AC impedance analyzer. Fast scan rate cyclic voltammetry (CV) experiments were conducted using an Ensman 400 bipotentiostat. All experiments were conducted under ambient conditions at ca. 25°C. Scanning electron microscopic (SEM) studies were conducted using an SEM-505 apparatus from Philips, operated at 200 kV.

2.3. Electrode preparation

Preparation of indicator electrodes

Several types of indicator electrodes made of different organic derivatives of trimethoxysilane were used. A typical preparation procedure was as follows: 1.5 ml of methanol (Frutarom, Haifa), 1.0 ml of methyltrimethoxysilane and 0.05 ml of hydrochloric acid (11 M) catalyst were mixed for 2 min, followed by the addition of 1.25 g of carbon and shaking for another minute. A 3×1 mm i.d. capillary was filled with the sol-gel carbon mixture and allowed to dry overnight under ambient conditions (ca. 25°C). Additional water for the hydrolysis step was provided by air humidity. Less acidic catalysis failed to produce rigid monoliths (or films) and yielded only silica covered carbon powder. [Strong base catalysis (> ca. 0.05 ml 10 M NaOH for the above procedure) yielded another range of suitable operating conditions, which will not be discussed here]. After drying, the electrode was polished with 600 grit polishing paper and polished gently by wiping the surface with weighing paper. Electrical contact was made by silver paint (Bio-Rad, A1208 Q-D colloidal silver).

A similar preparation procedure was used for preparation of other electrode configurations (Fig. 1) including, for example, carbon ceramic rod electrodes in different dimensions, miniature electrodes, flag electrodes made of a composite carbon–silica layer deposited on an insulating substrate or carbon coated electrodes made of glassy carbon covered by the composite material. The resulting electrodes were rigid, black and shiny (though not mirror-like), and had the shape and dimensions of the moulding vessels. The adhesion of the CCE to the capillary or the supporting (glass or carbon) substrate was good and channelling of the analyte along paths between the electrode and the capillary was never observed. The conductivity of the carbon silica composite material was approximately 1.0 mho cm^{-1}.

Electrode characteristics were relatively insensitive to the moulding procedures. Changes in the amount of acid catalysts (within the 0.05–1.0%, v/v, range of 11 M HCl in the starting solution) and change of water content (in the 1–25%, v/v, range) affected the electrode conductivity by less than 20%. However, when excess amount of water and a low acid–methyltrimethoxysilane ratio were used, a composite powder was formed instead of the desirable monolith.

Preparation of carbon electrodes

Three types of carbon electrodes were used for comparison. (1) Glassy carbon: a 3-mm diam. glassy carbon rod was placed in a glass tube and sealed by Torr-Seal epoxy (Varian, Lexington, MA). The electrode was polished with emery paper and 0.05 μm alumina powder (Buehler). (2) Graphite rod electrodes: graphite rods of ca. 1 cm (Alfa, Danvers, MA) were coated with Torr-Seal epoxy and polished according to the previous procedure. (3) Carbon paste electrodes: 0.3 g of carbon powder was mixed with 0.1 ml of paraffin oil and filled into 0.3 mm diam. glass capillaries. The electrodes were was wiped with weighing paper.

3. Results

3.1. SEM Studies

SEM micrographs of the surface of an indicator composite carbon electrode, prior to and following mechanical polishing are depicted in Fig. 2A and B. The micrographs show bare electrodes that were not spattered by an additional conductive layer. The conductivity of the carbon composite electrodes was sufficient to allow direct SEM analyses despite of the thin film of silica that covered the carbon particles prior to the mechanical polishing step. The ca. 10–20 μm carbon particles can be seen on the unpolished surface, but could hardly be distinguished on the surface of the polished electrodes, which, however, remained rough with > 0.1 μm ripples even after polishing (Fig. 2B).

3.2. Operating potential range in aqueous solution

Fig. 3 demonstrates the cyclic voltammograms of four types of graphite electrodes in 1 M HCl

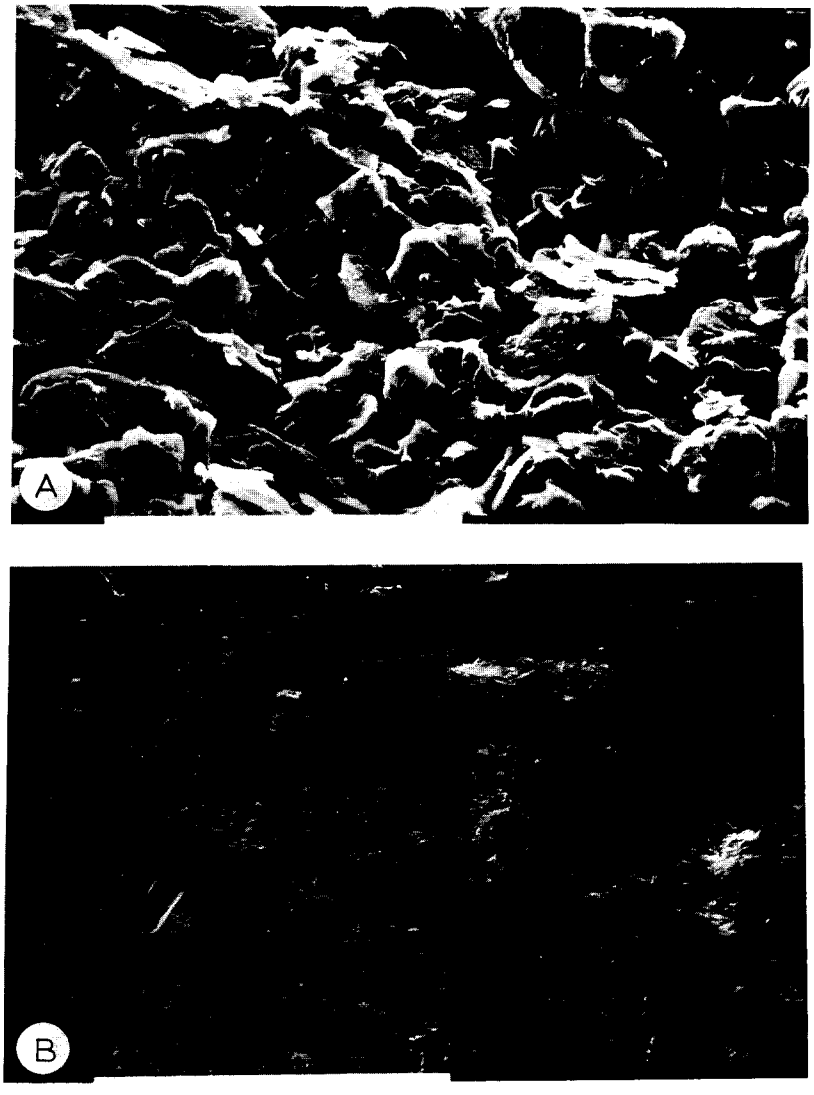

Fig. 2. SEM (200 kV) micrographs of silica carbon composite surface, (A) before and (B) after polishing. Bar = 100 μm.

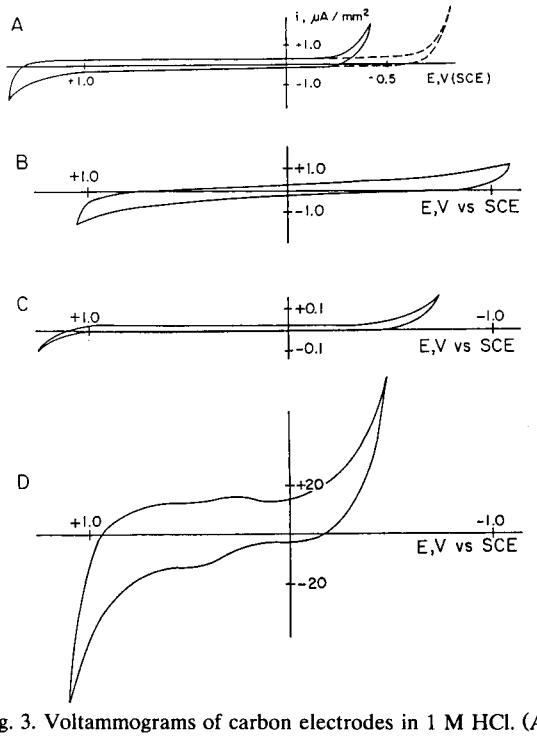

Fig. 3. Voltammograms of carbon electrodes in 1 M HCl. (A) Carbon–silica (dotted line represents deoxygenated conditions); (B) glassy carbon; (C) carbon paste; (D) graphite rod electrodes.

solution (scan rate = 100 mV/s) under nitrogen bubbling. Since the CCE electrodes are porous it was necessary to strip the oxygen not only from the solution but also from the bulk of the electrode before the experiment. This was done by introducing nitrogen through the back of the electrode (using a needle of a syringe to lead the purging gas through the conducting glue at the back of the electrode) or by an extended period of oxygen reduction (at −0.5 V vs. SCE) in nitrogen-bubbled solution. Fig. 3A depicts CCE voltammograms of a deoxygenated solution before and after oxygen removal from the bulk of the electrode. The cathodic operation range was extended by more than 200 mV by this procedure. The oxygen evolution took place at ca. 1200 mV vs. SCE in all four classes of electrodes. The cathodic overpotential (measured at the point where the current reaches twice its background level) of the CCE was similar to that of the carbon paste electrode. However, the CCEs exhibited steeper CV curves in the water splitting regions due to their larger active-to-geometrical surface area ratio. The cathodic overpotential of the CCE (ca. −700 mV) was smaller than that of glassy carbon electrodes (ca. −1000 mV), similar to the composite carbon-epoxy electrode (−600 mV [20]) and considerably larger than that of graphite rod (ca. −400 mV), and carbon–silicon (−300 mV [20]) electrodes.

3.3. Background current

Despite the progress in the development of background compensation and noise filters, low background current remains an essential prerequisite for most electroanalytical applications. The background current of graphite electrodes is contributed to by double layer charging and surface Faradaic reactions involving surface oxide groups (e.g., ketones, enols, and carboxylic groups) located at edge planes on the graphite structure [21]. Slow and fast scan rate voltammetry were used in order to compare the charging currents and the double layer capacitance of the four types of graphite electrodes. The observed capacity, C_{obs}, at 100 mV/s (CV) was calculated directly from Fig. 3 according to $C = i/v$, where i is the average cathodic and anodic current density, and v is the scan rate. The observed capacity was

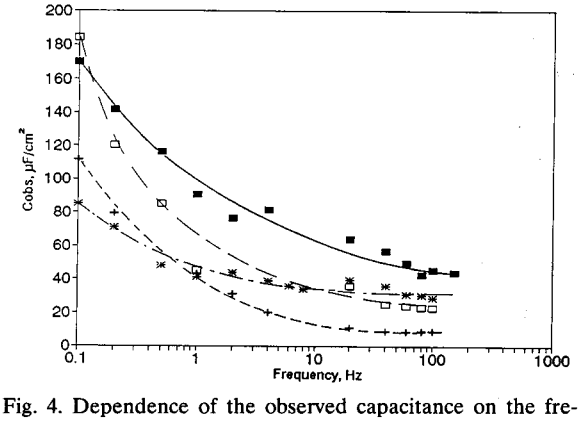

Fig. 4. Dependence of the observed capacitance on the frequency of the applied scan rate (1 M HCl; 100 mV amplitude triangular waveform). ■ = GC; □ = CCE; + = carbon rod/10; * = carbon paste.

Table 1
Double layer and charging capacity of carbon electrodes in 1 M HCl solution

Graphite electrode type	C_{dl} (μF/cm^2)	C_{obs} (μF/cm^2)
CCE	45.0	90.0
Glassy carbon	23.0	64.0
Carbon paste	3.0	4.0
Graphite rod	89.2	430.0

C_{obs} = Observed capacity at 100 mV/s scan rate.
C_{dl} = Electrode double-layer capacitance estimated by high scan rate small amplitude triangular wave experiment.

approximately uniform over the whole working potential range and despite the rough surface (observed in Figure 2) it was only 100 μF/cm^2 for the CCE. The glassy carbon and the silica–carbon electrodes exhibited approximately the same charging currents, which were intermediate to the favourable performance of the carbon paste electrode and the inferior performance of the graphite rod electrodes.

The dependence of the observed capacity (calculated as above) on the scan rate was determined by application of 100 mV peak-to-peak triangular waveforms and determination of the observed capacity from the square wave current response. The dependence of the observed capacities of the four model electrodes is presented in Fig. 4, which reveals that the choice of the 100 mV/s scan rate for determination of the observed capacity was somewhat arbitrary, since the observed capacity in this region is highly dependent on the voltammetric scan rate. At high scan rates (above 5 V/s) the observed capacity became practically independent of the applied scan rate. An estimate of the double layer capacitance can be obtained by the above equation for the high scan rate region according to Gileadi's technique [21,22].

Table 1 compares the estimates of the double-layer capacitance and the observed capacity at 100 mV/s of the four electrodes. In both the fast and slow scan rate methods, the observed capacities of the CCE and the glassy carbon electrode

Table 2
Formal CCE potentials of selected redox couples (mV vs. SCE)

Experimental data				Literature data	Ref.
Compounds	Conditions	$E^{0\prime}$	ΔE	Potential	
$Fe(CN)_6^{4-}/Fe(CN)_6^{3-}$	1 M HCl	+460	60	E_0 = +450 (1 F H_2SO_4)	23
$Mo(CN)_8^{3-}/Mo(CN)_8^{4-}$	pH 4.8	+490	90	E_0 = +480 (neutral medium)	24
$IrCl_6^{2-}/IrCl_6^{3-}$	1 M HCl	+700	60	E_0 = +700 (1 M HCl + 1 M NaCl)	24
$Ru(NH_3)_6^{3+}/Ru(NH_3)_6^{2+}$	0.1 M Acetate buffer (pH 4.6)	−265	70	E_0 = −290 (0.1 M $NaBF_4$)	24
I^-/I_2	1 M HCl	+400	160	E_0 = +380 (0.1 M HCl)	24
$Co(phen)_3^{3+}/Co(phen)_3^{2+}$	1 M HCl	+120	60	E_0 = +140 (1 M KCl)	24
$Fe(EDTA)^-/Fe(EDTA)^{2-}$	1 M KNO_3	−120	80	E_0 = −119 (neutral medium)	25
$Ru(bpy)_3^{3+}/Ru(bpy)_3^{2+}$	1 M HCl	+1000	60	E_0 = +1023 (neutral medium)	25
Fc	pH 7	+195	70	E_0 = +200 (neutral medium)	25
FcCOOH	pH 7	+295	80	E^0 = +290	26
1,4-Benzoquinone	1 M HCl,	+455	30	E^0 = +458	27
	pH 7.3	+35	30		
1,4-Naphthoquinone	1 M HCl,	+230	30	E^0 = +229	27
	pH 7	−190	30		
9,10-Phenanthroquinone	1 M HCl,	+200	30	E^0 = +201	27
	pH 7	−220	30		
Alizarin Red S	1 M HCl	−160	45	E^0 = −169	27
Toluidine Blue	1 M HCl,	+270	80	E^0 = +293	27
	pH 7.2	−235	90		
Methylene Blue	1 M HCl,	+265	60	E^0 = +284	27
	pH 7.2	−215	75		

$\Delta E \equiv E_{pa} - E_{pc}$; $E^{0\prime} \equiv \frac{1}{2}(E_{pa} + E_{pc})$; E_0 = formal potential; E^0 = standard potential. phen = 1,10-phenanthroline; bpy = 2,2′-bipyridyl; Fc = ferrocene.

were similar and intermediate to that of the carbon paste and graphite rod electrodes.

3.4. Generality

Table 2 depicts key voltammetric characteristics of representative inorganic, organic and organometallic redox couples. Despite the relative fast scan rate (100 mV/s) employed, most systems exhibited an almost reversible response and the peak potential separations were close to the expected 59 and 28.5 mV. Table 2 also compares the average anodic and cathodic peak potentials $[E'_0 = (E_{p,a} + E_{p,c})/2]$ with formal potentials reported for other carbon electrodes (E_0) or with standard redox potential values ($E°$). Indeed, the E'_0 values closely match the literature data [23–27], and the small deviations from the reported formal potential values can be attributed to kinetic effects that increase peak separation and also distort the symmetry of the cathodic and anodic waves. The deviations from the standard potential values were indeed larger due to ionic strength effects.

Fig. 5 demonstrates typical CV studies (100 mV/s, 1 M HCl) of hexacyanoferrate solutions using the composite carbon electrode. Reversible waveforms were obtained over two decades of concentrations (0.1–10 mM). A linear graph (Fig. 5B) describes the concentration–current dependence. The effective diffusion coefficient, D, can be estimated from

$$i_p = (2.69 \times 10^5) n^{3/2} A D^{1/2} v^{1/2} C \qquad (1)$$

$D = (D_o D_r)^{0.5}$ (cm^2/s); where D_r and D_o represent the diffusion coefficients of hexacyanoferrate(II) and -(III), respectively, and A is the surface area of the electrode (cm^2).

Fig. 6 demonstrates voltammograms obtained at constant concentration (1.0 mM in 1 M HCl) and various scan rates. Reversible electrode response was observed even at high sweep rates. Fig. 6B demonstrates the peak current–scan rate dependence. The effective diffusion coefficient, D, can also be estimated by Eq. 1. The diffusion coefficient calculated by the variable concentration experiment ($D = 5.8 \times 10^{-6}$ cm^2/s, $r = 0.997$, $n = 17$) falls within 5% of that calculated by the i–$v^{0.5}$ ($D = 5.6 \times 10^{-6}$ cm^2/s, $r = 0.998$, $n = 10$) dependence. In both cases the calibration graphs were independent of the direction of changes in concentration or sweep rates, which indicates the low ion-exchange capacity of the electrode surface.

3.5. Reproducibility

The renewal and preparation reproducibility of indicator CCEs were examined. Renewal re-

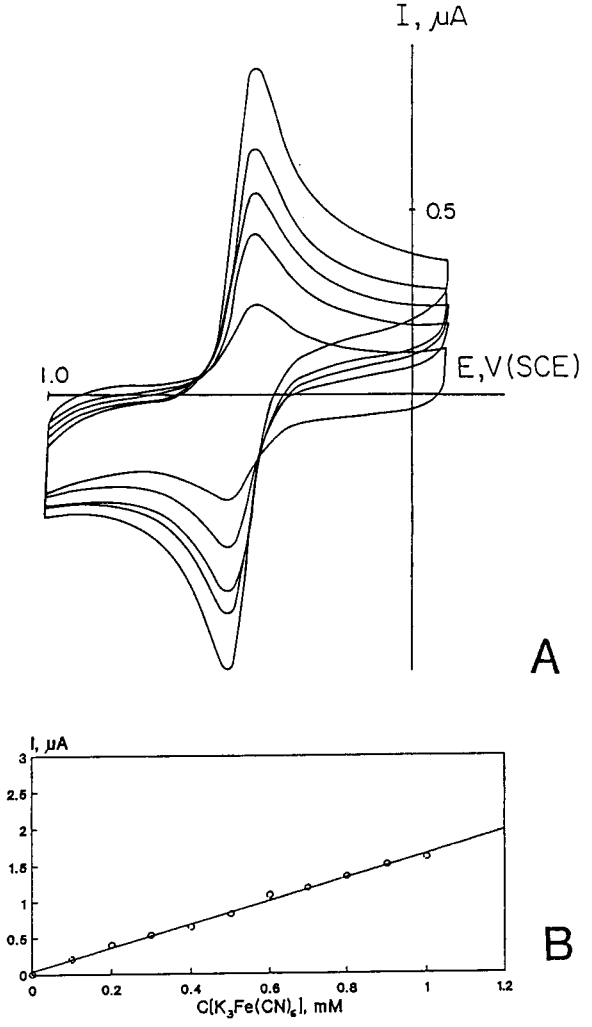

Fig. 5. (A) Cyclic voltammetry of several concentrations of hexacyanoferrate solutions (0.1, 0.2, 0.3, 0.4, 0.5 mM in 1 M HCl) and (B) cathodic peak current–concentration dependence.

peatability was checked by subjecting the same CCE to 10 cycles of renewal protocol that included surface roughening (with rough emery paper), surface polishing and smoothening followed by measurement of the background current (at 100 mV/s, 1 M HCl) and of the peak current of 1.0 mM hexacyanoferrate(III) in 1 M HCl. These studies revealed a 4.6% relative standard deviation (R.S.D.) in the measurement of the Faradaic current (or hexacyanoferrate concentration), and 4.2% R.S.D. in the measurement of the background current. Interelectrode reproducibility was evaluated by measurement of the background current (in 1 M HCl solution) and the hexacyanoferrate cathodic peak current using eight different electrodes prepared from the same batch of CCE precursors. The R.S.D. values were 5.0 and 4.8% for the peak current and the background current, respectively. The interelectrode and the renewal repeatability studies indicate that in spite of their rough surface (Fig. 2B) and heterogeneous composition, the geometric and active surface areas and surface composition are relatively insensitive to minor changes in preparation procedure. Thus, pre-prepared electrodes can be used even without prior calibration, and for some electroanalytical applications contaminated CCEs can be polished and renewed even without recalibration.

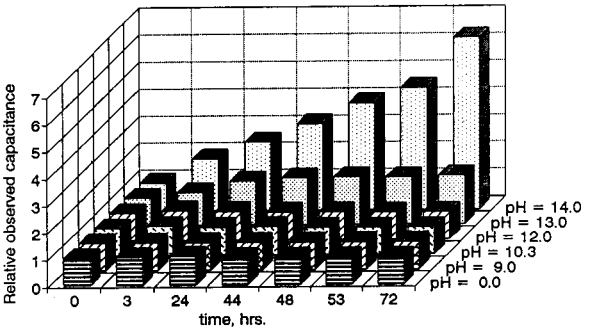

Fig. 7. Stability of the double layer capacity of CCEs in acid and base solutions.

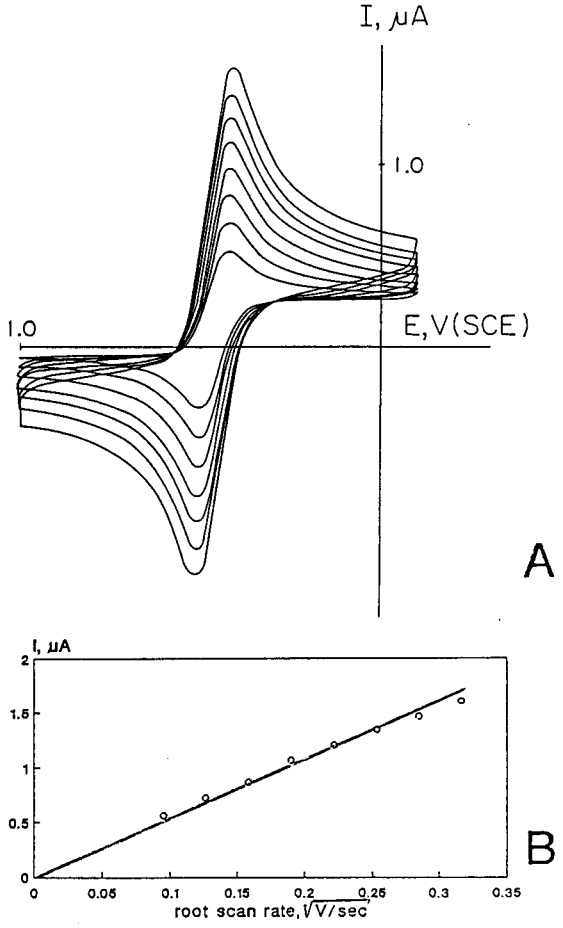

Fig. 6. A) Cyclic voltammograms of 1 mM hexacyanoferrate solutions (scan rate = 9, 16, 25, 36, 49, 64, 81, 100 mV/s) and (B) cathodic peak current–scan rate dependence.

3.6. Stability in aqueous solutions

The low stability of high surface area silica gel in basic solutions is well known. Therefore, it was interesting to investigate the stability of the response of modified silica carbon electrodes as a function of pH. The investigation was conducted by immersing CCEs in different pH solutions and recording the change in double layer capacity (C_{dl}) versus time. The double layer capacity is sensitive to minute changes in both surface area and surface characteristics, and can therefore probe minor changes in electrode surface better than the CV peak currents, which are more sensitive to changes in the geometric cross section area. Fig. 7 depicts the changes of C_{dl} normalized by its initial value ($C_{dl}/C_{dl,0}$) versus time. The

dimensionless presentation compensates for small interelectrode changes and for the effect of the changes in ionic strength on the initial values of the double layer capacity. The CCEs are very stable in acidic solution over periods of several weeks (not shown in Fig. 7), and can be used for prolonged operation even in basic conditions (pH 12).

3.7. Stability in mixed solvents

The relative instability of carbon paste electrodes in non-aqueous solutions hinders their application in instrumental flow-injection analysis and liquid chromatography, and in applications which require water–organic solvent mixtures. The stability of the hydrophobic CCE was determined by measurements of the electrode capacity (C_{dl}) during prolonged immersion in mixed solvents. Fig. 8A–C demonstrates the changes in double layer capacitance which is used as a measure of electrode deterioration. Different mixtures of aqueous 1 M HCl with acetonitrile, dimethylformamide or methanol were tested. The observed double layer capacitance was normalized relative to the C_{dl} of the same electrode in aqueous 1 M HCl. Fig. 8 illustrates the fact that the electrodes are stable in aqueous solutions containing up to 25% acetonitrile, 25% dimethylformamide and 50% (v/v) methanol. When these values are exceeded the electrode active surface increases gradually. For example, Fig. 9 demonstrates a voltammogram of 0.1 mM $K_4Mo(CN)_8$ in methanol–1 M aqueous HCl (1:1) immediately after immersion in the solution and after 48 h. The electrode maintains its (quasi-reversible) CV behaviour, though under such prolonged operation a recalibration of the electrode is required. The paraffin–carbon paste electrode was totally inoperable in this solution, though Svancara et al. [28] reported use of silicon oil–carbon paste electrodes in methanol–water (50:50) (the long term operational stability was not reported).

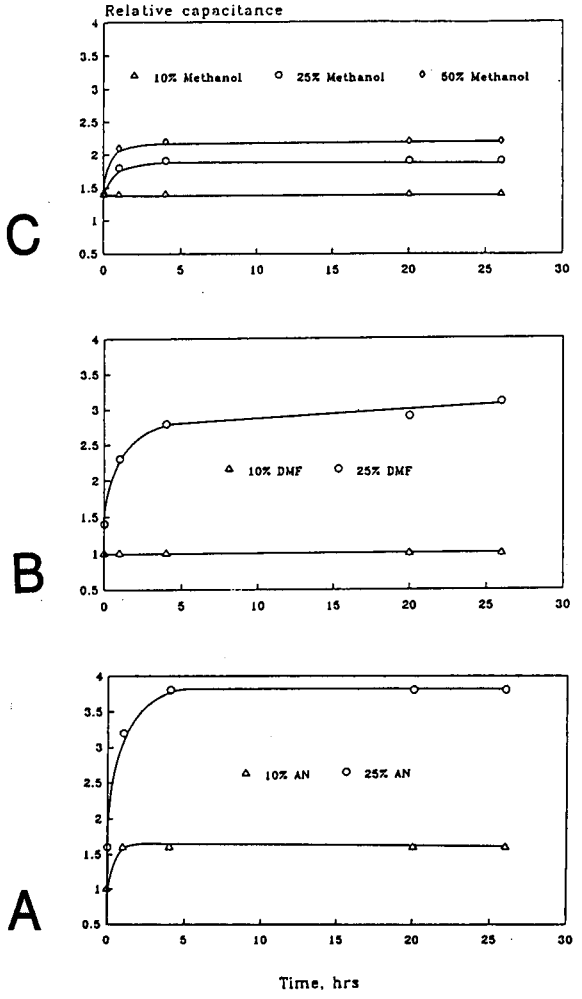

Fig. 8. Stability of CCE electrodes in mixed solvents. (A) Acetonitrile, (B) dimethylformamide and (C) methanol–water solutions.

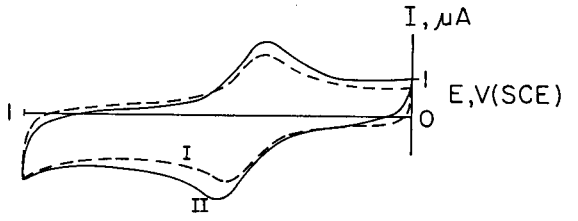

Fig. 9. Cyclic voltammograms of 0.1 mM $K_4Mo(CN)_8$ in methanol–water (1:1) immediately after immersion (I) and after 48 h (II).

4. Conclusions

Porous hydrophobic sol-gel derived graphite–organically modified silica matrices can be used as indicator "inert" electrodes. The water is re-

jected by the hydrophobic carbon and organically modified surfaces, and, despite the presence of the silica network, the electrodes do not adsorb cationic interferences. The electrodes can be manufactured virtually in any configuration, including flat plat geometry, unsupported or supported monoliths and even miniature configurations. The electrodes are therefore most amenable for screen printing technology as well as for specialized applications. Similar to the carbon paste electrodes the indicator CCEs can easily be renewed by mechanical polishing with good repeatability. Despite their rough surface the CCEs exhibit less background current compared with glassy carbon electrodes, though it is still much larger than that of the carbon paste electrodes. The CCEs show good stability and reproducible behaviour in aqueous and mixed solvent solutions.

References

[1] R.N. Adams and K.B. Prater, Anal. Chem., 38 (1966) 153.
[2] S.A. Wring and J.P. Hart, Analyst, 117 (1992) 1215; and references cited therein.
[3] S.L. Petersen and D.E. Tallman, Anal. Chem., 62 (1992) 1215; and references cited therein.
[4] E. Pungor and E. Szepesvary, Anal. Chim. Acta, 43 (1968) 289.
[5] L.N. Klatt, D.R. Connell, R.E. Adams, I.L. Honigberg and J.C. Price, Anal. Chem., 47 (1975) 2470.
[6] D.N. Armentrout, J.D. McLean and M.W. Long, Anal. Chem., 51 (1979) 1039.
[7] J. Wang, A. Brennsteiner and A.P. Sylwester, Anal. Chem., 62 (1990) 1102.
[8] H.S. Swofford and R.L. Carman III, Anal. Chem., 38 (1966) 966.
[9] K.E. Creasy and B.R. Shaw, Anal. Chem., 61 (1989) 1460.
[10] M.A. Lang and J.Q. Chambers, Anal. Chem., 58 (1986) 2872.
[11] J. Wang and J.M. Zadeii, J. Electroanal. Chem., 249 (1988) 339.
[12] (a) G. Scherer and J. Brinker, Sol-gel Science, Academic Press, San Diego, CA, 1990; (b) L.C. Klein (Ed.), Sol-gel Technology for Thin Films, Fibers, Preforms, Electronics and Specialty Shapes, Noyes, Park Ridge, NJ, 1990; (c) L.L. Hench and J.K. West (Eds.), Chemical Processing of Advanced Materials, Wiley, New York, 1992.
[13] G. Philipp and H. Schmidt, J. Non-Cryst. Solids, 63 (1984) 283.
[14] O. Lev, Analusis, 20 (1992) 543; and references cited therein.
[15] O. Dvorak and M.K. De Armond, J. Phys. Chem., 97 (1993) 2646.
[16] V. Glezer and O. Lev, J. Am. Chem. Soc., 115 (1993) 2533.
[17] P. Audebert, P. Griesmar, P. Hapiot and C. Sanchez, J. Mater. Chem., 2 (1992) 1293.
[18] M. Tsionsky, G. Gun, V. Glezer and O. Lev, Anal. Chem., 66 (1994) 1747.
[19] US Pat. Application, 08/080,520 (1993).
[20] G. Dryhurst, in P.T. Kissinger and W.R. Heineman (Eds.), Laboratory Techniques in Electroanalytical Chemistry, Marcel Dekker, New York, 1984
[21] R.L. McCreery, in A.J. Bard (Ed.), Electroanalytical Chemistry, Vol. 17, Marcel Dekker, New York, 1990, p. 221.
[22] E. Gileadi and N. Tshernikovski, Electrochim. Acta, 16 (1971) 579.
[23] CRC Handbook of Chemistry and Physics, CRC Press, Boca Raton, FL, 67th edn., 1991.
[24] A.J. Bard, R. Parsons and J. Jordan, Standard Potentials in Aqueous Solutions, Marcel Dekker, New York, 1985.
[25] A.J. Bard, F.-R.F. Fan and M.V. Mirkin, in A.J. Bard (Ed.), Electroanalytical Methods, Marcel Dekker, New York, in press.
[26] A.E.G. Cass, G. Davis, G.D. Fracis, H.A. Hill, W.J. Aston, I.J. Higgins, E.V. Plotkin, L.D.L. Scott and A.P.F. Turner, Anal. Chem., 56 (1984) 667.
[27] W.M. Clark, Oxidation–Reduction Potentials of Organic Systems, Williams and Wilkins, Baltimore, 1960.
[28] I. Svancara, K. Vytras, F. Renger and M.R. Smyth, Electrochim. Acta, 37 (1992) 1355.

ELSEVIER

Analytica Chimica Acta 294 (1994) 271–281

ANALYTICA CHIMICA ACTA

Influence of metal concentration at the electrode surface in differential pulse anodic stripping voltammetry in the presence of humic matter

M.G. Bugarin [a], A.M. Mota [b,*], J.P. Pinheiro [b], M.L.S. Gonçalves [b]

[a] *E.U.I.T.I., calle Conde Torrecedeira 86, 36208 Vigo, Pontevedra, Spain*
[b] *Centro de Quimica Estrutural, Instituto Superior Técnico, 1096 Lisbon Codex, Portugal*

Received 9th December 1993; revised manuscript received 7th February 1994

Abstract

The influence of metal concentration in bulk solution and of deposition time on voltammograms obtained by differential pulse anodic stripping voltammetry in the presence of humic matter is discussed based on the slow diffusion of complexes, adsorption of the ligand on the electrode and ligand to metal concentration ratio during the stripping step. The conditional stability parameters at pH 5, in the bulk solution and in the absorbed layer, are determined. The concentration of adsorbed sites is calculated from the saturation of the sites at the electrode surface with metal ions, estimated either from the critical deposition time or from the height of the shoulder presented in the voltammogram.

Key words: Anodic stripping voltammetry; Humic matter; Metals

1. Introduction

Humic matter, obtained by the slow degradation of dead bioorganisms, plays an important role in the circulation of trace metals in aquatic systems [1,2]. To study complexation reactions in natural water conditions (low concentration of organic compounds and very low concentration of trace metals), many researchers have used anodic stripping voltammetry (ASV) and differential pulse ASV (DPASV) with the hanging mercury drop electrode or thin mercury film electrode [3–10].

To determine speciation parameters of labile complexes from the voltammetric signal a large excess of ligand should be present compared to the total metal concentration (C_M), so that $C_L \approx |L'|$, where C_L and $|L'|$ stands respectively for the total ligand concentration and the ligand concentration not bound to the metal ion [11,12]. It should be noticed that if one of the concentrations, of ligand or of metal, is not in excess compared to the other one, the DPASV peak of labile systems becomes distorted [13]. In stripping techniques the condition $C_L \gg C_M$ is more severe than in direct voltammetry involving one step, because the metal concentration at the electrode surface during the stripping step (C_M^0) is higher than in the bulk solution, and the condi-

* Corresponding author.

0003-2670/94/$07.00 © 1994 Elsevier Science B.V. All rights reserved
SSDI 0003-2670(94)00149-G

tion $C_L \gg C_M^0$ should be verified in order to evaluate correctly the stability of the labile complexes formed.

In the presence of adsorption of the ligand on the electrode distortions on the voltammogram might became visible if the adsorbed ligand concentration is not in excess compared to C_M^0, due to a gradual saturation of adsorbed sites by the metal ion [8].

In this work the influence of the ligand to metal concentration ratio at the electrode surface on the DPASV signal, when adsorption occurs, will be discussed as well as the influence of other factors that also affect the voltammograms, namely [11,12]: (i) rate of the complexation and dissociation reactions, i.e., the lability of the complexes; (ii) diffusion coefficient of the metal species; (iii) heterogeneity of the natural organic ligands due to different complexing groups; (iv) adsorption of organic matter on the electrode. Some of those concepts (lability, heterogeneity and surface concentration effect) will be outlined below.

1.1. Lability

Lability is associated with the kinetics of complex dissociation, when the metal M is consumed at the electrode surface [11,12,14]. The complexes ML will be labile if the dissociation process is fast compared with the time scale of the technique, so that the thermodynamic equilibrium of ML dissociation is maintained at the electrode surface during the redox process. For labile complexes the voltammetric signal (i_p) will be related to the total metal concentration and the shift observed in the peak potential in the absence and presence of ligand (ΔE_p) takes into account the complexation affinity.

If ML has no time to dissociate, however, within the time scale of the technique when M is consumed (inert complex), ΔE_p will be zero in direct voltammetry and i_p will be proportional to the free metal concentration in the bulk solution for direct or stripping voltammetry.

It is worthwhile emphasizing that lability should not be confused with reversibility. The concept of reversibility is associated to the kinetics of the electrochemical reaction, the redox couple being reversible if the equilibrium is attained for all potentials within the time scale of the technique [11,12,14].

1.2. Heterogeneity

The thermodynamic meaning of the stability constant K_{ML} defined for a simple ligand L is lost for heterogeneous ligands with a large number of complexing sites; in this case the determination of K_{ML} leads to a mean stability parameter ($\bar{K}$) of all occupied sites over all site concentrations. Since the metal ion binds first with the strongest complexing sites of the ligand, $\bar{K}$ decreases with increase of the total metal concentration. To interpret in a better way the heterogeneity of organic matter the differential equilibrium function, K_{DEF} [1,15], can be determined instead of $\bar{K}$. In fact K_{DEF}, calculated on each point of a titration of the ligand with a metal ion or vice versa, includes a small range of sites around the corresponding titration point and therefore is more selective than $\bar{K}$. In the presence of a constant C_L value, K_{DEF} is given by:

$$K_{DEF} = -\frac{\alpha^2}{C_M}\left(\frac{1}{1+(\alpha-1)\,\mathrm{d}\ln C_M/\mathrm{d}\ln\alpha}\right) \quad (1)$$

where $\alpha = C_M/|M|$; C_M and $|M|$ are respectively the total metal concentration and the free metal ion concentration.

The degree of heterogeneity, Γ, can be determined from K_{DEF} assuming the Freundlich isotherm [16], as indicated by Eq. 2, where θ is the degree of occupation of ligand sites.

$$\Gamma = -\mathrm{d}\log\theta/\mathrm{d}\log K_{DEF} \quad (2)$$

Γ can vary between 0 and 1, where 0 corresponds to an infinitely broad distribution of K_{DEF} and 1 to a simple ligand.

1.3. Surface concentration effect

To evaluate complexing parameters from voltammetric measurements the concentration of the ligand not bound to the metal ($|L'|$) at the electrode surface should be the same as in the

bulk solution, i.e., $|L'|^0 \approx |L'| \approx C_L$, where C_L represents the total ligand concentration and the superscript 0 the concentration at the electrode surface. To satisfy this condition to within 5% the following relations should be verified: $C_L/|ML| \geq 20$ for voltammetry involving only one step (e.g., differential or normal pulse polarography), and $C_L/|ML|^0 \geq 20$ for stripping techniques (e.g., ASV, DPASV), where $|ML|$ represents the metal concentration bound to the ligand. These conditions implies that in the presence of strong complexation $C_L/C_M \geq 20$ and $C_L/C_M^0 \geq 20$, respectively.

The theoretical value of C_M^0 can be estimated from Eq. 3 [17], deduced in the absence of ligand, for reversible redox couples; its validity in the presence of complexants was confirmed with the system Pb(II)–triethylenetetraamine, which forms labile complexes with $D_{ML} \approx D_M$ [13].

$$C_M^0 = 2.3\frac{(D_M D_r)^{1/2}}{\delta R} t_d C_M \qquad (3)$$

The parameters D_{ML}, D_M and D_r are, respectively, the diffusion coefficients of the complex, of the metal ion in solution and of the amalgamated metal, R is the mercury drop radius, δ the thickness of the diffusion layer in solution during the deposition step, t_d the deposition time, and C_M the metal ion concentration in the bulk.

For typical parameter values ($t_d = 180$ s, $R = 0.04$ cm, $D_M \approx D_r \approx 10^{-5}$ cm^2 s^{-1} and $\delta = 2 \times 10^{-3}$ cm) it can be seen that $C_L/C_M^0 \geq 20$ corresponds to $C_L/C_M \geq 1000$.

For a labile and homogeneous system with $D_{ML} \approx D_M$ (the redox couple M^{n+}/M^0 being electrochemically reversible), and using different C_L/C_M values, obtained for the same C_L but different C_M and/or t_d values, it was shown that [13]:

(a) When $C_M \times t_d$ is so small that C_M^0 is negligible compared with C_L the peak heights and widths are the same as those obtained in the absence of ligand, and E_p is shifted cathodically with the increase of C_L following the DeFord-Hume equation; if C_M increases but C_L is constant E_p keeps its value constant.

(b) When C_M^0 is less than C_L but not negligible compared with the latter, the peak height decreases and the width increases compared with that in the absence of ligand, and E_p is shifted anodically with increase of $C_M \times t_d$ due to the surface concentration effect. In fact C_M^0 increases in the potential range corresponding to the rising part of the ASV curve, leading to a decrease in the concentration of sites not bound to M; the potential corresponding to a certain C_M^0 value is then shifted to more positive values, this shift increasing with increase of C_M^0, which leads to a broader and lower peak [16].

(c) Increasing $C_M \times t_d$ further, the ligand becomes fully saturated at the electrode surface ($C_M^0 \approx C_L$ for a 1:1 complex) giving a peak at potential E_{sat}. If $C_M^0 > C_L$, the remaining metal not bound to the ligand is present in the free form; in this case the voltammogram presents: (i) a *shoulder* that accounts for the metal bound to the ligand, whose height and potential depends mainly on C_L, and does not vary with $C_M \times t_d$; (ii) a *peak* due to the metal reoxidized to free M^{2+}, which potential tends to E_p^M obtained in the absence of ligand. It should be noticed that the shoulder begins to separate from the peak when the difference between their potentials is greater than 60 mV, i.e., only for strong ML complexes.

In the presence of adsorption of the ligand on the electrode, a surface concentration effect is also observed with a similar behaviour as that described above, due to a gradual saturation of adsorbed sites by the metal ion [8]. However the formation of the shoulder in the presence of adsorption is not mentioned in the literature.

In this work, where the results are clearly affected by adsorption, a shoulder is observed for sufficiently high values of C_M, and information about adsorption parameters can be obtained from its height.

2. Experimental

All chemicals used were of analytical grade and Suprapur mercury (Merck) was used for the hanging mercury drop electrode. Humic matter

was commercially obtained from Roth and a stock solution of 1.8 g l^{-1} was kept in the refrigerator.

Solutions were prepared in water passed through a Millipore Milli-Q system with an Organex column to remove organic matter; the water conductivity was below 0.1 μS cm^{-1}.

The number of protonation sites in the stock solution was determined from the inflection point obtained in a potentiometric titration of the ligand (diluted to 10%) in 0.1 M KNO_3 with 0.10 M KOH; the value found for the stock solution was $(7.0 \pm 0.3) \times 10^{-3}$ eq. l^{-1}.

Titrations of ligand solutions (40 or 80×10^{-6} eq. l^{-1}) with Pb(II), in 0.02 M KNO_3, pH = 5 and 22 ± 1°C, were followed by DPASV. A Metrohm 663VA stand with three-electrodes: working hanging mercury drop electrode (HMDE), reference Ag/AgCl and auxiliary (graphite or platinum) electrodes, was used for recording the voltammograms.

Unless otherwise specified the deposition time used was 120 s with stirring at 2000 rpm (mechanical stirring from the stand) followed by 30 s without stirring. The applied potential during the deposition step was −0.75 V and in the stripping step the potential was scanned to more positive values at 5 mV s^{-1}. The drop radius used was about 0.016 cm and the thickness of the diffusion layer ($\delta \approx 10^{-3}$ cm) was determined from the constant current measured during the deposition step ($i = nFDAC/\delta$) [18].

Alternating current (ac) polarographic measurements were carried out with a PAR 174A polarograph coupled to a PAR 5204 lock-in amplifier. The frequency and amplitude of the sinusoidal signal imposed were respectively 80 Hz and 10 mV; the current was measured at a phase angle of 90°. Under these conditions the current is proportional to the capacity of the double layer at the electrode surface, if no faradaic reactions occur and if the resistance of the cell is negligible. The plots of capacitive current vs time in ac experiments were recorded at $E_{ap} = -0.75$ V in stirred solutions of different concentration of ligand, at pH 5.0 and in 0.50 M KNO_3 (Fig. 1). The electrolyte concentration was chosen so that the resistence of the cell and the influence of the diffuse layer can be neglected.

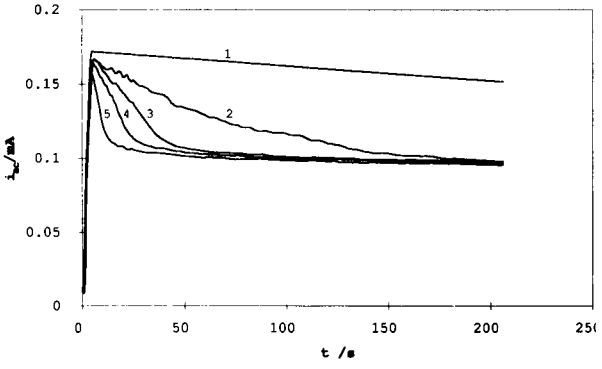

Fig. 1. Alternating current (i_{ac}), measured at a phase angle of 90°, versus time, for different concentrations of humic matter in 0.50 M KNO_3, at pH 5.0 and 22°C. Other experimental conditions: stirred medium, $E_{ap} \approx -0.75$ V; drop radius 0.042 cm; C_L (μeq. l^{-1}) = 0 (1); 4 (2); 20 (3), 40 (4), 80 (5).

In DPASV and ac polarographic experiments dissolved oxygen was removed from solutions in the polarographic cell by bubbling nitrogen with 99.995% purity. The glass call was decontaminated each day with 30% HNO_3, and between each titration curve (for 2 h at least).

3. Results and discussion

3.1. Adsorption of humic matter on the mercury electrode

From ac versus time curves obtained for different concentrations of humic matter (Fig. 1) it can be noticed that for the ligand concentrations of 40 and 80×10^{-6} eq. l^{-1} used in DPASV measurements (see Experimental), the electrode is fully saturated for intervals higher than 60 and 30 s, respectively. Therefore saturation of the electrode by adsorbed molecules is attained during the deposition step of DPASV, at −0.75V.

3.2. Rate of complexation and dissociation reactions

To check the degree of lability of the system during the deposition step the titration of humic species with Pb(II) was performed at different stirring rates (1000 and 3000 rpm). The normal-

Table 1
Normalised current $\Phi(=i_p^{M+L}/i_p^M$, where i_p^{M+L} and i_p^M stand, respectively, for the peak current in the presence and absence of ligand) for two different stirring rates, $V_1 = 1000$ and $V_2 = 3000$ rpm

C_{Pb} (M)	C_L/C_{Pb}	$100[\Phi(V_2)-\Phi(V_1)]/\bar{\Phi}$
2×10^{-8}	500	+7
	1000	+5
	2000	−8
	3000	−10
1×10^{-7}	250	−10
	500	+9
	1000	+1
	2000	−4
5×10^{-7}	250	+12
	500	+6

ized current Φ was the same, within experimental error, for each titration point and both stirring rates (Table 1), behaviour expected for fully labile or fully inert but reducible complexes. On the other hand it was checked that the system was not inert for lead concentrations in the range 10^{-7} to 10^{-6} M and C_L/C_{Pb} from 20 to 1000 (C_L given in number of protonation sites per liter), since the peak potential obtained by DPP was shifted to more cathodic values with increase of ligand concentration. The results are therefore discussed assuming fully labile complexes and reversible redox system.

3.3. Complexation parameters in solution

In the presence of a large excess of ligand site concentration compared to the total metal concentration during the stripping step, the peak currents obtained in the presence of ligand (i_p^{M+L}) and in its absence (i_p^M) should be equal for the same total concentration if the system is labile and $D_{ML} \approx D_M$.

Since the system is labile but $i_p^{M+L} < i_p^M$ then $D_{ML} < D_M$. In this work D_{ML} was determined from the peak current obtained in the presence of a sufficiently large excess of ligand so that the mean diffusion coefficient $\bar{D}$ is equal to D_{ML} (Eqs. 4 and 5, valid for labile systems). The value found was $D_{ML} = 5.5\times10^{-7}$ cm^2 s^{-1}, determined for a ligand site concentration of 326×10^{-6} eq. l^{-1} and lead concentration in the range from 0.01×10^{-6} to 0.05×10^{-6} M.

The mean conditional stability parameter $\bar{K}$, that includes all sites titrated, can be determined for labile systems either from current values since $D_{ML} < D_M$ (Eqs. 4 and 5 and $\bar{K}$ definition), or from potential values (Eqs. 4 and 6) (12):

$$i_p^{M+L}/i_p^M = \left(\bar{D}/D_M\right)^{1/2} \quad (4)$$

$$\bar{D} = \left(D_M|M| + D_{ML}|ML|\right)/C_M \quad (5)$$

$$\Delta E_p = \left(E_p^M - E_p^{M+L}\right) = (RT/nF)\ln\left(\bar{D}/D_M\right)^{1/2} + (RT/nF)\ln\alpha \quad (6)$$

where $\alpha = 1 + \bar{K}C_L$ (along the text C_L will always represent the number of protonation ligand sites per liter). The parameter $\bar{K}$ is given by $|ML|/(|M||L'|)$ assuming complexes of 1:1 type, where $|ML|$ and $|L'|$ represent the concentration of sites bound and not bound to the metal ion and the script M and M + L stand for the solutions in the absence and presence of ligand, respectively. The conditions of validity for Eqs. 5 and 6 are discussed in the appendix.

$\bar{K}$ values obtained either from i_p or from E_p vs. the degree of occupation of sites θ (fraction of number of ligand sites bound to the metal over total number of ligand sites, i.e., $|ML|/C_L$), are presented in Fig. 2. Since E_p is related to the complexing strength in the stripping step, the parameter $\bar{K}_{E_p}$ is associated to C_M^0 (total metal concentration at the electrode surface during stripping step). Consequently the same experimental point of the titration should show $\bar{K}_{E_p}$ lower than $\bar{K}_{i_p}$ (associated with the bulk concentration C_M), due to the heterogeneity of the ligand. Therefore $\bar{K}_{E_p}$ should be plotted vs. $\theta = |ML|^0/C_L$ and $\bar{K}_{i_p}$ versus $\theta = |ML|/C_L$ for real comparison of $\bar{K}_{i_p}$ and $\bar{K}_{E_p}$ ($|ML|^0$ and $|ML|$ stand, respectively, for the concentration of ML at the electrode surface and in bulk solution). The concentration $|ML|^0$ is determined from Eq. 6, where $\bar{K}C_L$ is equal to $|ML|^0/(C_M^0 - |ML|^0)$ and C_M^0 is estimated from Eq. 7.

$$C_M^0 = 2.3\frac{\left(\bar{D}D_r\right)^{1/2}}{\delta R}t_d C_M \quad (7)$$

Eq. 7 is formally identical to Eq. 3, where D_M has been substituted by the mean diffusion coefficient $\bar{D}$, determined from Eq. 4, in order to take into account the metal species that arrive to the electrode surface to be reduced during the deposition step. It should be mentioned that the validity of Eq. 7 was checked in the presence of ligand with $D_{ML} \approx D_M$ [13], but not for $D_{ML} < D_M$.

It was pointed out [13] that ASV measurements with typical parameter values should be done in the presence of an excess of ligand so that $C_L/C_M \geq 1000$, in order to have $C_L/C_M^0 \geq 20$ (see Introduction). However lower values of C_L/C_M are still possible if $D_{ML} < D_M$, since for ligands with similar complexing affinities but different D_{ML} values C_M^0 decreases with the decrease of D_{ML}.

Fig. 2 shows that log $\bar{K}_{E_p}$ is greater than log $\bar{K}_{i_p}$ for the same θ value, which is probably due to the adsorption of the ligand on Hg, which strongly affects the values of peak potential. In the presence of adsorption Eq. 6 should be redefined, adding the term $\bar{K}_{ad}|L'|_{ad}$ to $\bar{K}C_L$ in order to take into account the contribution of adsorbed sites [8]. The concentration of L'_{ad} (adsorbed ligand sites not bound to the metal) is similar to C_L^{ad} for $C_M^0 \ll C_L^{ad}$, and C_L^{ad} (total concentration of adsorbed ligand sites) is constant for different C_L values if the electrode is saturated; in this case and with increasing C_L the term $\bar{K}_{ad}C_L^{ad}$ becomes less and less important compared with $\bar{K}C_L$. This might be the reason why $\bar{K}_{E_p}$ in Fig. 2 is slightly lower for the highest ligand concentration used compared to the other concentrations, instead of being independent of C_L as expected in the absence of adsorption.

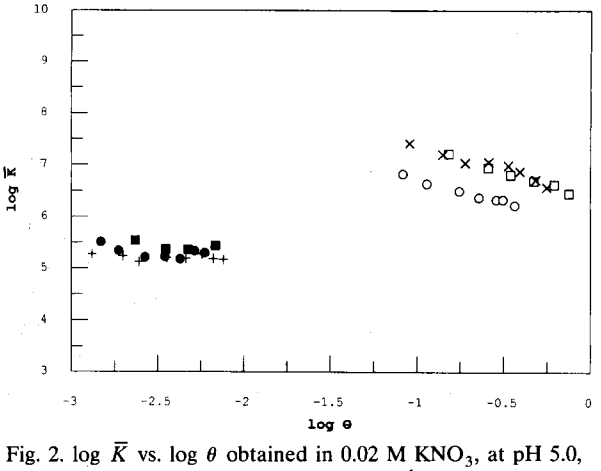

Fig. 2. log $\bar{K}$ vs. log θ obtained in 0.02 M KNO_3, at pH 5.0, 22°C, $C_{Pb} < 0.53$ μM and $C_L = 84$ μeq. l^{-1}; data from i_p (●) or E_p (○); $C_L = 64$ μeq. l^{-1}; data from i_p (+) or E_p (×); $C_L = 42$ μeq. l^{-1}; data from i_p (■) or E_p (□). θ is related to complexation in the bulk for data from i_p and to complexation at the electrode surface for data from E_p (see text).

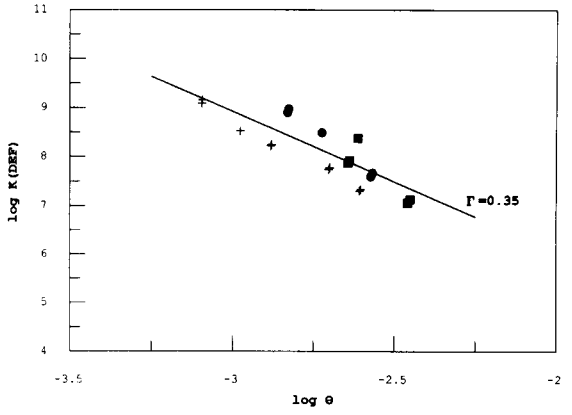

Fig. 3. log K_{DEF} vs. log θ obtained from i_p measurements. Same symbols and experimental conditions as Fig. 2.

The differential equilibrium function, K_{DEF}, was determined from Eq. 1 and i_p measurements that are less affected than E_p by adsorption of organic compounds on the electrode, as can be seen from the constancy of $\bar{K}_{i_p}$ within experimental errors for different C_L values and the same θ value (Fig. 2). From log K_{DEF} vs. log θ (Fig. 3) and Eq. 2 a degree of heterogeneity, $\Gamma = 0.35$, was found. This value shows that humic matter in the presence of lead behaves with high heterogeneity, since the usual range found for natural systems lies between 0.3 and 0.7 [16].

3.4. Complexation parameters in the absorbed layer

The stability parameter $\bar{K}_{ad}$ for complexation in the adsorbed layer can be obtained from Eq. 6 redefined in the presence of adsorption, i.e., replacing in this equation α by α_t, where $\alpha_t = 1 + \bar{K}_{ad}|L'|_{ad} + \bar{K}C_L$ (valid in the concentration range where $|L'| \approx C_L$). From this expression and the mass balance for adsorbed ligand ($C_L^{ad} =$

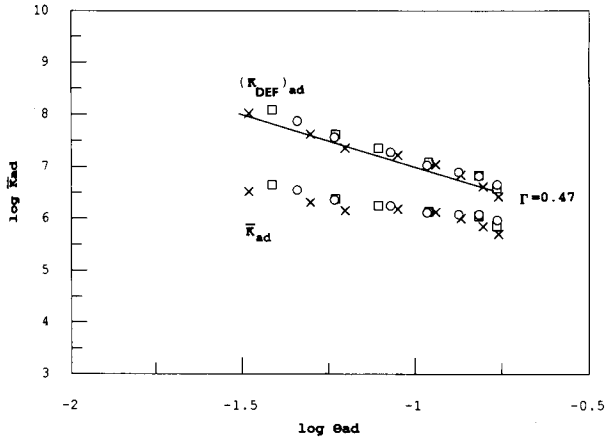

Fig. 4. log $\bar{K}_{ad}$ and log$(K_{DEF})_{ad}$ vs. log θ_{ad}, where ad stands for adsorbed layer. Same experimental conditions as Fig. 2; C_L (μeq. l^{-1}) = 84 (○); 64 (×); 42 (□).

$|L'|_{ad}$ $(1+\bar{K}_{ad}|M|^0)$, where $|M|^0$ is given by C_M^0/α_t) it was found that:

$$\bar{K}_{ad} = \frac{\alpha_t - 1 - \bar{K}C_L}{C_L^{ad} + C_M^0\left(\frac{1+\bar{K}C_L}{\alpha_t} - 1\right)} \quad (8)$$

The parameter $\bar{K}_{ad}$ is then determined from Eq. 8 using: (i) α_t obtained from the experimental values of ΔE_p (Eq. 6); (ii) $\bar{K}$ determined from i_p measurements; (iii) $C_L^{ad} = 1.6 \times 10^{-4}$ eq. l^{-1} calculated in Section 3.5; (iv) C_M^0 given by Eq. 7.

The variation of $\bar{K}_{ad}$ with the degree of occupation of adsorbed sites, θ_{ad} ($= |ML|_{ad}/C_L^{ad}$), is presented in Fig. 4, where the values of $(K_{DEF})_{ad}$ determined from α_t are also plotted. The value of θ_{ad} is calculated substituting the concentration $|ML|_{ad}$ by its expression determined from the mass balance of C_M^0 $(= |M|^0 + |ML|_{ad} + |ML|^0$, where $|ML|^0 = \bar{K}C_L|M|^0$ and $|M|^0 = C_M^0/\alpha_t$):

$$\theta_{ad} = \left\{C_M^0\left[1 + \frac{1}{\alpha_t}(1+\bar{K}C_L)\right]\right\}/C_L^{ad} \quad (9)$$

Comparing log K_{DEF} in Fig. 3 and 4 it can be seen that complexation of lead in the absorbed layer is stronger than in solution for the same degree of occupation of sites. This might be due either to a higher affinity of the adsorbed site, influenced by the spatial rearrangement of the molecule which is different in the absorbed layer and in solution, or to a higher ratio of stronger sites to total sites, influenced by the different affinity of each site and the vicinity of the mercury, negatively charged.

The degree of heterogeneity obtained from Fig. 4, $\Gamma_{ad} = 0.47$, should not be compared to the value obtained in solution since they correspond to a different θ ranges.

3.5. Influence of the metal concentration at the electrode surface in ASV

The influence of C_M^0 (metal concentration at the electrode surface during the stripping step) has been studied by increasing the deposition time and/or C_{Pb} at a constant C_L value.

When C_M^0 is no longer negligible compared with the concentration of complexing sites at the electrode surface (present either in the adsorbed layer or in solution) the peaks become distorted (Fig. 5) due to the surface concentration effect (see Introduction). In the following text the plots of characteristic peak parameters versus C_M and/or t_d are discussed in terms of this effect.

The variation of peak width and peak potential are characteristics of a surface concentration effect in the absorbed layer and/or in solution [8,13]. It should be pointed out that in the presence of heterogeneous ligands, the width is also affected by the heterogeneity of complexing sites bound to metal ions [16]. This is the reason why even in the presence of an excess of ligand (C_L and $C_L^{ad} \gg C_M^0$) the width is slightly larger than that observed in the absence of ligand ($W_{1/2}^{M+L} - W_{1/2}^{M} \approx 10$ mV).

The variation of peak currents will be discussed in detail since information about the concentration of complexing sites in the adsorbed layer can be obtained from them. It can be noticed from Fig. 6, where i_p vs. t_d are plotted for the same C_L and different C_M values, that the deposition time corresponding to the break point in each curve, represented by t_c, is inversely proportional to C_M. This corresponds to $\bar{D}$ and C_M^0 being constants in the concentration range used (Eq. 7). Then t_c should represent the critical

time for the saturation of complexing sites by metal ions, at the electrode surface; in this case C_M^0, equal to $C_L^{ad} + C_L$, has a constant value because the electrode is fully saturated with adsorbed molecules, i.e., C_L^{ad} is constant as well as the ligand concentration.

From Eq. 7 and $t_c(\text{min}) = 7.2$, 3.5 and 1.9 respectively for $C_{Pb}(\times 10^{-6}$ M) = 0.8, 2 and 4, using $R = 0.016$ cm, $\delta = 10^{-3}$ cm, $D_r = 1.2 \times 10^{-5}$ cm s^{-1}, $\bar{D} = 10^{-6}$ cm^2 s^{-1} and $C_L = 4.2 \times 10^{-5}$ eq. l^{-1} it was found $C_M^0 = (2.0 \pm 0.3) \times 10^{-4}$ eq. l^{-1} and so $C_L^{ad} = (1.6 \pm 0.3) \times 10^{-4}$ eq. l^{-1}, which represents the number of moles of adsorbed sites per litre in the absorbed layer.

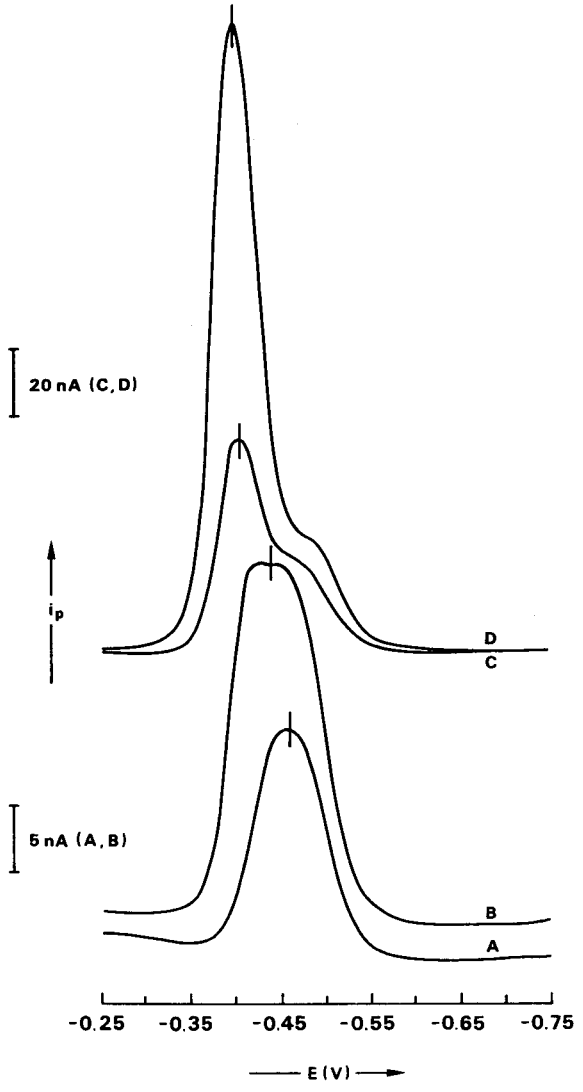

Fig. 5. Voltammograms obtained for $C_L = 42$ μeq. l^{-1} in 0.02 M KNO_3, 22°C, pH 5, $t_d = 1$ min; $C_{Pb}(\mu M) = 1$ (A); 2 (B); 4 (C), 8 (D).

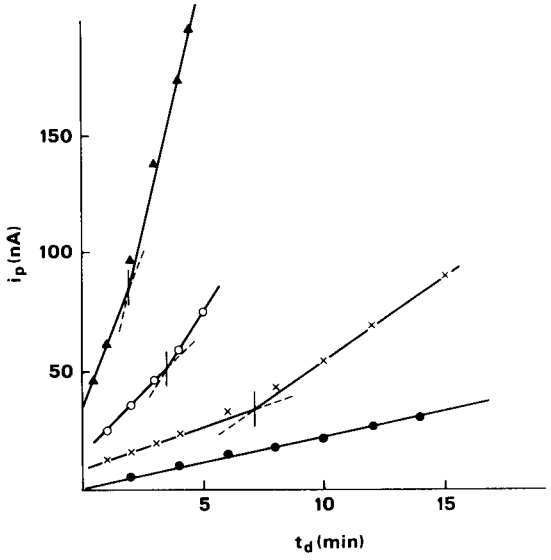

Fig. 6. i_p vs. t_d in the presence of $C_L = 42$ μeq. l^{-1} in 0.02 M KNO_3, pH 5 and 22°C; C_{Pb} (μM) = 0.2 (●); 1 (×); 2 (○); 4 (▲).

The same value of C_L^{ad} is obtained from Fig. 7 for C_L equal to 42 and 84×10^{-6} eq. l^{-1}, which indicates that the electrode is fully saturated for both C_L values, as previously checked from ac measurements.

It is worth while pointing out that if the difference between $\log(\bar{K}C_L)$ and $\log(\bar{K}_{ad}C_L^{ad})$ is greater than 3, two separate inflection points should be expected owing to the saturation at the electrode surface of the complexing sites in the absorbed layer and in solution, as it is usual in complexation measurements in the presence of ligands with different strengths. On the other hand if $C_L^{ad} \gg C_L$ the same t_c value should be obtained on increasing C_L if the electrode is fully saturated, as observed in [8].

Another result that has to be considered is the increase of i_p for the same $C_M \times t_d$ when C_{Pb} increases (Fig. 8). In fact for ligands with $D_{ML} \approx D_M$, C_M^0 is directly related to $C_M \times t_d$ and the same i_p vs. $C_M \times t_d$ curve should be obtained

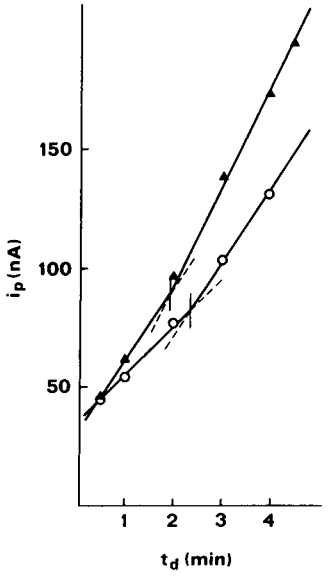

Fig. 7. i_p vs. t_d for $C_{Pb} = 4$ μM and two different ligand concentrations, in 0.02 M KNO_3, pH 5 and 22°C; C_L (μeq. l^{-1}) = 42 (▲) and 84 (○).

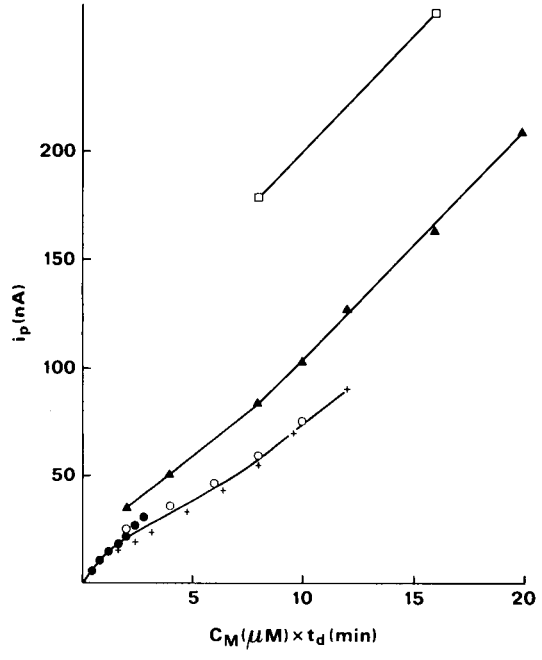

Fig. 8. i_p vs. $C_{Pb} \times t_d$ in the presence of $C_L = 42$ μeq. l^{-1} in 0.02 M KNO_3, pH 5 and 22°C; C_{Pb} (μM) = 0.2 (●); 1 (+); 2 (○); 4 (▲); 8 (□).

independent of the C_M value. However if $D_{ML} < D_M$, the $\bar{D}$ increases with increase of C_M since $|L'|$ decreases, leading to higher values of i_p, as observed in Fig. 8. Even for concentrations where $|L'| \approx C_L$ the value of i_p may be not constant for the same $C_M \times t_d$ if the parameter $\bar{K}$ influences significantly $\bar{D}$ in the concentration range used.

From Fig. 5 it can be seen the formation of a shoulder when $\Delta E_p < 15$ mV, with an approximately constant potential, $\Delta E_{sh} = E_p^M - E_{sh} \approx 80$ mV (where sh stands for shoulder), and constant current, $i_{sh} \approx (30 \pm 5)$ nA. On decreasing t_d the peak shifts to more negative values and when the difference between the potential of the peak and the shoulder is not sufficient to discriminate between them, a broadened peak is obtained.

The concentration of lead ions at the electrode surface responsible for i_{sh} can be obtained from Eq. 3 and the calibration plot i_p vs. $C_{Pb} \times t_d$ in the absence of ligand, giving $C_M^0 = (1.5 \times 0.3) \times 10^{-4}$ M. This value is of the same order of magnitude to that previously obtained for saturation of complexing sites at the electrode surface from t_c measurements, which clearly indicates that the shoulder is related to the saturation of those sites. Therefore, it can be concluded that saturation of complexing sites at the electrode surface, in the adsorbed layer and/or in solution, leads to the formation of a shoulder in anodic stripping voltammograms, with a constant potential and height for the same C_L value and different C_M and/or t_d values, since saturation of complexing sites by metal ions is independent of C_M or t_d.

It should be mentioned that shoulder formation has not been observed in the presence of other heterogeneous macromolecules studied in our group [9,19], although similar trends in $W_{1/2}$ as those observed in this paper and some asymmetric peaks are obtained when C_L/C_M^0 decreases due to an increase of C_M and/or t_d. Two possible effects might account for this: (i) lower ΔE_p values due to a lower complexing strength and/or a lower diffusion of ML, which decrease the term $(RT/nF) \times \ln(\bar{D}/D_M)^{1/2}$ in Eq. 6. Due to this fact, the potential of this shoulder is more positive making difficult its discrimination from the peak of the metal ion in the absence of

ligand; (ii) a lower concentration of adsorbed sites. In this case i_{sh} should be smaller and might not be detected.

Under the conditions used in this paper a well defined shoulder is obtained for $i_p/i_{sh} \approx 10$ and $\Delta E_p \approx 80$ mV. If the shoulder was lower it would disappear under the peak corresponding to the metal ion and/or under the base line at the sensitivity used.

4. Conclusions

From this study the following characteristics of lead complexes with humic matter can be summarized: (i) in the concentration range studied they show labile behaviour in ASV measurements; (ii) the diffusion coefficient of the complex is 5.5×10^{-7} cm^2 s^{-1}; (iii) the stability conditional parameter, log K_{DEF}, determined at pH 5.0, varies from 9.0 to 6.2 for log θ between -3 and -2, which corresponds to $\Gamma \approx 0.35$; (iv) $\log(K_{DEF})_{ad}$ varies from 6.5 to 5.8 for log θ_{ad} between -1.5 and -0.9; (v) the concentration of adsorbed sites in the absorbed layer is $(1.6 \pm 0.3) \times 10^{-4}$ eq. l^{-1}.

It was also shown that saturation of adsorbed sites leads to the formation of a shoulder in DP anodic stripping voltammograms, and C_M^0, and therefore C_L^{ad}, can be estimated from its height. To observe the shoulder in terms of experimental results the shift in the peak potential from that of the free metal ion should be > 60 mV, otherwice only some distortion and/or enlargement of the original peak will be observed.

In the environmental conditions the surface concentration effect might lead to erroneous conclusions if the break observed in i_p vs. C_M due to the saturation of the sites at the electrode surface is misunderstood with the break related to saturation of complexing sites in bulk solution, as discussed previously [8].

5. Appendix

The relative error of $\bar{K}$, $\Delta\bar{K}/\bar{K}$, is deduced from the measurements involved in its determination and their experimental errors. Experimental conditions are defined so that the relative error in $\bar{K}$ is always lower than 25%, which corresponds to an error of 0.25 units in log $\bar{K}$.

5.1. Conditions of validity of Eq. 5

Eq. 5 is valid if during the deposition step there is an excess of ligand so that $\bar{D}$ can be considered constant in the diffusion layer, i.e., $C_L \approx |L'|$, where L' represents the ligand not bound to the metal ion [13]. On the other hand the excess of ligand should not be so high that $\bar{D} \approx D_{ML}$ since in this case no speciation can be determined from i_p measurements. To define the best experimental conditions to be used, the relative error in $\bar{K}$ was determined for different $\bar{K}C_L$ values. The relative error in $\bar{K}$, determined from its definition and $|L'| \approx C_L$, is given by:

$$\left(\Delta\bar{K}/\bar{K}\right) = (\Delta M/M)\left[1 + 1/\left(\bar{K}C_L\right)\right] \qquad (11)$$

where the relative error in $|M|$, given by Eq. 12, is obtained from Eq. 5 and $\Delta\bar{D} = 0.1\ \bar{D}$; the relative error in $\bar{D}$ was calculated from Eq. 4 assuming an experimental error of 5% in i_p^{M+L}.

$$\Delta M/|M| = 0.1\bar{D}/\left(\bar{D} - D_{ML}\right) \qquad (12)$$

From Eq. 12 it can be seen that the relative error in $|M|$ is never $< 10\%$, value found when $D_{ML} \ll \bar{D}$. To obtain relative errors $< 25\%$ in $\bar{K}$, concentration ranges should be chosen so that $\bar{K}C_L$ varies from 1 to 25, for $D_{ML} = 5 \times 10^{-7}$ cm^2 s^{-1} (Table 2); this range is extended in both senses if D_{ML} decreases. On the other hand for $D_{ML} \geq 1.5 \times 10^{-7}$ cm^2 s^{-1} the relative error in $\bar{K}$ is always $> 25\%$; therefore, speciation from cur-

Table 2
Relative errors in $|M|$ and $\bar{K}$ obtained from i_p measurements for different $\bar{K}C_L$ values and $D_{ML} = 5 \times 10^{-7}$ cm^2 s^{-1}

$\bar{K}C_L$	$\Delta M/\|M\|$	$\Delta\bar{K}/\bar{K}$
0.02	0.11	11
0.1	0.11	1.2
1	0.11	0.22
10	0.16	0.17
25	0.24	0.25
50	0.37	0.38
100	0.63	0.63

rent measurements should be done only if $D_M/D_{ML} \geq 50$.

Another condition that should be fullfilled in order to have well defined peaks, in the absence of the surface concentration effect, is that $|ML|^0 < C_L$ and $|ML|_{ad} < C_L^{ad}$, where ^{0} and ^{ad} stand respectively for "solution at the electrode surface" and "adsorption layer". It should be noticed that for systems with high complexation affinity the condition $C_L > C_M^0$ might only be attained for C_L concentrations where $\bar{K}C_L > 25$; in those cases speciation from i_p measurements cannot be made within an error of 25% in the conditions of Table 2.

In this work determination based on i_p have been done for: (i) $|L'| > 99\%\ C_L$; (ii) $\bar{K}C_L \approx$ (13–26); (iii) $\%\ |ML|^0 < 10\%\ C_L$; (iv) $\%\ |ML|_{ad} < 17\%\ C_L^{ad}$.

5.2. Conditions of validity of Eq. 6

Eq. 6 is only valid in the absence of adsorption if there is an excess of ligand so that $C_L \approx |L'|^0$, where $|L'|^0$ represents the ligand concentration at the electrode surface not bound to the metal ion, during the stripping step. This condition is more severe in peak potential measurements than in peak current measurements, since $|L'|^0 < |L'|$. To determine $|L'|^0$, the parameter C_M^0 should be known (Eq. 7).

The relative error in $\bar{K}$ was determined from Eq. 6 for different $\bar{K}C_L$ values, assuming an error of 2.5 mV in ΔE and $\Delta\bar{D} = 0.1\ \bar{D}$:

$$\Delta\bar{K}/\bar{K} = 0.20\left[1 + 1/\left(\bar{K}C_L\right)\right] \qquad (13)$$

which shows that $\bar{K}C_L > 10$ in order to have a relative error of about 20% in $\bar{K}$ value. The minimum value of $\Delta\bar{K}/\bar{K}$ (20%) is attained for $\bar{K}C_L \geq 50$.

In this work experimental points have been obtained for $\bar{K}C_L$ between 13 and 26, and $|L'|^0 > 95\%\ C_L$.

Acknowledgments

M.G. Bugarin thanks the University of Vigo for the financial support in order to do the research work in Lisbon, Centro de Quimica Estrutural (IST).

References

[1] J. Buffle, in H. Sigel (Ed.), Natural Organic Matter and Metal-Organic Interactions in Aquatic Systems (Metal Ions in Biological Systems, Vol. 18), Marcel Dekker, New York, 1984.
[2] A. Beveridge and W.F. Pickering, Water, Air, Soil Pollut., 14 (1980) 171.
[3] G.A. Bhat and J.H. Weber, Anal. Chim. Acta, 141 (1982) 95.
[4] G. Capodaglio, K.H. Coale and K.W. Bruland, Mar. Chem., 29 (1990) 221.
[5] A.K. Hanson, Jr. Sakamoto-Arnold, M. Carole, D.L. Huizenga and D.R. Kester, Mar. Chem., 23 (1988) 181.
[6] K.W. Bruland, Limnol. Oceanogr., 34 (1989) 269.
[7] F.L.L. Muller and D.R. Kester, Mar. Chem., 33 (1991) 71.
[8] J. Buffle, J.J. Vuilleumier, M.L. Tercier and N. Parthasarathy, Sci. Total Environ., 60 (1987) 75.
[9] J.P. Pinheiro, A.M. Mota and M.L.S. Gonçalves, Anal. Chim. Acta, 284 (1994) 525.
[10] S. Capelo, A.M. Mota and M.L.S. Gonçalves, Electroanalysis, in press.
[11] A.M. Mota and M.C. Santos, in A. Tessier and D. Turner (Eds.), Interaction Between Trace Metals and Organisms, Lewis Publishers, Chap. 5, in press.
[12] J. Buffle, Complexation Reactions in Aquatic Chemistry, Ellis Horwood Chichester, 1988.
[13] A.M. Mota, J. Buffle, S.P. Kounaves and M.L.S. Gonçalves, Anal. Chim. Acta, 172 (1985) 13.
[14] J. Heyrovsky and J. Kuta, Principles of Polarography, Publishing House of the Czechoslovak Academy of Sciences, Prague, 1965.
[15] D.S. Gamble, A.W. Underdown and C.H. Langford, Anal. Chem., 52 (1980) 1901.
[16] M. Filella, J. Buffle and H.P. Van Leeuwen, Anal. Chim. Acta, 232 (1990) 209.
[17] J. Buffle, J. Electroanal. Chem., 125 (1981) 273.
[18] W. Davidson, J. Electroanal. Chem., 87 (1978) 395.
[19] M. Bejarano, L. Madrid, A.M. Mota and M.L.S. Gonçalves, Sci. Total Environ., in press.

ELSEVIER

Analytica Chimica Acta 294 (1994) 283–289

ANALYTICA CHIMICA ACTA

An ionization chamber as a gas sensor: theory of operation

Stevan A. Milinković *, Asim E. Sadibašić

Faculty of Technology and Metallurgy, University of Belgrade, Karnegijeva 4, 11000 Belgrade, Yugoslavia

Olga S. Milanko

Institute for Technical and Medical Protection, Katanićeva 15, 11 000 Belgrade, Yugoslavia

Received 9th October 1993

Abstract

In order to explain the operating principle of a simple ionization chamber with an internal radiation source as a sensor for compounds in the vapour phase, calculations of its basic parameters were made. The behavior of the reactant and product ions in a coaxial chamber powered with an alternating current is discussed. By setting the proper operating conditions, the chamber will operate in a resonance mode and produce the greatest change in the total current after formation of less mobile product ions. In an idealized situation, the measuring electrode will collect all reactant ions but none of the product ions. The mean current depends on the concentration of sample molecules, and therefore provides that this device could be used as a simple but powerful analytical sensor.

Key words: Gas sensors; Ionization chamber; Ion-molecule interactions; Vapour sensors

1. Introduction

Radiation source ionization chambers operating at atmospheric pressure are well-known detectors of gaseous and aerosol air pollutants [1]. They have numerous advantages over other gas sensing devices, e.g., good sensitivity, short response and recovery time, absence of wet chemistry and relatively simple sensor design. Ionization chambers have been used in gas chromatography for many years, primarily for the detection of gas molecules with high electron affinity [2,3]. In addition, the ionization technique has been applied in several portable detectors for chemical warfare agents [4–6].

In order to improve the selectivity of the method, various designs and operating principles were tried [4]. The main intention was to exploit the difference in ion mobilities in the electric field. Ion mobility spectrometry was a logical enhancement of the basic technique, aimed at improving the overall selectivity by adding a drift tube for a more efficient separation of ions according to their mobilities [7]. However, ion mobility spectrometry is a rather sophisticated technique, more suitable for laboratory use than for portable gas monitors that are to be widely employed. Simple ionization chambers still offer a lot of possibilities for performance improvement.

* Corresponding author.

0003-2670/94/$07.00 © 1994 Elsevier Science B.V. All rights reserved
SSDI 0003-2670(94)00152-C

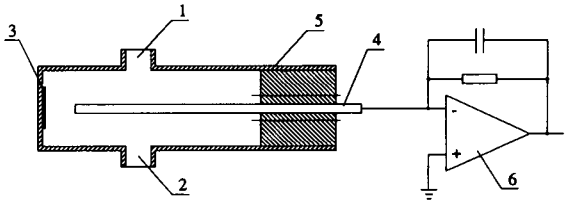

Fig. 1. Drift ionization chamber: (1) air inlet; (2) air outlet; (3) radiation source; (4) collector electrode; (5) outer electrode; (6) electrometer amplifier/integrator.

A potentially promising approach is operating a simple, radioactive source ionization chamber in an alternating current (AC) mode. Its selectivity can hardly be compared to that of an ion mobility spectrometer, but it is of a significantly simpler construction, and the operating principle itself deserves attention and offers possibilities for further optimization. This paper deals with the theory of operation of a cylindrical ionization chamber that is to be used as a sensor for various compounds in the vapour or gas phase.

The chamber, shown in Fig. 1, consists of a cylindrical housing (outer electrode), containing a radiation source mounted at the cylinder base, and a bar-shaped measuring electrode (collector). The air flows through the chamber perpendicular to the axis. The outer electrode is connected to a voltage source, and a collector is connected to an electrometer amplifier.

In operation, air is pumped through the chamber and is ionized by a built-in radioactive source. Primary ions start a sequence of ion–molecule reactions, resulting in the formation of reactant ions, both positive (N_2^+, O_2^+, $(H_2O)_nH^+$ etc. [8]) and negative (O^-, O_2^-, $(H_2O)_nO_2^-$, etc. [9,10]). In the presence of certain chemical species in the incoming air, the reactant ions undergo ion–molecule reactions with sample molecules to form product ions that are usually quasimolecular, larger in size and, therefore, less mobile.

Generally, if voltage is applied to the chamber electrodes, the ion current density J is given by [11]:

$$J = -D\nabla nq + v_d nq + D_g\left(\frac{Q}{P} - v_d\right)nq \qquad (1)$$

where q is the ion charge, n the number of ions, D the diffusion tensor, Q the volumetric flow-rate, P the cross-section of area of the chamber, D_g the pneumatic drag coefficient, v the drift velocity ($\approxeq kE$), k the ion mobility and E the electric field.

Eq. 1 holds both for positive and negative charge carriers. It is composed of three components:

(i) diffusion component, determined by ion concentration gradients and diffusion coefficients;
(ii) drift velocity component, which depends on ion mobility and electric field strength; and
(iii) flow-rate component.

The first two components are successfully exploited in gas detection. Consequently, there are basically two types of simple ionization chambers: a diffusion chamber and a drift chamber.

A diffusion chamber is characterized by a weak applied electric field, so that the diffusion current, greatly influenced by air flow, is dominant. By choosing an appropriate cell geometry [5], which promotes recombination of side diffused ions, the separation of ions will be related to their diffusion coefficients. The measured current is greater when an agent is present compared to the current when only clean carrier gas is sampled.

In a drift ionization chamber, a strong electric field is applied, so that the current due to diffusion can be neglected. In addition, if the air flows perpendicular to the chamber axis, the collector current is independent of the flow-rate. Since the current, I, due to the air flow is given by:

$$I = \int_S \boldsymbol{J}\,\mathrm{d}\boldsymbol{S} = \frac{D_g q}{P}\oint_S n\boldsymbol{Q}\,\mathrm{d}\boldsymbol{S} = 0 \qquad (2)$$

i.e. the total current due to the air flow is zero, because the flux through a closed surface is zero under the stationary conditions.

In this way, only the drift component of the current density is considered, and separation of ions according to their mobilities can be accomplished. The presence of detectable agents decreases the measured ion current.

All factors that enhance the difference in mobility between reactant ions and product ions can

be used to improve performance characteristics of a simple drift ionization chamber. The factor whose influence is discussed in this paper is the alternating field.

2. Theory of operation

Consider the ionization chamber of cylindrical geometry shown in Fig. 1. It could be assumed that the voltage applied to the outer electrode is given by the general sinusoidal function $u(t)$:

$$u(t) = U_0 \sin \omega t \tag{3}$$

where U_0 is the maximal amplitude and ω is the radial frequency.

The electric field in a cylindrical chamber is obtained by solving the Laplace equation [12], and will be

$$E(r, t) = \frac{U_0 \sin \omega t}{r \ln(b/a)} \tag{4}$$

where a and b are the radii of the inner and outer electrodes, respectively. According to the law of conservation of energy, the work done by the electric field in order to move a charge q_0 along an elementary path d_s is given by

$$q_0 E \, \mathrm{d}s = u(t) i_0(t) \, \mathrm{d}t \tag{5}$$

i.e., it is equal to the energy supplied by the voltage source, $u(t)$. Since the charge is moving along the field lines, it may be written as

$$q_0 E(r, t) \frac{\mathrm{d}r}{\mathrm{d}t} = u(t) i_0(t) \tag{6}$$

where $\mathrm{d}r/\mathrm{d}t$ is the instantaneous value of the particle radial velocity, v, i.e.,

$$v = \frac{\mathrm{d}r}{\mathrm{d}t} = kE(r, t) \tag{7}$$

where k is the mobility of the charge q_0. Consequently

$$i_0(t) = \frac{q_0 k E(r, t)^2}{u(t)} \tag{8}$$

i.e., after settling,

$$i_0(t) = \frac{q_0 k U_0 \sin \omega t}{r^2 [\ln(b/a)]^2} \tag{9}$$

The last equation practically describes the current pulse, beginning when the charge is generated and lasting until it is collected by one of the electrodes.

Let us now assume that the built-in radioactive source generates q ion pairs in unit volume per unit of time. Likewise, it can be assumed that the ionization of gas throughout the chamber volume is uniform because, due to the location of the radiation source and chamber geometry, the initial recombination is minimized by the influence of the radial electric field.

After primary ionization of the air molecules and a series of ion–molecule reactions, in which the initially formed electrons are thermalized and attached to oxygen molecules, positive and negative reactant ions are formed [8,9]. They are characterized by the presence of water molecules which are, being polar, easily incorporated in complex ions [13].

Among positive reactant ions, the most interesting are the ones of the type $(H_2O)_nH^+$, i.e. protonated water [14]. In the presence of compounds with high proton affinity, ion–molecule reactions with protonated water occur, resulting in the formation of complex ions of general formula $M_m(H_2O)_nH^+$ [15].

The effect of space charge can be neglected, because the number of ions is small compared to the number of neutral molecules. Therefore, from Eq. 9,

$$\frac{\mathrm{d}i(t)}{\mathrm{d}n} = \frac{ekU_0 \sin \omega t}{r^2 [\ln(b/a)]^2} \tag{10}$$

where $\mathrm{d}i(t)/\mathrm{d}n$ is the change in current vs. change in ion density in the chamber volume, and e is the unit charge. Under these circumstances, it can be considered that most ions are singly charged. In cylindrical geometry, the space distribution of ions depends only on the radial coordinate, r. Hence, the integration of Eq. 10 is done only along r and multiplied by $2\pi L$, where L is the chamber length.

The total ion current will be the sum of two components:

(1) Conduction current, consisting of the charge carriers reaching the electrodes. It is obtained by integration of Eq. 10 from a to b.

(2) Induction current, consisting of charge carriers moving between the electrodes without being collected, due to recombination. It is obtained by integration of Eq. 10 from $r_1 \geq a$ to $r_2 \leq b$.

Under the boundary conditions (for $r_1 = a$ and $r_2 = b$), the induction current becomes equal to the conduction current. By setting the operating parameters of the chamber so that the boundary conditions for positive reactant ions are satisfied, it is possible to obtain the greatest change in current after less mobile ions are formed in ion–molecule reactions.

The highest probability is that the reactant ions present in the region of mean field strength, $\bar{E}$, given by:

$$\bar{E} = \frac{E(a) + E(b)}{2} \tag{11}$$

will be collected last and hence contribute most to the induction current. After combining Eqs. 4 and 11 for $r = a$ and $r = b$

$$\bar{E} = \frac{(a+b)U_0 \sin \omega t}{2ab \ln(b/a)} \tag{12}$$

$$\frac{dr}{dt} = k\bar{E} \tag{13}$$

$$r(t) = k\int_0^t \bar{E}\, dt = \frac{kU_0(a+b)}{2\omega ab \ln(b/a)}(1 - \cos \omega t) \tag{14}$$

The mean distance, R, may be defined as

$$R = \bar{r}(t) = \frac{kU_0(a+b)}{2\omega ab \ln(b/a)} \tag{15}$$

Fig. 2 illustrates the oscillation of positive ions around R in an alternating field, with amplitude $R - r_1$ during the positive, and $r_2 - R$ during the negative half-period.

For the stated boundary conditions, $r_1 = a$ and $r_2 = b$,

$$\frac{kU_0(a+b)}{\omega ab \ln(b/a)} = b - a \tag{16}$$

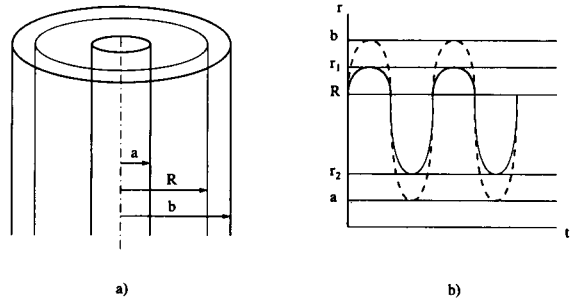

Fig. 2. The mean distance for the oscillation of ions. The dashed line represents reactant ions and the solid line product ions. (a) Space diagram; (b) time diagram.

and hence

$$f = \frac{kU_0(a+b)}{2\pi ab(b-a) \ln(b/a)} \tag{17}$$

In the previous equation, besides the chamber dimensions (i.e., a and b), the value for k – mean mobility of the reactant ions in the air under the standard conditions – may also be considered constant.

Therefore, in order to select the optimal frequency using Eq. 17, the peak amplitude of the supply voltage should be determined. This voltage should be high enough to enable the ionization chamber to operate at a point corresponding to the lower part of the saturation region of the static characteristic, in order to suppress excessive recombination. On the other hand, the chamber should not be allowed to operate in the saturation region, because, in that case, the total current would be equal to the conduction current, regardless of the composition of the ions present.

Since it is difficult to calculate the coefficient of recombination, the operating voltage can be determined experimentally from the static characteristic of the chamber, assuming the ion collection efficiency to be between 0.8 and 0.9 [16]. In that case, the current due to the reactant ions, i_r, will be the sum of two components:

$$i_r(t) = i_1(t) + i_2(t) \tag{18}$$

where $i_1(t)$ is the current due to the positive

reactant ions and $i_2(t)$ the current due to the negative reactant ions.

From the relation

$$i_r(t) = \int_{S_k} \boldsymbol{J}\, \mathrm{d}\boldsymbol{s} \tag{19}$$

and

$$\boldsymbol{J} = e\boldsymbol{E}(n_1 k_1 + n_2 k_2) \tag{20}$$

where the effect of diffusion is neglected, using Eq. 10, the current due to the reactant ions, $i_r(t)$, may be obtained as

$$i_r(t) = \frac{e(N_1 k_1 + N_2 k_2)U_0 \sin \omega t}{\ln(b/a)} \int_0^{2\pi}\int_0^{L} \frac{r\, \mathrm{d}\varphi\, \mathrm{d}z}{r} \tag{21}$$

i.e.,

$$i_r(t) = \frac{e(N_1 k_1 + N_2 k_2)U_0 \sin \omega t}{\ln(b/a)} 2\pi L \tag{22}$$

where N_1 is the total number of positive ions, N_2 the total number of negative ions, and $\mathrm{d}V$ is expressed as $\mathrm{d}V = r\mathrm{d}r\mathrm{d}\varphi\mathrm{d}z$.

Bearing in mind the asymmetry of the electric field inside a cylindrical chamber, it may be assumed that the concentration of positive reactant ions in the vicinity of the collector electrode during the positive half-period is much higher than the concentration of negative ions near the outer electrode [12]. For the negative half period, the opposite is true, i.e., there is a surplus of negative ions near the collector electrode. Therefore, the following mean ionization current, $\bar{i}_r$, would be obtained at the output of a suitable electrometer amplifier/integrator:

$$\bar{i}_r = \frac{1}{T}\int_0^{2\pi/\omega} i_r(t)\, \mathrm{d}t = \frac{1}{2T}\int_0^{\pi/\omega} i_1(t)\, \mathrm{d}t + \frac{1}{2T}\int_{\pi/\omega}^{2\pi/\omega} i_2(t)\, \mathrm{d}t \tag{23}$$

From here, using Eq. 22, we obtain

$$\bar{i}_r = \frac{eU_0 NL}{\ln(b/a)}(k_1 - k_2) \tag{24}$$

The mean current of the reactant ions is negative (because $k_2 > k_1$ [17]). However, after being inverted in the amplifier/integrator, it is obtained at the output as a positive voltage. In Eq. 24, N is the total number of ions inside the chamber. Under stationary conditions, $N_1 = N_2 = N$.

In the presence of various compounds, positive or negative reactant ions undergo ion–molecule reactions with sample molecules, forming cluster ions.

Let us first consider positive cluster ions (which are obtained when sample molecules have a high proton affinity). If the concentration of the newly formed product ions is n_p, the number of remaining reactant ions will be $n_1 - n_p$. The negative ion current remains the same while the current due to the positive ions, i_p, according to Eq. 10 and 15, will be

$$i_p(t) = \frac{2\pi LeU_0[(n_1 - n_2)k_1 + n_2 k_2] \sin \omega t}{\ln(b/a)} + \frac{2\pi LeU_0 n_p k_p \sin \omega t}{[\ln(b/a)]^2} \ln\frac{r_2}{r_1} \tag{25}$$

It is important to note that regardless of the fact that the recombination of positive reactant ions will be minimal if the condition expressed by Eq. 17 is fulfilled, it will not hold for the product ions. Because of their longer stay inside the chamber, the probability of recombination is higher. Fig. 3 shows the static characteristics of the chamber in the presence of reactant ions (curve 1), product ions when recombination is neglected (curve 2), and product ions when recombination is taken into account (curve 3). Since the difference between curves 2 and 3 at the chosen operating point is small, curve 2 is assumed to be valid.

After settling Eq. 25, we have

$$i_p(t) = i_r(t) + \frac{2\pi LU_0 \sin \omega t}{\ln(b/a)} \times \left[k_1 - k_p \frac{\ln(r_2/r_1)}{\ln(b/a)}\right] n_p \tag{26}$$

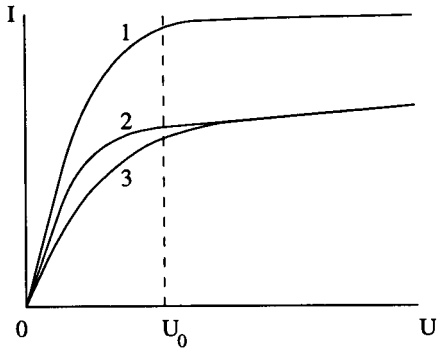

Fig. 3. Static characteristics of an ionization chamber: (1) reactant ions; (2) product ions, recombination neglected; (3) product ions, recombination included. U = applied DC voltage; I = measured ionization current.

where k_p is the effective mobility of product ions and

$$k_2 > k_1 > k_p \tag{27}$$

Keeping in mind what has been said about the mean current of reactant ions, the mean current of the product ions is given by

$$\bar{i}_p = \bar{i}_r - \frac{2eU_0L}{\ln(b/a)}\left[k_1 - k_p\frac{\ln(r_1/r_2)}{\ln(b/a)}\right]n_p \tag{28}$$

The second term in Eq. 28 is positive. It is subtracted from the mean current of reactant ions, which is negative, and inverted by the amplifier/integrator so that the corresponding output voltage rises with the increase in product ion concentration.

By further analysis of Eq. 28, the following conclusions can be made.

– In the absence of product ions, the current obtained is equal to the current of the reactant ions.

– When the concentration of product ions increases, the measured voltage increases too, at first linearly, and later asymptotically approaching the value for which $n_1 = 0$, that is, the value of the voltage when, for a given radiation source and chamber geometry, all positive reactant ions are consumed. It is presumed that the probability of direct ionization of sample molecules is negligible, due to the fact that their concentration is much lower compared with the concentration of air molecules. This asymptotic value is given by

$$\bar{i}_s = -\frac{eU_0L}{\ln(b/a)}k_2 - \frac{2eU_0L}{\ln(b/a)} \times\left[k_1 - k_p\frac{\ln(r_2/r_1)}{\ln(b/a)}\right]n \tag{29}$$

where n is the equilibrium concentration of ions. In the case of negative cluster ions, the mean current can be evaluated by an equation which is analogous to Eq. 28:

$$\bar{i}'_p = \bar{i}_r - \frac{2eU_0L}{\ln(b/a)}\left[k_2 - k'_p\frac{\ln(r_1/r_2)}{\ln(b/a)}\right]n'_p \tag{30}$$

where the superscript prime is related to negative ions.

In order to obtain the greatest signal for negative product ions, the ionization chamber should be tuned a little differently, because negative reactant ions are faster than positive reactant ions [17]. Therefore, the optimal operating frequency, calculated from Eq. 17, is somewhat higher for negative than for positive ions.

3. Conclusions

An ionization chamber with a built-in radiation source that is to be used as a gas and vapour sensor, can be brought in the dynamic resonance mode of operation when an alternating field is applied across its electrodes. The operating voltage and frequency are set to the values that provide the conditions in which positive reactant ions "barely" reach the electrodes. When an analyte with a high proton affinity is present in the chamber, the effective mobility of positive ions created in various ion–molecule reactions is lowered, causing a decrease in the measured current. In an alternating field, these positive ions (product ions) oscillate with a smaller amplitude and, therefore, reach the electrodes with a delay. Some of them are never collected because they recombine on their way to the electrodes. The recombination additionally lowers the measured chamber current, in fact, much more than the decrease in the mobility does. As the result, the sensitivity of

this type of ionization sensor is significantly increased.

The analytical application of the ionization chamber is based on its ability to measure the concentration of certain substances, due to the fact that the concentration is related to the ion current.

References

[1] J.E. Lovelock, Anal. Chem., 2 (1961) 162.

[2] G.E. Spangler and P.A. Lawless, Anal. Chem., 52 (1980) 193.

[3] E.B. Schmidel and L.I. Kalabina, J. Chromatogr., 446 (1988) 163.

[4] J. Boscher and Horst Adams, in Proceedings Supplement of the 3rd International Symposium on Protection Against Chemical Warfare Agents, Umeå, Sweden, 11–16 June 1989, National Defence Research Institute, Umeå, 1989, pp. 99–106.

[5] W.A. Harris, US Pat. 3835328.

[6] C.S. Harden and T.C. Imenson, Ionic Cluster Mass Spectrometry. I. Detection and Identification of Airborne Organic Vapors and Establishment of Operational Mechanism in the Ionization Detector System, NTIS AD-A 072 174, 1979.

[7] F.W. Karasek, W.D. Kilpatrick and M.J. Cohen, Anal. Chem., 43 (1971) 1441.

[8] D.I. Carroll, I. Dzidic, R.N. Stillwell and E.C. Horning, Anal. Chem., 47 (1975) 1956.

[9] G.E. Spangler and C.I. Collins, Anal. Chem., 47 (1975) 393.

[10] G.E. Spangler and J.P. Carrico, Int. J. Mass Spectrom. Ion Phys., 52 (1983) 267.

[11] T.W. Carr (Ed.), Plasma Chromatography, Plenum Press, New York, 1984, p. 23.

[12] J. Surutka, Elektromagnetika, Gradjevinska Knjiga, Beograd, 1975, p. 55.

[13] M.M. Metro and R.A. Keller, Sep. Sci., 9 (1974) 521.

[14] G.E. Spangler, D.N. Campbell, K.N. Vora and J.P. Carrico, ISA Trans., 23 (1984) 17.

[15] J.M. Preston, F.W. Karasek and S.H. Kim, Anal. Chem., 12 (1977) 1746.

[16] S. Milinković, O. Milanko and D. Novković, in Proceedings of the 3rd International Symposium on Protection Against Chemical Warfare Agents, Umeå, Sweden, 11–16 June 1989, National Defence Research Institute, Umeå, 1989, pp. 99–104.

[17] J.J. Thomson and G.P. Thomson, Conduction of Electricity through Gases, Vol I, Dover Publications, New York, 1969, p. 160.

ELSEVIER

Analytica Chimica Acta 294 (1994) 291–297

ANALYTICA CHIMICA ACTA

Development of an antibody-based biosensor for determination of 7-hydroxycoumarin (umbelliferone) using horseradish peroxidase labelled anti-7-hydroxycoumarin antibody

Brian Deasy [a], Eithne Dempsey [a], Malcolm R. Smyth [a,*], Denise Egan [b], Declan Bogan [b], Richard O'Kennedy [b]

[a] *School of Chemical Sciences, Dublin City University, Dublin 9, Ireland*
[b] *School of Biological Sciences, Dublin City University, Dublin 9, Ireland*

Received 22nd November 1993; revised manuscript received 11th March 1994

Abstract

An immunosensor based on a competitive electrochemical immunoassay was developed for the determination of 7-hydroxycoumarin. The antibody-based biosensor employed horseradish peroxidase-labelled anti-7-hydroxycoumarin, with the enzyme catalysed reaction involving the reduction of hydrogen peroxide in the presence of a mediator (hydroquinone). Sensor preparation involved immobilisation of the protein (ovalbumin/thyroglobulin)-bound 7-hydroxycoumarin antigen within a Nafion film on a glassy carbon surface. The electrode was then incubated in a solution containing both the enzyme-labelled anti-7-hydroxycoumarin and increasing concentrations of the free 7-hydroxycoumarin analyte. Competition between the free and immobilised forms of the antigen allows for the quantitation of free 7-hydroxycoumarin in solution. Injections of the enzyme substrate, hydrogen peroxide, resulted in an increase in the steady-state cathodic current (−0.03 V vs. saturated calomel reference electrode). This current output was inversely proportional to the concentration of analyte in solution. Free 7-hydroxycoumarin in solution was determined between 0 and 1 mM, with a detection limit of 24 μM.

Key words: Biosensors; Immunoassay; Immunosensor; 7-Hydroxycoumarin; Umbelliferone

1. Introduction

Coumarin is a naturally occurring constituent of many plants. It has been used in the treatment of a diverse range of ailments such as cancer, brucellosis, burns and rheumatic disease [1]. Coumarin undergoes rapid metabolism in the body, via the cytochrome P-450 system. In humans the main urinary metabolite is 7-hydroxycoumarin (7-OH-coumarin) [2,3]. Moran et al. [2] showed that, on average, 63% of the total dose of coumarin administered to patients was recovered as the 7-OH derivative within 24 h. A number of

* Corresponding author.

0003-2670/94/$07.00 © 1994 Elsevier Science B.V. All rights reserved
SSDI 0003-2670(94)00147-E

techniques have been applied to the determination of coumarin and 7-OH-coumarin. These techniques include paper and gas chromatography [4], liquid chromatography [5], spectrofluorimetry [6,7] and differential pulse voltammetry [8].

Immunoassay is a very selective and sensitive approach to trace metabolite analysis [9]. As a consequence of binding geometries the interaction between antigen and antibody molecules may be extremely specific under favourable conditions [10]. The utility of immunoassay in diagnostic medicine is well established with many routine clinical methods already in use for the determination of a wide variety of biologically important substances [11].

There are numerous means to study antibody–antigen interactions and antibody specificity. These include immunodiffusion, EMIT (enzyme multiplied immunoassay technique), radioimmunoassay, dialysis studies and blotting techniques [12]. The development of the Biacore system [13] offers a dynamic 'real time' method of monitoring antibody–antigen interactions. Recently, many other sensor systems have been described, which make use of antibody based methods [14]. Dempsey et al. [15] described a voltammetric method for studying the interaction of 7-OH-coumarin with its specific antibody. A well established method for studying antibody–antigen interactions is ELISA (enzyme linked immunosorbent assay) [12]. The competitive ELISA technique employs enzyme-labelled antibody with the antigen attached to a solid phase; the binding of enzyme-labelled antibody to immobilised antigen is competitively inhibited by an added standard or test antigen. The product concentrations measured at the end are inversely proportional to the concentration of the standard or test antigen in the incubation solutions.

This paper describes the development of a direct voltammetric method for the determination of 7-OH-coumarin in solution based on the decrease in current observed when free 7-OH-coumarin competes with 7-OH-coumarin immobilised as a protein metabolite conjugate on a glassy carbon electrode for their specific horseradish peroxidase (HRP)-labelled anti-7-OH-coumarin antibody. This results in a current output which is inversely proportional to the concentration of 7-OH-coumarin in the sample.

2. Experimental

2.1. Apparatus

A conventional 3-electrode system, with glassy carbon, saturated calomel and platinum gauze as working, reference and counter electrodes respectively, was connected to an EG&G PAR (Princeton Applied Research, Princeton, NJ) Model 264A polarographic analyser with output currents being measured by a WPA (Linton, Cambridge) Model CQ95 recorder. A batch amperometric mode of operation was used throughout, with a magnetic stirrer and bar providing the convective transport. A heat gun was used in the electrode preparation and an incubator (Memmert, Germany) was used in the temperature studies.

2.2. Electrode preparation

Before use the bare glassy carbon electrode was first polished with alumina slurry, after which it was sonicated in distilled water, rinsed with distilled water and allowed to dry in air. Modification of the electrode was achieved via drop coating of a 10 μl aliquot of the appropriate amount of conjugated protein (ovalbumin-7-OH-coumarin or thyroglobulin-7-OH-coumarin) in 5% Nafion, onto the electrode surface. The modified electrode was then dried for 1 h using the heat gun.

In the course of the optimisation studies the modified electrode was incubated in the appropriate concentration of HRP-labelled anti-7-OH-coumarin antibody (in 0.1 M phosphate buffer, pH 7.3) at the required temperature for 60 min. During the competitive assay the modified electrode was incubated in a solution of anti-7-OH-coumarin antibody (made up in 0.1 M phosphate buffer, pH 7.3) and the appropriate concentration of free 7-OH-coumarin (10 mM stock solution made up in 90:10 water–methanol daily).

2.3. Procedures

The modified electrode was rinsed in 0.1 M phosphate buffer, pH 7.3 and introduced into the electrochemical cell. DC voltammetry was carried out at a potential of −0.03 V vs. SCE after purging the phosphate buffer electrolyte solution (pH 7.3) with oxygen-free nitrogen for 20 min. The hydroquinone mediator (0.1 M stock solution made up in 0.1 M phosphate buffer immediately prior to use) was injected into the cell to reach a final concentration of 2 mM and the hydrogen peroxide substrate was added to give a final concentration of 1 mM in the cell. The reduction current of the mediator was then measured.

2.4. Reagents

Batch experiments were conducted at room temperature in 0.1 M phosphate buffer (pH 7.3), and all solutions were prepared in deionised water obtained by passing distilled water through a Milli-Q water purification system (Millipore, Milford, MA). 7-hydroxycoumarin (umbelliferone) was purchased from Sigma (St. Louis, MO). The anti-7-OH-coumarin antibodies were raised in rabbits [12] and the HRP-labelling was carried out according to Tijssen [12]. A 5 mg ml^{-1} solution of the HRP-labelled antibody was diluted with phosphate buffer. Diazotisation and conjugation of 7-OH-coumarin to BSA, ovalbumin and thyroglobulin was performed using a modification of methods reported by Morgan et al. [16] and Baker et al. [17].

Potassium dihydrogenphosphate and dipotassium hydrogenphosphate were obtained from Riedel-de-Haen (Hannover). Methanol (HPLC grade) was obtained from Labscan (Dublin). Hydroquinone was purchased from Aldrich (Poole). Nafion (perfluorinated ion-exchange powder, 5% solution in lower aliphatic alcohols and 10% water) was purchased from Aldrich (Poole). Hydrogen peroxide was obtained from Riedel-de-Haen. A 0.1 M solution of hydrogen peroxide was made up daily in 0.1 M phosphate buffer, pH 7.3.

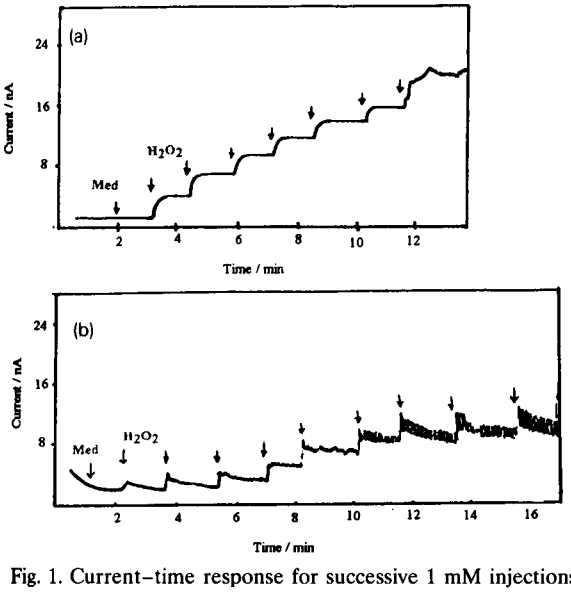

Fig. 1. Current–time response for successive 1 mM injections of H_2O_2 at (a) ovalbumin–7-OH-coumarin modified electrode and (b) ovalbumin only modified electrode. Operating potential −0.03 V with 450 rpm stirring rate and solution contains 2 mM hydroquinone. Electrolyte, 0.1 M phosphate buffer pH 7.3. The modified electrodes had been incubated in a 0.33 mg ml^{-1} anti-7-OH-coumarin antibody solution for 1 h at 37°C.

3. Results and discussion

3.1. Sensing mechanism

The enzyme horseradish peroxidase (HRP) catalyses the reaction between hydrogen peroxide and hydroquinone (HQ) and electrochemical biosensing is based on the amperometric monitoring of the electrochemical reduction of the oxidised mediator benzoquinone (BQ) [18].

$$H_2O_2 + HQ \xrightarrow{HRP} 2H_2O + BQ \quad (1)$$

$$BQ + 2H^+ + 2e^- \xrightarrow{\text{Applied Pot.}(-0.03\ V)} HQ \quad (2)$$

3.2. Development of an ovalbumin-7-OH-coumarin modified electrode

A 15% (w/v) ovalbumin–7-OH-coumarin modified electrode was prepared as described in the experimental section. This modified electrode

was then incubated in a 0.33 mg ml^{-1} anti-7-OH-coumarin antibody solution at 37°C for 1 h, after which it was rinsed with 0.1 M phosphate buffer (pH 7.3). The steady state response of this modified electrode to successive additions of 1 mM H_2O_2, in the presence of 2 mM hydroquinone as mediator, is shown in Fig. 1a.

The steady state response for the control electrode (ovalbumin only on surface) is shown in Fig. 1b. This demonstrates that there is a significant interference when using this protein to modify the electrode surface. This was not entirely unexpected as the rabbits were initially immunised with a bovine serum albumin (BSA) 7-OH-coumarin conjugate [12] and some of the antibodies produced have an affinity for the BSA itself. Ovalbumin is a very similar protein to BSA [19] (both being albumins) and this would explain the high response for the control. Globulins are significantly different proteins compared to albumins [19] and as a result a thyroglobulin–7-OH-coumarin conjugate was synthesised [16,17] and compared to the ovalbumin modified electrodes.

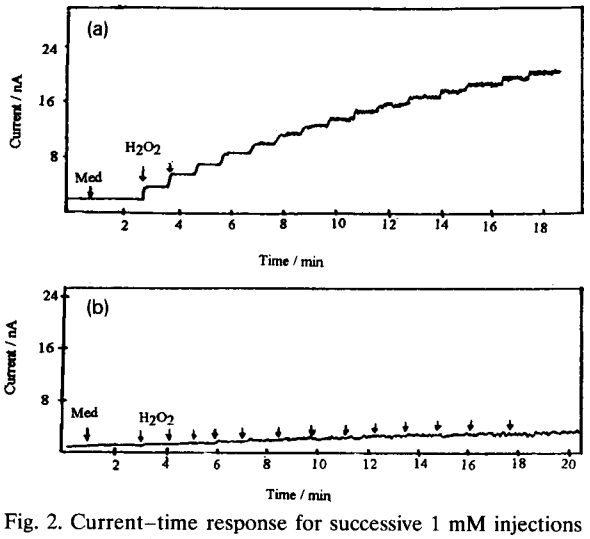

Fig. 2. Current–time response for successive 1 mM injections of H_2O_2 at (a) thyroglobulin–7-OH-coumarin and (b) thyroglobulin only modified electrode. Operating potential −0.03 V with 450 rpm stirring rate and solution contains 2 mM hydroquinone. Electrolyte 0.1 M phosphate buffer pH 7.3. The modified electrodes had been incubated in a 0.33 mg ml^{-1} anti-7-OH-coumarin antibody solution for 1 h at 37°C.

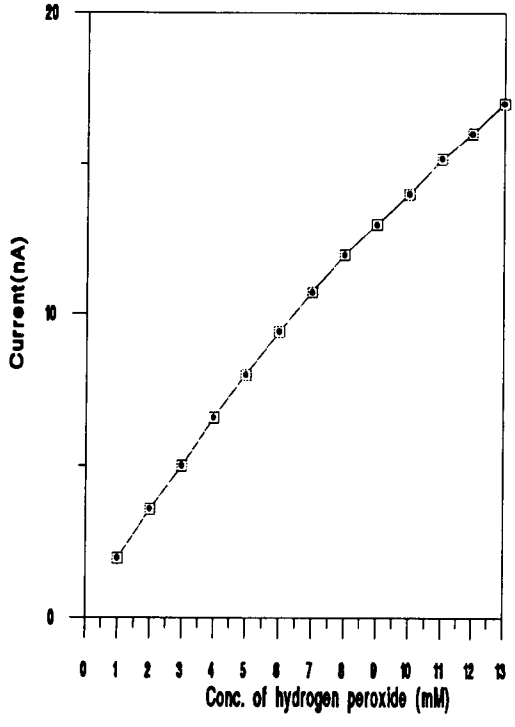

Fig. 3. Calibration plot for 15% (w/v) thyroglobulin–7-OH-coumarin modified electrode to successive additions of 1 mM hydrogen peroxide. Other conditions as in Fig. 2.

3.3. Development of a thyroglobulin–7-OH-coumarin modified electrode

These modified electrodes were prepared in a similar way to those using ovalbumin. A 15% (w/v) thyroglobulin–7-OH-coumarin modified electrode was prepared and incubated in a 0.33 mg ml^{-1} solution of anti-7-OH-coumarin antibody for 1 h at 37°C. Fig. 2a shows the steady state current response of this modified electrode to successive additions of 1 mM H_2O_2 (in the presence of 2 mM of mediator). It can also be seen from the figure that introduction of the mediator into the electrochemical cell produces no response until H_2O_2 is also present. Fig. 2b shows the response of a 15% (w/v) thyroglobulin control electrode. The resulting calibration plot for the thyroglobulin–7-OH-coumarin modified electrode is shown in Fig. 3. These results suggest that the anti-7-OH-coumarin antibodies have

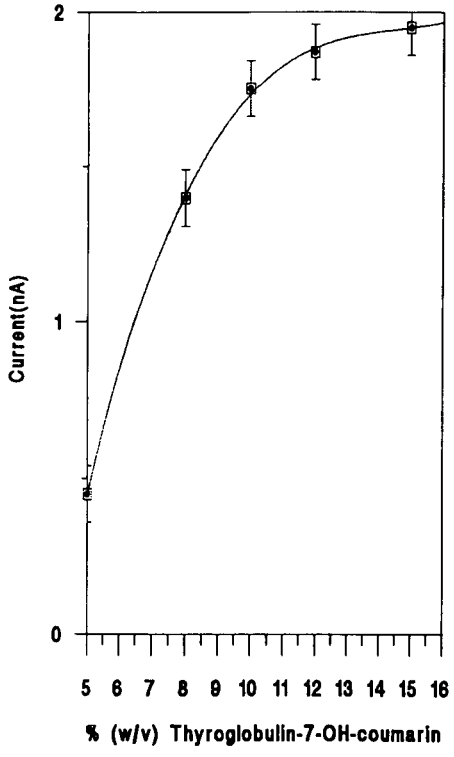

Fig. 4. Current dependence on thyroglobulin–7-OH-coumarin loading in the Nafion film upon injection of 1 mM hydrogen peroxide (in the presence of 2 mM hydroquinone). The antibody concentration was kept constant at 0.33 mg ml^{-1} and the temperature was 37°C throughout investigation.

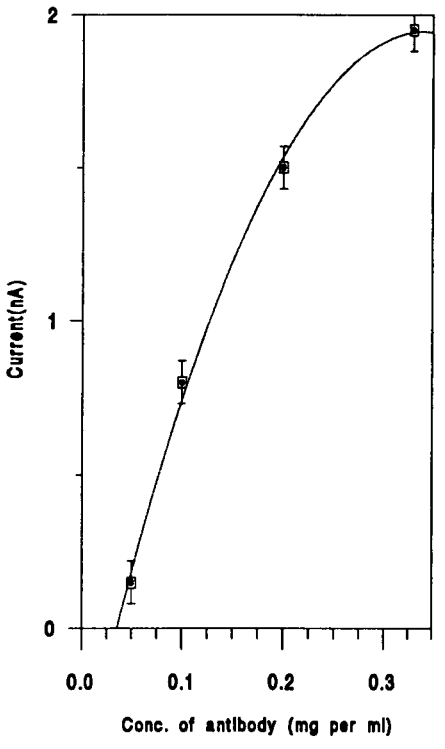

Fig. 5. Effect of anti-7-OH-coumarin antibody concentration on response to 1 mM injection of hydrogen peroxide (in the presence of 2 mM hydroquinone). Thyroglobulin–7-OH-coumarin loading was kept constant at 15% (w/v) and temperature of incubation was 37°C throughout the study.

much less affinity for the thyroglobulin protein compared to ovalbumin and for the remainder of the work the thyroglobulin conjugate was used in the development of an immunosensor for 7-OH-coumarin.

The effects of many experimental variables

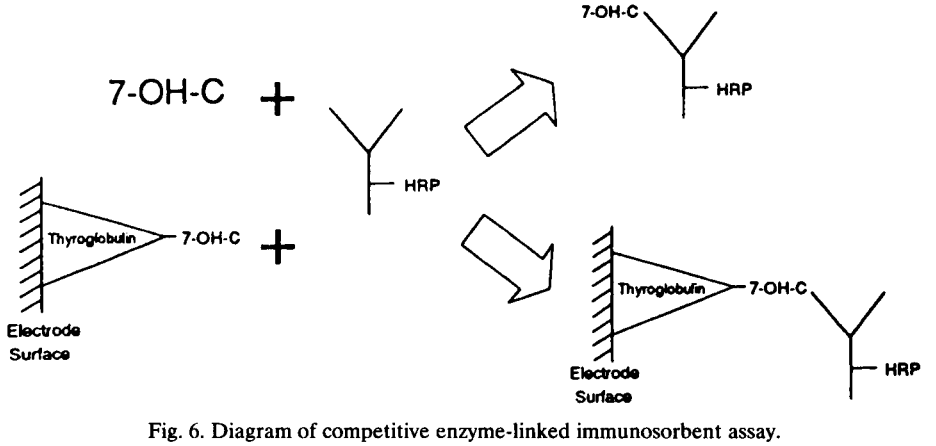

Fig. 6. Diagram of competitive enzyme-linked immunosorbent assay.

were investigated in order to optimise analytical performance. The optimum reaction of 7-OH-coumarin with its specific antibody takes place at pH 7.3, as determined in a previous study [15]. Nafion was used in the modified electrode preparation as it forms an insoluble film and is capable of keeping the protein conjugate immobilised within it. Various concentrations of Nafion were tried and a 5% Nafion film was shown to be optimum since lower concentrations of it either cracked on drying or resulted in the protein conjugate leaching out. Optimisation of the protein conjugate loading (thyroglobulin–7-OH-coumarin) in the Nafion film is shown in Fig. 4. In this case antibody concentration and temperature of incubation were kept constant. The optimum response was achieved using a 15% (w/v) loading. When higher loadings were attempted, the response time of the electrode became very slow.

The effect of antibody concentration is shown in Fig. 5. In this case protein loading in the Nafion film and temperature of incubation were kept constant. An optimum current response was observed for a concentration of 0.33 mg ml^{-1}.

The effect of temperature of incubation on antibody activity was also studied with an optimum being found near 37°C, i.e., the temperature where most antibodies are shown to bind to the antigen on the modified electrode surface. Therefore this temperature was taken as that providing maximum antibody activity for the operation of this immunosensor.

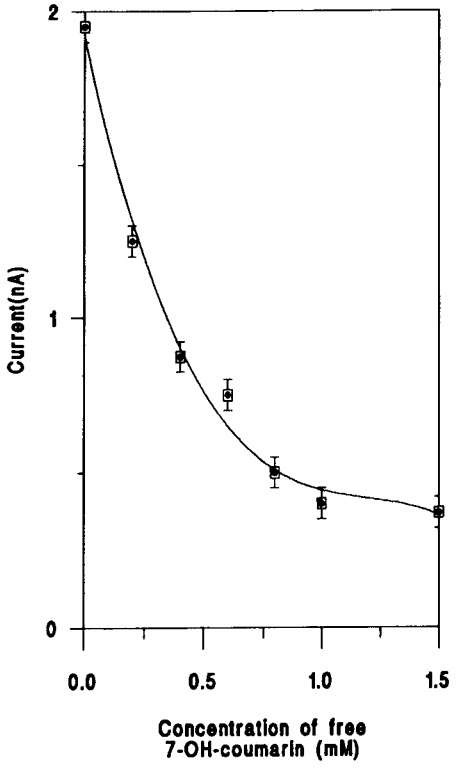

Fig. 7. Calibration graph for the determination of 7-OH-coumarin by electrochemical immunoassay. Thyroglobulin–7-OH-coumarin loading was 15% (w/v), antibody concentration was 0.33 mg ml^{-1} and the temperature of incubation was 37°C for each point on the calibration curve.

3.4. Competitive enzyme linked electrochemical immunoassay for the determination of 7-OH-coumarin

With all the experimental variables optimised, a calibration graph for 7-OH-coumarin was prepared for the immunosensor. A competitive enzyme-linked electrochemical assay was carried out where both free and solid phase antigens competitively react for the HRP-labelled anti-7-OH-coumarin antibody (Fig. 6). After rinsing with phosphate buffer, the enzyme attached to the electrode surface was determined by measuring the current after the addition of 1 mM hydrogen peroxide, in the presence of 2 mM of hydroquinone.

The calibration graph of current vs. concentration of 7-OH-coumarin is shown in Fig. 7. The response decreases exponentially, as less antibody binds to the immobilised antigen when the concentration of free 7-OH-coumarin in solution increases. Each point on the calibration graph represents an experiment with one electrode. From this plot 7-OH-coumarin can be determined between 0 and 1 mM in solution and has a limit of detection of 24 μM. This range has been shown to be physiologically relevant [3,8].

4. Conclusions

The system described in this paper clearly demonstrates a novel electrochemical approach for studying antibody–antigen binding and provides a further method for the determination of 7-OH-coumarin in solution. The metabolite can be determined between 0 and 1 mM in solution and has a limit of detection (3σ) of 24 μM. In the preparation of the modified electrodes it is important to use a protein conjugate which is significantly different from the protein conjugate used in the initial immunisation of the rabbits. Work is continuing into investigating how the antibody–antigen interaction on the electrode surface can be reversed after a determination, to produce a modified electrode capable of repeated use, for example in flow-injection analysis or liquid chromatography. It may be possible to do this by cleaning the modified electrode at the end of a determination in a buffer of low pH, which would cleave the antibody–antigen interaction on the electrode surface. Pulsed amperometric detection could also be used to reverse the antibody–antigen interaction, as has been suggested by Sadik and Wallace [20].

Acknowledgments

The authors acknowledge financial support from FORBAIRT for a Scientific Research Award (SC/92/340), and Maria Dolores Sanchez Suarez for assistance in the initial stages of this work.

References

[1] D. Egan, R. O'Kennedy, E. Moran, D. Cox, E. Prosser and R.D. Thornes, Drug Metab. Rev., 22 (1990) 503.
[2] E. Moran, R. O'Kennedy and R.D. Thornes, J. Chromatogr., 416 (1987) 165.
[3] D. Egan and R. O'Kennedy, J. Chromatogr., 582 (1992) 137.
[4] W.H. Schilling, R.F. Crampton and R.C. Longland, Nature (London), 221 (1969) 664.
[5] D.G. Walters, B.G. Lake and R.C. Cottrell, J. Chromatogr., 196 (1980) 501.
[6] H.S. Tan, W.A. Ritschel and P.R. Sanders, J. Pharm. Sci., 65 (1976) 30.
[7] D. Egan and R. O'Kennedy, Analyst, 118 (1993) 201.
[8] E. Dempsey, C. O'Sullivan, M.R. Smyth, D. Egan, R. O'Kennedy and J. Wang, J. Pharm. Biomed. Anal., 11 (1993) 443.
[9] J.I. Thorell and S.M. Larsond, Radioimmunoassay and Related Techniques, C.V. Mosby Co., St. Louis, 1978, p. 298.
[10] H.N. Eisen, in Microbiology, Harper and Row, New York, 1974, p. 547.
[11] E.M. Chalt and R.C. Ebersole, Anal. Chem., 53 (1981) 680.
[12] P. Tijssen, in R.H. Burdon and P.H. van Knippenberg (Eds.), Enzyme Linked Immunosorbent Assay in Laboratory Techniques, Biochemistry and Molecular Biology, Vol. 15, Elsevier, Amsterdam, 1985.
[13] U. Jonsson and M. Malmqvist, in A.P.F. Turner (Ed.), Advances in Biosensors, Vol. 2, JAI Press, London, 1992, pp. 291.
[14] F. Scheller and F. Schubert, Biosensors, Techniques and Instrumentation in Analytical Chemistry, Vol. 11, Elsevier, Amsterdam, 1992.
[15] E. Dempsey, C. O'Sullivan, M.R. Smyth, D. Egan, R. O'Kennedy and J. Wang, Analyst, 118 (1993) 411.
[16] G.T. Morgan, F.M.G. Michlethwait and M. Winfield, J. Biochem. Soc., 85 (1904) 1230.
[17] M.C. Baker, D.H. Campbell, S.I. Epstein and S.J. Singer, J. Am. Chem. Soc., 78 (1956) 312.
[18] P. Dominguez Sanchez, P. Tunon Blanco, J.M. Fernandez Alvarez, M.R. Smyth and R. O'Kennedy, Electroanalysis, 2 (1990) 303.
[19] T. Peters, J. Adv. Clin. Chem., 13 (1970) 37.
[20] O.A. Sadik and G.G. Wallace, Anal. Chim. Acta, 279 (1993) 209.

ELSEVIER

Analytica Chimica Acta 294 (1994) 299–304

ANALYTICA CHIMICA ACTA

Renewable miniature enzyme-based sensing devices

R. Gasparini [a], M. Scarpa [b], F. Vianello [a], B. Mondovì [c], A. Rigo [a,*]

[a] *Department of Biological Chemistry, University of Padova, Via Trieste 75, 35100 Padova, Italy*
[b] *Department of Physics, University of Trento, 38100 Trento, Italy*
[c] *Department of Biochemical Sciences and Center of Molecular Biology, University of Rome "La Sapienza", 00185 Rome, Italy*

Received 21st December 1993; revised manuscript received 21st March 1994

Abstract

A new approach to the preparation of electrochemical biosensors, based on a mixed Sepharose–carbon paste electrode, is described. The bioelectrode is made from carbon paste which is mixed, during preparation, with a mediator and with Sepharose containing an immobilized enzyme. The immobilized enzymes were glucose oxidase, from *Aspargillus niger*, and amine oxidase from bovine serum and from soybean seedlings. The Sepharose environment, favourable to the enzyme, and the close proximity of the enzyme redox-mediating and sensing sites, permits the required amount of enzyme to be decreased by two orders of magnitude and allows rapid response to the substrate. Response times as short as 15 s have been measured. The microelectrodes are easily fabricated, and the modified carbon paste can be incorporated in the various sensor configurations (micro, flow, etc.) relevant to clinical analysis.

Key words: Biosensors; Miniature enzyme-based sensors

1. Introduction

Mixed carbon paste electrodes, prepared by doping carbon paste with the modifying molecule, have received increasing attention in the last few years [1]. One of the most interesting developments in the field of electrochemical biosensors is the incorporation of biocomponents (enzymes, tissues, etc.) into a conventionally prepared carbon paste matrix [2–7]. Sensor fabrication is accomplished simply by mixing the biocomponent into the prepared carbon paste. However, the biological entities show a strong decrease in activity when incorporated in a carbon paste matrix due to their confinement in the hydrophobic environment. As a consequence, a large quantity of enzyme, up to 25% (w/w) [8], is required to obtain active bioelectrodes. This is a serious drawback when the biological component is available only in small amounts or it is highly expensive. This paper describes an approach to the preparation of carbon paste electrodes containing a Sepharose-immobilized enzyme. To illustrate the new concept of coupling biocomponents, immobilized in a favourable environment, with the technology of carbon paste, we chose three oxidases: glucose oxidase (GOD), a classical enzyme in biosensor testing, bovine serum amine oxidase

* Corresponding author.

Elsevier Science B.V.
SSDI 0003-2670(94)00148-F

(BSAO) and soybean seedling amine oxidase (SSAO), the last being an enzyme purified only in a small amount [9]. Such an approach results in an easy construction of high activity, reagentless enzyme electrodes requiring very small amounts of biocomponents.

2. Experimental

2.1. Materials

The chemicals for buffer solutions were of analytical grade. AH Sepharose, an agarose carrying free primary amino groups, was obtained from Pharmacia (Uppsala). All other materials were of the highest grade available.

Glucose oxidase, (E.C. 1.1.3.4. type X), from *Aspergillus niger*, specific activity 133 U/mg, and horseradish peroxidase, (E.C 1.11.1.7.), Type I, specific activity 95 U/mg, were supplied by Sigma (St. Louis, MO).

Soybean seedling amine oxidase was purified as previously reported [9].

Bovine serum amine oxidase, (amine:O_2 oxoreductase deaminating, E.C. 1.4.3.6), was purified according to a method described by Turini et al. [10].

2.2. Preparation of immobilized enzyme sensors

The enzymes were immobilized on AH Sepharose by cross-linking with *N*-(3-dimethylaminopropyl)-*N'*-ethylcarbodiimide hydrochloride. Alternatively amine oxidases were co-immobilized with horseradish peroxidase by use of the carbodiimide, mixing the enzymes together with the AH Sepharose. The molar amount of horseradish peroxidase loaded on the Sepharose was usually an order of magnitude higher than the amine oxidase.

The mixed Sepharose–carbon paste electrodes were obtained in the following manner: a graphite paste was prepared by carefully mixing 20 mg of graphite powder (Fluka), 10 mg of high vacuum silicone grease (Dow Corning), and 10 μl of 20 mM ferrocene in ethanol. The solution was cured at room temperature, for about 1 h, until the alcohol was completely evaporated. Then 4–7 mg of Sepharose containing the immobilized enzymes, partially dried on absorbent paper, were added to the prepared carbon paste and mixed thoroughly. In the case of standard carbon paste electrodes the lyophilized enzyme was added simply to carbon paste.

A small amount of the modified carbon paste was placed in a glass capillary (1.4 mm o.d., 0.6 mm i.d, 4 mm depth). A copper wire (0.6 mm o.d) provided tight closure of the capillary and the electrical contact in the voltammetric experiments. A fresh surface was obtained simply by extruding the carbon paste and the surface was smoothed on wax paper. The electrode has a calculated geometric area of 0.283 mm^2.

The electrode surface was checked by a Nikon stereoscopic microscope SMZ-ZT 102.

2.3. Apparatus

A 3-ml electrochemical cell equipped with a saturated calomel electrode (SCE) as reference, a Pt counter electrode and the modified carbon paste working electrode, was utilized. The electrodes were connected with an Amel 466 polarographic analyzer, the output of which was displayed on a Linseis y–t chart recorder.

2.4. Procedure

The sensor was equilibrated with 0.1 M potassium phosphate, pH 7.0, containing 50 mM KCl, in the case of glucose oxidase, or with 50 mM 4-(2-hydroxyethyl)-1-piperazineethanesulfonic acid (Hepes), pH 7.0, containing 50 mM NaCl, for the amine oxidases.

The amperometric detection of the various substrates was performed by application of an appropriate potential to the working electrode and the background current was allowed to decay to a steady-state. Aliquots of a stock solution of substrate were added, and, after brief stirring (10 s), the current for the quiescent solution was recorded. All the measurements were carried out at 22°C. The sensors, when not in use, were stored in 0.1 M potassium phosphate or 50 mM Hepes buffer, pH 7.0, containing 5 mM sodium azide, at 4°C.

3. Results and discussion

3.1. Sepharose–carbon paste electrodes containing glucose oxidase

To study the behaviour and demonstrate the advantages of the proposed Sepharose–carbon paste electrodes, conventional carbon paste and Sepharose–carbon paste electrodes, both containing glucose oxidase (GOD) and ferrocene, were prepared. The ferricinium ion (Fc^+), generated at the electrode surface by oxidation of ferrocene, was used as the acceptor of electrons from the reduced form of GOD.

Fig. 1a illustrates a typical chart recorder output of a carbon paste electrode containing GOD immobilized on Sepharose while Fig. 1b shows the calibration plot of carbon paste electrodes containing GOD in the presence and absence of AH Sepharose. We found that the electrode response increases linearly with the enzyme concentration in the range 2–40 U mg^{-1} carbon paste ($r = 0.997$; $n = 4$).

From Fig. 1 it appears that, notwithstanding that the Sepharose–carbon paste sensor contains a much smaller amount of enzyme than the usual carbon paste electrode, its current response is higher.

Since the void volume of the carbon paste due to the presence of Sepharose beads ranges from about 10 to 20%, thus increasing the electrode surface in contact with the solution, experiments were carried out where the enzymes were entrapped homogeneously in a carbon paste (enzyme–carbon paste, 10:90, w/w) containing about 15% (w/w) of AH Sepharose. A small decrease of the sensitivity was observed with respect to the sensitivity obtained when the same amount of enzyme was entrapped homogeneously in the carbon paste in the absence of AH Sepharose. This behaviour indicates that the presence of Sepharose in the carbon paste containing the oxidase is not responsible for the marked increase in activity obtained when the enzymes are covalently bound to the agarose matrix.

On the basis of the data reported in Fig. 1 and of the better signal-to-noise ratio obtained with the Sepharose containing electrodes, a simple

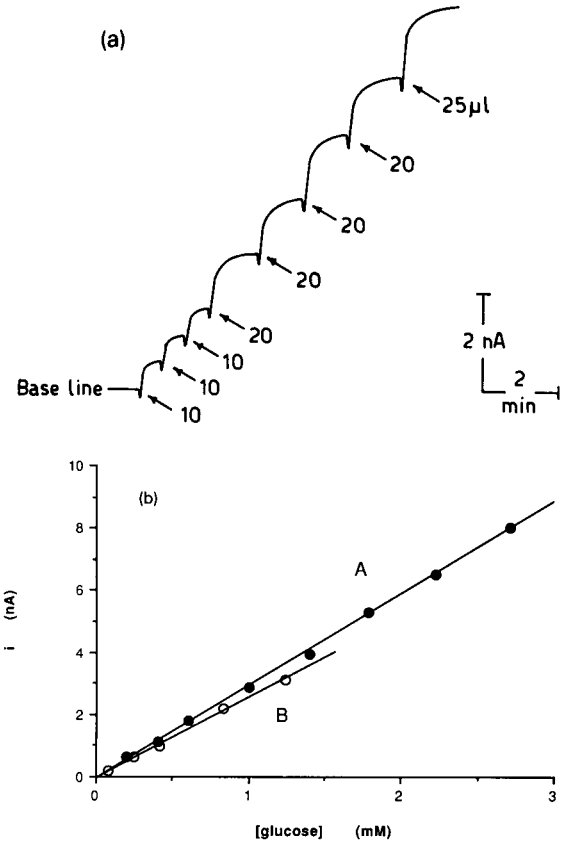

Fig. 1. (a) Typical response of glucose oxidase modified carbon paste electrode to addition of glucose. Glucose oxidase (enzyme unit ≤ 1) was immobilized on an AH Sepharose matrix mixed with carbon paste. 40 mM glucose was added to 2 ml 0.1 M potassium phosphate, pH 7.0, containing 50 mM KCl. (b) Calibration graphs for glucose obtained in the presence (•) and in the absence (○) of AH Sepharose: (A) glucose oxidase 0.177 U/mg carbon paste; (B) glucose oxidase 17 U/mg carbon paste, was simply mixed into the prepared carbon paste. The experiments were performed at $E = +400$ mV vs. SCE.

calculation shows that the carbon paste electrode containing the Sepharose-immobilized GOD permits a sensitivity similar to that of the conventional carbon paste–glucose oxidase electrodes to be achieved by a loading of enzyme at least two orders of magnitude less. The higher sensitivity of the Sepharose–carbon paste electrodes can be ascribed to the more 'natural' environment provided by Sepharose for the biocatalyst.

From Fig. 2, which shows the tip of an electrode, it appears that particles of AH Sepharose,

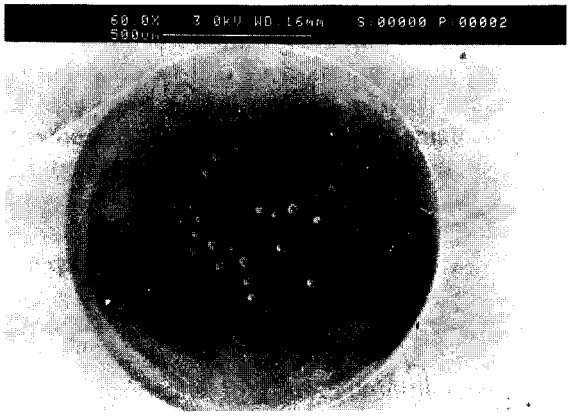

Fig. 2. Photograph of a Sepharose modified carbon paste electrode. The small round particles are the AH Sepharose grains.

characterized by a diameter in the 20–50 μm range, are present on the electrode surface. Accurate observations of the electrode surface by a stereoscopic microscope enables it to be calculated that 100–200 Sepharose particles are more or less exposed to the solution. Assuming that these particles are exposed as hemispheres a rough calculation showed that the amount of enzyme involved in the catalysis is of the order of 0.1 pmol.

Notwithstanding that the enzyme is immobilized into particles of ca. 50 μm diam., which may increase the diffusion path, the microelectrodes respond rapidly to changes in glucose concentration and the steady-state current is reached within 15–45 s. The Sepharose–carbon paste electrode shows a particularly favourable signal-to-noise ratio, which permits a detection limit of ca. 1×10^{-5} M glucose to be achieved. This detection limit appears as one of the best obtained for glucose oxidase biosensors [7], without enzyme amplification.

Typically, the calibration plots for the AH Sepharose carbon paste GOD electrodes are linear up to 3 mM glucose; the calibration graphs show an intercept of about zero and a slope of 15.9 nA mM^{-1} glucose U_{GOD}^{-1}, the standard deviation being $\leq 7.5\%$.

At glucose concentrations higher than 3 mM the electrode response displays a saturation effect. Since it was found that the steady-state current is virtually unaffected by turbulence in the solution, it was concluded that the response is limited by the enzyme reaction and that the small decrease in the current observed after sample addition, see Fig. 1, may be due to the response of the electrochemical circuit to the injection. Hence, an apparent Michaelis–Menten constant (K'_m can be calculated for the immobilized enzyme by plotting $1/I_{ss}$ vs. $1/$[glucose], where I_{ss} is the steady-state current (Lineweaver–Burk plot). The maximum current for this electrode was 260 nA/mm^2, with $K'_m = 12$ mM. The latter value is of the same order of magnitude of that found for the glucose oxidase electrode reported by Hale et al. [11]. However, the K'_m value we have measured is lower than that of the free enzyme (33–110 mM) [12,13]. Such K'_m shift may be due to the ferrocene mediated response or to the change of GOD microenvironment due to the enzyme immobilization into AH Sepharose particles.

3.2. Sepharose–carbon paste electrodes containing amine oxidase

An enhancement of the sensitivity with respect to the amount of loaded enzyme was also found for amine oxidases bound to Sepharose. Two enzymes were used: bovine serum amine oxidase (BSAO) and soybean seedling amine oxidase (SSAO), spermine and cadaverine being their substrates, respectively. As in the case of GOD, ferrocene was used as the mediator for the electron transfer between the enzyme and the electrode. However, since the electrochemically generated ferricinium ion does not act as an oxidant for reduced BSAO and SSAO, a kinetic excess of peroxidase relative to the oxidase was co-immobilized on Sepharose together with the amine oxidase. In this case the catalytic cycle is:

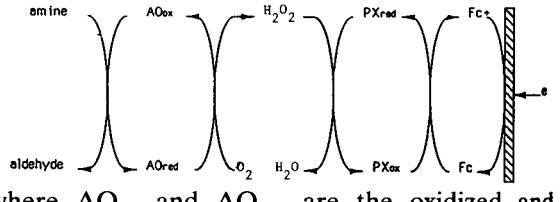

where AO_{ox} and AO_{red} are the oxidized and reduced form of the amine oxidase and PX_{ox},

PX_{red} are the oxidized and reduced form of the peroxidase, respectively.

In this way, hydrogen peroxide, which is one of the reaction products of the catalytic oxidation of the substrates and is electroactive at potentials higher than 600 mV vs. SCE, can be measured at potentials of the order of 200 mV or lower. Therefore, the interferences which may occur when real samples are examined at high electrode potentials may be minimized.

Typical characteristics of these electrodes are summarized in Table 1 together with those of GOD-containing electrodes. From this Table it appears that the Sepharose-modified carbon paste electrode, containing an amine oxidase, shows a much better performance than the conventional carbon paste electrode even if the amount of enzyme is one or two orders of magnitude less than in conventional carbon paste biosensors.

In Fig. 3 the steady-state response of the amine oxidase Sepharose–carbon paste electrodes to various concentrations of polyamines is reported. Fig. 3 underlines the good signal-to-noise ratio and detection limit achieved by this type of electrode, a detection limit of which, in the case of SSAO Sepharose–carbon paste electrodes, is better than that of the corresponding membrane biosensors [14].

It must be noted that the electrode containing the amine oxidase mixed directly with carbon paste shows a very poor signal-to-noise ratio, and the signal is not very stable. A saturation effect of

Table 1
Characteristics of the Sepharose modified carbon paste electrodes

Active component in the carbon paste	Amount of enzyme (mU mg^{-1} of carbon paste)	Detection limit (μM) [a]	Response time (s)
GOD–Sepharose	700	10	< 30
Lyophilized GOD	20000	50	180
BPAO–Sepharose	0.6	1	30
Lyophilized BSAO	30	3	90
SSAO–Sepharose	18.6	2	25
Lyophilized SAO	160	5	120

[a] The substrate was glucose, spermine and cadaverine for GOD, BSAO or SSAO, respectively. Other experimental conditions are given in the text.

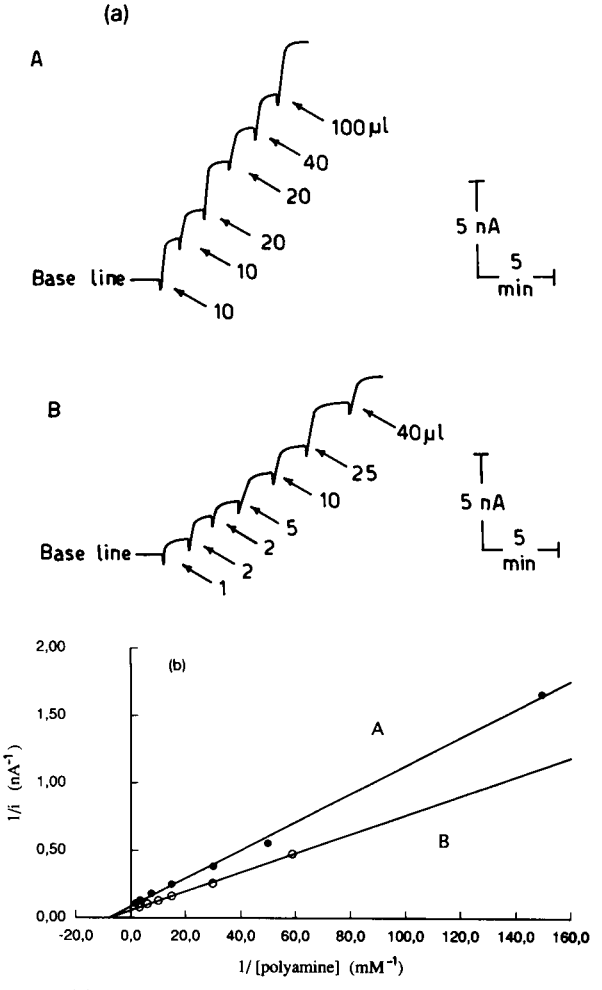

Fig. 3. (a) Typical response of amine oxidase modified carbon paste electrodes to addition of substrate. (A) Soybean seedling amine oxidase and horseradish peroxidase were immobilized in a Sepharose matrix mixed with carbon paste. 3.4 mM cadaverine was added to 2 ml of 50 mM Hepes, pH 7.0, containing 50 mM NaCl. (B) Bovine serum amine oxidase and horseradish peroxidase were mixed in the carbon paste matrix. 14 mM spermine was added to 2 ml of 50 mM Hepes, pH 7.0, containing 50 mM NaCl. (b) Calibration graphs as double reciprocal plot. The experiments were performed at $E = +200$ mV vs. SCE.

the AH Sepharose–carbon paste electrodes was also found for SSAO and BSAO, the apparent K'_m values being 126 and 125 μM, respectively. These values are higher than those found for the free amine oxidases under similar experimental conditions (65 μM and 30 μM for SSAO and BSAO, respectively) [15]. The increase of the K'_m

values could be due to a more difficult diffusion of substrate into the enzyme active sites.

3.3. Preparation and reproducibility of the electrodes

A set of data was acquired with independently fabricated GOD-containing Sepharose–carbon paste electrodes. The mean value of the slopes of the calibration graphs was characterized by a standard deviation of 8%. This result underlines the good reproducibility achieved in the preparation of the Sepharose-containing carbon paste electrodes, which is an important aspect to take into consideration in the large-scale production of biosensors. The re-use of these enzyme electrodes was also tested in the case of GOD containing electrodes. The active surface was renewed by extruding and polishing the GOD Sepharose–carbon paste material, and the electrode behaviour was recorded under the experimental conditions of Fig. 3. This procedure was repeated three times for each electrode. The mean value of the slope of the calibration plots obtained for the various surfaces was characterized by a standard deviation of 10.4%. This result shows the possibility of recreating an active surface by simply extruding the carbon paste when the activity of the sensing surface of the biosensor decreases because of enzyme denaturation by the test solutions.

3.4. Response time and stability

The response time of the GOD-containing Sepharose–carbon paste electrodes was measured by the time interval necessary to achieve 90% of the steady-state response current. As can be seen in Fig. 1, the steady-state current is achieved within 30 s in the presence of glucose concentrations ≤ 1 mM. The response time was found to increase to above 30 s at glucose concentrations in the mM range. For the amine oxidases, the response time was again < 30 s when the substrate concentration was $< K_m$ (Fig. 3). This appears to be a further proof that the sensor current is reaction limited and is in accord with the good flow properties of the Sepharose matrix.

The long-term stability of the sensor was determined by measuring the response to glucose. The sensor response decreased almost linearly to 60% of the initial level after two months when it was stored in phosphate buffer, pH 7, at 4°C. This change does not affect the practical analytical value of the enzyme electrode.

In conclusion the enzyme containing Sepharose–carbon paste electrodes are practical systems that can readily be used to prepare robust bioelectrodes for analytical applications. Such electrodes exhibit the advantage that the active surface may easily be renewed. The speed of response, small amount of enzyme, versatility, miniaturization, controlled bulk composition, incorporation of a second enzyme for sequence or amplification operations, and reproducibility of the surface represent others advantages of Sepharose–carbon paste bioelectrodes.

References

[1] P.D. Lyne and R.D. O' Neill, Anal. Chem., 62 (1990) 2347.
[2] J. Wang, L-H. Wu, Z. Lu, R. Li and J. Sanchez, Anal. Chim. Acta, 228 (1990) 251.
[3] T. Ikeda, F. Matsushita and M. Senda, Biosensors Bioelectronics, 6 (1991) 299.
[4] J. Wang and M.S. Lin, Anal. Chem., 60 (1988) 1545.
[5] W.W. Kubiak and J. Wang, Anal. Chim. Acta, 221 (1989) 43.
[6] J. Gerdea-Torresday, D. Dernall and J. Wang, Anal. Chem., 60 (1988) 72.
[7] W. Matuszewski and M. Trojanowicz, Analyst, 113 (1988) 735.
[8] J. Wang and K. Varughese, Anal. Chem., 62 (1990) 318.
[9] F. Vianello, M.L. Di Paolo, R. Stevanato, R. Gasparini and A. Rigo, Arch. Biochem. Biophys., 307 (1993) 35.
[10] P. Turini, S. Sabatini, O. Befani, F. Chimenti, C. Casanova, P.L. Riccio and B. Mondovi, Anal. Biochem., 125 (1982) 294.
[11] P.D. Hale, L.I. Boguslavsky, T. Inagaki, H.I. Karan, H.S. Lee and T.A. Skotheim, Anal. Chem., 63 (1991) 677.
[12] H.E. Welter, in H.U. Bergmeyer, J. Bergmeier and M. Grasse (Eds.), Methods of Enzymatic Analysis, Vol. 2, Verlag Chemie, Weinheim, 1983, p. 201.
[13] L. Goldstein, Methods Enzymol., 44 (1976) 397.
[14] R. Gasparini, M. Scarpa, M.L. Di Paolo, R. Stevanato and A. Rigo, Bioelectrochem. Bioenerg., 25 (1991) 307.
[15] R. Stevanato, B. Mondovì, O. Befani, M. Scarpa and A. Rigo, Biochem. J., 299 (1994) 317.

ELSEVIER

Analytica Chimica Acta 294 (1994) 305–309

ANALYTICA CHIMICA ACTA

Conductimetric assay of pyroglutamyl peptidase activity

Christine Besson [a], Sandrine Vessillier [a], Thierry Gonzales [b], Joëlle Saulnier [a], Jean Wallach [a,*]

[a] *Laboratoire de Biochimie Analytique et de Synthèse Bioorganique, ICBMC, Bât. 303, 43 Boulevard du 11 Novembre 1918, 69622 Villeurbanne Cedex, France*

[b] *Laboratoire de Génétique Moléculaire des Microorganismes et des Interactions Cellulaires, URA CNRS 1486, INSA, Bât. 406, 20 avenue Albert Einstein, 69621 Villeurbanne Cedex, France*

Received 16th December 1993; revised manuscript received 31st January 1994

Abstract

A conductimetric method was applied to assay *Streptococcus pyogenes* pyroglutamyl peptidase (E.C. 3.4.8.11) activity using pyroglutamylalanine or pyroglutamyltyrosine. A spectrophotometric comparison using pyroglutamyl-β-naphthylamide indicated that the sensitivity was much increased when using conductimetry. The use of a C-protected dipeptide such as pyroglutamylalanineamide also increased the sensitivity. Kinetic parameters have been measured for both dipeptides, with K_M values of 0.34 mM and 0.47 mM, respectively, for the alanine and tyrosine derivatives.

Key words: Conductimetry; Spectrophotometry; Pyroglutamyl peptidase

1. Introduction

Conductimetry has only quite recently been used for measurements of enzymatic activity [1]. In our laboratory we have developed various assays for the monitoring of reactions catalyzed by butyrylcholinesterase [2], alcohol and aldehyde dehydrogenases [3], lipases [4] and elastases [5,6]. The principle is based on the changes of charge distribution during the reaction; for example, charges may appear after cleavage of a peptide bond, oxidation of a substrate and release of protons.

In this paper the development of a new assay for pyroglutamyl peptidase (Pgp) activity measurements using a conductimetric technique is described. This type of enzymes selectively removes amino terminal L-pyroglutamic acid from peptides and proteins and is largely distributed in animal and plant tissues and micro-organisms [7,8]. The first assays developed used ninhydrin which reacted as free NH_2 was released. The methods currently used are based on the hydrolysis of pyroglutamic acid coupled with chromogenic or fluorogenic groups such as β-naphthylamine (βNA) [9] or *para*-nitroaniline [10], the reaction being monitored either by spectrophotometry or fluorimetry.

We have compared the spectrophotometric assay using pyroglutamyl-β-naphthylamide and the

* Corresponding author.

0003-2670/94/$07.00 © 1994 Elsevier Science B.V. All rights reserved
SSDI 0003-2670(94)00150-K

conductimetric assay using a pyroglutamylamino acid.

2. Materials and methods

2.1. Enzyme source

Pgp was purified from *Streptococcus pyogenes* [10]. The enzyme was kept at 4°C in a 50 mM phosphate buffer pH 8 containing 2 mM dithiothreitol (DTT) and 5 mM EDTA. Its concentration was 3.8 mg ml^{-1}.

2.2. Substrates

L-pGlu–$AlaNH_2$ was chemically synthesized using 1.5 mmol of L-pGlu (Bachem) and L-$AlaNH_2$ (Sigma, A-3521) in ethyl acetate. Dicyclohexylcarbodiimide (Jansen) and hydroxybenzotriazole (Milligen) were used as carboxyl activator and catalyst, respectively. After the reaction was complete, the solvent was evaporated and the product recrystallized from water. The purity of the product was demonstrated by TLC and LC. L-pGlu–Tyr was a gift from the Laboratory of Organic Chemistry (INSA, Lyon). L-pGlu–Ala and L-pGlu–βNA were obtained from Sigma. A 1 mM stock solution of pGlu–Ala or pGlu–Tyr was prepared in 5 mM Tris and the pH was adjusted to 8.6. A 10 mM pGlu–βNA solution was prepared in methanol. A 2 mM stock solution of pGlu–$AlaNH_2$ was prepared in 5 mM Tris. This solution was diluted to 1 mM with 5 mM Tris–HCl buffer (pH 8.6) for conductimetric measurements.

2.3. Other products

pGlu (Bachem), Ala (Merck), Tyr (Prolabo) and all other products were of analytical grade. Solutions of pGlu, Ala, Tyr, (pGlu + Ala) and (pGlu + Tyr) were prepared in 5 mM Tris–HCl buffer (pH 8.6) at a final concentration of 1 mM.

2.4. Conductimetry

The conductimetric measurements were performed in a 4-ml temperature-regulated cell which was connected to a CD-810 conductimeter (Solea-Tacussel) and conductance was recorded on a Kipp and Zonen BD40 recorder. The temperature was 30°C ± 0.1°C, the variations being kept under 0.02°C with a PTR Regler R-20/2 Lauda thermostat. In a typical experiment, the 4-ml cell is filled with the substrate solution and its conductance recorded after thermal equilibrium is reached (about 10–15 min). A small volume of enzyme is added to start the reaction and the variations of the conductance are recorded (see Fig. 1). Using solutions of known concentrations, the variation of conductances were correlated with the rates of the reaction.

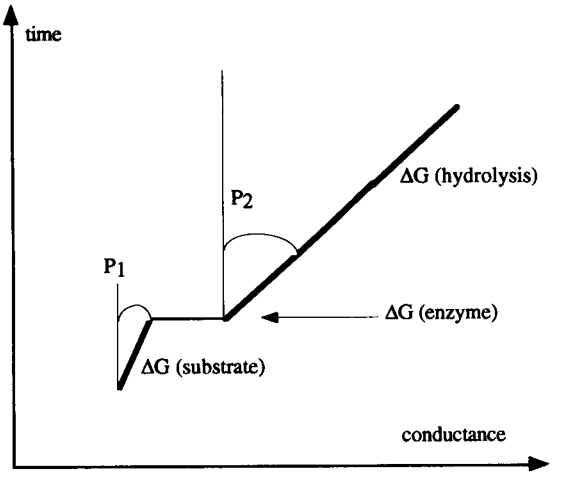

Fig. 1. Typical conductimetric recording (ΔG = change in conductance).

2.5. Spectrophotometry

The spectrophotometric measurements were performed using an Uvikon 941 spectrophotometer (Kontron). A small volume of enzyme was added to 0.9 ml of 50 mM phosphate buffer (pH 7) as described by Lee et al. [12]. After 3 min at 30°C, 100 μl of 10 mM pGlu–βNA were added to start the reaction. Absorbances were measured at 340 nm. The rates of hydrolysis are given in mM of substrate hydrolyzed per hour (ε_{NA} = 2070 l mol^{-1} cm^{-1}).

3. Results and discussion

3.1. Calibration of the conductimetric assay

The hydrolysis of the substrate may be summarized as follow:

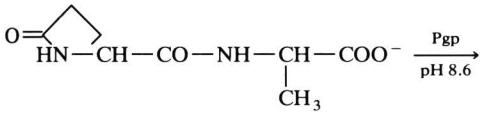

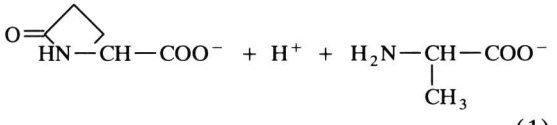

(1)

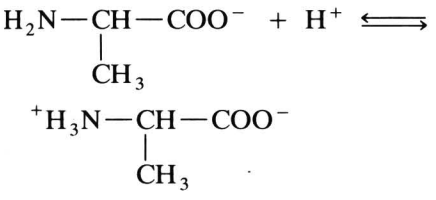

(2)

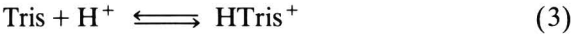

(3)

Considering the pH of the reaction, substrate hydrolysis leads to the pyroglutamyl anion, to the base form of alanine and to a proton (reaction 1). The liberated proton may combine with the amino group of either alanine (reaction 2) or tris(hydroxymethyl)aminomethane (Tris) (reaction 3). If we consider the conductimetric yield, reaction 1 and 3 are associated with an increase of conductance whereas reaction 2 leads to a decrease. It is therefore difficult to calculate the theoretical conductance variation due to substrate hydrolysis. We have determined separately the conductance changes of pGlu, Ala and Tris under the present experimental conditions.

Fig. 2 gives the relationship of conductance with concentrations for several solutions and particularly for pGlu + Ala and pGlu + Tyr mixtures. Using curve fitting, we have demonstrated that these relationships are linear. We have also determined similar relationships for pGlu, Ala and Tyr. First, we may observe that the conductances of Ala and Tyr are smaller than those of pGlu (9.2, 27.2 and 61.2 μS for Ala, Tyr and pGlu, respectively). In practice, in pH 8.6 Tris buffer, the amino group is only partially ionized,

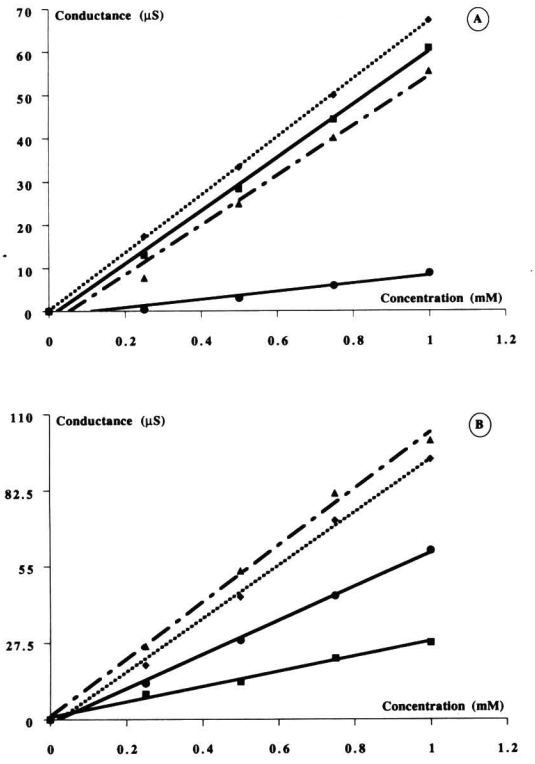

Fig. 2. Variation of the conductance (G, μS) as a function of substrate concentration. Equations are obtained by simple linear regression (standard deviation ($n = 3$) of slopes and intercept are given in parentheses). (A) (●) Ala: $G = -1.0$ (± 0.7) + 9.2 (± 1.1) [Ala], (▲) pGlu: $G = -1.3$ (± 0.9) + 61.2 (± 1.5) [pGlu], (◆) pGlu–Ala: $G = 0.2$ (± 0.3) + 66.7 (± 0.5) [pGlu–Ala], (■) pGlu + Ala: $G = -3.0$ (± 2.2) + 57.2 (± 3.6) ([pGlu] + [Ala]). (B) (■) Tyr: $G = 0.8$ (± 0.9) + 27.2 (± 1.5) [Tyr], (●) pGlu: $G = -1.3$ (± 0.9) + 61.2 (± 1.5) [pGlu], (◆) pGlu–Tyr: $G = -2.2$ (± 1.8) + 95.8 (± 3.0) [pGlu–Tyr], (▲) pGlu + Tyr: $G = 1.1$ (± 2.2) + 102.3 (± 3.6) ([pGlu] + [Tyr]).

whereas pGlu is fully ionized. Hydrolysis of pyroglutamylalanine (or tyrosine) will therefore be accompanied with an increase of conductance (in Tris buffer). Secondly, we have checked that the conductance of pGlu + Ala mixtures are quite equal to the sum of the conductance of pGlu and Ala (or Tyr).

3.2. Rates of substrate hydrolysis as a function of enzyme concentration

Fig. 3A and B shows the results of the conductimetric (A) and spectrophotometric (B) measure-

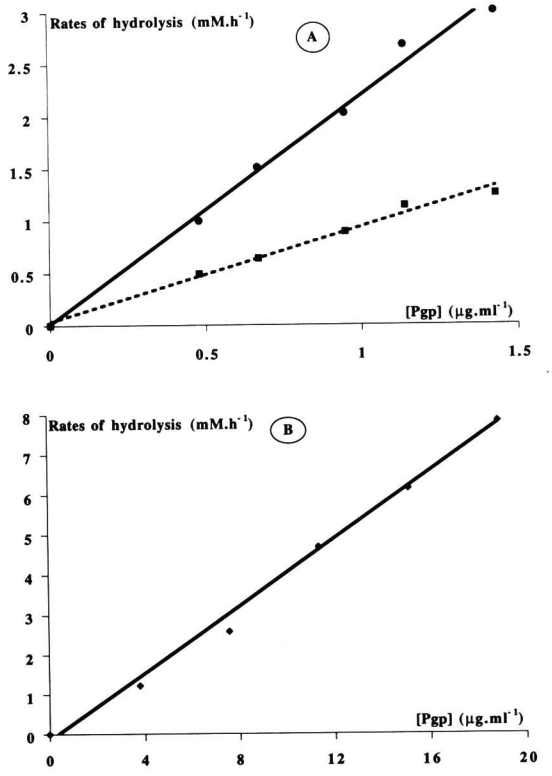

Fig. 3. Calibration graphs based on the comparison of the conductimetric method (A) and on the spectrophotometric method (B) for assaying Pgp. Equations are obtained by linear regression (standard deviation of slopes and intercept are given in parentheses). (A) pGlu–Ala (●): $v = 2.18$ (± 0.11) [Pgp] + 0.01 (± 0.3), $r = 1.00$. pGlu–Tyr (■): $v = 0.90$ (± 0.05) [Pgp] + 0.03 (± 0.04), $r = 0.99$. (B) pGlu–βNA (●): $v = 0.42$ (± 0.02) [Pgp] − 0.26 (± 0.18), $r = 1.00$. Each point is the mean of at least 2 values, the standard deviation being always lower than 5%.

ments of Pgp activity. The lowest measurable concentration of Pgp was about 4 μg ml^{-1} using the spectrophotometric method and 1 μg ml^{-1} for conductimetry for all substrates. If we use pGlu–Ala as a substrate in a conductimetric assay, the sensitivity is about 10 times higher then when using pGlu–βNA spectrophotometrically. The method would be improved by replacing pGlu–Ala by its amide derivative. Indeed, the substrate conductance would initially be equal to zero, and splitting of peptide bond would lead to two ionized molecules: pGlu, fully negatively charged and alaninamide, partially positively charged. The total change would be higher than with pGlu–Ala, thus increasing the sensitivity. In a preliminary study, we have synthesized pyroglutamylalaninamide (pGlu–AlaNH$_2$), and demonstrated that the experimental conductance changes are twice as high as with pGlu–Ala at the same concentration.

3.3. Kinetic parameters of pGlu-X hydrolysis by Pgp

Fig. 4 shows the results obtained for pGlu–Ala and pGlu–Tyr hydrolysis. The K_M values are 0.34 and 0.47 mM for pGlu–Ala and pGlu–Tyr, respectively. The maximal velocities (V_m) are 2.80 and 1.63 mM h^{-1} for pGlu–Ala and pGlu–Tyr, respectively. These values are in good agreement with those observed for calibration. The affinity constant of pGlu–βNA is 1.79 mM [11] which is 4 or 5 times higher than the values for pGlu–Ala or pGlu–Tyr. pGlu–βNA may be considered as a poor substrate for this Pgp, mainly because it is quite non-specific.

When comparing the affinity constants with those for other Pgps, the values are quite in good agreement. Fujiwara et al. determined K_M values of 0.1–0.15 mM with pGlu–Val, pGlu–Phe or pGlu–Trp as substrates for *Bacillus amyloliquefaciens* Pgp [13]. The value was 0.83–0.85 mM for

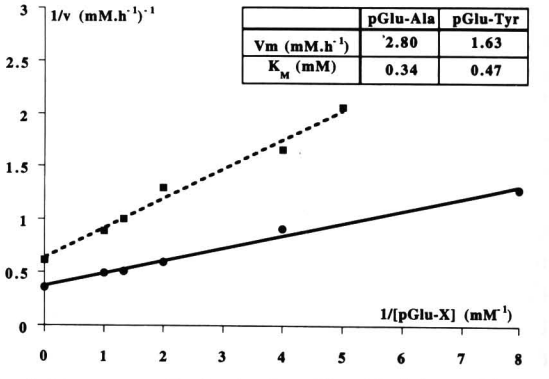

Fig. 4. Lineweaver–Burk plot for pGlu–Ala (●) or pGlu–Tyr (■) hydrolysis by Pgp. The concentration of the enzyme was 0.95 μg ml^{-1}. The kinetic parameters have been determined using k●cat software (BioMetallics). The standard deviations are: pGlu–Ala (●): $K_M = 0.34 \pm 0.05$, $V_m = 2.80 \pm 0.15$; pGlu–Tyr (■): $K_M = 0.47 \pm 0.08$, $V_m = 1.63 \pm 0.13$.

pGlu-Ala or pGlu-Val when using *Streptococcus faecium* Pgp [14].

In conclusion, conductimetry appears to be a very competitive alternative technique for measuring Pgp activity because its sensitivity and activities are continuously monitored. One disadvantage is that the method is limited to low ionic strength solutions, as sensitivity is defined by the relative change of conductance. The higher the background conductance, the higher must be the change in conductance to be measured, thus decreasing the sensitivity. The choice of a pyroglutamylamino acid led to lower K_M values, as P_1' (nomenclature of Schechter and Berger [15]) (and P_2' when amide derivatives were used) were occupied. With such a technique, it will be possible not only to measure enzyme activities in crude media, during purification, for example, but also to precisely define the specificity of Pgps by comparing the enzymatic parameters of various pyroglutamylamino acid substrates. This is particularly important if enzymes without specificity on P_1' positions are needed, for example, for *N*-terminal deprotection of peptides before sequencing.

Acknowledgments

We wish to thank Kerry McArtney for her very skilful technical assistance and Sandrine Croze for typing the manuscript. We also thank B. Chanterel and A. Doutheau for providing us with pGlu–Tyr. T. Gonzales was funded by the Région Rhône-Alpes.

References

[1] M. Hanss and A. Rey, Biochem. Biophys. Acta, 227 (1971) 630.
[2] P. Duffy and J. Wallach, Biotechnol. Appl. Biochem., 8 (1986) 479.
[3] I. Saad and J. Wallach, Anal. Lett., 25 (1992) 37.
[4] C. Ballot, B. Saizonou-Manika, C. Mealet, G. Favre-Bonvin and J. Wallach, Anal. Chim. Acta, 163 (1984) 305.
[5] B. Manika-Saizonou, K. Bostancioglu, C. Mealet, G. Favre-Bonvin and J. Wallach, Anal. Lett., 18 (1985) 901.
[6] H. Bakala, J. Wallach and M. Hanss, Biochimie, 60 (1978) 1205.
[7] A. Szewczuk and J. Kwiatkowska, Eur. J. Biochem., 15 (1970) 92.
[8] M. Mulczyk and A. Szewczuk, J. Gen. Microbiol., 61 (1970) 9.
[9] T. Yoshimoto, T. Shimoda, A. Kitazono, T. Kabashima, K. Ito and D. Tsuru, J. Biochem., 113 (1993) 67.
[10] A. Szewczuk and M. Mulczyk, Eur. J. Biochem., 8 (1969) 63.
[11] A. Awadé, T. Gonzales, P. Cleuziat and J. Robert-Baudouy, FEBS, 308 (1992) 70.
[12] H.J. Lee, J.N. Larue and I.B. Wilson, Anal. Biochem., 41 (1971) 397.
[13] K. Fujiwara, R. Koyabashi and D. Tsuru, Biochem. Biophys. Acta, 570 (1979) 140.
[14] J.J. Sullivan, E.E. Muchnicky, B.E. Davidson and G.R. Jago, Aust. J. Biol. Sci., 30 (1977) 543.
[15] I. Schechter and A. Berger, Biochem. Biophys. Res. Commun., 27 (1967) 157.

ELSEVIER

Analytica Chimica Acta 294 (1994) 311–318

ANALYTICA CHIMICA ACTA

Circuit network analysis method applied to surface acoustic wave impedance system in liquids

Shouzhuo Yao *,[a], Kang Chen [b], Dezhong Liu [b], Lihua Nie [b]

[a] *New Material Research Institute, Hunan University, Changsha 410082, China*
[b] *Department of Chemistry and Chemical Engineering, Hunan University, Changsha 410082, China*

Received 3rd January 1994; revised manuscript received 11th March 1994

Abstract

The circuit network theory was applied to analyse a surface acoustic wave (SAW) impedance system constructed from a 61-MHz SAW resonator and a pair of conductive electrodes in series. Two oscillation equations were derived and used to explain the effects of solution capacitance and cell constant on the frequency characteristics. The effects of the solution density and the viscosity on the frequency response of the SAW impedance system were also investigated. The SAW impedance system can be applied to conductivity measurements in solution with a high concentration background of foreign electrolytes.

Key words: Acoustic methods; Conductimetry; Impedance; Liquids; Surface acoustic wave

1. Introduction

The use of surface acoustic wave (SAW) devices for sensing chemical vapours was first reported in 1979 [1] and has since been investigated for its application to a variety of measurements, both chemical and physical [2–7]. SAW devices function by generating mechanical Rayleigh surface waves on a thin slab of a piezoelectric material that oscillates at a characteristic resonant frequency when placed in a feedback circuit with a radiofrequency amplifier [8]. Conductivity measurements are widely applied in analytical chemistry [9] e.g., for end-point detection in conductimetry and high-frequency titrimetry [10]. However, the sensitivity of such methods is limited and the accuracy is poor in solution systems when foreign electrolytes are present.

In previous papers [11,12], a new kind of SAW impedance system was introduced by combining a 61-MHz SAW resonator with a pair of parallel electrodes. We became interested in such a SAW impedance system because it can respond to changes in conductance and capacitance of the solution between the two electrodes. Recently we have developed two correlations between the frequency shift (Δf) of the SAW impedance system and the conductivity (χ) and the permittivity (ϵ) of the liquid:

$$\Delta f = a\chi + b \quad (1)$$

$$\Delta f = c\epsilon + d \quad (2)$$

* Corresponding author.

0003-2670/94/$07.00 © 1994 Elsevier Science B.V. All rights reserved
SSDI 0003-2670(94)00143-A

where a, b, c and d are constants depending on the SAW device, the circuit used and other experimental conditions. We also found that in a certain conductance region, the higher the conductance, the higher is the sensitivity of the impedance system.

We present here the results of further studies carried out in an attempt to clarify the earlier observations. The SAW impedance system including the amplifier was analysed with emphasis on its frequency behaviour with respect to electrolyte solutions by using the circuit network theory. Two oscillation equations were formulated. Experiments were then performed to determine the effect of the solution permittivity on the SAW impedance system and the influence of the cell constant. The effects of the density and viscosity of solution were also investigated.

2. Theory

The SAW impedance system consists of a SAW resonator and a pair of conductive electrodes. When the electrodes are immersed in a liquid, the electrical circuit representation of the SAW impedance system is as illustrated in Fig. 1a. The circuit of the series combination of a capacitor (C_m), an inductor (L_m) and a resistor (R_m) in parallel with a capacitor (C_o) and a resistor (R_o) is equivalent electrically to the SAW resonator. The motional resistance R_m and the radiation resistance R_o correspond to the loss of mechanical energy dissipated to the surrounding medium and the supporting structures [13–15]. The solution resistance is the reciprocal of the solution conductance (G) and the solution capacitance (C_s) depends on the permittivity of the solution and the cell constant (k):

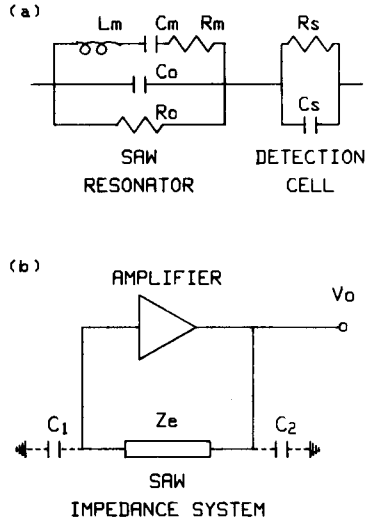

Fig. 1. (a) Equivalent electrical circuit of the SAW impedance system and (b) basic oscillator circuit.

$$G = k\chi \tag{3}$$

$$C_s = k\epsilon + C' \tag{4}$$

where C' is the parasitic capacitance. The impedance of the equivalent circuit (Z_e) shown in Fig. 1a is a complex, $Z_e = R_e + jX_e$; the real part (R_e) is called the resistance and the imaginary part (X_e) is called the reactance:

$$R_e = \frac{G}{G^2 + \omega^2 C_s^2} \tag{5}$$

$$X_e = \frac{-\omega C_s}{G^2 + \omega^2 C_s^2} + \frac{\omega L_m - 1/\omega C_m}{1 + C_o/C_m - \omega^2 L_m C_o} \tag{6}$$

where ω is angular frequency (in rad s^{-1}). Since the SAW resonator is operated in vacuum and is separated from the analyte in the experiment, the energy loss is much smaller than that of the normal polymer-coated SAW devices. For simplification, R_m and R_o are therefore ignored in Eqs. 5 and 6.

Most types of oscillator are constituted of an amplifier and a positive feedback. Fig. 1b shows the basic circuit of the SAW oscillator used in the experiment. C_1 and C_2 are parasitic capacitances between the leading wires of the SAW impedance system and ground and Z_e is the impedance of the equivalent circuit of the SAW impedance system (Eqs. 5 and 6). Z_e, C_1 and C_2 constitute the positive feedback network.

For purposes of oscillator analysis, the amplifier is represented by a four-terminal network described by its Y parameters (Y_i, Y_o, Y_f, Y_r) and the positive feedback network is represented by its Z parameters (Z_i, Z_o, Z_f, Z_r). In most instances, the amplifier can be considered as an

ideal one in circuit analysis. In this circuit, it is assumed that the amplifier input admittance Y_i and the reverse transfer admittance Y_r will be negligible and the output admittance will be purely real, $Y_o = g_o$. The forward transfer admittance Y_f is often broken into its real part (transconductance) and imaginary part (susceptance): $Y_f = g_f + jb_f$. The Z parameters can also be calculated by definitions as follows [16]:

$$Z_i = -X_2(X_1 + X_e - jR_e)/Z \quad (7)$$

$$Z_o = -X_1(X_2 + X_e - jR_e)/Z \quad (8)$$

$$Z_f = Z_r = -X_1X_2/Z \quad (9)$$

where $Z = R_e + j(X_1 + X_2 + X_e)$, $X_1 = -1/\omega C_1$ and $X_2 = -1/\omega C_2$.

There are two criteria that must be satisfied for an oscillation to occur in a network: the magnitude of loop gain is unity and the phase shift around the loop is zero. These two criteria can be included by solving a complex oscillation equation based on the Y and Z parameters of the network [17]:

$$Y_fZ_f + Y_iZ_o + Y_oZ_i + Y_rZ_r + \Delta Y \Delta Z + 1 = 0 \quad (10)$$

where

$$\Delta Y = Y_iY_o - Y_fY_r$$

$$\Delta Z = Z_iZ_o - Z_fZ_r$$

This equation is general and can be applied to almost any kind of oscillation. By substituting Eqs. 7–9 and the above assumptions of Y parameters into the general equation (Eq. 10) and separating it into real and imaginary components, we obtain the real part:

$$-X_1X_2g_f - X_2g_o(X_1 + X_e) + R_e = 0 \quad (11)$$

and the imaginary part:

$$-X_1X_2b_f - X_2R_eg_o + X_1 + X_2 + X_e = 0 \quad (12)$$

Define A as the phase angle of the forward transfer admittance: $A = b_f/g_f$. When an amplifier is operated at high frequency, there is a phase lag between the output current and the input voltage, so A is negative at high frequency and is a function of frequency. It is convenient to assume that, to a certain degree of accuracy, A is a constant because the relative frequency variation during the experiment is very small. Then Eqs. 11 and 12 can be rearranged as

$$R_e(A - g_oX_2) - X_e(1 + g_oX_2A) - (X_1 + X_2 + g_oX_1X_2A) = 0 \quad (13)$$

$$g_f = \frac{R_e - g_oX_2 \cdot (X_1 + X_e)}{X_1X_2} \quad (14)$$

Eq. 13 yields the necessary reactance of the SAW resonator to satisfy the phase shift requirement which determines the oscillation frequency of the circuit, while Eq. 14 yields the amplifier transconductance g_f required for oscillation.

Let

$$-X(\omega) = R_e(A - g_oX_2) - X_e(1 + g_oX_2A) - (X_1 + X_2 + g_oX_1X_2A)$$

Fig. 2 shows a typical plot of $X(\omega)$ and g_f of the SAW impedance system operated at 61 MHz. There are two frequencies at which the phase shift is zero: f_s is the low frequency at zero phase, called the series resonant frequency, and f_p is the high frequency at zero phase, called the parallel resonant frequency. The two frequencies are solutions of Eq. 13, which is a quadratic function of frequency. As g_f is much smaller at f_s than at f_p, especially when R_m and R_p are taken into account, oscillation will build up on the series resonant frequency [15].

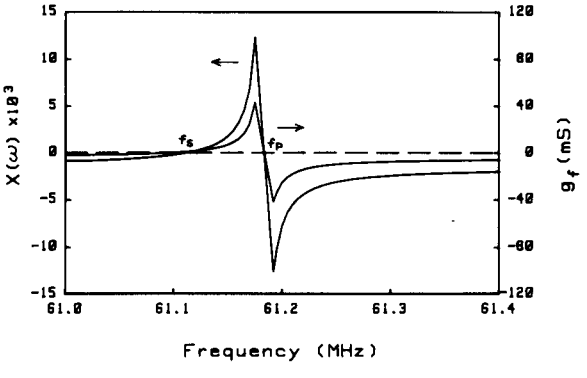

Fig. 2. Display of solutions of the oscillation equations (Eqs. 13 and 14).

When the solution conductance G changes, the impedance of the SAW impedance system Z_e also changes, so the oscillation frequency will shift until the two oscillation conditions are satisfied. This is the theoretical basis for the SAW impedance system to be applied to conductivity measurements. The effect of varying G on the g_f and the oscillation frequency of the SAW impedance system are demonstrated in Fig. 3. These are calculated for $L_m = 227\ \mu H$, $C_m = 0.03$ pF, $C_0 = 5$ pF, $C_1 = C_2 = 10$ pF, $g_0 = 1$ mS, $C_s = 9$ pF, $A = -0.5$ and $k = 1$ cm. As can be seen from Fig. 3, increasing G drives the oscillation frequency to lower frequency.

The conductance sensitivity of the SAW impedance system ($d\Delta f/dG$) is defined as the incremental change in oscillation frequency occurring in response to an incremental change in conductance. The conductance sensitivity of the SAW impedance system as a function of conductance is shown in Fig. 4. It can be seen that in a certain region, the conductance sensitivity of the SAW impedance system increases with increasing solution conductance. Therefore, the SAW impedance system offers an advantage over the classical conductimetric method in a solution system of high electrolyte background. If the conductance of foreign electrolytes is much greater than that of the analyte, the sensitivity and accuracy of the classical conductimetric method become worse, whereas those of the SAW impedance system improve.

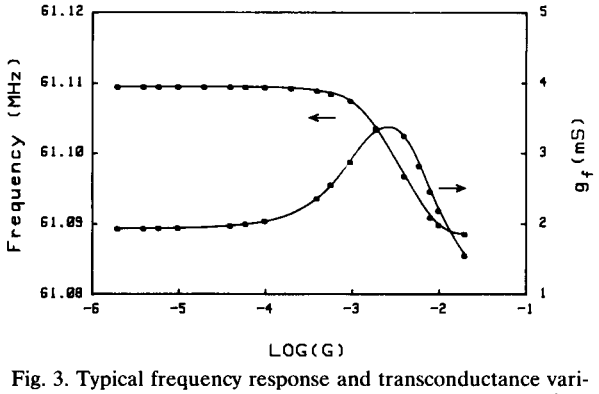

Fig. 3. Typical frequency response and transconductance variation with solution conductance. G ranges from 2×10^{-6} to 2×10^{-2} S.

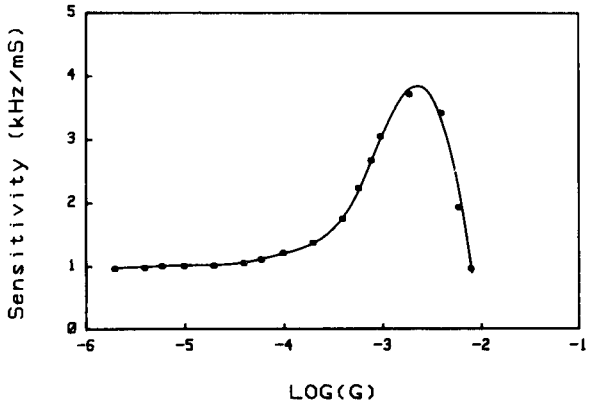

Fig. 4. Dependence of conductance sensitivity of the SAW impedance system on solution conductance.

3. Experimental

3.1. Apparatus and reagents

The experimental set-up with the SAW impedance system used in this work was the same as reported previously [10]. Two platinum electrodes of dimensions 0.5×0.5 cm were selected, ground with sandpaper and placed parallel into a detection cell at a fixed distance. The two leading wires were kept as short as possible to reduce the parasitic capacitance. The instrument used to characterize the SAW resonator was an HP 8753A network analyser with an HP 85046A S-parameter test set. The operational frequency range was from 300 kHz to 3.0 GHz. An HP 4192A LF impedance analyser was employed to measure the conductance and the capacitance of the liquids with the same conductive electrodes in the experiment. The data were transferred over an HPIB bus to an HP 300 computer and were used in the theoretical calculation.

All chemicals were of analytical-reagent grade and used as received. Data for the density and viscosity for sucrose solutions of different concentration at 20°C were taken from [18]. Doubly distilled water was used throughout.

3.2. Procedure

A period of 30 min was needed to stabilize the whole set-up, including the frequency counter and power supply. The baseline noise was determined by using frequency data collected for 5 min prior to the experiments. After the mean frequency (f_0) had been measured in the background solution (10 ml), 10 μl of standard electrolyte solution were injected into it using a microsyringe. The frequency shift ($\Delta f = f_0 - f$) observed was then recorded. The procedure was carried out consecutively from dilute solution to more concentrated solution. The measurements were repeated in 1,4-dioxane–water mixed solvents of different concentrations and with conductive electrodes of different cell constants.

To examine the effects of density and viscosity on the SAW impedance system, frequency shift measurements were performed with sucrose solutions from 0% to 25% in increments of 5%.

All experiments were conducted at a fixed stirring speed and a constant temperature thermostated at 20.0 ± 0.1°C.

4. Results and discussion

4.1. Effects of density and viscosity of solution

The influence of density and viscosity on the behaviour of the SAW impedance system was investigated in 0–25% aqueous sucrose solutions. The changes in capacitance and the frequency shift of the SAW impedance system with variation in the solution density and viscosity are shown in Table 1. It can be seen that the frequency shift increases but the capacitance decreases with increasing density and viscosity. The solution conductance was less than 0.01 mS and remained almost unchanged during the experiment. Hence its effect on the SAW impedance system response can be ignored. Frequency shifts were also calculated according to Eq. 13 due to the varying solution capacitance with other factors being constants ($C_m = 0.03$ pF, $L_m = 227$ μH, $C_0 = 5$ pF, $k = 0.972$ cm and $G = 0.01$ mS). The results are close to the frequency shifts measured experimentally. That is, the density and viscosity of the solution have little effect on the frequency of the SAW impedance system, but do affect the capacitance and conductance. This result is as expected because the SAW resonator is not in contact with the solution and its frequency should depend only on solution parameters such as electrolytic conductivity and permittivity. The acoustic impedance and the energy loss of the SAW resonator are much less, so the impedance system possesses a low noise level, a high quality factor (Q) and hence a low detection limit. The typical noise level is less than 2 Hz.

Table 1
Frequency shift and solution parameters in sucrose solutions

C (%)	ρ (g cm^{-3})	η/η_0	C_s (pF)	$\Delta f_{pred.}$ (Hz)	$\Delta f_{expt.}$ (Hz)	R.S.D. ($n = 5$)(%)
0	0.9982	1	9.216	0	0	
5.0	1.0178	1.144	9.094	209	201	1.0
10.0	1.0381	1.333	8.976	418	405	1.2
15.0	1.0592	1.589	8.859	632	611	1.0
20.0	1.0810	1.914	8.747	851	826	0.8
25.0	1.1036	2.447	8.630	1075	1039	0.9

ρ = Density and η/η_0 = relative viscosity at 20°C; all the data are from [18]. $\Delta f_{pred.}$ = frequency shift calculated according to Eqn. 13 with a 0% solution as the reference.

4.2. Responses of SAW impedance system to electrolyte solutions

The influence of solution capacitance on the response of the SAW impedance system to conductance was examined by investigating the frequency characteristics in 1,4-dioxane–water mixed solvents of different volume percentages and with varying electrolyte concentrations. Dioxane–water was chosen because it has a wide permittivity range varying from 2.209 to 78.54 (at 25°C). The lower the percentage of water, the smaller is the mixed solvent capacitance.

The frequency shift vs. conductance curves are plotted in Fig. 5. Curves for mixed solvents with 0 and 5% water are not shown owing to overlapping with the curve for mixed solvent with 10% water (curve 1). It can be seen from Fig. 5 that

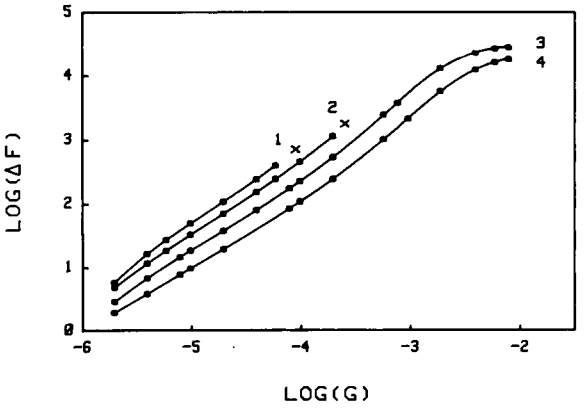

Fig. 5. Effect of solution capacitance on frequency conductance characteristics. The solid lines represent the predicted values based on Eq. 13. Water concentration in the dioxane–water mixed solvent (v/v): (1) 10; (2) 30; (3) 60; (4) 100%.

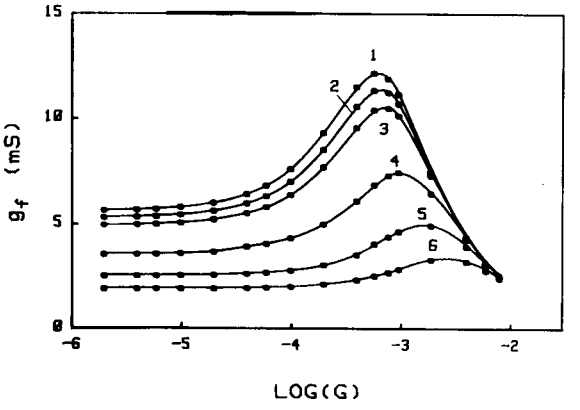

Fig. 7. Effect of solution capacitance on transconductance. Water concentration in the dioxane–water mixed solvent (v/v): (1) 0; (2) 5; (3) 10; (4) 30; (5) 60; (6) 100%.

there is a linear relationship between the frequency shift and the solution conductance over a wide conductance range, and the solution capacitance has a strong influence on the SAW impedance system; the impedance system has higher sensitivity but narrower linear range in solutions of smaller capacitance. Conductance sensitivities of the response of the SAW impedance system were also calculated according to Eq. 13 with the measured values of capacitance and conductance and the following parameters of the SAW resonator and circuit: $L_m = 227$ μH, $C_m = 0.03$ pF, $C_0 = 5$ pF, $C_1 = C_2 = 10$ pF, $g_o = 1$ mS, $A = -0.5$ and $k = 0.972$ cm. The results are shown in Fig. 6. The points represent the calculated values of conductance sensitivity based on Eq. 13. The agreement between the calculated and experimental values is very good.

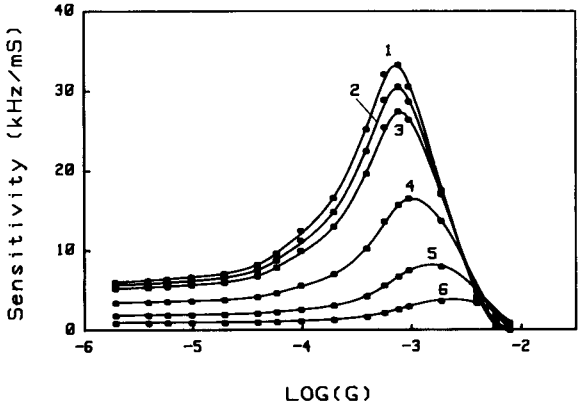

Fig. 6. Effect of solution capacitance on conductance sensitivity. Water concentration in the dioxane–water mixed solvent (v/v): (1) 0; (2) 5; (3) 10; (4) 30; (5) 60; (6) 100%.

A phenomenon observed in this experiment was that when the conductance became greater in small-capacitance solutions, the frequency stability of the SAW impedance system became worse and the oscillation even ceased. The smaller the solution capacitance, the lower was the cease-to-oscillate point (see Fig. 5). The transconductance g_f, which indicates the amplifier gain needed to support the oscillation, was calculated according to Eq. 14 as a function of conductance and is shown in Fig. 7. The results clearly show that Eq. 14 explains the above phenomenon well: g_f increases with increasing G until the point is reached at which the amplifier gain of the electrical circuit is no longer sufficient to maintain oscillation. The effect of g_f on frequency stability is difficult to investigate experimentally. However, the greatest value of g_f that can be obtained in our circuit under these experimental conditions can be estimated as approximately 6 mS, on comparing Figs. 5 and 7. This indicates that g_f is an important characteristic parameter for the design of the SAW impedance system.

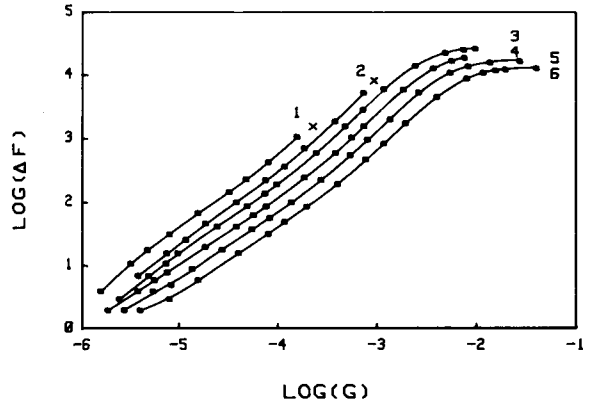

Fig. 8. Effect of cell constant on frequency conductance characteristics. The solid lines represent the predicted values based on Eq. 13. Cell constant: (1) 0.164; (2) 0.385; (3) 0.630; (4) 0.972; (5) 1.41; (6) 2.04 cm.

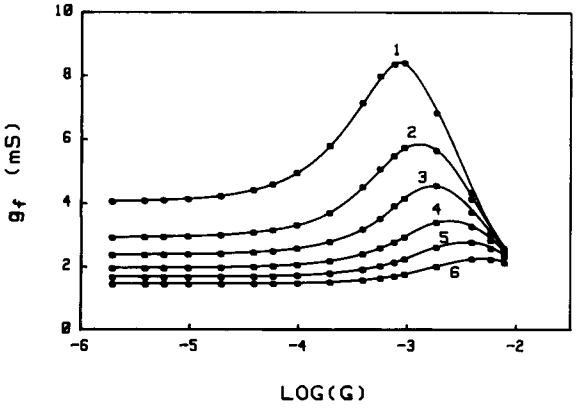

Fig. 10. Effect of the cell constant on transconductance. Cell constant: (1) 0.164; (2) 0.385; (3) 0.630; (4) 0.972; (5) 1.41; (6) 2.04 cm.

4.3. Effect of cell constant

Because both the solution capacitance and conductance are proportional to the cell constant of conductive electrodes in series with the SAW resonator (Eqs. 3 and 4), the effect of the cell constant on the frequency conductance characteristics was investigated. The results of frequency shift due to conductance variation obtained with different cell constants from 0.164 to 2.04 cm (Fig. 8) show that the impedance system has higher sensitivity, a narrower linear range and a lower cease-to-oscillate point when a pair of electrodes of smaller cell constant is employed. Figs. 9 and 10 illustrate the calculated conductance sensitivity and transconductance with different cell constants. The plots show almost the same features as those in Figs. 6 and Fig. 7, and agree well with the experimental results. The most important result of this experiment is that if the amplifier can provide sufficient transconductance, conductive electrodes of small cell constant have a high sensitivity. This offers an advantage in miniaturizing the impedance system.

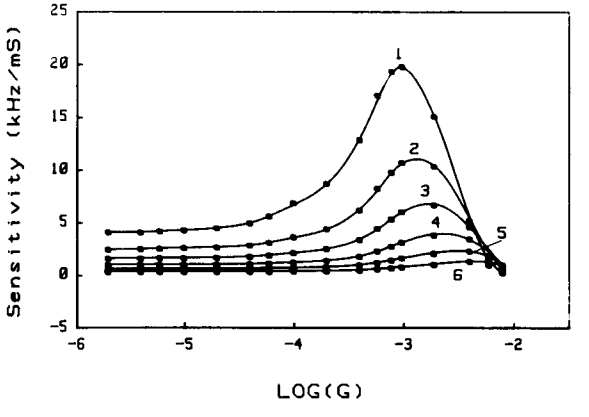

Fig. 9. Effect of the cell constant on conductance sensitivity. Cell constant: (1) 0.164; (2) 0.385; (3) 0.630; (4) 0.972; (5) 1.41; (6) 2.04 cm.

5. Conclusions

The circuit network analysis method was applied to characterize the SAW impedance system and the amplifier circuit. Two oscillation equations were formulated and found to be in good agreement with the experimental results. The SAW impedance system can respond linearly to solution conductance and in a certain region the conductance sensitivity increases with increasing solution conductance. The linearity range and the response sensitivity are greatly affected by the solution capacitance and cell constant, but the solution density and viscosity have little effect.

Acknowledgement

This work was supported by funds from the National Science Foundation and the Education Commission Fund of China.

Glossary

ω angular frequency
C_m motional capacitance of the SAW resonator
L_m motional inductance of the SAW resonator
R_m motional resistance of the SAW resonator
R_0 radiation resistance of the SAW resonator
C_0 radiation capacitance of the SAW resonator
G conductance of the solution
k cell constant of the conductive electrodes
χ conductivity of the solution
C_s capacitance of the solution
X_1 reactance of the parasitic capacitor C_1
X_2 reactance of the parasitic capacitor C_2
Z_e impedance of the SAW impedance system
R_e real part of Z_e
X_e imaginary part of Z_e
Y_i input admittance
Y_o output admittance
Y_f forward transfer admittance
Y_r reverse transfer admittance
Z_i input impedance
Z_o output impedance
Z_f forward transfer impedance
Z_r reverse transfer impedance
g_o output conductance of the amplifier
g_f forward transfer conductance (transconductance)
A phase lag of the forward transfer admittance

References

[1] H. Wohltjen and R. Dessy, Anal. Chem., 51 (1979) 1458.
[2] D.S. Ballantine and H. Wohltjen, Anal. Chem., 61 (1989) 704A.
[3] A. D'Amico and E. Verona, Sensors Actuators, 17 (1989) 55.
[4] C.G. Fox and J.F. Alder, Analyst, 114 (1989) 997.
[5] A.J. Ricco, S.J. Martin and T.E. Zipperian, Sensors Actuators, 8 (1985) 319.
[6] M.S. Nieuwenhuizen and A. Venema, Sensors Mater., 5 (1989) 261.
[7] J.W. Grate and M. Klusty, Anal. Chem., 63 (1991) 1719.
[8] H. Wohltjen, Sensors Actuators, 5 (1984) 307.
[9] I.M. Kolthoff and P.J. Elving, Treatise on Analytical Chemistry, Part I, Vol. 4, Interscience, New York, 1963, Chap. 51.
[10] E. Pungor, Oscillometry and Conductometry, Pergamon, Oxford, 1965.
[11] S. Yao, K. Chen, F. Zhu, D. Shen and L. Nie, Anal. Chim. Acta, 287 (1994) 65.
[12] S. Yao, K. Chen and L. Nie, Anal. Chim. Acta, 289 (1994) 47.
[13] J.S. Schoenwald, W.R. Shreve and R.C. Rosenfeld, in 29th Annual Symposium on Frequency Control, 1975, p. 86 (in Chinese).
[14] A.A. Oliner, Acoustic Surface Waves, Springer, Berlin, 1978.
[15] F.X. Zhang and K. Sun, Piezoelectricity, National Defence Industry Publishing House, Beijing, 1984 (in Chinese).
[16] M.E. Frerking, Crystal Oscillator Design and Temperature Compensation, Van Nostrand Reinhold, New York, 1978.
[17] H.J. Reich, Functional Circuits and Oscillators, Van Nostrand, Princeton, NJ, 1961.
[18] R.C. Weast, D.R. Lide, M.J. Astle and W.H. Beyer (Eds.) CRC Handbook of Chemistry and Physics, CRC, Boca Raton, FL, 70th edn., 1989.

ELSEVIER

Analytica Chimica Acta 294 (1994) 319–327

ANALYTICA CHIMICA ACTA

A comparative study of proton and alkaline earth metal binding by humic substances

J.R. Lead [a], J. Hamilton-Taylor [a,*], N. Hesketh [b], M.N. Jones [b], A.E. Wilkinson [b], E. Tipping [c]

[a] *Institute of Environmental and Biological Sciences, Lancaster University, Lancaster LA1 4YQ, UK*
[b] *Department of Biochemistry and Molecular Biology, Manchester University, Manchester M13 9PT, UK*
[c] *Institute of Freshwater Ecology, Ambleside, Cumbria LA22 0LP, UK*

Received 29th November 1993; revised manuscript received 7th March 1994

Abstract

Humic substances (HS) were extracted from the soil and water of an upland catchment and characterised with respect to molecular weight, C, H, O, N and S contents and ash content. Three samples were obtained: peat humic acid, aquatic humic acid and aquatic fulvic acid. The weight average molecular weights were found to increase from 2400 for aquatic fulvic acid, to 6300 for aquatic humic acid and to 16500 for peat humic acid. Acid–base titrations were performed to assess the proton binding behaviour at different ionic strengths in NaCl and in the presence of important cation competitors (calcium and magnesium). The results from the titrations were fitted to a recently developed discrete-site/electrostatic model of cation–humic binding. Model parameters showed systematic trends with molecular weight and good agreement with parameters derived from the analysis of literature data. In the order peat humic, aquatic humic and aquatic fulvic acid, the milli-equivalents of carboxylic acid groups per gram of HS (n_A) increased. In the same order both the negative $\log_{10}$ of the mid-range intrinsic proton dissociation constant for the strong acid groups (pK_A) and the empirical constant, P, which accounts for electrostatic effects, decreased.

Key words: Humic substances; Proton and alkaline earth binding

1. Introduction

Humic substances (HS) are ubiquitous in the environment and potentially have important effects on the speciation of cations in both soils and natural waters. Both humic acids (HA) and fulvic acids (FA) are defined operationally, i.e., by the procedure used to extract them, rather than structurally or functionally. Despite this limitation a large amount of data in the literature indicates consistent differences in the physical and chemical characteristics between HA and FA and between soil HS and aquatic HS. In general FA have a lower molecular weight than HA [1–3]. They also have higher oxygen content and lower carbon content [4].

* Corresponding author.

0003-2670/94/$07.00 © 1994 Elsevier Science B.V. All rights reserved
SSDI 0003-2670(94)00142-9

Development and testing of Model V, a discrete site/electrostatic model of humic–ion binding [5], have suggested consistent differences between the binding properties of HA and FA. However uncertainties remain, firstly because the organic acids have been extracted from different source materials and may therefore have intrinsically dissimilar properties with regard to cation binding, and secondly because methodologies may vary between laboratories. Therefore available results cannot be compared straightforwardly. Humic and fulvic acids from the same source have not previously been interpreted by this model, for instance.

In order to minimise these uncertainties, work in this laboratory was performed on peat and aquatic humic and fulvic acids from the same catchment. The results from this work may help to decide to what extent the properties of HS can be generalised from site to site.

2. Experimental

Approximately 1.5 kg of peat was collected from Whitray Fell, North Yorkshire (Latitude 54°5′N, Longitude 2°30′) and the humic acid fraction was extracted by methods previously described [1–3]. Briefly, a dilute acid and base extraction was used, with the HA being purified by the addition of dilute HF and subsequent dialysis. Approximately 730 l of water were collected in polythene containers from Whitray Beck (which drains Whitray Fell) and the humic and fulvic acid fractions extracted as previously described [1–3]. The extraction was carried out by chromotographic use of XAD-8 resin and dilute acid and base separation of the HA and FA. The FA was purified on a cation exchange resin and the HA by addition of HF and dialysis. The three freeze dried samples were stored in brown glass, screw top containers in a desiccator. Stock solutions/suspensions of ~1 g/l were made up when required and kept in the dark at 4°C. The HS was diluted to 0.5 g/l for the titrations.

Ash contents of the freeze dried samples were determined by heating to constant weight in a muffle furnace at 550°C and water content by heating to constant weight at 60°C. The latter temperature was selected as a compromise between the removal of all water present and possible alteration of the sample [6]. C, H, N and S contents were determined with a Carlo Erba EA1108 elemental analyser and the oxygen was calculated by difference.

2.1. Titrations

Acid–base titrations of the aquatic HS were carried out in continuous mode and on the peat HS in batch mode. The model compound *p*-hydroxybenzoic was titrated at 0.003 M and 0.1 M NaCl in continuous mode, to assess the performance of the experimental set-up. The aquatic FA and aquatic HA were titrated in the two salt concentrations mentioned and also at 0.0333 M $CaCl_2$ and $MgCl_2$. Due to the surfactant properties of the HS and to the low pH of the starting solution the samples were not degassed. However they were kept under N_2 prior to and during the titrations. The samples and NBS buffers were pre-equilibrated at 25°C. Titrations typically took two hours to perform with addition of carbonate-free NaOH every 60–120 s from a Schott T 90/10 10-ml burette. Titrant was added when the drift on the electrode was less than 0.001 mV/s and then a wait time had elapsed; the time was usually set to 60 s. Particularly in the initial stages of the work the pH over the course of the titration was monitored by eye to make sure equilibrium had been reached before the next addition of base. The titrations were run over the pH range 3–11.

Batch titrations were performed on the peat humic acid in separate solutions of NaCl, $MgCl_2$ and $CaCl_2$ at 25°C and at the concentrations given above. The suspensions were degassed with water-saturated N_2 and kept in a shaking water bath overnight. The pH was measured, an aliquot of base added and the procedure repeated. A measurement was taken when the drift in pH was < 0.005 over 5 min. The pH was taken in the range 3–7.5 and not to higher values due to difficulties in minimising exposure to CO_2 over long periods of time. Batch titrations were used

because of the long periods of time over which equilibrium was attained with peat HA.

The pH in all titrations was measured using a Whatman double junction combination electrode which underwent a quality control procedure as recommended by Davison [7].

Acid–base titrations were performed on the three HS samples. The aquatic HS was titrated in the pH range 3–11. However, values above pH 10 were found to be unreliable in view if the inconsistency of the calculated charge on the *p*-hydroxybenzoic acid. The charge was found to reach the expected value of 2 meq/mmol at around pH 10, but to fall thereafter. Therefore, only results for pH $\leq$ 10 were accepted for analysis. This could in part be due to errors in pH measurement which in turn lead to magnified errors in the charge balance at high pH. However comparison of theoretical and actual strong acid–strong base titration curves suggest that the sort of experimental errors required in order to give such errors at pH 10 were not occurring. Wait times between addition of aliquots of base were varied and the system was found to be at equilibrium. A possible explanation of the problem is that the organic ligands had some (unknown) effect on the electrode at high pH.

Derivation of model parameters for the *p*-hydroxybenzoic acid titrations showed that the experimental set-up was working satisfactorily. The pK_A and pK_B derived were comparable to pK values of the benzoic and phenolic groups on *p*-hydroxybenzoic acid [8]. Also the ΔpK and P values were small as expected (see Model section for explanation of terms).

2.2. Molecular weights

Weight-average molecular weights of the three fractions were found by sedimentation equilibrium ultracentrifugation [9]. Measurements were taken with a Beckman L8-70 ultracentrifuge fitted with a UV scanner working at 280 nm. Samples were centrifuged at the required speed until equilibrium was reached, usually more than 72 h. Equilibrium was judged to have been reached when there was no significant change in the absorbance–distance profiles through the cells over a 5 h period.

Weight average molecular weights were calculated from the equation,

$$\overline{M}_W = \left[\frac{2RT}{(1-\bar{\nu}_2\rho)\omega^2}\right] 2.303\left(\frac{\mathrm{d}\log c}{\mathrm{d}(r^2)}\right) \qquad (1)$$

where R is the gas constant, T is the temperature in Kelvin, ν_2 is the partial specific volume, ρ is the solution density, ω is the angular velocity, c is the concentration and r is the radius from the centre of rotation of the rotor.

2.3. Humic ion binding model V

The model of humic–ion binding (Model V) has been described in full elsewhere for fulvic acids [5], humic acids [10] and the effects of calcium and magnesium competition on trace metal binding [11]. It is a discrete site model, in which binding is modified by electrostatic interactions. Two types of groups are postulated: carboxylic groups (p$K < 7$) and weaker acid groups (p$K > 7$). One pK value for each type, as well as a range parameter, are derived from the titration data (pK_A, pK_B and ΔpK_A, ΔpK_B). A fifth fitting parameter is the number of carboxylic groups (n_A) in meq/g of HS. The number of weaker acid groups is assumed to be half the number of carboxylic groups, to avoid overparameterisation. This simplifying assumption arises from the common problem of not being able to identify the end-point of the titration of the weak acid groups. The ΔpK_A and ΔpK_B values in a simple way represent the chemical heterogeneity of the humic material. The last fitting parameter for describing proton binding is an empirical proportionality constant (P) which relates w, the electrostatic interaction factor, to ionic strength via the relationship $w = P \log_{10} I$. The intrinsic binding constants refer to conditions where the humic molecule is in a hypothetical chargeless state. The extra attraction of cations to the negatively charged humic surface is allowed for by the term exp $(-2wzZ)$ where z and Z are the charge on the cation and on the HS respectively. Once these 6 parameters are fixed then two metal binding parameters can be fitted

(pK_{MHA} and pK_{MHB}). The pK_{MHB} can be approximated from the pK_{MHA} by a simple relationship derived from previous data fitting [5]. Mono- and bidentate binding are both permitted as is binding simply due to the accumulation of counter ions in the diffuse layer.

3. Results and discussion

The streamwater collected had measured dissolved organic carbon (DOC) values of 10–12 mg/l and a pH of 4.0. The ash content, elemental analyses and weight-average molecular weights of

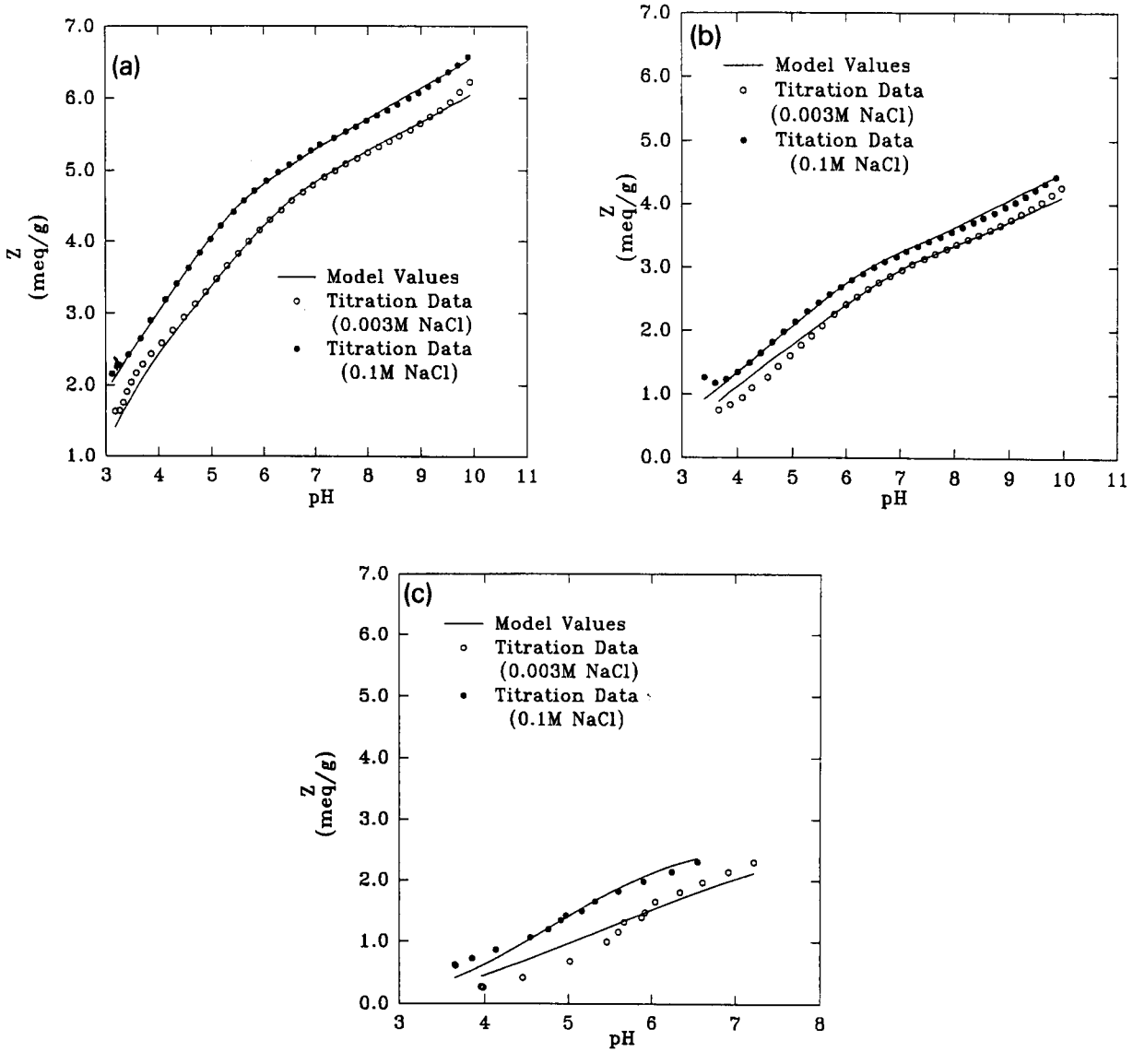

Fig. 1. Variation of Z (net humic charge) with pH for (a) aquatic FA, (b) aquatic HA and (c) peat HA. (●) denotes 0.1 M NaCl, (○) denotes 0.003 M NaCl and the solid line denotes model values.

Table 1
Major elements, ash content and weight average molecular weights of the HS fractions.

	Peat HA	Aquatic HA	Aquatic FA
Carbon	56.3	51.9	51.0
Hydrogen	5.8	4.4	3.8
Oxygen	34.4	40.1	43.8
Nitrogen	2.2	1.5	0.7
Sulphur	0.4	0.0	0.0
Ash	0.9	2.1	0.7
M_w	16 500	6 300	2 400

the extracted HS are presented in Table 1. The data are within the ranges of literature values available and show expected trends [1–4] with oxygen content decreasing and carbon content and molecular weight increasing in the order aquatic FA–aquatic HA–peat HA.

3.1. Proton binding

Fig. 1a–c shows the variation of net humic charge with pH. Satisfactory fits are obtained with the model with respect to ionic strength effects. The curves in 0.1 M NaCl are offset as a result of the salt shielding the humic charge and decreasing its attraction for the protons, i.e., at higher salt concentrations the term $\exp(-2wzZ)$ is reduced in importance. A clear trend is shown of decreasing humic charge from aquatic FA to aquatic HA to peat HA at a particular pH (see also Fig. 2). The fits for the peat HA titrations are somewhat poorer than for the aquatic HS. This may in part be due to the differences in experimental procedure, but the model is generally better at describing the behaviour of fulvic acid than humic acid.

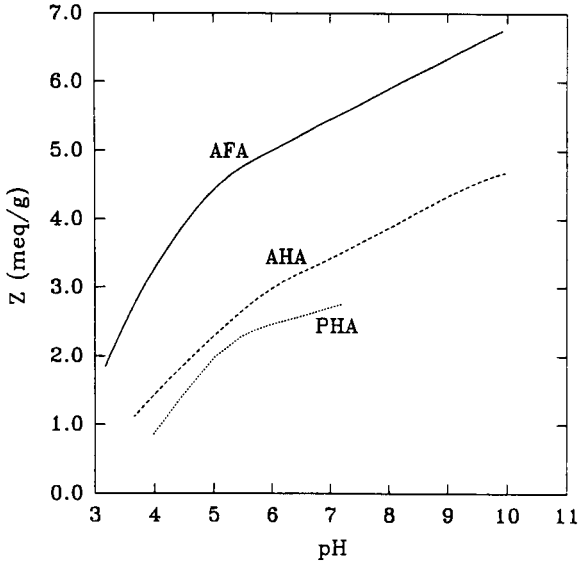

Fig. 2. Model derived curves showing the variation of Z with pH at ionic strength 1.0 M. At this ionic strength the model predicts that electrostatic interactions are negligible. The solid line represents aquatic FA; – – –, aquatic HA; and · · · ·, peat HA.

Table 2 gives the parameters derived from the data by Model V. The standard errors of the parameters were estimated by the jackknife method of Nash and Walker-Smith [12]. In the main the parameter values show good agreement with average parameters derived from the analysis of literature data [5], also shown in Table 2.

Table 2
Model V parameters derived from titrations (peat and aquatic humic and fulvic acids, PHA, AHA and AFA) and mean values from literature data (HA and FA). Figures in brackets are standard errors. The root mean squared error (RMSE) in Z (meq/g) for the acid base titrations are: 0.152 (PHA), 0.088 (AHA) and 0.093 (AFA). RMSE in pH for the metal titrations are: 0.26 (PHA), 0.23 (AHA) and 0.17 (AFA).

	PHA	AHA	AFA	HA	FA
n_a	2.46 (0.03)	3.43 (0.04)	4.86 (0.1)	3.3	4.7
pK_A	4.31 (0.03)	4.23 (0.05)	3.23 (0.04)	4.0	3.3
pK_B	-	8.88 (0.14)	8.37 (0.28)	8.6	9.6
ΔpK_A	1.08 (0.12)	3.35 (0.12)	3.00 (0.10)	1.8	3.3
ΔpK_B	-	2.68 (0.09)	4.14 (0.07)	3.4	5.5
$-P$	435 (10)	171 (6)	116 (1)	370	103
pK_{MHA} Ca	3.31 (0.05)	3.18 (0.02)	1.98 (0.00)	3.2	2.2
pK_{MHA} Mg	3.21 (0.02)	3.23 (0.01)	2.07 (0.05)	3.3	2.2

This shows clearly that fulvic acids from different sources, extracted by different means are similar with regard to their ion binding properties. The same is true for humic acids, but the FA and HA show marked differences between each other. To some extent, however, this may be an artifact caused by the various extraction methods, e.g., some homogenisation of HS caused by the use of XAD resins [13]. XAD-8 resin was used in this study for the aquatic HS but not the peat HA.

Inspection of the pK_A and n_A values show aquatic HS to be more acidic and to contain a greater number of carboxyl groups than the peat HS. From the ΔpK values it can be seen that the pK values are spread over a wider range indicating a greater diversity in functional group content. The same trends are also apparent if fulvic and humic acids are compared. It is interesting to note that aquatic HA, the intermediate of the three humic fractions, resembles peat HA most in terms of n_A and pK_A (the "chemical" parameters) but that it shows greater similarity to aquatic FA when P (the electrostatic term) is considered. This is illustrated by Fig. 2 which shows Model V curves at an ionic strength of 1.0 M, at which value the model predicts that electrostatic modifications of cation binding disappear, and where the aquatic FA curve is displaced to a much larger degree than peat HA from the aquatic HA curve.

P is also found to be related to the molecular weight (Fig. 3) as expected. The model derives P from data fitting and it is related to w, a parameter used to account for the interaction between discrete sites caused by the charge on the HS, i.e., electrostatic interactions. As derived by Tanford [14] w increases with increasing radius of the humic macro-ion, which can in turn be related to the molecular weight, if assumptions about the geometry of the humic molecules are made.

3.2. Calcium and magnesium binding

The parameter values in Table 2 show that calcium and magnesium behaved similarly to each other with respect to their binding to the three humic fractions. Therefore only calcium will be discussed. The differences in the pK_{MHA} between the three HS fractions are not necessarily a reflection of their respective metal binding strengths as the model envisages binding as an exchange with the protonated acid sites and not the bare (deprotonated) sites. For the reaction,

$$\equiv COO^- + Ca^{2+} = \equiv COOCa^+$$

$K = [COOCa^+]/[COO^-][Ca^{2+}]$. The pK values are 1.2, 0.9 and 1.1 for aquatic FA, aquatic HA and peat HA respectively. This shows that the binding strengths of the carboxylic groups of the humic fractions are similar to each other. These pK values are similar to the analogous values for acetate and lactate, 1.1 and 1.45 respectively [8]. The pK_{MHA} values suggested that the carboxylic groups of the aquatic FA were much stronger at binding calcium, but it appears that the differences in the pK_{MHA} are more a reflection of the relative proton affinities of the carboxylic groups, i.e., the sites on the three HS fractions appear similar with respect to calcium binding, but different in their ability to bind hydrogen ions.

Fig. 4a–c shows the curves of pH versus added volume of base when HS is titrated in 0.0333 M $CaCl_2$. The fits, while generally satisfactory, are rather poor for the peat HA data with observed

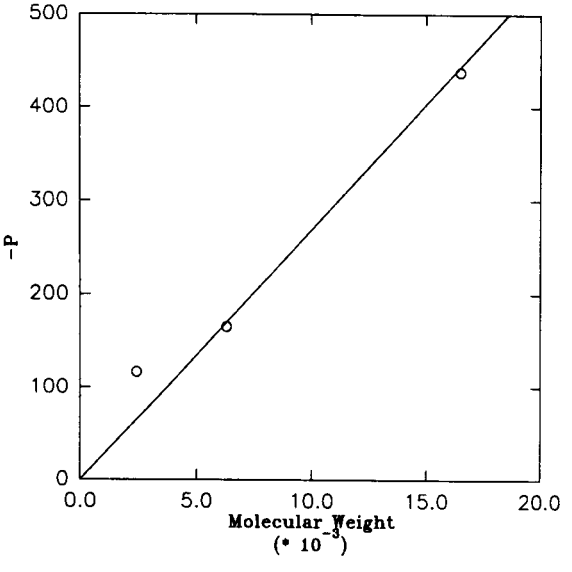

Fig. 3. Change in $-P$ with molecular weight. The line is the best straight line through the points when constrained to go through the origin.

pH being substantially less than that predicted, at pH < 5. The same is true, to a lesser extent, for aquatic HA. In this case, however, the fits are very good in the neutral pH range (pH 5–9), before becoming worse at high pH. This suggests that, at low pH, calcium binding is much stronger than that predicted by Model V, resulting in displacement of protons into solution. It should be noted, however, that the model fits the data somewhat poorly at low pH for both the acid–base and calcium titrations. It is therefore difficult to say whether the failure with Ca at low pH is due to the failure to describe the acid base titrations, the calcium titrations or both. Strong calcium binding was not seen in one other data set interpreted with an earlier version of the model [15]. The poor description of the data cannot be improved as there is only one adjustable metal

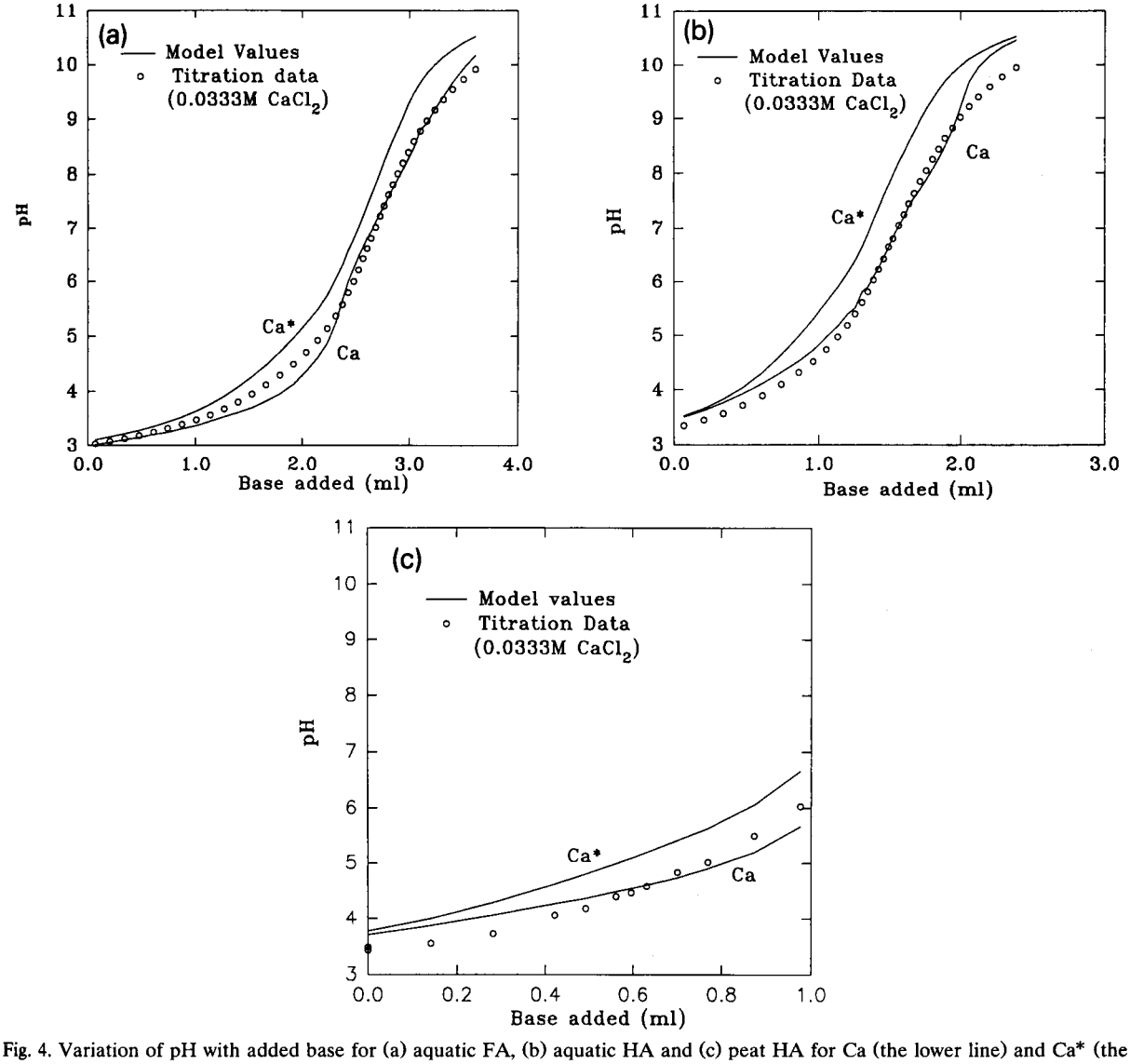

Fig. 4. Variation of pH with added base for (a) aquatic FA, (b) aquatic HA and (c) peat HA for Ca (the lower line) and Ca* (the upper line). See Results and Discussion for explanation of Ca*. (○) Denotes titration values.

binding parameter and better predictions could only be obtained by the use of more parameters. This is possible but would increase the complexity and computational effort necessary which would partially negate some of the objectives of the Model V: to model humic–ion binding in a realistic but practical way.

The curve labelled Ca* is model derived and assumes that there is no specific binding of Ca to the discrete sites of the HS. As there is no discrete binding the only humic–calcium interactions are electrostatic in nature, i.e., Ca binding is only by accumulation in the diffuse layer. Ca* is therefore analogous to Na, as the model assumes Group 1 metals interact only in this manner. The difference between the two curves is thus a measure of the protons removed from the humic material into solution by the direct competition of Ca at specific sites.

3.3. Humic behaviour in relation to physico-chemical properties

The humic samples studied in this work underwent fractionation within the soil–water system of the catchment, and this is reflected in their physico-chemical properties. The most obvious factor is net charge. The results of Fig. 1a–c show that at the pH (ca. 4) and ionic strength (ca. 10^{-3} M) of the soil the aquatic FA and aquatic HA are appreciably ionised, whereas the peat HA has a charge close to zero. By the same principle that is exploited in fractionating humic extracts into HA and FA, the charge differences mean that the mobilities of the aquatic FA and aquatic HA will be greater than that of the peat HA.

Charge may not be the sole determinant of mobility however. Tipping and Woof [16] had to invoke differences in hydrophobicity, as well as charge, within the fulvic acid type fractions of organic soils in order to explain sorption behaviour. Thus they viewed mobility as increasing with net charge and decreasing with hydrophobicity, both effects tending to diminish sorption. If C and O contents of the HS are taken as rough indications of hydrophobicity, it is seen (Table 1) that hydrophobicity increases in the order aquatic FA < aquatic HA < peat HA. This is the reverse of the variation in the extent of ionisation. Therefore the trend towards higher mobility with higher charge is reinforced.

A third factor to consider is molecular weight. As can be seen from the results in Table 1, increase in molecular weight is associated with a decrease in mobility. This could be explained simply by the correlation between hydrophobicity and molecular weight. However, it may also be that larger molecules sorb more strongly than smaller ones, possibly by virtue of more contacts being possible between the sorbate and sorbent.

A final point that should be emphasised is that the individual humic fractions are mixtures of molecules. The peat HA may contain some molecules more typical of the average aquatic HA, but which are sorbed to soil solids. Similarly, aquatic FA may contain molecules with the proton binding characteristics of average aquatic HA, but perhaps being relatively hydrophilic do not precipitate when the aquatic FA/HA mixture is acidified.

Acknowledgments

Financial support for this work was provided through a Research Studentship (grant number GT4/91/AAPS/25) from the Natural Environment Research Council. Thanks are due to C. Woof for help with the water sampling, to J. Turner for the elemental analyses and to W. Davison for helpful discussions and comments on the manuscript. We would also like to acknowledge the helpful and perceptive comments of two anonymous referees.

References

[1] P.M. Reid, A.E. Wilkinson, E. Tipping and Jones M.N. Geochim. Cosmochim. Acta, 54 (1990) 131.
[2] B.M. Beckett, Z. Jue and J.C. Giddings, Environ. Sci. Technol., 21 (1987) 289.
[3] E.M. Thurman, R.L. Wershaw, R.L. Malcolm and D.J. Pinckney, Org. Geochem., 4 (1982) 27.
[4] G.R. Aiken, D.M. McKnight, R.L. Wershaw and P. MacCarthy (Eds.), Humic Substances in Soil, Sediment and Water, Wiley, New York, 1985.

[5] E. Tipping and M.A. Hurley, Geochim. Cosmochim. Acta, 56 (1992) 3627.
[6] E.W.D. Huffman and H.A. Stuber, in G.R. Aiken, D.M. McKnight, R.L. Wershaw and P. MacCarthy (Eds.), Humic Substances in the Soil Sediment and Water, Wiley, New York, 1985.
[7] W. Davison, Trends Anal. Chem., 9 (1990) 80.
[8] A.E. Martell and R.M. Smith, Critical Stability Constants, Vol. 3, Other Organic Ligands, Plenum, New York, 1977.
[9] A.E.Wilkinson, N.Hesketh, J.J.W. Higgo, E. Tipping and M.N. Jones, Colloids Surf. A, 73 (1993) 19.
[10] E. Tipping, Colloids Surf. A, 73 (1993) 117.
[11] E. Tipping, Environ. Sci. Technol., 27 (1993) 520.
[12] J.C. Nash and M. Walker-Smith, Nonlinear Parameter Estimation. An Integrated System in Basic, Dekker, New York, 1987.
[13] M.S. Shuman, in E.M. Perdue and E.T. Gjessing (Eds.), Organic Acids in Aquatic Ecosystems, Wiley, New York, 1990, p. 97.
[14] C. Tanford, Physical Chemistry of Macromolecules, Wiley, New York, 1961.
[15] E. Tipping, C.A. Backes and M.A. Hurley, Water Res., 22 (1988) 597.
[16] E. Tipping and C.J. Woof, Soil Sci., 41 (1990) 573.

ELSEVIER

Analytica Chimica Acta 294 (1994) 329–335

ANALYTICA CHIMICA ACTA

Liquid–liquid extraction of copper(II) with cyclic tetrathioethers

Keiitsu Saito *,[a], Satomi Murakami [a], Akihiko Muromatsu [a], Eiichi Sekido [b]

[a] *Division of Natural Environment and Chemistry, Faculty of Human Development, Kobe University, Tsurukabuto, Nada, Kobe 657, Japan*

[b] *Department of Chemistry, Faculty of Science, Kobe University, Rokkodai, Nada, Kobe 657, Japan*

Received 15th March 1994

Abstract

Liquid–liquid extraction of the divalent metal ions manganese(II), cobalt(II), nickel(II), copper(II), zinc(II) and cadmium(II) with 1,4,8,11-tetrathiacyclotetradecane was examined using the tetraphenylborate ion (TPB^-) for the formation of the ion pairs. Copper(II) was quantitatively extracted into 1,2-dichloroethane, whereas the other metals were hardly extracted. The extraction behaviour of copper(II) with 12–16-membered cyclic tetrathioethers ([*n*]aneS_4, where *n* represents the total number of carbon and sulphur atoms in the cyclic ligand ring) was examined. Chloroform and 1,2-dichloroethane were used as extraction solvents. The order of the extractability of copper(II) was as follows: [15]aneS_4 > [16]aneS_4 > [14]aneS_4 > [13]aneS_4 > [12]aneS_4 at 2.5×10^{-4} M of ligands, [16]aneS_4 > [15]aneS_4 > [14]aneS_4 > [13]aneS_4 > [12]aneS_4 at 2.5×10^{-5} M of ligands. The extracted species were examined at ligand concentrations higher than 2.5×10^{-4} M. Copper(II) was extracted with [13]aneS_4 and [16]aneS_4 as $[CuL_2]^{2+}(TPB^-)_2$ and $[CuL_4]^{2+}(TPB^-)_2$ depending upon the relative concentration of the ligand to copper(II). Where L represents cyclic tetrathioethers. The extracted species with [14]aneS_4 and [15]aneS_4 were $[CuL_2]^{2+}(TPB^-)_2$ and $[CuL_4]^{2+}(TPB^-)_2$, respectively. In case of [12]aneS_4, the following three species were observed depending upon concentrations of the ligand and TPB^-: $[CuL_2(OH)]^+TPB^-$, $[CuL_2]^{2+}(TPB^-)_2$ and $[CuL_4]^{2+}(TPB^-)_2$.

Key words: Copper; Cyclic tetrathioethers; Extraction

1. Introduction

Since a thioether group is a soft Lewis base, macrocyclic polythioethers react selectively with soft Lewis acids such as copper(I), silver(I) and mercury(II) [1–4]. Although copper(II) is classified as a borderline acid [5], it reacts with polythioethers, and studies concerning copper(II) complexes with polythioethers have been reported [6–8]. The equilibrium constants and thermodynamic parameters of copper(II)–cyclic polythioether complexes in aqueous solution have been determined and macrocyclic, ring-size and anion effects have been discussed [6]. Copper(II) complexes with 12–16-membered cyclic tetrathioethers have been isolated and characterized and ring-size effects on the structure of macrocyclic ligand complexes have been discussed [7]. Recently, the extraction behaviour of copper(II) with cyclic and non-cyclic tetra-

* Corresponding author.

0003-2670/94/$07.00 © 1994 Elsevier Science B.V. All rights reserved
SSDI 0003-2670(94)00139-D

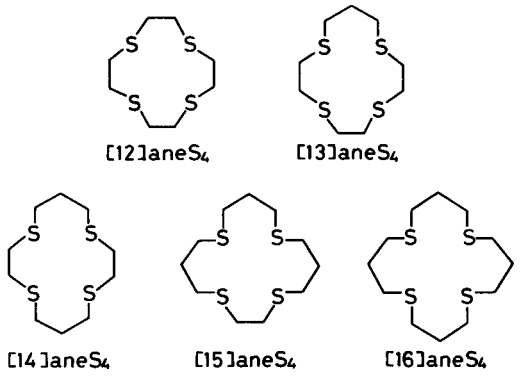

Fig. 1. Cyclic tetrathioethers investigated.

thioethers has been examined using hexanitrodiphenylamine ion as the counter anion [9]. However, the extraction behaviour of copper(II) with a continuous series of homologous macrocyclic polythioethers has not been reported.

In this study, the liquid–liquid extraction of several divalent metal ions with 1,4,8,11-tetrathiacyclotetradecane was examined using the tetraphenylborate ion (TPB^-) as the anion of the ion pair. The extraction behaviour of copper(II) with 12–16-membered cyclic tetrathioethers (Fig. 1) was examined with chloroform and 1,2-dichloroethane as extraction solvents. The effects of the lipophilicity and ring size on the extractability of copper(II) are discussed. Compositions of the extracted species were determined and compared with those in the presence of hexanitrodiphenylamine ion [9] or thymol blue ion as the counter anion.

2. Experimental

2.1. Reagents

All cyclic tetrathioethers were synthesized according to the method of Ochrymowycz et al. [10]. The products were purified by the method described previously [11]. All 0.01 M stock standard solutions of the metal ions were prepared by dissolving the metal sulphates (analytical-reagent grade) in water and standardized by titration with EDTA. A solution of sodium tetraphenylborate (Dojindo Labs.) was prepared fresh for each experiment. Chloroform and 1,2-dichloroethane were purified as described previously [2]. Other reagents were of analytical-reagent grade.

2.2. Apparatus

A Taiyo M-100 incubator was used for shaking the solutions. A Seiko SAS-725 atomic absorption spectrometer was used for the determination of metal ions. A Hitachi U-3200 spectrophotometer was used for absorption measurements. The pH of the aqueous phase was measured with a Toa HM-7E pH meter.

2.3. Liquid–liquid extraction of metal ions

A 10-ml volume of an aqueous solution containing metal ion, sodium tetraphenylborate and acetic acid–sodium acetate buffer (0.01 M) was maintained at an ionic strength of 0.1 with sodium sulphate. This solution was kept in a stoppered 50-ml cylindrical glass tube. After the addition of 10 ml of a cyclic tetrathioether solution in 1,2-dichloroethane or chloroform, the mixture was shaken for 30 min at 200 strokes min^{-1} at 25 ± 0.1°C. The mixture was then centrifuged for 5 min at 2000 rpm (530 *g*). After the two phases had separated, the pH of the aqueous phase was measured. The concentration of metal ion in the aqueous phase was determined by atomic absorption spectrometry. The metal ion concentration in the organic phase was determined as follows: 5 ml of the organic phase were allowed to evaporate, the residue was decomposed with 1 ml of concentrated nitric acid and diluted with water to 10 ml and the concentration of metal ion was determined by atomic absorption spectrometry.

2.4. Determination of tetraphenylborate ion

When the compositions of the extracted species of copper(II) with cyclic tetrathioethers were examined, the concentration of TPB^- in the aqueous phase was determined spectrophotometrically at 272 nm. The absorption spectrum of the aqueous solution of sodium tetraphenylborate showed a discernible shoulder near 272 nm. The calibra-

tion graph for of TPB^- was a straight line passing through the origin. The molar absorption coefficient of TPB^- was 2.03×10^3 l mol^{-1} cm^{-1}. Copper(II) sulphate (2.5×10^{-5} M), sodium sulphate (0.033 M) and acetate buffer (0.01 M) did not interfere with the determination of TPB^-.

3. Results and discussion

3.1. Extraction of divalent metal ions with [14]aneS$_4$

The extraction of several divalent metal ions with [14]aneS$_4$ into 1,2-dichloroethane was examined at pH 5.9 using TPB^- for the formation of the ion pair. The concentrations of the metal ion, [14]aneS$_4$ and TPB^- were 5×10^{-5} M, 5×10^{-3} M and 5×10^{-4} M, respectively. The following metal ions were examined: the latter half of the first transition metal group, i.e., manganese(II), cobalt(II), nickel(II) and copper(II); and the post-transition metals, zinc(II) and cadmium(II). Copper(II) was extracted quantitatively (over 99%) into 1,2-dichloroethane, whereas copper(II) was only slightly extracted (6–7%) in the presence of picrate ion [2]. Manganese(II), cobalt(II), nickel(II), zinc(II) and cadmium(II) were hardly extracted (below 1%) even when TPB^- was used as the counter anion. The extraction of nickel(II) with [14]aneS$_4$ into nitrobenzene was also examined in the pH range 1.5–5.0. Although nitrobenzene is better than 1,2-dichloroethane for the extraction of ion associates, nickel(II) was hardly extracted.These results show that copper(II) is selectively extracted with cyclic tetrathioethers from tetraphenylborate solution so that it is possible to separate copper(II) from manganese(II), cobalt(II), nickel(II), zinc(II) and cadmium(II) by liquid–liquid extraction.

3.2. Extraction of copper(II) with cyclic tetrathioethers

The extraction of the copper(II)–cyclic tetrathioether complex into 1,2-dichloroethane was examined at pH 5.0. The concentration of TPB^- was ten times in excess of that of copper(II) ion (2.5×10^{-5} M). The results are given in Table 1. It was found that the order of the extractability of copper(II) is [12]aneS$_4$ < [13]aneS$_4$ < [14]aneS$_4$ < [15]aneS$_4$, [16]aneS$_4$ with 2.5×10^{-4} M ligands. No difference in the extractability of copper(II) between [15]aneS$_4$ and [16]aneS$_4$ could be observed because of the high extractability of copper(II) ($E > 99\%$). It has been reported for the ion-pair extraction of copper(I) with [14]aneS$_4$ and picrate ion that the extractability of copper(I) decreases with decreasing dielectric constant of organic solvents [2]. Therefore, the extraction of the copper(II)–cyclic tetrathioether complex into chloroform was tried at pH 4.9. The concentrations of the ligand and TPB^- were ten times in excess of that of copper(II). The results are given in Table 1.

Table 1
Data for the extraction (E) of copper(II) with five cyclic tetrathioethers in the presence of TPB^-

Ligand	E (%)		
	1,2-Dichloroethane (pH 5.0)		Chloroform (pH 4.9)
	2.5×10^{-4} M	2.5×10^{-5} M	2.5×10^{-4} M
[12]aneS$_4$	41.3 ± 4.2(10)	8.8 ± 0.6(8)	Ppt. [a]
[13]aneS$_4$	88.6 ± 3.4(13)	21.2 ± 1.0(8)	< 1
[14]aneS$_4$	97.5 ± 1.5(6)	35.2 ± 1.5(11)	78.9 ± 2.8(8)
[15]aneS$_4$	> 99	43.7 ± 3.1(11)	91.7 ± 2.0(8)
[16]aneS$_4$	> 99	46.0 ± 3.2(11)	86.4 ± 3.3(8)

Results are means ± standard deviations with the numbers of measurements in parentheses.
[a] Precipitation.

With the use of chloroform as the extraction solvent, it was found that the order of the extractability is [14]aneS$_4$ < [16]aneS$_4$ < [15]aneS$_4$. Consequently, the order of the extractability is [12]aneS$_4$ < [13]aneS$_4$ < [14]aneS$_4$ < [16]aneS$_4$ < [15]aneS$_4$ with 2.5×10^{-4} M ligands. On the other hand, the order of extractability is [12]aneS$_4$ < [13]aneS$_4$ < [14]aneS$_4$ < [15]aneS$_4$ < [16]aneS$_4$ with 2.5×10^{-5} M ligands in 1,2-dichloroethane (Table 1). The extractability with [16]aneS$_4$ is higher than that with [15]aneS$_4$ at lower ligand concentrations. This may be due to the difference in the composition of the extracted species. The equilibrium constants of the 1 : 1 copper(II)–cyclic tetrathioether complexes in aqueous solution have

been reported by Sokol et al. [6]. According to their studies, the order of the stability constants is [16]aneS$_4$ < [15]aneS$_4$ < [12]aneS$_4$ < [13]aneS$_4$ < [14]aneS$_4$. It was found that the order of the stability constants of the copper(II)–cyclic tetrathioether complexes is not reflected in the extractability of copper(II). Although [14]aneS$_4$ gives a cavity in which the copper(II) ion just fits and the stability constant is 15 and 140 times larger than that with [15]aneS$_4$ and [16]aneS$_4$, respectively the extractability of copper(II) with [14]aneS$_4$ is lower than with [15]aneS$_4$ or [16]aneS$_4$. This suggests that the extractability of copper(II) depends on the lipophilicity of the ligand in addition to ring size. Further, the composition of the extracted species may be different from that of the copper(II)–cyclic tetrathioether complexes in aqueous solution, so the stability constants of the 1:1 complexes may not be reflected in the extractability. This may be of interest and will be discussed later.

If the species extracted into an organic solvent is represented by $CuL_m(TPB)_n$ (L = ligand), the extraction equilibrium and the extraction constant, K_{ex}, are given by the equations

$$Cu^{2+} + mL(o) + nTPB^- \overset{K_{ex}}{\rightleftharpoons} CuL_m(TPB)_n(o) \quad (1)$$

$$K_{ex} = [CuL_m(TBP)_n]_o / [Cu^{2+}][L]_o[TPB^-]^n \quad (2)$$

respectively, where (o) and the subscript o indicate the species in the organic phase. The logarithmic distribution ratio of copper(II), log D, is represented by the equation

$$\log D = \log K_{ex} + m \log[L]_o + n \log[TPB^-] \quad (3)$$

3.3. Determination of the number of tetraphenylborate ions involved in the extracted species

The extraction of copper(II) at pH 5 was examined at various concentrations of TPB^- with a constant concentration of the ligand. 1,2-Dichloroethane was used as the extraction solvent for [12]aneS$_4$ and [13]aneS$_4$ because the copper(II) complex with [12]aneS$_4$ was precipitated and that with [13]aneS$_4$ was hardly extracted when chloroform was used. Chloroform was used as the extraction solvent for [14]aneS$_4$, [15]aneS$_4$ and [16]aneS$_4$ because of the high extractability of copper(II) into 1,2-dichloroethane in the presence of a large excess of the ligand. Plots of log D vs. the logarithmic concentration of TPB^- in the aqueous phase are shown in Fig. 2.

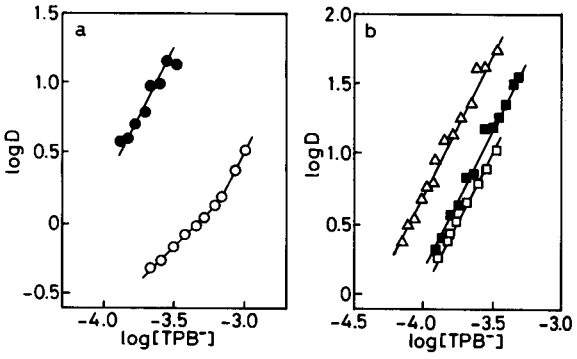

Fig. 2. Distribution ratio as a function of TPB^- concentration when copper(II) (2.5×10^{-5} M) was extracted from TPB^- solution with cyclic tetrathioethers (2.5×10^{-4} M). pH: (a) 4.9 and (b) 5.0. Extraction solvent: (a) 1,2-dichloroethane and (b) chloroform. Ligands: ○ = [12]aneS$_4$; ● = [13]aneS$_4$; □ = [14]aneS$_4$; △ = [15]aneS$_4$; ■ = [16]aneS$_4$.

The concentration of TPB^- was determined spectrophotometrically at 272 nm because the distribution of sodium tetraphenylborate between the organic solvent used and the aqueous phase was not negligible. For [13]aneS$_4$, [14]aneS$_4$, [15]aneS$_4$ and [16]aneS$_4$, four straight lines were obtained with slopes close to 2, indicating that $n = 2$. For [12]aneS$_4$, a straight line with a slope of 2 which indicates $n = 2$ was obtained in the region of log[TPB^-] > −3.2. At concentrations of TPB^- below 6.5×10^{-4} M, a straight line with the slope of 1 was obtained, which indicates $n = 1$. In this region an anion other than TPB^- such as acetate or hydroxide ion should neutralize the charge of the complex cation. Participation of a hydroxide ion in the ion-pair extraction of cobalt(II) with crown ethers has been reported by Khalifa and Aly [12]. Chayama and Sekido [9] have also reported that hydroxide ion participates in the extraction of copper(II) with cyclic and non-cyclic tetrathioethers. Therefore, it is as-

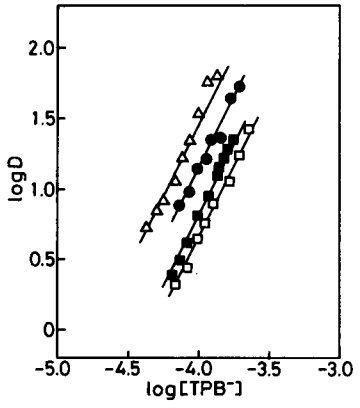

Fig. 3. Relationships between log D and log[TPB^-] when copper(II) (2.5×10^{-5} M) was extracted from TPB^- solution with 4×10^{-4} M (●) [13]$aneS_4$ in 1,2-dichloroethane and 5×10^{-4} M (□) [14]$aneS_4$, (△) [15]$aneS_4$ and (■) [16]$aneS_4$ in chloroform. pH: 4.9 ± 0.1.

sumed that a hydroxide ion is involved in the extraction of copper(II) with [12]$aneS_4$ at the concentration of TPB^- below 6.5×10^{-4} M.

Fig. 3 shows the relationships between log D and log[TPB^-] when copper(II) was extracted from TPB^- solution with 13-, 14-, 15- and 16-membered cyclic tetrathioethers at higher concentration. Four straight lines with slopes of 2, which indicates $n = 2$, were obtained for these four cyclic tetrahioethers.

3.4. Determination of the number of ligand molecules involved in the extracted species

The extraction of copper(II) at pH 5 was examined at various concentrations of the ligand. The initial concentrations of TPB^- were 1×10^{-3} M for [12]$aneS_4$ and 2×10^{-4} M for 13-, 14-, 15- and 16-membered cyclic ligands. As $n = 2$ at these TPB^- concentrations, Eq. 3 becomes

$$\log D - 2\log[TPB^-] = \log K_{ex} + m\log[L]_o \quad (4)$$

The concentration of TPB^- in the aqueous phase was determined spectrophotometrically at 272 nm. The relationships between log $D-2$ log[TPB^-] and $\log[L]_o$ are shown in Fig. 4. For [12]$aneS_4$, [13]$aneS_4$ and [16]$aneS_4$, three straight lines with slopes close to 2 were obtained at lower ligand concentrations (below 5.0×10^{-4}, 3.4×10^{-4} and 4.0×10^{-4} M for [12]$aneS_4$, [13]$aneS_4$ and [16]$aneS_4$, respectively) and lines with slopes close to 4 at higher ligand concentrations. These results indicate that the value of m changes from 2 to 4 depending on the concentration of the ligand relative to copper(II). In the case of [14]$aneS_4$, a straight line was obtained with a slope close to 2, indicating that $m = 2$. The formation of a 1:4 copper(II)–[14]$aneS_4$ complex was not observed. For [15]$aneS_4$, a straight line with a slope close to 4 was obtained, indicating that $m = 4$, and the formation of the 1:2 copper(II)–[15]$aneS_4$ complex was hardly observed in the presence of more than a tenfold excess of the ligand over copper(II).

3.5. Composition of the extracted copper(II)–cyclic tetrathioether complexes

The molar ratios of copper(II), ligand and TPB^- in the extracted species obtained from Figs. 2, 3 and 4 are summarized with the proposed formulae in Table 2. The values of log K_{ex} which were calculated from Eq. 3 and the results in Figs. 2, 3 and 4 are also given in Table 2.

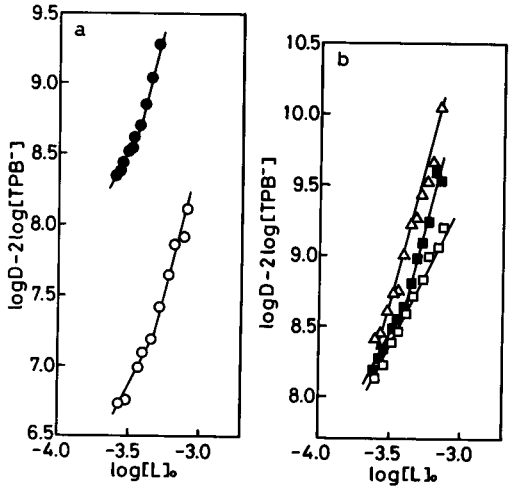

Fig. 4. Plots of log $D-2$ log[TPB^-] vs. $\log[L]_o$ for (a) (○) [12]$aneS_4$ and (●) [13]$aneS_4$ at pH 5.0 and (b) (□) [14]$aneS_4$, (△) [15]$aneS_4$ and (■) [16]$aneS_4$ at pH 4.9. Extraction solvent: (a) 1,2-dichloroethane and (b) chloroform. Initial concentrations: copper(II), 2.5×10^{-5} M; tetraphenylborate ion, 1.0×10^{-3} M for [12]$aneS_4$ and 2.0×10^{-4} M for [13]$aneS_4$, [14]$aneS_4$, [15]$aneS_4$ and [16]$aneS_4$.

Crystallographic studies have indicated that the copper(II) ion is too large to fit into the cavity of [12]aneS$_4$ and [13]aneS$_4$ and the copper(II) ion is located 0.53 and 0.38 Å above the plane of the four sulphur donor atoms [7]. Therefore, an extracted species in which more than one ligand was bound to copper(II) was expected for these two smaller ligands under the condition of a large excess of the ligand. As expected from crystallographic data, the extracted complexes in which two or four ligand molecules were bound to copper(II) were observed. According to crystallographic studies [7], the copper(II) ion fits into the cavity of [14]aneS$_4$, [15]aneS$_4$ and [16]aneS$_4$ so that the copper(II) ion is coplanar with the four sulphur donor atoms in the complexes with the three larger ligands. Consequently, the molar ratio of the extracted species was expected to be Cu(II):L = 1:1 for the three larger ligands, especially for [14]aneS$_4$, which provides an optimum fit for planar coordination around copper(II) [6,7]. However, the results obtained in this study indicate that the 1:2 or 1:4 copper(II)–cyclic tetrathioether complex is formed in the presence of a large excess of ligands. The formation of the 1:1 copper(II)–[14]aneS$_4$ complex was observed when hexanitrodiphenylamine ion was used as the counter anion [9].

These facts suggest that the composition of the extracted species is altered by the counter anion. In order to confirm this, the extraction of copper(II) with [13]aneS$_4$ and [16]aneS$_4$ into 1,2-dichloroethane was carried out at pH 6 using thymol blue ion (TB^-) as the counter anion. The relationships between log D and the logarithm of the ligand concentration in the organic phase are shown in Fig. 5a. Two straight lines with slopes close to 1 were obtained. These results indicate that the ratio of the extracted species is Cu(II):L = 1:1, which is different from the composition in the presence of TPB^-. A plot of log D vs. the logarithmic concentration of TB^- in the aqueous phase for [16]aneS$_4$ is shown in Fig. 5b. A straight line with a slope close to 1 was obtained, which indicates a 1:1 ratio of copper(II) to TB^-. As mentioned before, it is assumed that a hydroxide ion is involved in the extraction of copper(II) in the presence of TB^-, the extracted species being $[CuL(OH)]^+TB^-$. Consequently, the ratio of copper(II) to cyclic tetrathioether in the extracted species is altered by the pairing anion. That is, the ratio of copper(II) to the ligand is 1:2 or 1:4 in the presence of tetraphenylborate ion as the counter anion, whereas it is 1:1 when thymol blue or hexanitrodiphenylamine anion is used.

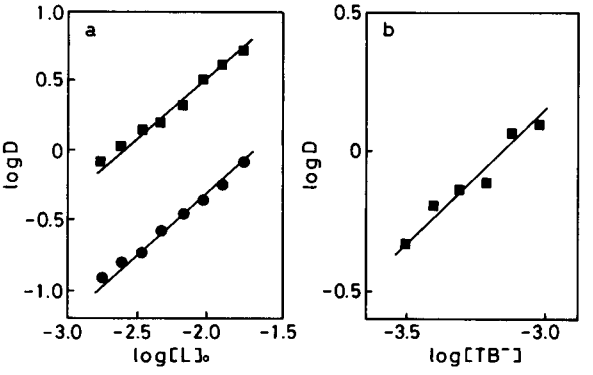

Fig. 5. Plots of (a) log D vs. log[L]$_0$ for (●) [13]aneS$_4$ and (■) [16]aneS$_4$ and (b) log D vs. log[TB$^-$] for [16]aneS$_4$. pH: 6.0. Extraction solvent: 1,2-dichloroethane. Initial concentrations; copper(II), 5×10^{-5} M; thymol blue ion, 5×10^{-4} M for (a); ligand, 5×10^{-3} M for (b).

Table 2
Compositions and extraction constants for copper(II)–cyclic tetrathioether complexes extracted into the organic solvent

Ligand	Cu(II):L:TPB$^-$	Proposed formula	Log K_{ex}
[12]aneS$_4$ [a]	1:2:1	$[CuL_2(OH)]^+TPB^-$	
	1:2:2	$[CuL_2]^{2+}(TPB^-)_2$	
	1:4:2	$[CuL_4]^{2+}(TPB^-)_2$	
[13]aneS$_4$ [a]	1:2:2	$[CuL_2]^{2+}(TPB^-)_2$	15.48
	1:4:2	$[CuL_4]^{2+}(TPB^-)_2$	22.48
[14]aneS$_4$ [b]	1:2:2	$[CuL_2]^{2+}(TPB^-)_2$	15.30
[15]aneS$_4$ [b]	1:4:2	$[CuL_4]^{2+}(TPB^-)_2$	22.85
[16]aneS$_4$ [b]	1:2:2	$[CuL_2]^{2+}(TPB^-)_2$	15.39
	1:4:2	$[CuL_4]^{2+}(TPB^-)_2$	22.07

[a] Extraction solvent, 1,2-dichloroethane.
[b] Extraction solvent, chloroform.

References

[1] D. Sevdic and H. Meider, J. Inorg. Nucl. Chem., 39 (1977) 1403.
[2] K. Saito, Y. Masuda and E. Sekido, Anal. Chim. Acta, 151 (1983) 447.

[3] K. Saito, Y. Masuda and E. Sekido, Bull. Chem. Soc. Jpn., 57 (1984) 189.
[4] E. Sekido, H. Kawahara and K. Tsuji, Bull. Chem. Soc. Jpn., 61 (1988) 1587.
[5] R.G. Pearson, J. Am. Chem. Soc., 85 (1963) 3533.
[6] L.S.W.L. Sokol, L.A. Ochrymowycz and D.B. Rorabacher, Inorg. Chem., 20 (1981) 3189.
[7] V.B. Pett, L.L. Diaddario, Jr., E.R. Dockal, P.W. Corfield, C. Ceccarelli, M.D. Glick, L.A. Ochrymowycz and D.B. Rorabacher, Inorg. Chem., 22 (1983) 3661.
[8] E. Sekido, K. Chayama and H. Iwamoto, Anal. Sci., 4 (1988) 511.
[9] K. Chayama and E. Sekido, Anal. Chim. Acta, 248 (1991) 511.
[10] L.A. Ochrymowycz, C.P. Mak and J.D. Michna, J. Org. Chem., 39 (1974) 2079.
[11] K. Saito, S. Murakami, A. Muromatsu and E. Sekido, Anal. Chim. Acta, 237 (1990) 245.
[12] S.M. Khalifa and H.F. Aly, Talanta, 36 (1989) 406.

ELSEVIER

Analytica Chimica Acta 294 (1994) 337–341

ANALYTICA CHIMICA ACTA

Book Reviews

Kh. Brainina and E. Neyman, *Electroanalytical Stripping Methods*, Wiley, New York, 1993 (ISBN 0-471-59506-3). xiii + 198 pp. Price £49.50.

This book presents a concise overview of recent progress in electrochemical stripping methods of analysis. Discussion of the various topics, although not comprehensive, is well supported with many references and numerous easy to read tables. Chapter 1 discusses the thermodynamic and kinetic aspects of metal electrodeposition, nucleation and electrodissolution. The next chapter describes briefly the different types of stripping techniques, the associated analytical signals and the most common interferences.

Chapter 3 summarises the range of electrodes, including chemically modified electrodes, and some of the electrochemical cell designs currently available. The first part of chapter 4 describes the methods for deposition and concentration of metals used prior to the stripping step. The second part presents many examples of applications of electrochemical stripping techniques to the analysis of industrial, environmental and biological materials.

The last two chapters are dedicated to what the authors call stripping electroanalytical chemistry of solids. This is a welcome addition since the subject is not usually included in similar books. Treatment of the area is divided into phase analysis (chapter 5) and examination of specific features of the structure of solids (chapter 6). In these methods the test substance is used as the working electrode in either pure form or dispersed into a carbon paste electrode. Processes investigated include redox reactions, chemisorption and crystallization.

In summary, electroanalytical chemists will find this review a useful complement to similar books already on their bookshelves. In this respect, one of the most important achievements of *Electroanalytical Stripping Methods* is to provide an account of developments in this research area in Russia. This should help fill the gap currently existing in the Western scientific literature.

Joseph N. Barisci

C. Vandecasteele and C.B. Block, *Modern Methods for Trace Element Determination*, Wiley, Chichester 1993 (ISBN 0-471-94039-9). xi + 330 pp. Price £45.00.

This is a very nice production, in the style of a handbook, of particular interest to scientists who would like to focus in on the methodology of modern spectroscopic techniques for trace element determination. Following a brief account of the occurrence and importance of elements in chapter 1, a detailed account of sample preparation methods is provided, including microwave decomposition, combustion and fusion methods. Interestingly, sections on systematic errors in decomposition methods and preconcentration techniques for metal ions are added to complete the picture. Chapter 3, on methodology in trace element determination, deals exclusively with statistics. An introduction to spectrochemical measurements in the next chapter leads on to chapters on atomic absorption, atomic emission and atomic fluorescence spectrometry, and a brief but useful comparison of the performances of these tech-

0003-2670/94/$07.00 © 1994 Elsevier Science B.V. All rights reserved
SSDI 0003-2670(94)00257-M

niques is provided in chapter 8. Comprehensive chapters on mass spectrometry, x-ray methods and activation analysis follow. The book finishes with a not-so-comprehensive look at metal speciation.

With the emphasis on the practical aspects of the methods, the authors have taken a refreshing approach to the subject, unlike previous textbooks. This is achieved through the emphasis on newer and more sensitive techniques and through the careful selection and reproduction of illustrative diagrams and tables. Surprisingly, the book fails to cover modern chromatographic or electrochemical methods for trace element determination.

Jeremy D. Glennon

Hans G. Seiler, Astrid Sigel and Helmut Sigel, *Handbook on Metals in Clinical and Analytical Chemistry*, Marcel Dekker, New York, 1994 (ISBN 0-8247-9094-4). xx + 753 pp. Price US$ 195.00.

This book has a format very similar to the *Handbook of Toxicity of Inorganic Compounds* by the same authors and reviewed earlier in this journal. It comprises three major sections. The first (28 pp.) deals with the general aspects of inorganic species in relation to physiological intake (sources, intake, clinical and toxicological significance). The second describes the analytical approaches to the determination of these species in biological (clinical) samples, with accounts of sample handling and quality aspects, followed by individual chapters describing the main techniques used in such analysis (UV–visible spectrophotometry, AAS, ISEs, voltammetry, ion chromatography, GC–MS, ICP-AES and ICP-MS, and NAA and γ-spectrometry), all written by well-known experts. This section concludes with chapters on solid samples analysis and analysis of human hair. The final section is a sequence of 43 chapters on individual elements (or groups of elements), arranged alphabetically and each generally organised into descriptions of basic chemistry, distribution and technical uses, physiology and analysis. In total, 80 authors have contributed to the book. It ends with extensive subject and author indexes.

This is a splendid text. It provides an excellent source of information on the impact of inorganic species on clinical systems. And, notwithstanding the title, it concludes the metalloids arsenic and antimony and the distinctly non-metallic selenium, and does deal with clinical samples, not with analytical chemistry in general. Thus it can be recommended as an essential reference text for all concerned with trace analysis in a clinical (or even a wider, biological) context.

Alan Townshend

E. Castillo and E. Alvarez, *Expert Systems: Uncertainty and Learning*, Elsevier Applied Science, London, New York, 1991 (ISBN 1-85166-664-8). xi + 331 pp. Price £58.00. Computational Mechanics Publications, Southampton (ISBN 1-85312-050-2). Computational Mechanics Publications, Boston (ISBN 0-945824-33-5).

This book provides a good overview of the development and use of expert systems, based both on rules and probability, and the contribution of statistics in this field. It is addressed to readers interested in utilizing as well as intending to develop expert systems. The latter will be assisted with four appendices, written in Pascal and Lisp, which are essentially useful. Due evidently to the authors' own experience, probability-based expert systems are given broader coverage than ruled based ones. The book is readable for a very wide range of specialists although for complete understanding of the text some general mathematical skills are required. However, the included examples will make all readers familiar with the scope and limitations of expert systems' utilization. The bibliography is not exhaustive and lists primarily landmark papers and books published until 1987. Overall, this book will serve as a good resource for practical implementation of different expert systems' approaches. Contents: (1) An Overview of Expert Systems. (2) Ruled Based Expert Systems. (3) Probability Based Ex-

pert Systems. (4) The Problem of Measuring and Propagating Uncertainty. (5) Other Contributions of Statistics to Expert Systems. (6) Learning Procedures. (7) Tools, Shells and Commercial Expert Systems. Appendix A – Rule Based Expert System in Pascal. Appendix B – Rule Based Expert System in Lisp. Appendix C – Probability Based Expert System in Pascal. Appendix D – Probabilistic Models. Bibliography. Glossary of Terms. Index.

George Andreev

C.N. Hegarty, *An Introduction to the Management of Laboratory Data: A Tutorial Approach using Borland's Paradox Relational Database*, Royal Society of Chemistry, Cambridge, 1992 (ISBN 0-85186-219-5). 587 pp. Price £85.00.

This heavyweight book is designed to take a total novice in the use of databases through the construction of a complete Laboratory Information Management System (LIMS) using Borland's Paradox Relational Database. The LIMS created in this tutorial cannot rival the large commercially available systems but at the end the user will have a basic LIMS and should be capable of constructing extra modules.

Some 540 pages are devoted to taking the user through creating the LIMS, essentially key press by key press. Consequently, I cannot describe the text as inspiring and I have to question its value to a complete novice in programming, databases or LIMS as there is little discussion on the vital planning stages for a project of this size. In particular, there is no discussion of the overall structure of the LIMS nor any plan or schematic diagram to show the relationships between the various modules and files contained in it. This makes it difficult to identify the market for this text; the novice could easily follow the instructions but will learn little, and the more experienced will find little substance to extend their knowledge.

A working run-time only DOS version of the program on a disk is supplied with the text. The compressed program loaded without problem and expanded to 264 files occupying 2.18Mb of disk space. Apart from one or two quirks (using F2 to leave a form takes you to the main toplevel menu instead of the parent menu and on a fast PC some of the information screens flash by) it seemed to function as described in the text.

R.L. Tranter

Barry H. Gump and David J. Pruett (Eds.), *Beer and Wine Production: Analysis, Characterization, and Technological Advances*, ACS Symposium Series No. 536, American Chemical Society, Washington, DC, 1993 (ISBN 0-8412-2714-4). xi + 275 pp. Price Clothbound US$59.95.

This book reports on a symposium held at the 203rd National Meeting of the ACS in San Francisco 1992. The art of beer and wine making is very old, definitely much older than the art of writing. Traditional brewing and wine-making relied on experience and on sensory tests for quality control. Improvements of the products were slow and brought about by a combination of observation, guesswork and luck. This has very much changed in the recent past, as modern analytical and technological innovations have found their way into the production process. It is a direct consequence of this development that we currently drink the best wine and beers ever produced.

This book deals with various aspects of modern beer and wine making technology. The first two chapters give a general review on the general analytical methods in the field. The next section (5 chapters) is devoted to the sensory characterization and control, followed by another 5 chapters on the state and progress of technological applications. Finally, two chapters on the home making of beer and wine and the index section close the collection of papers.

This book is interesting for the general analytical chemist, who will discover many new and interesting aspects of practical analytical chemistry. As wine making and brewing is of an extremely multidisciplinary nature, much of the relevant information tends to be scattered in diverse

literature fields, e.g., food science, agriculture, and microbiology. This book, collecting together an excellent overview of the field, is thus quite useful for the expert. It will also certainly make good reading for not-so-technical wine and beer drinkers, helping them to understand the science and technology of wine and beer making and to appreciate the technical sophistication achieved in the last few decades. Even though detailed understanding of the science and technology of wine and beer making is not required to enjoy a good glass of wine or beer, such an understanding may lead to greater appreciation of the products.

J.T. Clerc

E.W. Schlag (Ed.), *Time-of-flight Mass Spectrometry and its Applications*, Elsevier, Amsterdam, 1994 (ISBN 0-444-81875-8). ix + 413 pp. Price US$ 122.75/Dfl 215.00 (paperback).

Time-of-flight mass spectrometry (TOFMS) is undergoing a considerable resurgence as a fast and versatile analytical technique. This volume, which was previously published as a special issue of the *International Journal of Mass Spectrometry and Ion Processes*, Vol. 131 (1994), is a collection of 21 articles, largely by authors from the USA and Germany, intended *to give a survey of current applications from many of the active groups in the field*. It also includes an article by Mamyrin on laser-assisted reflectron TOFMS. There is a subject index.

Charles L. Wilkins (Ed.), *Computer-enhanced Analytical Spectroscopy*, Vol. 4, Plenum Press, New York, 1993 (ISBN-0-306-44456-9). xviii + 308 pp. Price US$89.50.

This book contains the keynote lectures presented at the *Fourth Symposium on Computer-Enhanced Analytical Spectroscopy*, June 17–19, 1992, near Salt Lake City. The twelve chapters, with 32 authors, cover aspects of NMR spectroscopy (4 papers), mass spectroscopy (2), IR spectroscopy (2), ion mobility spectrometry, UV–visible spectrometry, chromatography and molecular structure and dynamics at interfaces.

Takayuki Skibamoto (Ed.), *Lipid Chromatographic Analysis*, Marcel Dekker, New York, 1994 (ISBN 0-8247-8941-5). viii + 412 pp. Price US$ 135.00.

This is a useful text in which the application of modern chromatographic techniques to lipid analysis is reviewed. The first chapter (49 pp) co-authored by the editor, deals with solid-phase extraction to separate lipids into classes. This is followed by eleven chapters covering TLC (with FID), capillary GC of myocardial cholesterol oxides, GLC of neutral lipids and, with LC, of neutral glycerolipids and of lipid peroxidation products. There are two further LC articles, one on ether-linked glycerolipids, two on GC–MS and finally one on SFC. The articles are well produced and illustrated, and extensively referenced. There is a large subject index.

Gary D. Christian, *Analytical Chemistry*, 5th edn. Wiley, New York, 1994 (ISBN 0-471-305-820). xx + 812 pp. Price £18.95 (paperback).

There can be no doubt that this is one of the favourite text books on undergraduate analytical chemistry. Its frequent revisions have meant that the contents have been kept up-to-date, and that its organisation meets current needs. This is certainly true for this fifth edition. For example, there are changes in the way which titrimetry and potentiometry are dealt with, and a focus on electrochemical sensors and voltammetry has displaced techniques like classical polarography and coulometry. There have also been changes in the treatment of chromatography. The book retains its collection of experiments and of applications to specific types of samples (clinical and environmental). The "problems" section has been extensively revised.

IARC Monographs on the Evaluation of Carcinogenic Risk to Humans, Vol. 56, *Some Naturally Occurring Substances: Food Items and Constituents, Heterocyclic Aromatic Amines and Mycotoxins*, IARC, Lyon, 1993 (ISBN 92-832-1256-8). 599 pp. Price SF 95.00.

This volume has a similar format to other volumes in the series, presenting, in great detail, and with full references, the evidence relating to carcinogenic risks to humans, of certain substances and compounds. In this instance, the items covered are certain food items and constituents (salted fish, picked vegetables, caffeic acid and *d*-limonene), four aromatic amines found in cooked foods, mycotoxins (especially aflatoxins (150 pp.), but also those from various *Fusarium* species and ochratoxin A). The book concludes with a summary of final evaluations, summary tables and activity profiles for genetic and related effects, and the usual cumulative index to the series.

ELSEVIER

Analytica Chimica Acta 294 (1994) 343–345

ANALYTICA CHIMICA ACTA

Author Index

Calendar of forthcoming meetings

★ *indicates new or amended entry*

September 18–22, 1994
Ambleside, UK
Geoanalysis 94 — An International Conference on the Analysis of Geological and Environmental Materials. *Contact*: Geoanalysis 94 Conference Secretariat, Analytical Geochemistry Group, British Geological Survey, Keyworth, Nottingham NG12 5GG, UK. Tel.: +44 (0)602 363349; Fax: +44 (0)602 363200; Telex: 378173 bgskey g; E-mail: k_snrc@uk.ac.nerc-keyworth.vaxa.

September 18–22, 1994
Chambéry, Savoy, France
14th International CODATA Conference. Data and Knowledge in a Changing World: The Quest for a Healthier Environment. *Contact:* Prof. J.-E. Dubois, ITODYS, Université Paris 7, 1 rue Guy de la Brosse, 75005 Paris, France. Fax: +33 1 42881466. E-mail: codata@paris7.jussieu.fr (Internet).

September 19–22, 1994
Turin, Italy
International Ion Chromatography Symposium 1994. *Contact*: Century International, P.O. Box 493, Medfield, MA 02052, USA. Tel.: +1 508/359-8777; Fax: +1 508/359-8778.

September 21–24, 1994
Stockholm, Sweden
5th International Symposium on Pharmaceutical and Biomedical Analysis: *Contact*: Swedish Academy of Pharmaceutical Sciences, P.O. Box 1136, S-111 81 Stockholm, Sweden. Tel.: +46 8 245085; Fax: +46 8 205511.

September 22–24, 1994
Constanta, Romania
12th Conference on Analytical Chemistry. *Contact:* Dr. Gabirel-Lucian Radu, Romanian Society of Analytical Chemistry, 13 Blvd. Carol I, Sector 3, 70346 Bucharest, Romania.

September 25–30, 1994
Goa, India
ISMEBC '94. International Conference on Molecular Electronics and Biocomputing. *Contact*: Dr. Ratna S. Phadke, Scientific Secretary for ISMEBC '94, Chemical Physics Group, Tata Institute of Fundamental Research, Homi Bhabha Road, Bombay 400 005, India. Tel: +91 (22) 215 2971; Fax: +91 (22) 215 2110 e-mail: mebc@tifrvax.bitnet mebc@tifrvax.tifr.res.in.

September 25–30, 1994
Bristol, UK
1994 European Workshop in Chemometrics. *Contact*: Janice Green, School of Chemistry, University of Bristol, Cantock's Close, Bristol BS8 1TS, UK. Tel: +44 (0)272 303030 ext. 4421 (ansaphone) or +44 (0)272 303672; Fax: +44 (0) 272 251295.

September 26–28, 1994
Basel, Switzerland
Chemometrics: Multivariate Analysis and Design in Chemical Research and Development. *Contact*: S. Morgenthaler, ASS, EPFL, Dept. de Mathématiques, CH-1015 Lausanne, Switzerland.

★ ***October 2–7, 1994***
St. Louis, MO, USA
21st Annual Federation of Analytical Chemistry and Spectroscopy Societies Conference. *Contact:* Ms. Jo Ann Brown, 198 Thomas Johnson Dr., Suite S2, Frederick, MD 21702-4317, USA.

October 3–7, 1994
St. Peterburg, Russia
ISCMS '94. International Symposium: Chromatography and Mass Spectrometry in Environmental Analysis. *Contact:* ISCMS '94, Dr. Alexander Rodin, State Institute of Applied Chemistry, Dobrolubov Ave. 14, 197198, St. Petersburg, Russia. Tel.: +7 812 2389786; Fax: +7 812 2338989; Telex: 121345 ptb sigma.

October 11–13, 1994
Amsterdam, The Netherlands
6th International Colloquium Solid Sampling with Atomic Spectroscopy. *Contact*: Prof. Dr. R.F.M. Herber, Coronel Laboratory, University of Amsterdam, Meibergdreef 15, 1105 AZ Amsterdam, The Netherlands.

October 14–15, 1994
Hong Kong
CITAC '94 Hong Kong Symposium on Traceability and Comparability of Analytical Measurements. *Contact*: Dr. T.L. Ting, CITAC 94 Hong Kong Symposium Secretariat, c/o Government Laboratory, Ho Man Tin Government Offices, 88 Chung Hau Street, Homantin, Hong Kong. Tel.: (+852) 7623706; Fax: (+852) 7144083

October 17–19, 1994
Strasbourg, France
3rd International Symposium on Supercritical Fluids: Thermodynamics, Physico-chemical Properties, Technology and Applications. *Contact:* ISASF, Mle. Brionne, ENSIC, P.O. Box 451, F-54001 Nancy Cedex, France. Tel.: +33 83175003; Fax: +33 83350811.

October 19–22, 1994
Pasadena, CA, USA
Personal Identification. Meeting of the Forensic Science Society. *Contact:* Forensic Science Society, Clarke House, 18a Mount Parade, Harrogate, UK. Tel.: +44 423-506068; Fax: +44 423-530948.

★ ***October 24–25, 1994***
Amsterdam, Netherlands
DART '94. Data Handling, Automation, Regulation, and Technology Conference and Table-Top Exhibition. *Contact:* Zena Barrick, Conference Manager DART '94, Advanstar House, Park West, Sealand Road, Chester CH1 4RN, UK. Tel.: +44 244 378-888; Fax: +44 244 370-011.

October 31–November 2, 1994
Minneapolis, USA
Anabiotec '94. 5th International Symposium on Analytical Methods, Systems and Strategies in Biotechnology. *Contact*: Anabiotec Conference Secretariat, Elsevier Advanced Technology, Mayfield House, 256 Banbury Road, Oxford, OX2 7DH, U.K., Tel: +44 (0)865 512242, Fax: +44 (0)865 310981.

November 6–12, 1994
Venezuela
Third Rio Symposium on Atomic Spectrometry. *Contact*: José Alvarado, Departamento de Química, Universidad Simón Bolívar, Apartado 89000, Caracas 1080-A, Venezuela. Fax: +58-2 9621695/938322.

November 7–8, 1994
Montreux, Switzerland
Short Course on LC/MS, SFC/MS and CE/MS (preceding 11th Montreux Symposium). *Contact*: Dr. A. Donzel, Scitec S.A., Lausanne, Switzerland. Tel.: +41 21-241533; Fax: +41 21-241549.

November 8–10, 1994
Helsinki, Finland
KEMIA 94. The Finnish Chemical Congress and Exhibition. *Contact*: Ms Ritva Becker. Tel.: +358-0-1509 211.

November 9–11, 1994
Montreux, Switzerland
11th Montreux Symposium on Liquid Chromatography–Mass Spectrometry (LC/MS; SFC/MS; CE/MS; MS/MS). *Contact:* M. Frei-Häusler, Postfach 46, CH-4123 Allschwil 2, Switzerland. Tel.: +41 61-4812789; Fax: +41 61-4820805.

November 21–22, 1994
Enschede, The Netherlands
μTAS'94. Workshop on Micro Total Analysis Systems. *Contact:* Dr. Albert van den Berg, University of Twente, MESA Research Institute, P.O. Box 217, 7500 AE Enschede, The Netherlands. Tel. +31 53 892 691; Fax: +31 53 309 547.

★ ***January 8–13, 1995***
Cambridge, UK
1995 Winter Conference on Plasma Spectrochemistry. *Contact:* Janice M. Gordon, Royal Society of Chemistry, Thomas Graham House, Science Park, Milton Road, Cambridge CB4 4WF, UK. Tel.: +44 223 420066; Fax: +44 223 420247.

January 22–25, 1995
Yokohama, Japan
International Symposium on Chromatography. 35th Anniversay of Research Group on Liquid Chromatography in Japan. *Contact*: Dr. Toshihiko Hanai, International Institute Technol. Analysis, 3-492 Marsumi, Eclairer 2-913, Kanagawaku, Yokohama 221, Japan. Fax: +81 45-402-6361.

★ ***February 7–10, 1995***
Montreux, Switzerland
4th International Conference on Automation, Robotics and Artificial Intelligence applied to Analytical Chemistry and Laboratory Medicine. *Contact:* International Conference on Automation and Robotics, c/o SCITEC, Av. de Provence 20, CH-100 Lausanne 20, Switzerland. Tel.: +41 21 624 15 33; Fax: +41 21 625 15 46. *USA:* Tel.: +1 (804) 924 5691; Fax: +1 (904) 924 5718.

March 6–10, 1995
PITTCON '95. Pittsburgh Conference on Analytical Chemistry and Applied Spectroscopy. *Contact:* Pittsburgh Conference, Suite 332, 300 Penn Center Blvd., Pittsburgh, PA 15235-9962, USA.

★ ***March 13–15, 1995***
Durham, NC, USA
Low- and No-VOC Coating Technologies. 2nd Biennial International Conference. *Contact:* Ms. Coleen M. Northeim, Research Triangle Institute, P.O. Box 12194, Research Triangle Park, NC 27709-2194. Tel.: +1 (919) 541-5816; Fax: +1 (919) 541-7155.

April 4–7, 1995
Rome, Italy
Short Course on Chiral Resolution. *Contact*: Dr. Salvatore Fanali or Dr. Massimo Sinibaldi, CNR, Istituto di Cromatografia, C.P{. 10, 00016 Monterotondo Scalo (Roma), Italy. Tel.: +39 6-90625328/90625836; Fax: +39 6 90625849; Telex: 624809 CNR MLI.

★ ***May 7–10, 1995***
Lund, Sweden
7th Symposium on Handling of Environmental and Biological Samples in Chromatography. *Contact:* IAEAC Secretariat, M. Frei-Häusler, Postfach 46, CH-4123 Allschwil 2, Switzerland. Tel.: +41 61-4812789; Fax: +41 61-4820805.

May 9–12, 1995
Jülich, Germany
6th International Hans Wolfgang Nürnberg Memorial Symposium on Metal Compounds in Environment and Life, 6: Analysis, Speciation and Specimen Banking. *Contact:* Dr. H.W. Dürbeck, Institute of Applied Physical Chemistry, Research Center, Jülich (KFA), D-52425 Jülich, Germany.

June 5–8, 1995
Singapore
Fifth Symposium on Our Environment and First Asia-Pacific Workshop on Pesticides. *Contact:* The Secretariat, 5th Symposium on Our Environment, c/o Department of Chemistry, National University of Singapore, Kent Ridge, Rep. Singapore 0511. Fax: +65 779-1691.

★ ***July 9–13, 1995***
Barcelona, Spain
3rd International Symposium on Applied Mass Spectrometry in the Health Sciences and 3rd European Tandem Mass Spectrometry Conference. *Contact:* Prof. Emilio Gelpi, Palau de Congressos, Dept. Convencions, Av. Reina M. Cristina, s/n, 08004 Barcelona, Spain. Tel.: +34 3 4233101 ext. 8208-8213; Fax: +34 3 4262845.

★ ***July 9–14, 1995***
Darwin, NT, Australia
13AC/4EC. 13th Australian Symposium on Analytical Chemistry: "Initiatives in Quality Solutions", in conjunction with 4th Environmental Chemistry Conference: "Chemistry in Tropical and Temperate Environments". *Contact:* Symposium Secretariat, 13AC/4EC, Convention Catalysts Int., GPO Box 2541, Darwin, NT 0801, Australia. Tel.: +61 89 811 875; Fax: +61 89 411 639.

July 9–15, 1995
Hull, UK
SAC 95. *Contact:* Analytical Division, The Royal Society of Chemistry, Burlington House, Piccadilly, London W1V 0BN, UK. Tel.: +44 71 437-8656; Fax: +44 71 734-1227.

★ ***August 13–17, 1995***
Seattle, WA, USA
ICFIA 95. Seventh International Conference on Flow Injection Analysis. *Contact:* ICFIA 95, c/o Gary D. Christian, Department of Chemistry BG-10, University of Washington, Seattle, WA 98195, USA. Tel.: +1 (206) 543-5340; Fax: +1 (206) 685-3478; E-mail: christia@chem.washington.edu

August 27–September 1, 1995
Leipzig, Germany
CSI XXIX. Colloquium Spectroscopicum Internationale XXIX. *Contact:* Gesellschaft Deutscher Chemiker, Abt. Tagungen, P.O. Box 90 04 40, D-60444 Frankfurt/ Main, Germany.

August 27–September 1, 1995
Budapest, Hungary
10th International Conference on Fourier Transform Spectroscopy. *Contact:* Mrs. Klára Láng/Mr. Attila Varga, Conference Office, Roland Eötvös Physical Society, P.O. Box 433, H-1371 Budapest, Hungary. Tel./Fax: +36 1 201-8682.

September 3–8, 1995
Villeneuve d'Ascq, France
6th European Conference on the Spectroscopy of Biological Molecules. *Contact*: Professor J.C. Merlin or Dr. S. Turrell, ECSBM'95, LASIR, Université des Sciences et Technologies de Lille, Bât. C5, 59655 Villeneuve d'Ascq Cedex, France. Tel.: +33 20436988 (JCM) or +33 20434920 (ST); Fax: +33 20436755; E-mail: ECSBM95@univ-lille1.fr.

September 4–5, 1995
Paris, France
Sample Handling of Pesticides in the Aquatic Environment. Short course preceding the 5th Workshop on Chemistry and Fate of Modern Pesticide. *Contact:* Prof. M.-C. Hennion, ESPCI, Lab. Chimi Analytique, 10 rue Vauquelin, 75005 Paris, France.

★ ***September 4–7, 1995***
Potsdam, Germany
Design of Bioactive Compounds: Possibilities for Industrial Applications. *Contact:* SCI Conference Office, 14/15 Belgrave Square, London SW1X 8PS, UK.

September 6–8, 1995
Paris, France
5th Workshop on Chemistry and Fate of Modern Pesticides. *Contact:* Prof. M.-C. Hennion, ESPCI, Lab. Chimi Analytique, 10 rue Vauquelin, 75005 Paris, France.

September 12–15, 1995
Leuven, Belgium
5th International Symposium on Drug Analysis. *Contact:* Prof. J. Hoogmartens, Drug Analysis '95, Institute of Pharmaceutical Sciences, Van Evenstraat 4, B-3000 Leuven, Belgium. Tel.: +32 16 283440; Fax: +32 16 283448.

★ ***September 25–28, 1995***
Moscow, Russia
5th Symposium on Kinetics in Analytical Chemistry (KAC '95). *Contact:* Prof. H.A. Mottola, Department of Chemistry, Physical Sciences 107, Oklahoma State University, Stillwater, OK 74078-0447, USA. Tel.: +1 (405) 744-5920; Fax: +1 (405) 744-6007.

February 6–9, 1996
Bruges, Belgium
HTC 4. Fourth International Symposium on Hyphenated Techniques in Chromatography: Hyphenated Chromatographic Analyzers. *Contact*: Royal Flemish Chemical Society, Working Party on Chromatography, c/o Dr. R. Smits, BASF Antwerpen N.V., Central Laboratory, Haven 725, Scheldelaan 600, B-2040 Antwerp, Belgium. Tel.: +32 3-5612831; Telex: 31047 basant b; Fax: +32 3-5613250.

PUBLICATION SCHEDULE FOR 1994

	J	F	M	A	M	J	J	A	S	O	N	D
Anal. Chim. Acta	284/3 285/1–2 285/3	286/1 286/2 286/3	287/1–2 287/3 288/1–2	288/3 289/1 289/2	289/3 290/1–2 290/3	291/1–2 291/3 292/1–2	292/3 293/1–2 293/3	294/1 294/2 294/3	295/1–2 295/3 296/1	296/2 296/3 297/1–2	297/3 298/1 298/2	298/3 299/1 299/2
Vib. Spec.	6/2		6/3		7/1		7/2		7/3		8/1	

INFORMATION FOR AUTHORS

Detailed "Instructions to Authors" for *Analytica Chimica Acta* was published in Volume 289, No. 3, pp. 381–384. Free reprints of the "Instructions to Authors" of *Analytica Chimica Acta* and *Vibrational Spectroscopy* are available from the Editors or from: Elsevier Science B.V., P.O. Box 330, 1000 AH Amsterdam, The Netherlands. Telefax: (+31-20) 5862459.

Manuscripts. The language of the journal is English. English linguistic improvement is provided as part of the normal editorial processing. Authors should submit three copies of the manuscript in clear double-spaced typing on one side of the paper only. *Vibrational Spectroscopy* also accepts papers in English only.

Rapid publication letters. *Letters* are short papers that describe innovative research. Criteria for letters are novelty, quality, significance, urgency and brevity. Submission data: max. of 2 printed pages (incl. Figs., Tables, Abstr., Refs.); short abstract (e.g., 3 lines); *no* proofs will be sent to the authors; submission on floppy disc; *no* revision will be possible.

Abstract. All papers and reviews begin with an Abstract (50–250 words) which should comprise a factual account of the contents of the paper, with emphasis on new information.

Figures. Figures should be prepared in black waterproof drawing ink on drawing or tracing paper of the same size as that on which the manuscript is typed. One original (or sharp glossy print) and two photostat (or other) copies are required. Attention should be given to line thickness, lettering (which should be kept to a minimum) and spacing on axes of graphs, to ensure suitability for reduction in size on printing. Axes of a graph should be clearly labelled, along the axes, outside the graph itself. All figures should be numbered with Arabic numerals, and require descriptive legends which should be typed on a separate sheet of paper. Simple straight-line graphs are not acceptable, because they can readily be described in the text by means of an equation or a sentence. Claims of linearity should be supported by regression data that include slope, intercept, standard deviations of the slope and intercept, standard error and the number of data points; correlation coefficients are optional.

Photographs should be glossy prints and be as rich in contrast as possible; colour photographs cannot be accepted. Line diagrams are generally preferred to photographs of equipment. Computer outputs for reproduction as figures must be good quality on blank paper, and should preferably be submitted as glossy prints.

Nomenclature, abbreviations and symbols. In general, the recommendations of IUPAC should be followed, and attention should be given to the recommendations of the Analytical Chemistry Division in the journal *Pure and Applied Chemistry* (see also *IUPAC Compendium of Analytical Nomenclature, Definitive Rules*, 1987).

References. The references should be collected at the end of the paper, numbered in the order of their appearance in the text (*not* alphabetically) and typed on a separate sheet.

Reprints. Fifty reprints will be supplied free of charge. Additional reprints (minimum 100) can be ordered. An order form containing price quotations will be sent to the authors together with the proofs of their article.

Papers dealing with vibrational spectroscopy should be sent to: Dr J.G. Grasselli, 150 Greentree Road, Chagrin Falls, OH 44022, U.S.A. Telefax: (+1-216) 2473360 (Americas, Canada, Australia and New Zealand) or Dr J.H. van der Maas, Department of Analytical Molecular Spectrometry, Faculty of Chemistry, University of Utrecht, P.O. Box 80083, 3508 TB Utrecht, The Netherlands. Telefax: (+31-30) 518219 (all other countries).

© 1994, ELSEVIER SCIENCE B.V. All rights reserved.

0003-2670/94/$07.00

No part of this publication may be reproduced, stored in a retrieval system or transmitted in any form or by any means, electronic, mechanical, photocopying, recording or otherwise, without the prior written permission of the publisher, Elsevier Science B.V., Copyright and Permissions Dept., P.O. Box 521, 1000 AM Amsterdam, The Netherlands.

Upon acceptance of an article by the journal, the author(s) will be asked to transfer copyright of the article to the publisher. The transfer will ensure the widest possible dissemination of information.

Special regulations for readers in the U.S.A.–This journal has been registered with the Copyright Clearance Center, Inc. Consent is given for copying of articles for personal or internal use, or for the personal use of specific clients. This consent is given on the condition that the copier pays through the Center the per-copy fee for copying beyond that permitted by Sections 107 or 108 of the U.S. Copyright Law. The per-copy fee is stated in the code-line at the bottom of the first page of each article. The appropriate fee, together with a copy of the first page of the article, should be forwarded to the Copyright Clearance Center, Inc., 27 Congress Street, Salem, MA 01970, U.S.A. If no code-line appears, broad consent to copy has not been given and permission to copy must be obtained directly from the author. The fee indicated on the first page of an article in this issue will apply retroactively to all articles published in the journal, regardless of the year of publication. This consent does not extend to other kinds of copying, such as for general distribution, resale, advertising and promotion purposes, or for creating new collective works. Special written permission must be obtained from the publisher for such copying.

No responsibility is assumed by the publisher for any injury and/or damage to persons or property as a matter of products liability, negligence or otherwise, or from any use or operation of any methods, products, instructions or ideas contained in the material herein.

Although all advertising material is expected to conform to ethical (medical) standards, inclusion in this publication does not constitute a guarantee or endorsement of the quality or value of such product or of the claims made of it by its manufacturer.

(∞) The paper used in this publication meets the requirements of ANSI/NISO 239.48-1992 (Permanence of Paper).

PRINTED IN THE NETHERLANDS

Elsevier's Dictionary of Microscopes and Microtechnique

In English (with definitions), French and German

R. Serré

The publication of this dictionary encompassing the terminology of all types of microscopes and of various aspects of microtechnique fills a major communications gap in an area of scientific research and instrumentation that has evolved over more than 350 years. The reader will discover all the key concepts linked to optical, electron, phase-contrast, polarizing, and other types of microscopes, as well as many terms related to the preparation of specimens for examination under the microscope, including microtomy, staining, and fixation. Translators and terminologists will find in this dictionary such useful features as definitions, synonyms, cross references, and bibliographic sources, a separate listing of acronyms and abbreviations, and French and German indexes. As a multilingual tool, this dictionary contains features that language specialists have come to expect: definitions and bibliographic sources. As a technical work, it brings order and coherence to a multitude of terms and expressions from a broad spectrum of scientific and technical disciplines.
The layout of this dictionary is such that each language included may be used as a target as well as a source language.

©1993 viii + 286 pages
Hardbound
1827 terms
Price: Dfl. 250.00 (US$142.75)
ISBN 0-444-889973-6.

A sample page from this dictionary available from the publisher.

ORDER FORM

Send this form (or a photocopy) to your usual supplier or to one of the addresses listed below:
ELSEVIER SCIENCE, Attn: Rina Terstall, P.O. Box 1991, 1000 BZ Amsterdam, The Netherlands
in the USA/Canada: Attn: Judy Weislogel, P.O. Box 945, Madison Square Station, New York, NY 10160-0757

☐ **Yes, please send me ..... copy(ies) of Elsevier's Dictionary of Microscopes and Microtechnique** (R. Serré). ISBN 0-444-889973-6. Price: Dfl. 250.00 (US$ 142.75)

☐ **Payment enclosed:** (BankDraft/Eurocheque/International Money Order/Personal Cheque/PostalCheque/OfficePurchaseOrderForm)

☐ **Charge my credit card:**

☐ MasterCard ☐ Eurocard ☐ Access ☐ VISA ☐ American Express

Card no. _____ Expiry Date _____ _____

☐ **Please send an invoice**/postage will be added

Name _____

Address _____

City _____ Zip Code _____ Country _____

VAT Registration no.: _____ Date _____ Signature _____

The Dutch Guilder (Dfl.) price quoted applies worldwide. US Dollar (US$) price quoted may be subject to exchange rate fluctuations. Prices are subject to change without prior notice. No postage will be added to prepaid book orders. Non VAT registered customers in the European Community should add the appropriate VAT rate applicable in their country to the price(s). In New York State, please add applicable sales tax.

419\B\DICT6

0003-2670(19940830)294:3;1-0